

UNIVERSITY OF CINCINNATI

Date: _____

I, _____,
hereby submit this work as part of the requirements for the degree of:

in:

It is entitled:

This work and its defense approved by:

Chair: _____

A Model for Dry- and Wet-Casting of Polymeric Membranes
incorporating Convection due to Densification
- Application to Macrovoid Formation

by

Hanyong Lee

B.S. Yonsei University, Korea (ROK), 1996

M.S. Yonsei University, Korea (ROK), 2000

Committee Members:

Dr. William B. Krantz (Chair)

Dr. Sun-Tak Hwang (Co-chair)

Dr. Chia-Chi Ho

Dr. James E. Mark

This thesis is submitted to
the Faculty of the Research Committee at the
University of Cincinnati in partial fulfillment
of the requirements for the degree of
Doctor of Philosophy
in Chemical Engineering
in the year 2005.

ABSTRACT

The dry-casting process and the wet-casting process are two typical phase-inversion techniques for manufacturing synthetic polymeric membranes. Although extensive modeling studies have been done for both casting processes in order to achieve an optimization of a membrane recipe, all models developed heretofore allow for mass transfer only by diffusion. A proper model for membrane casting should incorporate both the diffusive and convective contributions to the mass transfer fluxes. Therefore, the objective of this thesis is the developments of a dry-casting model and a wet-casting model based on the fundamental and general approach to construct well-defined mass-transfer problems incorporating both convection and diffusion.

This new more general approach produces well-defined description of wet- and dry-casting processes that are solvable with currently available PDE solvers and accurately describe the effects of density variation in the system. Non-equilibrium thermodynamics allows further generalization of this approach to multicomponent mass-transfer problems. The predictions of the dry-casting model developed with this general approach show much better agreement with experimental data in the literature for the CA/acetone/water system. The new wet-casting model predicts the presence of a metastable region in the casting solution depending on the initial thickness that is not predicted by model that incorporates only diffusive mass transfer. Low-gravity experiments using a newly developed membrane casting apparatus show that macrovoids are formed in the CA/acetone/water casting solution when a metastable region is

predicted by the new wet-casting model. Furthermore, membrane casting experiments that incorporated surfactant in the precipitation bath reveal that macrovoid formation is strongly associated with the coalescence of microdroplets having a high surface energy in the metastable region of the casting solution. Therefore, both the experimental and modeling results support the coalescence-induced coalescence macrovoid formation mechanism.

To my parents,

My parents-in-law,

My wife,

And To my sons, Caton and Brandt Lee

ACKNOWLEDGMENTS

During all years I spent with Professor William B. Krantz and Professor Sun-Tak Hwang, they have served me as all the followings; advisors, guides, teachers, friends. The moment whenever I felt frustration, they were willing hands and gave me a very important advice for my life and for my research. Their encouragement and enthusiasm were the driving force to be what I am. Like guiding angels, they always stood at both sides of me and dragged me into the right place. I am really afraid to imagine how I was a stupid student to them. They also gave me eyes, ears, a brain and a heart to understand and to manage many cultural differences between U.S. and Korea. It was invaluable experience to learn how to manage my life from our perfect cultural spectrum from Americanized American (Professor Krantz) through Americanized Korean (Professor Hwang) to Koreanized Korean (me). They also gladly acted as the worst enemy for me. Whenever they felt my overexcitement possessed with a wrong idea, they make me frustrated without any hesitation and gave another chance to rethink from the beginning. Now I am possessed by their voices; ‘I completely agree on this, B.U.T.....’(Professor Krantz) and ‘NO!, IT IS WRONG’ (Professor Hwang). Their voices are ringing throughout my head automatically, whenever I am forcing to convince myself. However, I am deeply appreciating their intellectual and mental ‘torture’ to make me stronger. I already miss our enthusiastic discussion which, to anybody else, would look like a severe fighting.

The financial support of this research was provided by NASA's Office of Biological and Physical Sciences Research via Grant No. NAG3-2451. I would like to thank all the participants of NASA for their support of this project. Especially, I will never forget the greatest and also worst experience of flying around in front of dozens of people with an upset stomach in KC-135A low-G flight.

Making the apparatus for low-G experiments was one of the challenges in this project. It would be impossible to build the excellent membrane-casting apparatus (MCA) without the great help of Dr. Paul W. Todd and Mr. Andy Kirk in Space Hardware Optimization Technology, Inc. I also would like to thank Dr. Robert L. Sani in University of Colorado at Boulder for his help to test our new idea of the MCA. I have to mention Dr. Alan R. Greenberg and Dr. Vivek P. Khare in University of Colorado at Boulder who gave me excellent advices on this project and helped to refresh Professor Krantz's memory whenever needed. They also contributed many important advices to build FORTRAN programs. In spite of unstable stomach in low-G, Mr. Jeremiah Zartman and Mr. Chris S. Howard helped me a lot to conduct low-G experiment.

My colleagues, Shaun Howard and Siladitya Ray Chaudhuri, made me happy in the lab no matter how hard and stressful things I have. I am sure that most of our chat was not constructive at all and the most subjects of our talking were not even close to our research. However, it was really nice feeling that I have two good friends who can gladly waste their time for my diversion in the lab. Also, I cannot forget to mention the nice discussions with Ray on our researches. These were really helpful to me. My friend, Yi-Chuan Chen, also contributed his time to cheer me up. I also remember the time spent on the group study with

Shigao Cheng and Bo Sun. Joo-Youp Lee and Kyesang Yoo helped me a lot to accommodate myself to sudden change of my life. I also would like to thank Dr. Il Moon in Yonsei University at Korea and Seunghoon Lee, my friend, for their many good advices from Korea.

Finally, I would like to thank my whole family; my parents, my wife's parents, my wife and my sons. Their existence itself is the reason and the driving force of my life. They sacrificed many things for me to study. I cannot be too thankful for their love and confidence gave me.

CONTENTS

LIST OF TABLES.....	8
LIST OF FIGURES.....	9
LIST OF SYMBOLS.....	21
CHAPTER	
I. GENERAL INTRODUCTION.....	26
1.1 Polymeric Membrane Industry.....	26
1.2 Polymeric Membrane Formation.....	28
1.3 Research Challenges.....	32
1.4 Focus of This Research.....	33
1.5 Organization of Thesis.....	36
II. CONVECTIVE TRANSPORT.....	38
2.1 Scope of Chapter.....	38
2.2 Introduction.....	39
2.3 Review of Prior Studies.....	42
2.3.1 Diffusion.....	42
2.3.2 Convection.....	43
2.4 Motivation for This Study.....	44

2.5 Multi-component Convection-Diffusion Mass-Transfer Problem.....	45
2.5.1 Mass Balance for Individual Fluxes.....	45
2.5.2 Equation-of-State.....	47
2.5.3 Mass-Average Velocity.....	47
2.5.4 Modified Peclet Number.....	49
2.5.5 Example Study 1: Rapid Unsteady-State Evaporation.....	50
2.5.5.1 System of Interest.....	50
2.5.5.2 Derivation of Model Equations.....	53
2.5.5.3 Solution Methodology.....	56
2.5.5.4 Results and Discussion.....	58
2.6 Generalized Flux Equation from Non-equilibrium Thermodynamics.....	68
2.6.1 Flux Equation.....	68
2.6.2 Example Study 2: Steady-State Binary Gas Permeation through Membrane.....	70
2.6.2.1 System of Interest.....	70
2.6.2.2 Derivation of Model Equations.....	73
2.6.2.3 Mass-Average Velocity and Modified Peclet Number.....	76
2.7 Summary.....	77
III. DEVELOPMENT OF THE DRY-CASTING MODEL INCORPORATING CONVECTIVE TRANSPORT.....	78

3.1 Scope of Chapter.....	78
3.2 Introduction.....	79
3.3 Review of Prior Studies.....	80
3.4 Motivation of This Study.....	81
3.5 Model Development.....	82
3.5.1 System of Interest.....	82
3.5.2 Thermodynamic Model.....	84
3.5.3 Mass-Transport Model in Casting solution.....	85
3.5.3.1 Species-Balance Equations.....	85
3.5.3.2 Equation-of-State.....	86
3.5.3.3 Multicomponent Diffusive Flux Equations.....	87
3.5.3.4 Mass-Average Velocity.....	88
3.5.3.5 Final Governing Equations.....	90
3.5.3.6 Initial and Boundary Conditions.....	91
3.5.3.7 Displacement of the Liquid-Gas Interface of the Casting Solution.....	92
3.5.4 Energy-Transport Model.....	92
3.5.4.1 Energy-Balance Equations.....	92
3.5.4.2 Initial and Boundary Conditions.....	93
3.5.5 Gas-Phase Transport Model.....	94

3.6 Solution Methodology.....	94
3.7 Presentation of Model Results.....	95
3.8 Discussion of Results.....	112
3.8.1 Corroboration with Membrane Morphology.....	112
3.8.2 Corroboration with Light-Reflection Measurements.....	118
3.8.3 Corroboration with Surface Temperature and Total Solution Mass.....	120
3.8.4 Modified Peclet Number.....	128
3.9 Summary.....	130
IV. DEVELOPMENT OF THE DRY-CASTING MODEL INCORPORATING CONVECTIVE TRANSPORT.....	131
4.1 Scope of Chapter.....	131
4.2 Introduction.....	132
4.3 Review of Prior Studies.....	132
4.4 Motivation for This Study.....	135
4.5 Model Development.....	136
4.5.1 System of Interest.....	136
4.5.2 Thermodynamic Model.....	139
4.5.3 Mass-Transport Model in Casting Solution.....	139
4.5.4 Mass-Transport Model in the Nonsolvent Bath.....	142
4.5.5 Interfacial Local Equilibrium Concentration.....	148

4.6 Solution Methodology.....	149
4.7 Presentation and Discussion of Results.....	150
4.7.1 Local Pseudo-equilibrium.....	150
4.7.2 Local Equilibrium.....	153
4.7.3 Extended Simulation after Vitrification on Interface.....	155
4.7.3.1 Convection-Diffusion Model Results.....	156
4.7.3.2 Diffusion-only Model Results.....	172
4.8 Summary.....	180
V. MACROVOID FORMATION MECHANISM.....	182
5.1 Scope of Chapter.....	182
5.2 Introduction.....	183
5.2.1 Nucleation and Growth (NG) and Spinodal Decomposition (SD).....	183
5.2.2 Coalescence.....	186
5.2.3 Macrovoid Pores (MV).....	189
5.3 Review of Prior Studies.....	192
5.3.1 Hypotheses for Macrovoid Formation Mechanism.....	192
5.3.2 Phenomenological Approach to Macrovoid Formation.....	196
5.3.3 Membrane Casting in Low Gravity.....	198
5.4 Motivation for This Study.....	199

5.5 Experimental Design.....	201
5.5.1 Materials.....	201
5.5.2 Parabolic flight research aircraft (KC-135A).....	201
5.5.3 Membrane Casting Apparatus (MCA).....	204
5.5.4 Light Reflection Measurement.....	219
5.5.5 Surfactant-Induced Membrane Formation.....	219
5.6 Presentation of Experimental Results.....	219
5.7 Discussion of Results.....	233
5.7.1 Elimination of Undesirable Convection.....	233
5.7.2 Corroboration with Model Predictions.....	233
5.7.3 Effects of Gravity.....	238
5.7.4 Surfactant-Induced Macrovoid Formation.....	239
5.7.5 Coalescence-Induced Coalescence Macrovoid Formation Mechanism.....	242
5.8 Summary.....	248
VI. CONCLUSIONS ²⁴⁵ AND RECOMMENDATIONS.....	249
6.1 Scope of Chapter.....	249
6.2 Conclusions.....	249
6.2.1 Convective Transport.....	249
6.2.2 Dry-Casting Model.....	251

6.2.3 Wet-Casting Model.....	252
6.2.4 Macrovoid Formation Mechanism.....	254
6.3 Recommendations.....	257
BIBLIOGRAPHY.....	261
APPENDIX	
A. EVAPORATION PROGRAM.....	273
B. DRY-CASTING MASS-TRANSPORT PROGRAM.....	281
C. TERNARY DIAGRAM.....	319
D. VOLUME-AVERAGE VELOCITY.....	323
E. WET-CASTING MASS-TRANSPORT PROGRAM.....	325

LIST OF TABLES

Table	
2.1 Physical Parameters used in model calculation	57
3.1 Summary of Initial Conditions of the Casting Solutions used in the Numerical Solution of the Dry-Casting Model	96
3.2 Predicted and measured time for the onset of phase-separation [12]	119
5.1 Summary of the convective velocity due to viscous drag and the diffusion velocity	211
5.2 Summary of systemic change of the wet-cast membrane structure formed with the studied initial thicknesses and gravity conditions. The darker color of the membrane represents denser or less porous structure of the membrane	236

LIST OF FIGURES

Figure	
1.1	Scanning electron micrograph showing a cross-sectional view of an asymmetric cellulose acetate membrane having macrovoids. The thickness of the membrane is about $200 \mu m$. 30
1.2	Schematic representation of the phase-inversion process. a: homogenous polymer solution, b: agglomerate, c: gelation, d: phase-separation and e: skin. 31
2.1	Schematic representation of evaporation from a binary liquid phase into a gas phase. 52
2.2	Change of weight fraction of volatile component A in a binary liquid mixture evaporating into a gas. Pure component densities of A and C are 0.7 and 1.0, respectively. 61
2.3	Change of weight fraction of volatile component A in a binary liquid mixture evaporating into a gas phase. Pure component densities of A and C are 0.9 and 1.0 respectively. 62
2.4	Change of weight fraction of volatile component A in a binary liquid mixture evaporating into a gas phase. Pure component densities of A and C are both 1.0. 63
2.5	Change of mass-average velocity in a binary liquid mixture during evaporation of volatile component A into a gas phase. Pure species densities of A and C are 0.7 and 1.0 respectively. 64

2.6	Change of mass-average velocity in a binary liquid mixture during evaporation of volatile component A into a gas phase. Pure component densities of A and C are 0.9 and 1.0 respectively.	65
2.7	Thickness change of liquid phase during evaporation. Model predictions from well-defined convection-diffusion equations (solid line) and from ill-defined diffusion-only equations (dashed line) are presented for three different cases of density of A (0.7, 0.9 and 1.0).	66
2.8	Change of the modified Peclet number of volatile component A at the liquid/gas interface in binary liquid phase during evaporation into gas phase for various cases of pure component density of A. Pure densities of C are same as 1.0 for all cases.	67
2.9	Schematic representation of binary mass transfer of components A and B through perfect membrane that allows only component A to permeate.	72
3.1	Schematic of the dry-cast process for polymeric membrane formation	83
3.2	Concentration change of the liquid-gas interface (●) and solid-liquid interface (○) during the dry-cast membrane-formation process for casting solution 1.	98
3.3	Chemical potential profile change of water in the casting solution during the dry-casting process for casting solution 1.	99
3.4	Chemical potential profile change of acetone in the casting solution during the dry-casting process for casting solution 1.	100
3.5	Mass-average velocity in the casting solution during the dry-casting process for casting solution 1.	101

3.6 Concentration change of liquid-gas interface (●) and solid-liquid interface (○) during the dry-casting membrane-formation process for casting solution 2.	103
3.7 Chemical potential profile change of water in the casting solution during the dry-casting process for casting solution 2.	104
3.8 Chemical potential profile change of acetone in the casting solution during the dry-casting process for casting solution 2.	105
3.9 Mass-average velocity in the casting solution during the dry-casting process for casting solution 2.	106
3.10 Concentration change of liquid-gas interface (●) and solid-liquid interface (○) during the dry-cast membrane formation process for casting solution 3.	108
3.11 Chemical potential profile change of water in the casting solution during dry-casting process for solution 3.	109
3.12 Chemical potential profile change of acetone in the casting solution during the dry-casting process for casting solution 3.	110
3.13 Mass-average velocity in the casting solution during the dry-casting process for casting solution 3.	111
3.14 Concentration paths for the liquid-gas interface and the solid-liquid interface predicted by the convection-diffusion model (solid lines) and Shojaie et al.'s diffusion model (dashed line) during the dry-cast membrane formation process for casting solution 1.	115

3.15 Concentration paths for the liquid-gas interface and the solid-liquid interface predicted by the convection-diffusion model (solid lines) and Shojaie et al.'s diffusion model (dashed line) during the dry-cast membrane formation process for casting solution 2.	116
3.16 Concentration paths for the liquid-gas interface and the solid-liquid interface as predicted by the convection-diffusion model (solid lines) and Shojaie et al.'s diffusion model (dashed line) during the dry-cast membrane formation process for casting solution 3.	117
3.17 Predicted (—) and measured (X) total casting solution mass as a function of time for casting solution 1 in Table 3.1.	122
3.18 Predicted (—) and measured (X) total casting solution mass as a function of time for casting solution 2 in Table 3.1.	123
3.19 Predicted (—) and measured (X) total casting solution mass as a function of time for casting solution 3 in Table 3.1.	124
3.20 Predicted (—) and measured (X) temperature of the liquid/gas interface as a function of time for casting solution 1 in Table 3.1.	125
3.21 Predicted (—) and measured (X) temperature of the liquid/gas interface as a function of time for casting solution 2 in Table 3.1.	126
3.22 Predicted (—) and measured (X) temperature of the liquid/gas interface as a function of time for casting solution 3 in Table 3.1.	127
3.23 Modified Peclet number of acetone near the gas/casting solution interface as a function of time for casting solutions 1, 2, and 3.	129
4.1 Schematic representation of wet-casting process for membrane formation.	138

4.2 Phase diagram of the water (1)/ acetone (2)/cellulose acetate (3) system in which the concentration has a discontinuity at the interface between the polymer-rich and polymer-lean phases in equilibrium	144
4.3 Polynomial fit to the binary diffusion coefficient data for the water (1)/acetone (2) system.	147
4.4 Composition change of the upper interface during wet-casting of a ternary solution of water/acetone/cellulose acetate (0, 0.15, 0.85 mass fraction). Initial casting solution thicknesses of 75 μm and 125 μm gave identical results.	152
4.5 Composition change of the upper interface during wet-casting of a ternary solution of water/acetone/cellulose acetate (0, 0.15, 0.85 mass fraction). The initial casting solution thicknesses are 75 μm and 125 μm . The composition changes on the binodal (from 3.3×10^{-10} sec to 2.0×10^{-9} sec) were calculated using the tie-lines from the Flory-Huggins model. The composition trajectory for contact times less than 3.3×10^{-10} sec in Figure 4.4 is also shown here.	154
4.6 Composition changes for a membrane wet-cast from a ternary solution of water/acetone /cellulose acetate (0/0.15/0.85 mass fraction) having an initial solution thickness of 75 μm . Each curve shows the composition from the lower substrate to the upper interface for a different time after immersion.	158
4.7 Chemical potential profiles for water for a membrane wet-cast from a ternary solution water/acetone /cellulose acetate (0/0.15/0.85 mass fraction) having an initial solution thickness of 75 μm .	159

4.8	Chemical potential profiles for acetone for a membrane wet-cast from a ternary solution water/acetone /cellulose acetate (0/0.15/0.85 mass fraction) having an initial solution thickness of $75 \mu m$.	160
4.9	Thickness change for a for a membrane wet-cast from a ternary solution water/acetone /cellulose acetate (0/0.15/0.85 mass fraction) having an initial solution thickness of $75 \mu m$.	161
4.10	Flux change at the upper interface for a for a membrane wet-cast from a ternary solution water/acetone /cellulose acetate (0/0.15/0.85 mass fraction) having an initial solution thickness of $75 \mu m$	162
4.11	Mass-average velocity profiles for a for a membrane wet-cast from a ternary solution water/acetone /cellulose acetate (0/0.15/0.85 mass fraction) having an initial solution thickness of $75 \mu m$.	163
4.12	Modified Peclet number profiles for a for a membrane wet-cast from a ternary solution water/acetone /cellulose acetate (0/0.15/0.85 mass fraction) having an initial solution thickness of $75 \mu m$.	164
4.13	Composition changes for a membrane wet-cast from a ternary solution of water/acetone /cellulose acetate (0/0.15/0.85 mass fraction) having an initial solution thickness of $125 \mu m$. Each curve shows the composition from the lower substrate to the upper interface for a different time after immersion.	165
4.14	Chemical potential profiles for water for a membrane wet-cast from a ternary solution water/acetone /cellulose acetate (0/0.15/0.85 mass fraction) having an initial solution thickness of $125 \mu m$.	166

4.15	Chemical potential profiles for acetone for a membrane wet-cast from a ternary solution water/acetone /cellulose acetate (0/0.15/0.85 mass fraction) having an initial solution thickness of $125 \mu m$.	167
4.16	Thickness change for a membrane wet-cast from a ternary solution water/acetone /cellulose acetate (0/0.15/0.85 mass fraction) having an initial solution thickness of $125 \mu m$.	168
4.17	Flux change at the upper interface for a membrane wet-cast from a ternary solution water/acetone /cellulose acetate (0/0.15/0.85 mass fraction) having an initial solution thickness of $125 \mu m$.	169
4.18	Mass-average velocity profiles for a for a membrane wet-cast from a ternary solution water/acetone /cellulose acetate (0/0.15/0.85 mass fraction) having an initial solution thickness of $125 \mu m$.	170
4.19	Modified Peclet number profiles for a for a membrane wet-cast from a ternary solution water/acetone /cellulose acetate (0/0.15/0.85 mass fraction) having an initial solution thickness of $125 \mu m$.	171
4.20	Model predictions when convection is ignored: Composition changes for a membrane wet-cast from a ternary solution of water/acetone /cellulose acetate (0/0.15/0.85 mass fraction) having an initial solution thickness of $75 \mu m$. Each curve shows the composition from the lower substrate to the upper interface for a different time after immersion.	174
4.21	Model predictions when convection is ignored: Flux change at the upper interface for a membrane wet-cast from a ternary solution of water/acetone /cellulose acetate (0/0.15/0.85 mass fraction) having an initial solution thickness of $75 \mu m$	175

4.22 Model predictions when convection is ignored: Thickness change for a membrane wet-cast from a ternary solution of water/acetone /cellulose acetate (0/0.15/0.85 mass fraction) having an initial solution thickness of $75 \mu m$	176
4.23 Model predictions when convection is ignored: Composition changes for a membrane wet-cast from a ternary solution of water/acetone /cellulose acetate (0/0.15/0.85 mass fraction) having an initial solution thickness of $125 \mu m$. Each curve shows the composition from the lower substrate to the upper interface for a different time after immersion.	177
4.24 Model predictions when convection is ignored: Flux change at the upper interface for a membrane wet-cast from a ternary solution of water/acetone /cellulose acetate (0/0.15/0.85 mass fraction) having an initial solution thickness of $125 \mu m$	178
4.25 Model predictions when convection is ignored: Thickness change for a membrane wet-cast from a ternary solution of water/acetone /cellulose acetate (0/0.15/0.85 mass fraction) having an initial solution thickness of $125 \mu m$.	179
5.1 Schematic representation of Gibbs free energy as a function of the size of the nucleus.	185
5.2 Schematic representation of the flow field created by shape relaxation of two small coalescing droplets (peanut-shaped solid line). The coalescence results in the round shape of the single large droplet (dotted line).	188
5.3 Environmental scanning electron micrograph (ESEM) of typical macrovoids in the cross-section of a cellulose-acetate membrane.	191

5.4 Schematic representation of parabolic flight of NASA-KC135A.	203
5.5 Membrane-casting apparatus used by Pekny et al [92, 102] and Khare [103]: (a) Before moving the absorbent block and (b) after moving the absorbent block.	205
5.6 Representative illustration of MCA (membrane casting apparatus) testing apparatus filled with dye or aluminum powder, the glycerin/water mixture and pure glycerin to visualize effects of viscous drag.	208
5.7 Dimensionless parallel velocity change with dimensionless time at the top of the casting-solution well having aspect ratio = 1:2 (width:depth).	212
5.8 Dimensionless parallel velocity change with dimensionless time at the top of the casting-solution well having aspect ratio = 1:3 (width:depth).	213
5.9 Dimensionless parallel velocity change with dimensionless time at the top of the casting-solution well having aspect ratio = 40:1 (width:depth).	214
5.10 Schematic side view of the new membrane casting apparatus for low gravity in the three experimental stages: (a) setup; (b) membrane formation; and (c) storage of the membrane.	217
5.11 Photograph of (a) the new membrane casting apparatus (MCA) and (b) nonsolvent chamber in the moving block of the MCA.	218
5.12 Environmental scanning electron micrograph of a membrane cast from a ternary water/acetone/cellulose-acetate solution with a pure water bath in low gravity. The initial water and acetone mass fractions and film thickness are $\omega_1^\circ = 0$, $\omega_2^\circ = 0.15$, and $L_c = 75\mu m$, respectively.	221
5.13 Light intensity data for cellulose-acetate membrane formation corresponding to the initial casting condition used for Figure 5.12.	222

- 5.14 Environmental scanning electron micrograph of a membrane cast from a ternary water/acetone/cellulose-acetate solution with a water/surfactant (20ppm) bath in low gravity. The initial water and acetone mass fractions and film thickness are $\omega_1^\circ = 0$, $\omega_2^\circ = 0.15$, and $L_o = 75\mu m$, respectively. 223
- 5.15 Environmental Scanning micrograph of a membrane cast from a ternary water/acetone/cellulose-acetate solution with a pure water bath in normal gravity. The initial water and acetone mass fractions and film thickness are $\omega_1^\circ = 0$, $\omega_2^\circ = 0.15$, and $L_o = 75\mu m$, respectively. 224
- 5.16 Environmental Scanning micrograph of a membrane cast from a ternary water/acetone/cellulose-acetate solution with a pure water bath in high gravity. The initial water and acetone mass fractions and film thickness are $\omega_1^\circ = 0$, $\omega_2^\circ = 0.15$, and $L_o = 75\mu m$, respectively. 225
- 5.17 Environmental Scanning micrograph of a membrane cast from a ternary water/acetone/cellulose-acetate solution with a pure water bath in low gravity. The initial water and acetone mass fractions, film thickness are $\omega_1^\circ = 0$, $\omega_2^\circ = 0.15$, and $L_o = 125\mu m$, respectively. 227
- 5.18 Light intensity data for cellulose-acetate membrane formation corresponding to the initial casting condition of Figure 5.17. 228
- 5.19 Environmental Scanning micrograph of a membrane cast from a ternary water/acetone/cellulose-acetate solution with a water/surfactant (20ppm) bath in low gravity. The initial water and acetone mass fractions, film thickness are $\omega_1^\circ = 0$, $\omega_2^\circ = 0.15$, and $L_o = 125\mu m$, respectively. 229

- 5.20 Environmental Scanning micrograph of a membrane cast from a ternary water/acetone/cellulose-acetate solution with a pure water bath in normal gravity. The initial water and acetone mass fractions, film thickness are $\omega_1^\circ = 0$, $\omega_2^\circ = 0.15$, and $L_0 = 125\mu m$, respectively. 230
- 5.21 Environmental Scanning micrograph of a membrane cast from a ternary water/acetone/cellulose-acetate solution with a pure water bath in high gravity. The initial water and acetone mass fractions, film thickness are $\omega_1^\circ = 0$, $\omega_2^\circ = 0.15$, and $L_0 = 125\mu m$, respectively. 231
- 5.22 Environmental Scanning micrograph of a membrane cast from a ternary water/acetone/cellulose-acetate solution with a pure water bath in normal gravity. The initial water and acetone mass fractions, film thickness are $\omega_1^\circ = 0$, $\omega_2^\circ = 0.15$, and $L_0 = 500\mu m$, respectively. 232
- 5.23 Composition profiles from the top to the bottom of the casting solution depending on initial thickness as predicted by our wet-casting model using the same initial composition of casting solution of water/acetone/cellulose-acetate = 0 / 0.15 / 0.85 (mass fraction). 237
- 5.24 Magnified view showing the MV-like pores surrounding a huge void (megavoid) that is located at the bottom of the membrane shown in Figure 5.19. 241
- 5.25 Schematic representation of normal pore formation from a thin metastable region: (a) formation of the thin metastable region (b) formation of normal pores and a new metastable region. 245
- 5.26 Schematic representation of initial MV formation from a thick metastable region: (a) formation of the thick metastable region (b) formation of nascent MVs. 246

5.27 Schematic representation of MV growth in a metastable region. The arrows inside the macrovoid represent the spatial expansion rate of the MV.	247
C.1 Ternary phase diagram for an A / B / C system and an example composition X of the mixture.	320
C.2 Hypothetical ternary phase diagram for a polymer / solvent / nonsolvent system which can be one-phase or two-phase.	322

LIST OF SYMBOLS

$\langle a \rangle$	Mean radius of droplet
c	Molar density
c_i	Molar density of component i
C_p	Heat capacity of polymer solution
D_{ij}	Mutual diffusion coefficient of components i and j
J	General flux matrix
j_i	Mass flux of component i with respect to mass average velocity
J_i^*	Molar flux of component i with respect to molar average velocity
F	General phenomenological coefficients matrix
h	Free-convection heat transfer coefficient
K	Thermal conductivity
k_i^G	Mass transfer coefficient of component i in gas phase

$L(t)$	Location of the solution / gas or the solution / liquid interface
L°	Initial thickness of the solution
L_{sub}	Thickness of the glass support plate
L_{ij}	Phenomenological coefficient of $i - j$ pair
M_i	Molecular weight of pure component i
\overline{M}	Number average molecular weight
N	Total molar flux with respect to stationary coordinates
N_i	Molar flux of component i with respect to stationary coordinates
n	Total mass flux with respect to stationary coordinates
n_i	Mass flux of component i with respect to stationary coordinates
n_i^G	Mass flux of component i with respect to stationary coordinates in gas phase
n_i^B	Mass flux of component i with respect to stationary coordinates in nonsolvent bath
P	Total pressure

\bar{p}_i	Partial pressure of component i
Pe_i^M	Modified Peclet number of component i
R	Universal gas constant
T	Temperature
T_a	Ambient temperature
T°	Initial temperature of the system
T_{sub}	Temperature of the glass support plate
V	Total volume
\bar{V}_i	Partial molar volume of component i
v_i	Velocity of component i
W	Mass-average velocity
W^V	Volume-average velocity
X	General driving force matrix
x_i	Mole fraction
x_i^B	Mole fraction of component i in nonsolvent bath

y_i Mole fraction of component i in gas phase

z Spatial coordinate

ΔH_i^v Heat of vaporization of component i

Greek

α Thermal diffusivity

γ_i Activity coefficient

γ_i^B Activity coefficient of component i in nonsolvent bath

δ Effective film thickness

ε Emissivity of the polymer solution

μ_i^j Chemical potential of component i in phase j

$\Delta\mu_i$ Change in chemical potential with respect to a reference state

ξ Growth exponent of droplet

ξ_{ij} Friction coefficient between components i and j

ρ Overall solution density

ρ_i Density of component i in solution

ρ_i°	Density of pure component i
σ	Stefan-Boltzmann constant
ϕ_i	Volume fraction of component i
ω_i	Mass fraction of component i
ω_i^B	Mass fraction of component i in nonsolvent bath
ω_i°	Initial mass fraction of component i
$\omega_i^{B^\circ}$	Initial mass fraction of component i in nonsolvent bath

Subscripts

sub	Substrate properties
-------	----------------------

Superscripts

B	Nonsolvent bath
G	Gas phase

CHAPTER I

GENERAL INTRODUCTION

1.1 Polymeric Membrane Industry

Environmental degradation is now a world-wide concern. In particular, demands for more efficient production processes that are less hazardous to the environment have spurred the development of new technologies. The rapid growth of membrane technology, which is projected to have a US \$8 billion global membrane equipment market by 2007 [1], is not a surprising evolution but a rational development in view of these new demands. Owing to decreasing supplies of fresh water, membrane application to desalination for potable drinking water is a growing market; moreover, the equipment demands for this application alone are projected to be US \$1.8 billion by 2007 [1]. Membrane technology also is used for new applications in the chemical, food, pharmaceutical, biotechnology and other industries. The US and Canadian membrane bioreactor markets totaled US \$32.2 million in 2003 and are projected to reach US \$89 million by 2010 [2].

Over the past four decades, synthetic polymers have provided an inexpensive and effective material for most commercial membranes. Because of their good performance at high temperatures and in corrosive environments, inorganic membranes are drawing increased attention of many researchers. However, the majority of membranes are still made from polymeric materials owing to their low cost and ability to be mass-produced. The efficiency and performance of polymeric membranes under harsh operating

conditions also has been considerably improved by the development of new polymeric materials and modification techniques. Interestingly, the demand for membrane materials is forecasted to grow by 7.1% per year and to reach US \$2.1 billion by 2006, of which 94.1% will involve polymeric membranes [3].

Polymeric membranes may be considered as barriers that can selectively allow the passage of certain species depending on their chemical and/or mechanical properties, while greatly restricting the passage of others. The pioneering work of Loeb and Sourirajan [4] has permitted the development of highly selective asymmetric polymeric membranes while maintaining substantially higher fluxes. This breakthrough led to rapid commercialization of the process and development of the associated membrane technology as an attractive alternative to conventional, energy-intensive and environmentally unfriendly separation processes. Due to recent advances in research, membrane processes are being extended to various new applications.

Development of an efficient membrane process is key to a successful industrial application. It is not surprising that there are extensive studies to achieve optimization of both the membrane and the operating conditions for the membrane process. The selectivity and flux achieved with a polymeric membrane strongly depend on its morphology, such as the size and distribution of pores, asymmetric/symmetric structure and presence of skin. Various needs demand that the membrane be optimized for each specific application. However, membrane fabrication recipes are still perfected based on a trial-and-error scheme via extensive experimentations.

1.2 Polymeric Membrane Formation

Polymeric membranes are generally classified based on their two distinct types of morphologies: asymmetric and symmetric membranes. Asymmetric membranes have a sharp gradient in pore density. A dense skin (10-200 nm) on top of a thicker porous support layer (100 μm) is believed to be responsible for the perm-selective properties. For this reason asymmetric membranes are sometimes referred to as integrally-skinned membranes. The thicker porous support can sometimes contain macrovoids, i.e., abnormally large pores. Figure 1.1 shows an asymmetric membrane having macrovoids. In contrast, a symmetric membrane displays a homogeneous structure. The type of morphology displayed by a membrane strongly depends on the casting conditions during its fabrication.

Several fundamentally different techniques can be employed to fabricate polymeric membranes for a given membrane material. Among these, phase inversion is the most common and versatile route for manufacturing synthetic polymeric membranes. According to Kesting, phase inversion refers to a "... process by which a polymer solution (in which the solvent is the continuous phase) inverts into a swollen three-dimensional macromolecular network or gel (where the polymer is the continuous phase)" [5]. A schematic representation of this phase inversion process is shown in Figure 1.2. For a particular polymer, a system of suitable solvent(s) and nonsolvent(s) are chosen so that they form a homogenous polymer solution, *a* in Figure 1.2. Once the homogenous solution is cast into the desired shape, subsequent mass and/or heat transfer and close proximity make the polymer molecules interact and physically be entangled to form agglomerates, *b*. Further interaction makes them form a continuous matrix

throughout the solution, c , which is commonly referred to as “gelation”. As the polymer solution becomes thermodynamically metastable or unstable, the system lowers its free energy by converting into a two-phase solution. Often both resultant phases are liquid, in which case the process is referred to as liquid-liquid demixing, although solid-liquid demixing is also possible. In this phase-separated system, d , one phase has higher concentration of polymer (polymer-rich phase) than the other (polymer-lean phase). This is the ‘phase inversion’ step described by Kesting. The polymer-rich phase eventually undergoes an additional solid-liquid phase transition through gelation, vitrification or crystallization thereby forming the structural matrix of the membrane. The polymer-lean phase, containing mainly solvent(s) and/or non-solvent(s), ultimately gives rise to the porous substructure of the membrane. Often a dense region, e , or “skin” may also form at the polymer solution/fluid interface. This thermodynamic instability can be induced by nonsolvent/solvent exchange (wet-casting process), cooling (thermal-casting process) or solvent evaporation (dry-casting process). The principal focus of this thesis is the development of mathematical models for both the dry- and wet-casting processes for the formation of polymeric membrane.

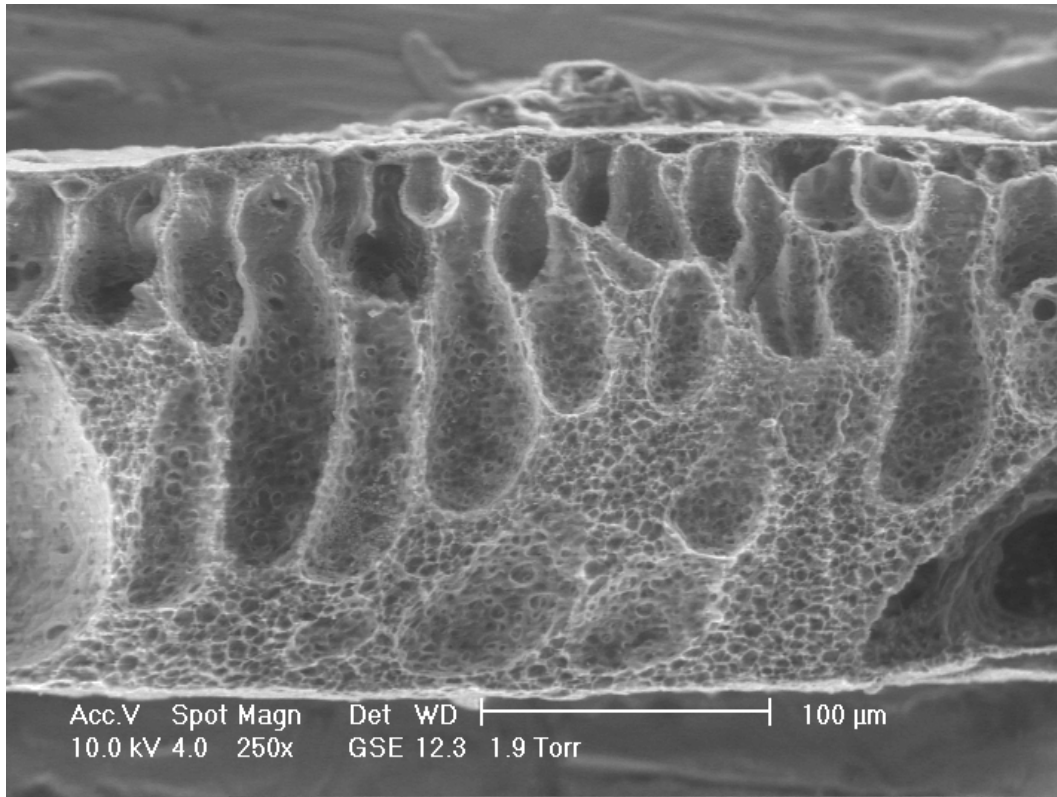


Figure 1.1: Scanning electron micrograph showing a cross-sectional view of an asymmetric cellulose acetate membrane having macrovoids. The thickness of the membrane is about 200 μm .

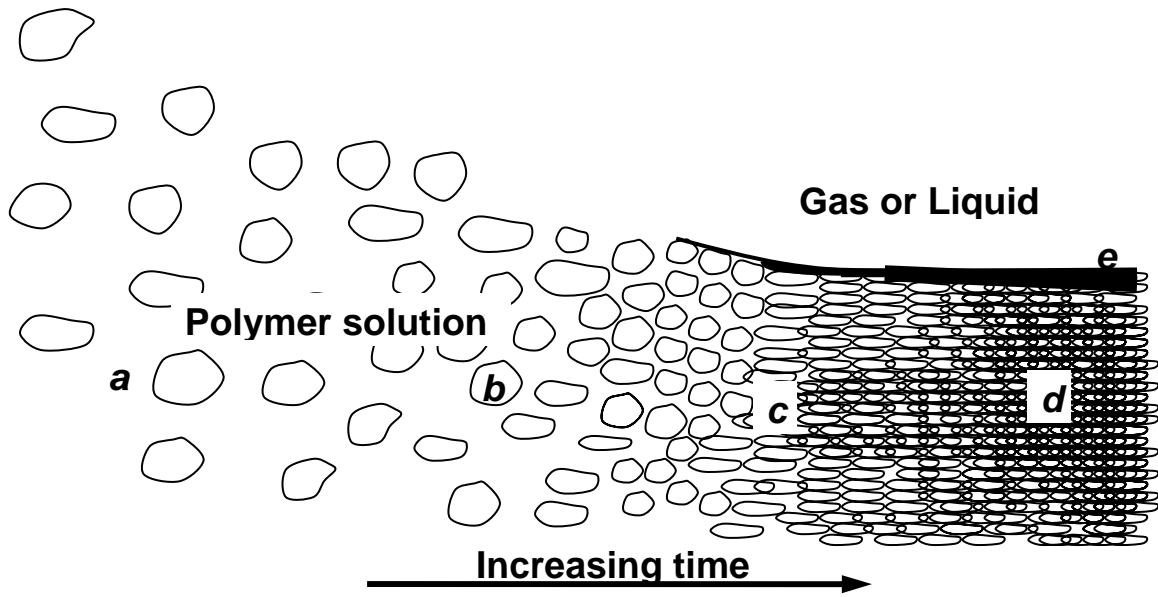


Figure 1.2: Schematic representation of the phase-inversion process. a: homogenous polymer solution, b: agglomerate, c: gelation, d: phase-separation and e: skin.

1.3 Research Challenges

The optimization of a membrane process requires a membrane chosen and perhaps modified for the specific needs of the application. The functional behavior of polymeric membranes is intimately tied to the membrane morphology. A slight change in the fabrication recipe for a membrane can greatly influence the final membrane morphology. Indeed, reproducible uniform membrane morphology can hardly be produced without an extremely carefully controlled membrane fabrication process.

In order to achieve the desired final membrane morphology for some specific need, extensive trial-and-error experimentation is still required. This procedure demands tremendous time and effort. An attractive alternative is to use mathematical models to reduce the cost and make it easier to develop improved membrane fabrication recipes. Having a rigorous mathematical model is also beneficial to study and control various phenomena that are not well understood, such as the macrovoid formation. Macrovoids are usually observed in polymeric membranes fabricated via the wet-cast process. The real-time measurement of relevant variables in the wet-cast process is very hard to achieve due to its very fast mass transfer. The ongoing controversy regarding the macrovoid formation mechanism is due to a lack of relevant experimental data and a rigorous mathematical model [5].

Although extensive modeling studies have been done for both the wet-cast and dry-cast processes, all models developed heretofore allow for mass transfer only by diffusion. None of models in the current literature include all the mechanisms that can affect the membrane morphology. A proper model for membrane casting should incorporate both the diffusive and convective contributions to the mass transfer flux.

However, it is hard to find a model in the literature that deals with both diffusion and convection in a mass transfer problem. In most of cases, either diffusion or convection is assumed to have a dominant contribution *a priori* and the other is neglected. Therefore, a fundamental study of diffusion and convection should be done to develop a rigorous model for dry and wet-cast processes.

1.4 Focus of This Research

A general procedure for addressing a mass transfer problem without assuming a dominant transport contribution (either diffusion or convection) is essential for developing a rigorous mass transfer model. This procedure provides a tool for studying any mass transfer process, including membrane casting. Developing this procedure for assessing the importance of convective mass transfer and properly incorporating it into a mass transfer model constitutes one of the major foci of this thesis

In view of the need for mathematical models for membrane formation, the main focus of this thesis is to develop an improved model for the dry and wet-cast polymeric membrane formation processes. Although the mass transfer in both processes is similar, substantial latent-heat effects must be considered in modeling the dry-cast process. The dry-cast process is the oldest phase inversion method for fabricating polymeric membranes and is seldom used alone in modern industry due to environmental concerns related to containing the evaporating solvent. However, a study of dry-casting is still important because an evaporation step is often used as a precursor in other phase-inversion processes. Moreover, it is much easier to obtain real-time data for the dry-cast process in order to validate a mathematical model; that is, experimental

validation of a dry-cast model provides some assurance that the fundamental modeling approach can be used in constructing a wet-cast model for which it is far more difficult to obtain real-time data.

A complicating factor in validating a wet-cast model is that the mass transfer in batch-scale laboratory experiments is generally multidimensional owing to buoyancy-induced free convection in the precipitation bath. Interestingly, commercial scale membrane casting usually involves one-dimensional mass transfer since the bath phase involves forced convection created by continuously drawing the supported casting solution through the precipitation bath. Hence, there is a need to conduct carefully controlled laboratory scale-experiments for which buoyancy-induced convection is eliminated. This can be done by casting membranes in a low gravity environment, which can be achieved via NASA's aircraft flight program. Hence, another focus of this thesis is to carry out membrane casting experiments on the laboratory scale for which spurious free convection mass transfer is eliminated by conducting these studies under low gravity conditions.

A mathematical model can assist in understanding complex phenomena such as macrovoid pore formation. In particular, it can be used to test various hypotheses that have been advanced for macrovoid formation. Prior studies of macrovoid formation have been complicated owing to multi-dimensional mass transfer associated with free convection in the precipitation bath. Hence, another focus of this thesis is to carry out experimental studies of macrovoid formation under conditions for which free convection has been eliminated by utilizing an effective low gravity environment. The mathematical model developed in this research will be applied to predict the conditions that prevail

when macrovoids are observed to form. These studies will provide fundamental insight that will permit discriminating between the various hypotheses advanced for macrovoid formation.

The aforementioned goals then lead to the following objectives for this thesis research:

- To develop a general well-defined formalism for incorporating both diffusion and convection in describing membrane casting and other related mass-transfer processes
- To develop a fully-predictive, non-isothermal transport model for the dry-cast membrane formation process that incorporates both diffusion and convection
- To validate quantitatively the dry-cast model with experimental data in the literature
- To develop a fully-predictive transport model for the wet-cast membrane formation process that incorporates both diffusion and convection
- To utilize the wet cast model to investigate the macrovoid formation mechanism
- To construct a membrane casting apparatus that will permit fabricating polymeric membranes under low gravity conditions in order to ensure one-dimensional mass-transfer during the wet-cast process
- To utilize the low gravity environment to elucidate the conditions required for macrovoid formation

1.5 Organization of Thesis

This thesis involves four independent unique subjects: convective transport (Chapter 2); development of a dry-casting model incorporating convective transport (Chapter 3); development of a wet-casting model incorporating convective transport (Chapter 4); and macrovoid formation (Chapter 5). Although these four subjects are interrelated, each involves a unique body of prior literature. Hence, the development in each of these chapters is complete in that it includes a review of prior studies and a detailed development and discussion of the contributions of this thesis to the subject.

In Chapter 2, a generalized approach for developing a comprehensive mass-transfer model that incorporates both diffusion and convection will be given. This generalized approach will be illustrated using several simple examples. This generalized approach developed in Chapter 2 is applicable to any process involving mass transfer. In Chapter 3 this approach is applied to develop a model for the dry-cast process for polymeric membrane formation. The model developed is also validated in Chapter 3 using extensive real-time data available in the literature. This validation provides some confidence that the same formalism can be applied to develop a model for the wet-cast process for polymeric membrane formation that is discussed in Chapter 4. Chapter 5 discusses the macrovoid formation - a problem endemic to the wet-casting process. In particular, the wet-casting model is applied to predict the conditions present when macrovoids are detected. This chapter also describes the experimental program in which a low-gravity environment is used to suppress buoyancy-induced free convection in order to insure one-dimensional mass transfer. This chapter describes the results of these experiments that provide fundamental insight into the conditions required for macrovoid

pore formation. Chapter 6 then summarizes the conclusions and recommendations emanating from this research.

CHAPTER II

CONVECTIVE TRANSPORT

2.1 Scope of Chapter

The general approach to construct a well-defined mass-transfer problem is developed in this chapter. Both diffusive and convective contributions to the mass flux should be incorporated in any mass-transfer model including dry- and wet-cast process models. The equation-of-continuity is of particular importance in developing a mathematical expression for the convective flux. Also it should be noted that a mathematical model is useful only when its solution is tractable. A major difficulty in dealing with the species-balance equations in conjunction with the equation-of-continuity is that there is still no numerical method to solve such nonlinear coupled hyperbolic and parabolic partial differential equations. Therefore, a judicious manipulation of the equations will be shown to avoid this difficulty. The validity of the general approach will be shown by the comparison between results from the proposed approach in this thesis and misleading results obtained by simplifications often used in the literature. Furthermore, the relationship between the fundamental mass-flux formalism of diffusion-convection and the total flux formalism in non-equilibrium thermodynamics will be established. The approach using non-equilibrium thermodynamics is very convenient to describe coupling effects of fluxes as well as to consider multiple driving forces (e.g., concentration gradient, pressure gradient, temperature gradient). In particular, coupling

effects should be considered in the development of dry-casting model and wet-casting model involving multicomponent mass-transfer.

This chapter is organized in the following manner. First, an introduction to the mass-transfer problem is presented. Then, a review of prior works and the motivation for this study are presented. The multicomponent convection-diffusion mass-transfer problem and the generalized flux equation from non-equilibrium thermodynamics will follow to show how to handle well-defined mass-transfer problems and their interrelationship. Sample problems for each approach are presented. Finally, a summary of this chapter is given.

2.2 Introduction

Modeling is the procedure for obtaining mathematical expressions and their solutions with variables that symbolize the nature of a given problem. A useful mathematical model has a good description of the nature of the problem and a well-defined set of equations. The mathematical terminology of a “well-defined problem”, sometimes referred to as “well-posed problem”, originates from the definition that appears in the paper of Hadamard [6]. According to his definition, mathematical models composed of a well-defined problem should have a unique solution that depends continuously on the data [7]. In order to obtain a solution from a set of equations, it is necessary to specify as many independent equations as there are dependent variables. An equation is independent when no equation is redundant; that is, no equation can be derived from the other equations. Checking the number and dependency of equations and variables is an important step to verify if the problem is well-defined.

The use of mathematical models is central to a quantitative description of transport processes. These models constitute (usually partial) differential equations and their associated conditions (initial, boundary and auxiliary) and are developed through the use of the fundamental physical principles of conservation of mass and energy (and also momentum). In recent times, this idea has been extended to develop a generalized conservation equation for any physical entity, which may then be used for describing mass and heat transfer [8, 9]. The obvious similarities in describing the differential equations for various transport processes have long been recognized and used to develop suitable analogies between them, whereby, the results of one can be successfully used to predict the other [10, 11]. However, such analyses can only be successfully implemented for purely 'diffusive' or 'conductive' processes, that explicitly preclude the possibility of bulk motion of materials within the system [12, 13]. Although the use of such analogies is quite popular, they often lead to approximate or an oversimplified representation of physical processes, especially when dealing with mass transfer. Mass transfer is unique and different from other transport processes such as heat transfer or fluid mechanics in several aspects. This difference is most prominent for multicomponent systems, whereby each species has its own identity and contribution. For such systems, the velocity of each species will be different from the other, resulting in a non-zero mass-average velocity, thereby leading to a non-zero bulk mass-transport component or convection. This bulk mass-transport component will be present even if there is no explicit fluid flow in the system owing to a pressure drop and similar external driving forces.

Although the bulk mass-transport term, represented by the mass-average velocity, is critical for several practical chemical engineering problems involving mass transport in

multicomponent systems, a lack of knowledge of the individual species velocity or mass-average velocity often forces researchers to either completely neglect it or make simplified assumptions. One of the most popular ways to neglect convection for binary systems is by considering the net flux of one species to be equal in magnitude and opposite in direction to the other [8, 12]. This is commonly referred to as ‘equimolar (or equimass) counter-diffusion’ and forces the mass-average velocity to be identically zero. This assumption is very limiting for systems for which all the species move in the same direction, for instance, evaporative casting (or dry-casting) of dense films and polymer membranes, evaporation of liquid mixtures etc. Convective mass transport can also be neglected through the ‘dilute solution approximation’, whereby all the species in a mixture are assumed to be dilute, which is an impossible supposition. Another popular and widely used means of approximating the convective mass flux is by considering one or more components in a multicomponent system to be ‘stationary’ i.e., not directly participating in mass transfer or movement [8, 12]. Bulk mass transport can also be approximated by assuming the (mass or molar) density of a multicomponent solution to be constant and independent of the system composition. It is surprising that even though sophisticated models have been proposed that depict variation of solution density with pressure and temperature (assuming the system to be either compressible [14, 15] or incompressible [16-18]), there is practically no definitive study that considers the local density as a function of local composition. Moreover, even though the above assumptions and approximations enable us to devise tractable analytical or numerical solutions to mass-transport problems, they represent a highly specialized situation. An effort to apply such results to a generalized system can seriously jeopardize the quality of the model’s

predictive power and will eventually lead to a poor correlation with experimental or analytical results.

2.3 Review of Prior Studies

2.3.1 Diffusion

Historically, Fick's 1st Law of Diffusion was proposed by Adolf Fick via a loose analogy to Fourier's Law of Heat Conduction as has been discussed in [19]:

$$J_i = -D\nabla c_i \quad (2.1)$$

However, in interpreting Fick's suggestion for formulating a diffusive relationship, various researchers have assumed different relationships. Although, most of the literature employs Fick's law as given in Equation (2.1), some of the literature [8,13,20,22 and 24] use a slightly different form:

$$J_i = -cD\nabla x_i \quad (2.2)$$

Although the two forms are identical for systems having constant molar density, there is a slight difference for systems having variable densities. Sherwood et al. [24] claimed that the form in Equation (2.2) is more generalized, based on a rigorous derivation from kinetic theory as shown by Hirschfelder et al.[21]. Similar claims have been made by Welty et al. [22] who consider the form in Equation (2.2), based on the proposition of de Groot [23] that Equation (2.1) is the constant-density form for Equation (2.2). However, a careful analysis of the original derivation in [22] that serves as the foundation for Equation (2.2) reveals that it is valid only for ideal light gases. It cannot be directly used for dense or real gases, liquids, and solids, thereby making it highly specialized.

Furthermore, if one chooses to use Equation (2.2), then the values of diffusivity should also be a theoretical expression based on kinetic theory, thereby further limiting the accuracy of the expression. The most reliable sources of diffusivity values are experimental data and studies that result in predictive correlations. Almost all published values of diffusivities are based on the use of Equation (2.1) to interpret experimental data [24], which is nearly always the accepted form. Hence, for this study, the former expression as given in Equation (2.1) shall be employed to describe Fickian diffusion. In terms of mass units, Fick's First Law is written as:

$$j_i = -D_{AB} \nabla \rho_i \quad (2.3)$$

2.3.2 Convection

There are few studies on convective mass transport in literature. However, there are several numerical approaches to deal with convection-diffusion problem in momentum transfer. The compressibility of the fluid is considered in these studies. Matsumura et al. [16] and Feireisl et al. [17] considered the compressibility of the fluid as a function of temperature and pressure in their momentum-transfer model. These are more realistic models than the incompressible fluid models of Qui et al. [15] and Driessen et al. [14] since compression or expansion of the fluid will affect the bulk fluid velocity and, thereby, convective velocity. However, compressibility effects that depend on the concentration of each species in the fluid mixture are not considered in any of the above models.

Bardow et al. [25] attempted to advance the description of mass-transfer processes by considering a 'well-defined convection-diffusion mass-transfer problem' with an

impermeable wall at one side. Based on a mathematical tool proposed by Unger et al. [26], the authors suggested an expression for the mass-average velocity, assuming that it had a 'lower index' than the diffusive term in the species-balance equation. Although their approach is novel and considerably closer to accurately describing realistic mass-transfer processes, it is limited due to a key assumption that one of the system boundaries is impermeable.

2.4 Motivation for This Study

Although Bardow et al. [25] constructed a "well-defined convection-diffusion mass-transfer problem", their approach is not general in that the numerical implementation involved assuming a lower index for the convective term. This approach needs intense iterative calculation. Moreover, there is no guarantee that the index of the convective term in the partial differential equation is always lower than that of the diffusive term. Thereby, the goal of this study is to describe practical mass-transfer problems through the development of well-posed generalized mass-transport equations with a detailed in-depth analysis of the significance and importance of the bulk mass-transport term.

In addition, it should be noted that non-equilibrium thermodynamics treats the total flux as a combination of each individual driving force and its phenomenological constants, while the driving force, in its classic definition of diffusion and convection, is limited to concentration gradients. This implies that the mass-transfer equation can be generalized further for any kind of driving force.

2.5 Multi-component Convection-Diffusion Mass-Transfer Problem

2.5.1 Mass Balance for Individual Fluxes

For one-dimensional mass transfer involving N species, the conservation-of-species equation can be written as:

$$\frac{\partial \rho_i}{\partial t} = -\frac{\partial n_i}{\partial z} \quad \text{for } i = 1, 2, \dots, N \quad (2.4)$$

where ρ_i is the mass concentration of species i , t and z are the time and spatial coordinates, respectively, and n_i is the total mass flux of species i . The total species flux, in turn, can be spilt into its constituent terms, diffusive and bulk flow, as formulated in [12]

$$n_i = j_i + \rho_i W \quad (2.5)$$

where j_i is the diffusive flux of species i and W is the mass-average velocity, representing the bulk or ‘convective’ contribution. It should be noted that the words ‘bulk’ and ‘convective’ have been used interchangeably in this study, with particular reference to mass transport. This similarity in terminology might have its roots in the historical analogy drawn between mass and heat transfer. In heat transfer, convection means flows resulting from the presence of external forces and gradients in the system such as body forces (free convection due to gravity) or pressure gradients (forced convection). In the presence of such external forces, there will be appreciable bulk mass transfer. However, even in the absence of such external forces, there can be bulk motion of matter within a system, due to the development of density gradients owing to either swelling or densification. Thus, there is a need for a clear demarcation between bulk motion of material owing to external forces and those owing to purely density gradients

developed in mixtures. However, such a demarcation has not been explicitly done anywhere in the literature, and hence, for the purposes of this study, the latter *i.e.* bulk motion due to density gradients has been also referred to as ‘convective flow’. In any case, using the definition of species mass flux given in Equation (2.5), the conservation-of-species equation can be rewritten as:

$$\rho \left(\frac{\partial \omega_i}{\partial t} + W \frac{\partial \omega_i}{\partial z} \right) = - \frac{\partial j_i}{\partial z} \quad (2.6)$$

where ρ is solution mass density, and ω_i is the mass fraction of species i . Since the mass fractions of the individual species add to one, for a system containing N components, one needs to solve $N - 1$ conservation-of-species equations and an overall mass balance. In order to solve these equations, one needs to obtain appropriate expressions for the unknowns in these equations in terms of known or measurable quantities. The unknown variables in the species equations are the diffusive fluxes, the total solution density and the mass-average velocity. As already described earlier, the total solution density can be expressed through a suitable equation-of-state. The mass-average velocity can be calculated by solving the continuity equation coupled with the conservation-of-species equation. The former can be written as:

$$\frac{\partial \rho}{\partial t} = - \frac{\partial}{\partial z} (\rho W) \quad (2.7)$$

It should be noted that the above continuity equation is a hyperbolic partial differentiation equation (PDE), while the one-dimensional conservation-of-species equation is a (linear or nonlinear) parabolic PDE., Solving coupled hyperbolic PDEs and parabolic PDEs for complex situations such as moving boundary problems is not possible as yet even with the most sophisticated available numerical routines. In such situations, the only options

are to express the mass-average velocity as an explicit algebraic expression or to completely neglect or approximate it by means as already mentioned above.

2.5.2 Equation-of-State

For an isothermal and isobaric situation, the overall mass density (henceforth referred to as ‘density’) of the system can be related to its composition and the pure component densities through an appropriate equation-of-state.

$$\rho = F(\omega_i, \rho_i^0) \quad \text{for } i=1,2,\dots,N \quad (2.8)$$

where ρ_i^0 is the pure component density for species i . The function F depends on the system. Volume-of-mixing effects should be considered to formulate the function F . One of the simplest forms for the function F can be obtained for a system having no volume-of-mixing effects as:

$$\frac{1}{\rho} = \sum_{i=1}^N \frac{\omega_i}{\rho_i^0} \quad (2.9)$$

2.5.3 Mass-Average Velocity

The mass-average velocity is defined as

$$W = \frac{\sum_{j=1}^N \rho_j v_j}{\sum_{j=1}^N \rho_j} \quad (2.10)$$

where v_i is the velocity of the individual species [12]. From this equation, it is clear that the mass-average velocity is a variable that changes with time and the spatial coordinate in accordance with changes in solution density and species velocity.

Once the equation-of-state for the density is available, it can be used in conjunction with the equation-of-continuity to obtain an expression for the mass-average velocity. This can be done by differentiating both sides of Equation (2.8) with respect to time and the spatial coordinate

$$\frac{\partial \rho}{\partial t} = \sum_{i=1}^N f(\rho_i^0, \rho) \frac{\partial \omega_i}{\partial t} \quad \text{for } i=1,2,\dots,N \quad (2.11)$$

$$\frac{\partial \rho}{\partial z} = \sum_{i=1}^N f(\rho_i^0, \rho) \frac{\partial \omega_i}{\partial z} \quad \text{for } i=1,2,\dots,N \quad (2.12)$$

where $f(\rho_i^0, \rho)$ is a function of the total and pure component densities. Combination of equations (2.6), (2.7), (2.11) and (2.12) yields

$$\frac{\partial W}{\partial z} = -\frac{1}{\rho} \sum_{i=1}^N f(\rho_i^0, \rho) \left(\frac{\partial \omega_i}{\partial t} + W \frac{\partial \omega_i}{\partial z} \right) \quad (2.13)$$

Equation (2.13) can be expressed in terms of the diffusive flux as:

$$\frac{\partial W}{\partial z} = \frac{1}{\rho^2} \sum_{i=1}^N f(\rho_i^0, \rho) \frac{\partial j_i}{\partial z} \quad (2.14)$$

The above equation can be integrated with the appropriate boundary conditions to obtain an explicit expression for the mass-average velocity:

$$W = \int \frac{1}{\rho^2} \sum_{i=1}^N f(\rho_i^0, \rho) \frac{\partial j_i}{\partial z} + W_c(t) \quad (2.15)$$

where $W_c(t)$ is the integration constant, which may be a constant number or a function of time only. It can be evaluated from appropriate boundary conditions. For an open system, this boundary condition would constitute specifying a combination of mass transfer due to external forces (convection) and the intrinsic densification flow term at a boundary.

For a closed system, the appropriate boundary is the no-flux condition at the impermeable boundary.

2.5.4 Modified Peclet Number

In accordance with the analogy to heat transfer, the convective contribution to mass transfer has been primarily attributed to fluid-flow processes that, in turn, have been expressed in terms of the dimensionless Peclet number [12]. However, this conventional Peclet number is limited and is adequate only for systems where convective mass flux takes place due to the presence of external forces such as pressure gradients, etc. For specific mass-transfer situations, researchers have redefined the Peclet number to adequately describe the convective flow characteristics. For the most generalized mass-transfer situation where convective mass flux takes place due to the development of density gradients in the system, in absence of any external pressure or body forces, the appropriate terminology is the ‘modified Peclet number’, as introduced by Bhattacharya and Hwang [27]. It can be represented mathematically as:

$$Pe_i^M = \frac{LW}{D_{im}} \quad (2.16)$$

where L is the characteristic length of the system and D_{im} is the extrapolated binary diffusivity of species i in the mixture. In this definition of the Peclet number, the convective mass flux is parallel to the diffusive flux, as opposed to the conventional Peclet number for which it is perpendicular. This definition is convenient and realistic for unidirectional mass transfer, especially where the possibility of explicit fluid flow due to external gradients is precluded. For the limiting case when the modified Peclet number is low, the contribution of the convective flux to the total flux can be approximated to be

zero. This approximation is justifiable when either the characteristic length of the system or the mass-average velocity is sufficiently small or the diffusivities of the system are very high. This reflects the fact that for the aforementioned conditions the diffusive mass transfer outweighs densification flow by orders of magnitude. On the other hand, if the system is subjected to steep density gradients, the convective flux or mass-average velocity will be sufficiently high, thereby making the contribution of diffusive flux negligible with respect to convection. For all other intermediate situations, *i.e.* systems having a moderate modified Peclet number, neither the convective flux nor the diffusive flux can be neglected and both fluxes should be expressed in terms of determinable quantities and included in the describing equation(s). In the following section, an example problem will show the importance of convection via the modified Peclet number.

2.5.5 Example Study 1: Rapid Unsteady-State Evaporation

2.5.5.1 System of Interest

Let us consider a simple problem focused at determining the unsteady-state composition of a binary mixture containing liquids A and C, as is illustrated in Figure 2.1. Instead of having to make limiting assumptions on densification flow, as long as a suitable equation-of-state for the solution density is available for the system under consideration, the complete convective-diffusion model can be developed and solved. For the purposes of making the example realistic, let us assume that the components have different pure component densities. Moreover, we will assume that the thickness of liquid solution changes with time owing to evaporation. In order to simplify the model,

component C is assumed to be non-volatile, which would still make it a moving-boundary problem and thereby retain the essence of a realistic situation. Evaporation of liquid A into the gas phase is dependent on the variable concentration of A at the liquid-gas interface and is described through a constant mass-transfer coefficient (k_A^G) and a constant thermodynamic partition coefficient (α). Also the binary diffusivity in the liquid phase is assumed to be invariant with composition.

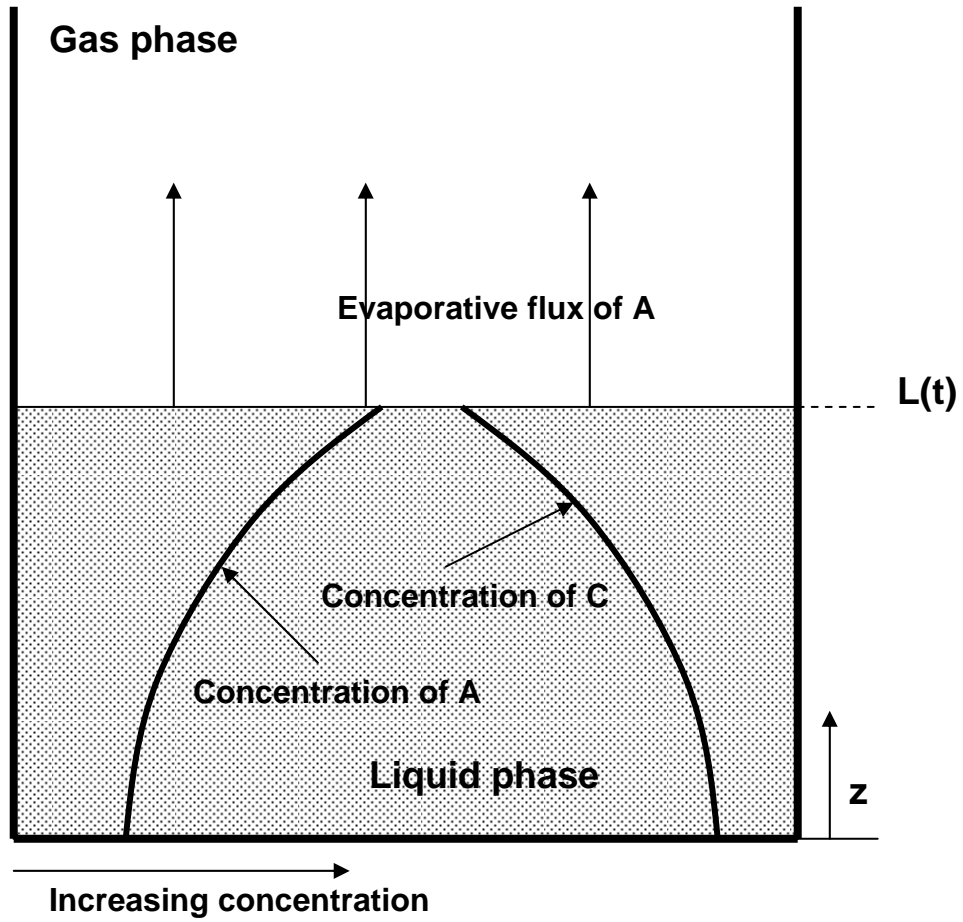


Figure 2.1: Schematic representation of evaporation from a binary liquid phase into a gas phase.

2.5.5.2 Derivation of Model Equations

The assumption of zero volume-of-mixing leads to the following equation-of-state for a binary system:

$$\frac{1}{\rho} = \frac{\omega_A}{\rho_A^\circ} + \frac{1-\omega_A}{\rho_C^\circ} \quad (2.17)$$

Using this equation-of-state, one can obtain an explicit algebraic expression for the mass-average velocity, subjected to a no-flux boundary condition at the bottom. Differentiating Equation (2.17) with respect to time results in the following:

$$\frac{\partial}{\partial t} \left(\frac{1}{\rho} \right) = \left(\frac{1}{\rho_A^\circ} - \frac{1}{\rho_C^\circ} \right) \frac{\partial \omega_A}{\partial t} \quad (2.18)$$

The derivatives of the reciprocal density and of the density are related by

$$\frac{\partial}{\partial t} \left(\frac{1}{\rho} \right) = -\frac{1}{\rho^2} \frac{\partial \rho}{\partial t} \quad (2.19)$$

Therefore, from Equations (2.18) and (2.19), the derivative of the density with respect to time is

$$\frac{\partial \rho}{\partial t} = -\rho^2 \left(\frac{1}{\rho_A^\circ} - \frac{1}{\rho_C^\circ} \right) \frac{\partial \omega_A}{\partial t} \quad (2.20)$$

The derivative of the density with respect to the spatial coordinate can be obtained by the same procedure.

$$\frac{\partial \rho}{\partial z} = -\rho^2 \left(\frac{1}{\rho_A^\circ} - \frac{1}{\rho_C^\circ} \right) \frac{\partial \omega_A}{\partial z} \quad (2.21)$$

The individual species-balance equation for one-dimensional mass transfer of species A is

$$\frac{\partial \rho_A}{\partial t} = -\frac{\partial n_A}{\partial z} \quad (2.22)$$

The flux of species A is

$$n_A = -D_{AC} \frac{\partial \rho_A}{\partial z} + \rho_A W \quad (2.23)$$

Combining Equations (2.22) and (2.23), and applying $\rho_A = \rho \omega_A$ yields the following equation.

$$\frac{\partial \omega_A}{\partial t} = \frac{1}{\rho} \frac{\partial}{\partial z} \left(\rho D_{AC} \frac{\partial \omega_A}{\partial z} + \omega_A D_{AC} \frac{\partial \rho}{\partial z} \right) - W \frac{\partial \omega_A}{\partial z} \quad (2.24)$$

Combining Equations (2.24) and (2.21) yields

$$\frac{\partial \omega_A}{\partial t} = \frac{1}{\rho} \frac{\partial}{\partial z} \left[\rho D_{AC} \left\{ 1 - \omega_A \rho \left(\frac{1}{\rho_A^\circ} - \frac{1}{\rho_C^\circ} \right) \right\} \frac{\partial \omega_A}{\partial z} \right] - W \frac{\partial \omega_A}{\partial z} \quad (2.25)$$

Equation (2.25) can be simplified using Equation (2.17), to give the following equation.

$$\frac{\partial \omega_A}{\partial t} = \frac{1}{\rho} \frac{\partial}{\partial z} \left[\frac{\rho^2}{\rho_C^\circ} D_{AC} \frac{\partial \omega_A}{\partial z} \right] - W \frac{\partial \omega_A}{\partial z} \quad (2.26)$$

Equation (2.26) allows one to eliminate the time-derivative term from the equation for the mass-average velocity. The equation for the mass-average velocity can be obtained from the equation-of-continuity, Equation (2.7). Substituting Equation (2.7) into Equations (2.20) and (2.21) yields

$$-\rho^2 \left(\frac{1}{\rho_A^\circ} - \frac{1}{\rho_C^\circ} \right) \frac{\partial \omega_A}{\partial t} = -\rho \frac{\partial W}{\partial z} + \rho^2 W \left(\frac{1}{\rho_A^\circ} - \frac{1}{\rho_C^\circ} \right) \frac{\partial \omega_A}{\partial z} \quad (2.27)$$

Substituting Equation (2.25) into Equation (2.27) and rearranging yields the following differential equation for the mass-average velocity.

$$\frac{\partial W}{\partial z} = \left(\frac{1}{\rho_A^\circ} - \frac{1}{\rho_C^\circ} \right) \frac{\partial}{\partial z} \left(\frac{\rho^2}{\rho_C^\circ} D_{AC} \frac{\partial \omega_A}{\partial z} \right) \quad (2.28)$$

Integration of this equation with a proper boundary condition provides an expression for mass-average velocity. Since the bottom of the liquid container is impermeable in this example, the mass-average velocity at $z=0$ is zero. Therefore, a closed-form equation for the mass-average velocity is

$$W = \left(\frac{\rho^2}{\rho_C^\circ} \right) \left(\frac{1}{\rho_A^\circ} - \frac{1}{\rho_C^\circ} \right) D_{AC} \frac{\partial \omega_A}{\partial z} \quad (2.29)$$

Thus, the describing mass-transfer equation for the binary liquid mixture is the conservation-of-species equation:

$$\frac{\partial \omega_A}{\partial t} = \frac{1}{\rho} \frac{\partial}{\partial z} \left[\frac{\rho^2}{\rho_C^\circ} D_{AC} \frac{\partial \omega_A}{\partial z} \right] - \left(\frac{\rho^2}{\rho_C^\circ} \right) \left(\frac{1}{\rho_A^\circ} - \frac{1}{\rho_C^\circ} \right) D_{AC} \left(\frac{\partial \omega_A}{\partial z} \right)^2 \quad (2.30)$$

The above is a nonlinear second-order partial differential equation requiring one initial and two boundary conditions for a particular solution. The initial condition is given by a known initial composition

$$\omega_A = \omega_A^I \quad \text{at } t = 0 \quad (2.31)$$

The impermeable bottom yields a zero-flux boundary condition at $z=0$ as

$$\frac{\partial \omega_A}{\partial z} = 0 \quad \text{at } z = 0 \quad (2.32)$$

The boundary conditions at the liquid solution/gas interface can be derived through a combination of the instantaneous integral mass balance for one of the species and a total mass balance and results in the following expression:

$$\left\{ 1 - \rho \omega_A \left(\frac{1}{\rho_A^\circ} - \frac{1}{\rho_C^\circ} \right) \right\} \rho D_{AC} \frac{\partial \omega_A}{\partial z} = -k_A^G \alpha \omega_A \Big|_{z=L(t)} - \rho_A \Big|_{L(t)} \frac{dL}{dt} \quad (2.33)$$

In order to complete the description, an auxiliary equation is required to locate the instantaneous position of the interface defined by $L(t)$. This is obtained from an integral total mass balance given by the following ordinary differential equation (ODE):

$$\rho \frac{dL}{dt} = -k_A^G \alpha \omega_A \Big|_{z=L(t)} + \rho^2 \left(\frac{1}{\rho_A^\circ} - \frac{1}{\rho_C^\circ} \right) D_{AC} \frac{\partial \omega_A}{\partial z} \Big|_{z=L(t)} \quad (2.34)$$

The above ODE requires an initial condition, which is given by the initial thickness of casting solution.

$$L = L^\circ \quad \text{at} \quad t = 0 \quad (2.35)$$

2.5.5.3 Solution Methodology

The model equations for the current example are solved using a commercially available partial differential equation solver, D03PPF, from National Algorithms Group, Inc. This solver uses finite difference methods to solve non-linear parabolic partial differential equations with coupled ordinary differential equations. The spatial location is normalized by the instantaneous thickness of casting solution to convert the problem from a moving to a fixed coordinate system.

The expression for the mass-average velocity expressed by Equation (2.29) for this problem indicates that the convective flow will be larger for greater differences in density between the two components. In order to examine this effect, three different cases have been considered, where the ratio of the pure component density of the evaporating species (A) to that of the non-evaporating component (C) has been taken to be 0.7, 0.9 and 1.0, respectively. The other physical parameters are kept constant during the process; their exact values are given in Table 2.1.

Table 2.1: Physical Parameters used in model calculations

Parameter	Value used in calculation
Binary Liquid Diffusivity, D_{AC}	$10^{-4} \text{ cm}^2/\text{sec}$
Mass-transfer Coefficient in the Gas Phase, k_A^G	$10^{-2} \text{ g}/(\text{cm}^2\text{sec})$
Thermodynamic Partition Coefficient, α	1.0
Initial Thickness of the Mixture, L_0	10^{-1} cm
Pure Component Density of A, ρ_A°	1.0 or 0.9 or 0.7
Pure Component Density of C, ρ_C°	1.0
Initial Composition, ω_A'	0.5

2.5.5.4 Results and Discussion

Figures 2.2–2.4 show the change in the concentration profile inside the binary liquid phase during the evaporation process. In these three figures the pure component density of species C was kept constant, whereas that of A was varied gradually increased to see the effect that the decreasing density gradients and the associated convective mass flux has on the mass-transfer characteristics of the system. It should be noted that both the shape of the concentration profile as well as the depth over which it occurs vary. This is due to the fact that the thickness of the binary liquid solution decreases with time, which is reflected in both the shape and extent of the concentration profiles. In order to represent rapid evaporation its rate has been kept high. The relatively higher evaporation rate as compared to the diffusion rate, results in a very steep concentration gradient at the liquid/gas interface. As time progresses, there is a decay in the concentration profile such that it eventually flattens out at the end of the evaporation process. The time required for complete evaporation of the lighter component in Figures 2.2, 2.3, and 2.4 is 221 s, 277 s and 298 s, respectively.

Figures 2.5 and 2.6 show the mass-average velocity profiles corresponding to the conditions for Figures 2.2 and 2.3. As expected, due to the steep concentration gradients at the liquid/gas interface, the mass-average velocity is a maximum at the interface, thereby resulting in steep gradients. It should be noted that the profile is much steeper and curved in Figure 2.5 than in Figure 2.6. This is because a lower pure component density of the lighter species in Figure 2.5 means that the mass-average velocity will be higher, as already dictated by equation 29. When both components have the same density, the mass-average velocity is identically zero at any location for all times during the process.

The solution of the coupled ODE in the model permits predicting the variation in liquid-layer thickness with time as shown in Figure 2.7. Since one of the components in the mixture is non-volatile, the final thickness of the solution is predetermined by the known initial composition. Hence, the solution thickness should asymptotically approach this known final value. However, if the model equations are approximate or incomplete, the material balance within the system of equations will not be satisfied. Hence, as a result the simulated thickness will asymptotically approach a value different from the known final value. The difference between these two values is an indication of the error incorporated into the system as a result of such approximations. In order to assess the implications and importance of this convective term, numerical solutions of the purely diffusive equations were also carried out. In this situation the convection term was purposely eliminated from the conservation-of-species equation and boundary conditions. The effect of ignoring the convective term is shown in Figure 2.7. The largest error is encountered for the lighter component density of 0.7 for the three cases studied. Note that the final thickness of the mixture should be 41.2% of the initial thickness based on the pure component densities and the initial composition of 0.5 assuming a zero volume-of-mixing. However, there is nearly an 11% error in the final simulated thickness as compared to the true value as a result of ignoring the convective flux. If the pure component densities of the two species are the same, then convection is ideally zero and the solution thickness predicted by both the convective and purely diffusive models approach the same true final value. This is also shown in Figure 2.7 and confirms that the numerical solutions of the model equations are accurate.

Figure 2.8 shows the variation of modified Peclet number with time for different density differences. It is clear from this figure that larger density differences correspond to increased modified Peclet numbers. Moreover, the value of this dimensionless group decreases with time and becomes zero at very long times. Most, importantly, for $\rho_A^\circ=0.7$, and evaporation times up to 42 seconds, the absolute value of Pe_A^M is greater than 1, thereby indicating that convective flow should not be neglected in such situations.

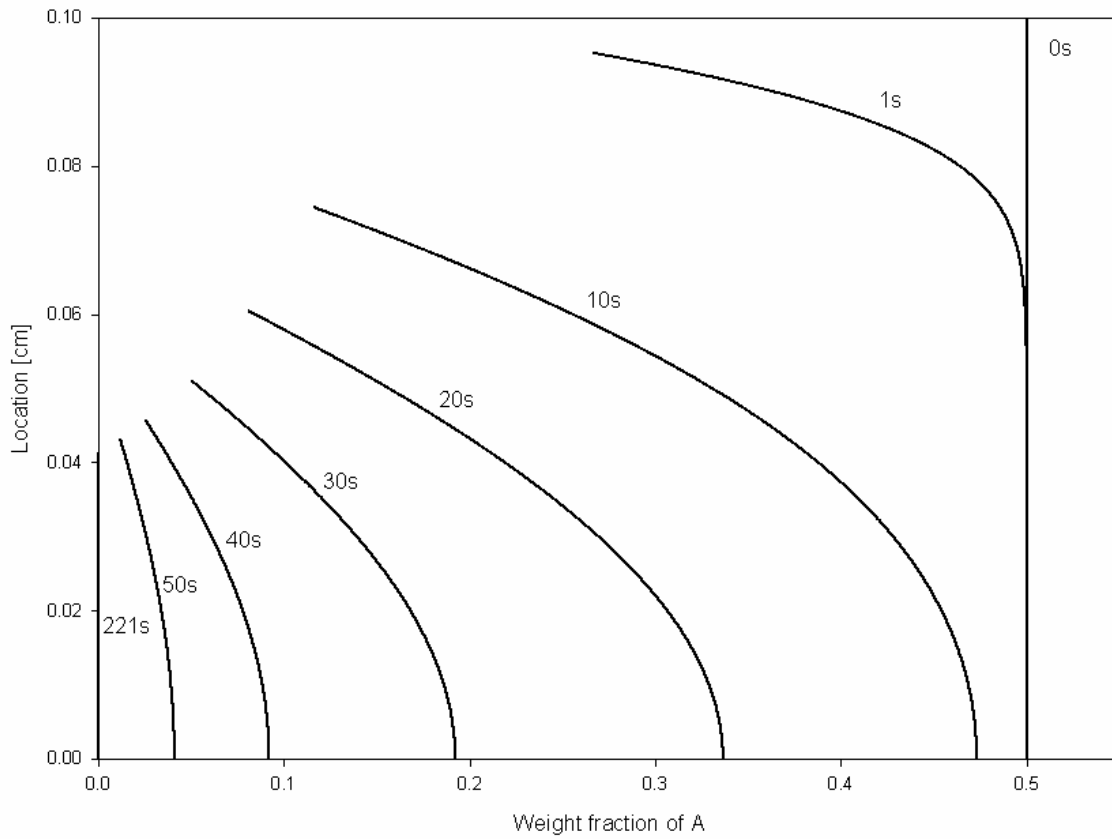


Figure 2.2: Change of weight fraction of volatile component A in a binary liquid mixture evaporating into a gas. Pure component densities of A and C are 0.7 and 1.0, respectively.

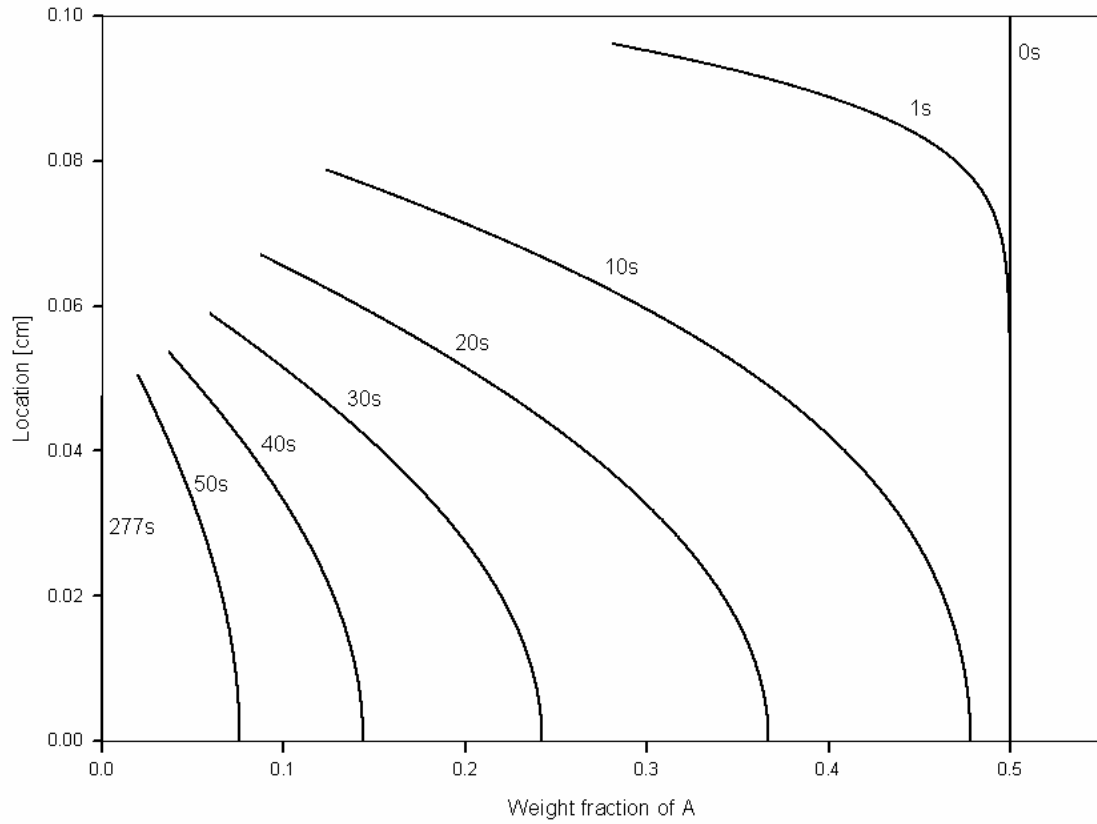


Figure 2.3: Change of weight fraction of volatile component A in a binary liquid mixture evaporating into a gas phase. Pure component densities of A and C are 0.9 and 1.0 respectively.

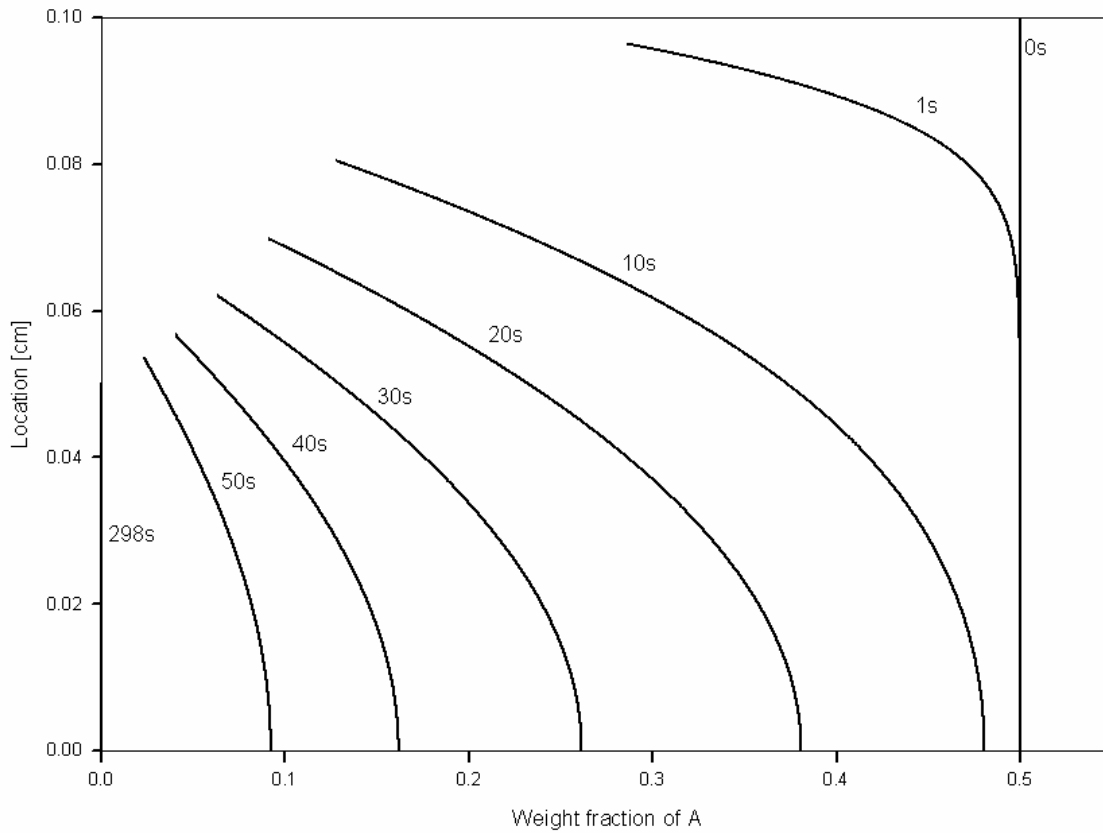


Figure 2.4: Change of weight fraction of volatile component A in a binary liquid mixture evaporating into a gas phase. Pure component densities of A and C are both 1.0.

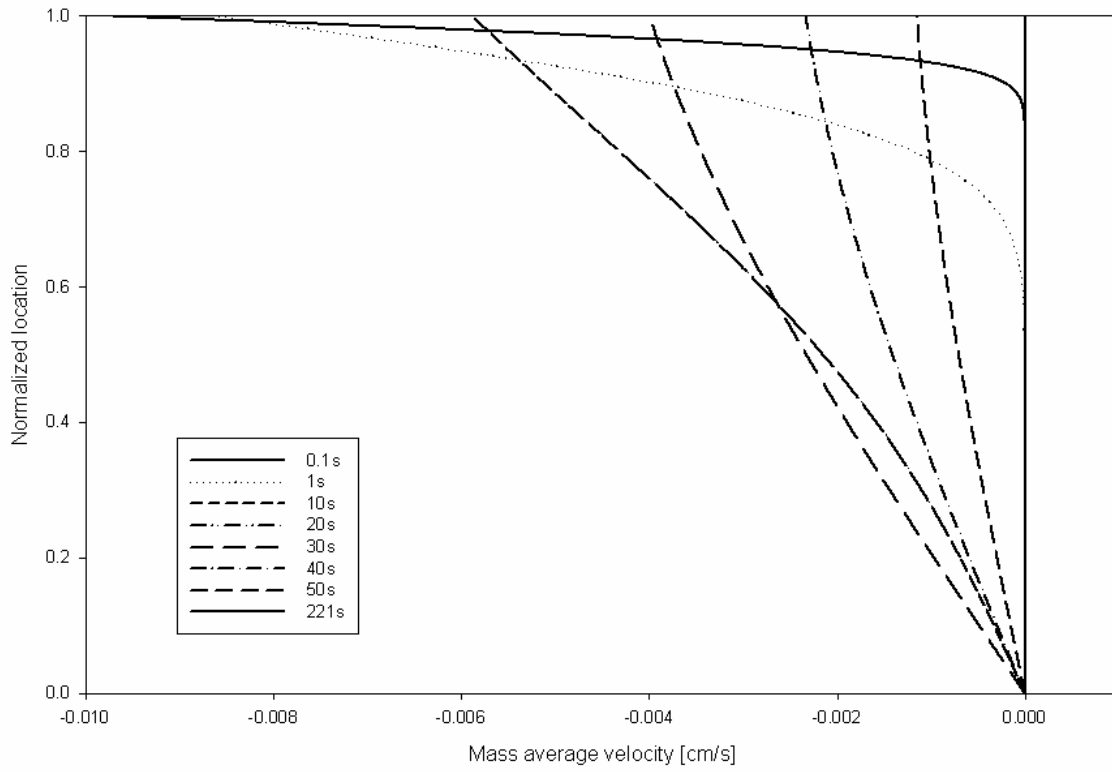


Figure 2.5: Change of mass-average velocity in a binary liquid mixture during evaporation of volatile component A into a gas phase. Pure species densities of A and C are 0.7 and 1.0 respectively.

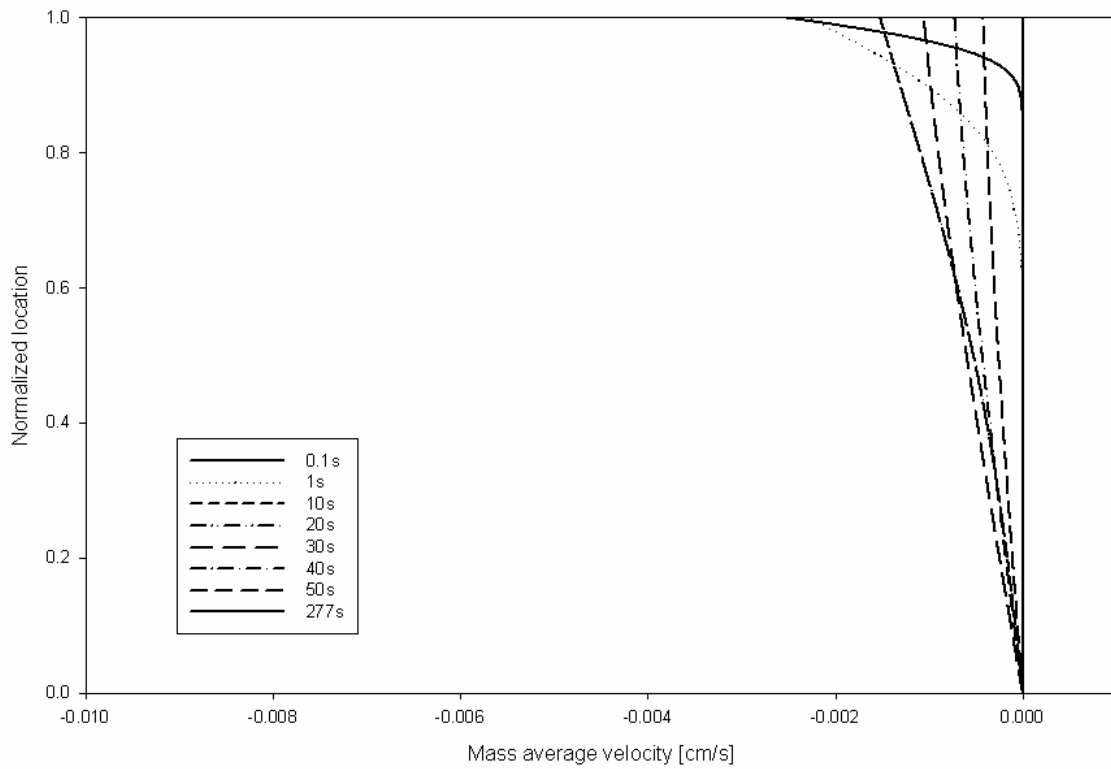


Figure 2.6: Change of mass-average velocity in a binary liquid mixture during evaporation of volatile component A into a gas phase. Pure component densities of A and C are 0.9 and 1.0 respectively.

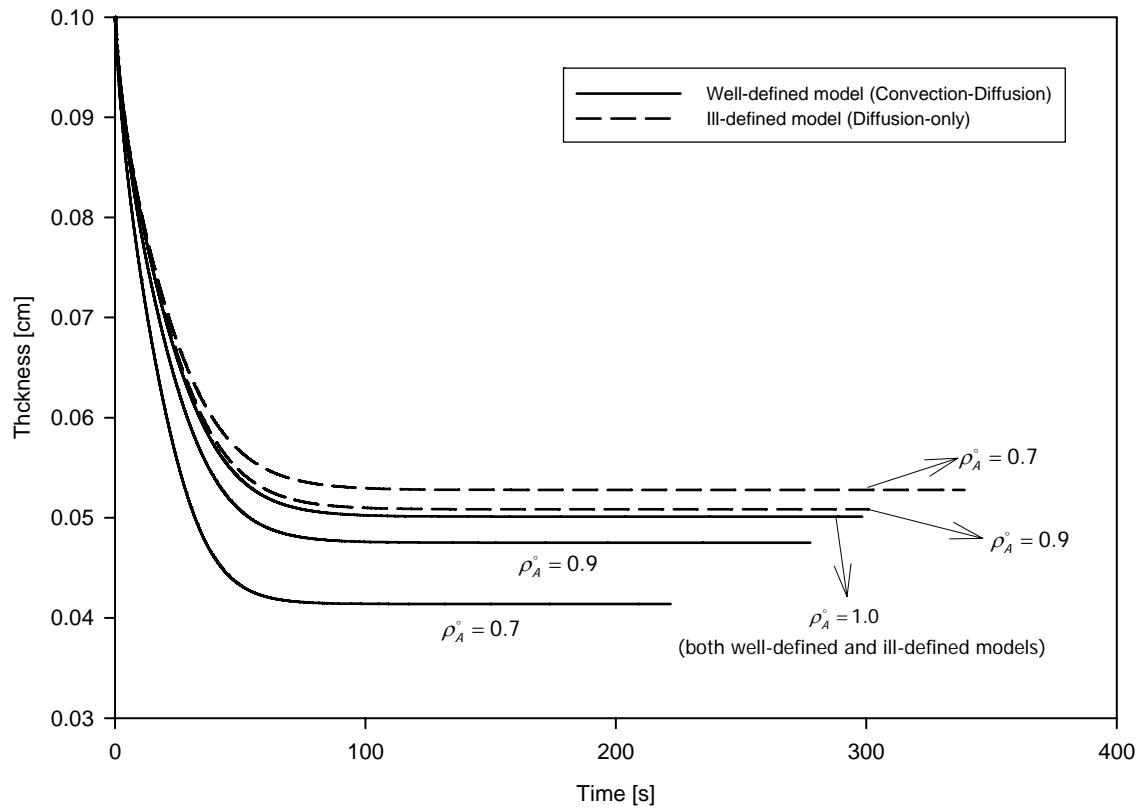


Figure 2.7: Thickness change of liquid phase during evaporation. Model predictions from well-defined convection-diffusion equations (solid line) and from ill-defined diffusion-only equations (dashed line) are presented for three different cases of density of A (0.7, 0.9 and 1.0).

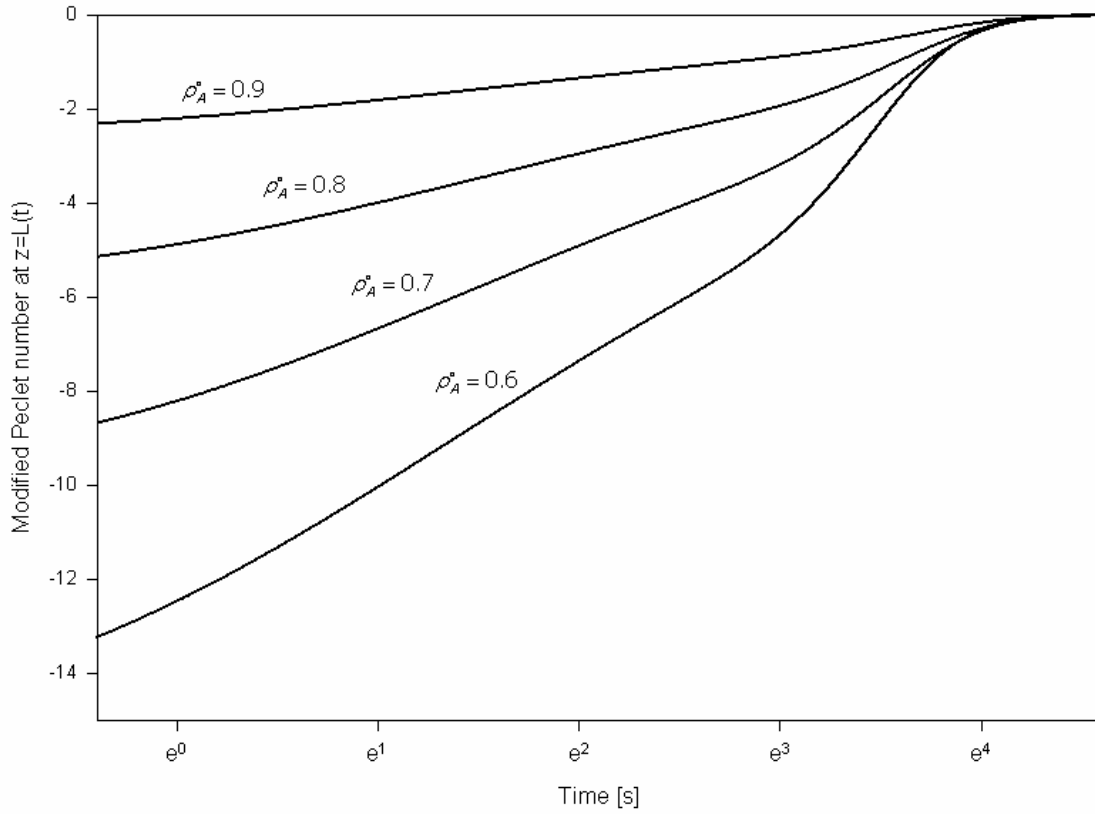


Figure 2.8: Change of the modified Peclet number of volatile component A at the liquid/gas interface in binary liquid phase during evaporation into gas phase for various cases of pure component density of A. Pure densities of C are same as 1.0 for all cases.

2.6 Generalized Flux Equation from Non-equilibrium Thermodynamics

2.6.1 Flux Equation

A generalized system of equations that describes a practical mass-transfer problem usually includes driving forces other than the concentration gradient. These driving forces can be included in mass-transfer analyses through the use of the fundamental principles of non-equilibrium thermodynamics. Linear non-equilibrium thermodynamics relates fluxes and driving forces (or simply ‘forces’) for a system by the following relationship [21]:

$$n_i = M_i \sum_{j=1}^N L_{ij} X_j \quad \text{for } i = 1, 2, \dots, N \quad (2.36)$$

The current formulation splits the total material flux into diffusive and convective contributions. The convective contribution has already been derived explicitly in the earlier section. For the diffusive contribution, instead of using a form of Fick’s law which is limited in its application, one needs to use a form that is suitable for ternary or higher systems and also incorporates all possible external forces or gradients that may be responsible for causing mass transfer. However, the basic formulation of non-equilibrium thermodynamics relates total flux to phenomenological coefficients and driving forces. Recently, Hwang has related the diffusive molar flux with the appropriate coefficients and driving forces [28]. For a mass-transfer system this can be done as follows. From the entropy balance equation for a one-dimensional transport, one can write

$$T\sigma = \sum_i N_i \frac{d\mu_i}{dz} = \sum_i n_i \frac{d}{dz} \left(\frac{\mu_i}{M_i} \right) \quad (2.37)$$

The species flux n_i can be expanded in terms of the usual diffusive and convective contributions and written as:

$$n_i = j_i + \omega_i n_T \quad (2.38)$$

where n_T is the total mass flux of all the species taken together. Substituting the expression for the total species flux given by Equation (2.37) into Equation (2.38), one obtains:

$$T\sigma = \sum_i j_i \frac{d}{dz} \left(\frac{\mu_i}{M_i} \right) + n_T \sum_i \omega_i \frac{d}{dz} \left(\frac{\mu_i}{M_i} \right) \quad (2.39)$$

The chemical potential driving force in the above equations can be rewritten in terms of the Gibbs–Duhem (G–D) equation. The mathematical form for the generalized G–D equation in terms of mass units is written as [23]:

$$\frac{1}{\rho} dP + \bar{s} dT = \sum_i \omega_i d \left(\frac{\mu_i}{M_i} \right) \quad (2.40)$$

For an isothermal one–dimensional situation, it can be rewritten as

$$\frac{1}{\rho} \frac{dP}{dz} = \sum_i \omega_i \frac{d}{dz} \left(\frac{\mu_i}{M_i} \right) \quad (2.41)$$

Combining Equations (2.40) and (2.41), one obtains

$$T\sigma = \sum_i j_i \frac{d}{dz} \left(\frac{\mu_i}{M_i} \right) + \frac{n_T}{\rho} \frac{dP}{dz} = \sum_i j_i \frac{d}{dz} \left(\frac{\mu_i}{M_i} \right) + W \frac{dP}{dz} \quad (2.42)$$

Thus, once the fluxes and forces have been identified, the expressions are:

$$J = LX \quad (2.43)$$

Where J is the flux matrix, L is the phenomenological coefficient matrix and X is the matrix for driving forces. As an example, for a four–component system, they can be written as

$$J = \begin{bmatrix} j_1 \\ j_2 \\ j_3 \\ W \end{bmatrix} \quad (2.44)$$

$$L = \begin{bmatrix} L_{11} & L_{12} & L_{12} & L_{14} \\ L_{21} & L_{22} & L_{23} & L_{24} \\ L_{31} & L_{32} & L_{33} & L_{34} \\ L_{41} & L_{42} & L_{43} & L_{44} \end{bmatrix} \quad (2.45)$$

$$X = \begin{bmatrix} \frac{d}{dz} \left(\frac{\mu_1}{M_1} \right) \\ \frac{d}{dz} \left(\frac{\mu_2}{M_2} \right) \\ \frac{d}{dz} \left(\frac{\mu_3}{M_3} \right) \\ \frac{dP}{dz} \end{bmatrix} \quad (2.46)$$

Thus, a system can be fully defined for a generalized mass-transfer situation incorporating all possible gradients and convective mass flux for a multicomponent system.

2.6.2 Example Study 2: Steady-State Binary Gas Permeation through Membrane

2.6.2.1 System of Interest

Simple steady-state binary gas permeation through a membrane can be illustrated as shown in Figure 2.9. The differences of pressure and concentration between upstream and downstream produce a flow through membrane. Here let us assume a ‘perfect membrane’ that is capable of allowing passage only to one species, that will be

designated as component A in this example. To simplify the problem, both gas species are assumed to be ideal gases. When there is a pressure difference between the upstream and downstream boundaries, gas molecules move from the high pressure side to low pressure side in order to neutralize a chemical potential gradient due to pressure. This example assumes higher pressure in the upstream gas chamber. Since component B cannot pass through the membrane, the flux of component B with respect to stationary coordinates appears to be zero at any location in steady state. Non-equilibrium thermodynamics can relate individual fluxes to the driving forces. Our goals in this example are to employ non-equilibrium thermodynamics to find expressions for the flux of component A and to construct the proper expression for the corresponding modified Peclet number.

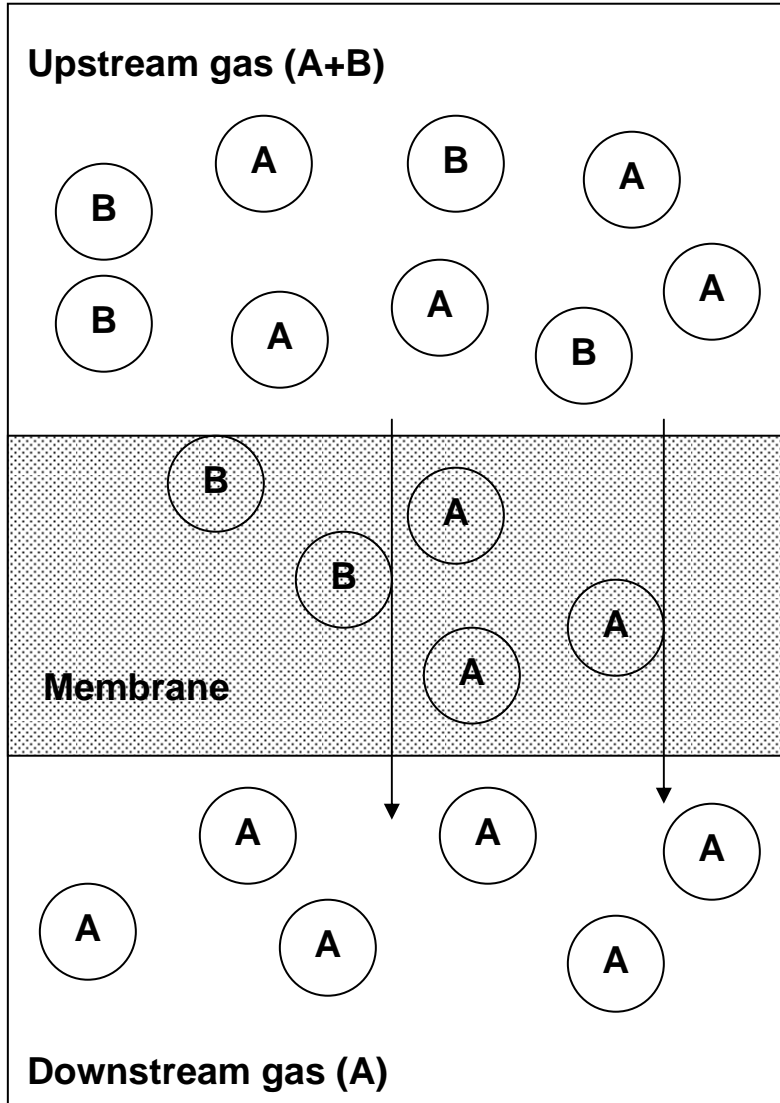


Figure 2.9: Schematic representation of binary mass transfer of components A and B through perfect membrane that allows only component A to permeate.

2.6.2.2 Derivation of Model Equations

For a binary system the rate of lost work for a steady-state membrane process can be expressed as:

$$T\sigma = -N_A \frac{d\mu_A}{dz} - N_B \frac{d\mu_B}{dz} \quad (2.47)$$

Applying the Gibbs-Duhem equation for an ideal gas to the above equation yields

$$T\sigma = -N_A RT \frac{d \ln \bar{p}_A}{dz} - N_B RT \frac{d \ln \bar{p}_B}{dz} \quad (2.48)$$

Therefore, the following identification of flux and driving force results

$$\begin{pmatrix} N_A \\ N_B \end{pmatrix} = \begin{pmatrix} L_{AA} & L_{AB} \\ L_{BA} & L_{BB} \end{pmatrix} \begin{pmatrix} -RT \frac{d \ln \bar{p}_A}{dz} \\ -RT \frac{d \ln \bar{p}_B}{dz} \end{pmatrix} \quad (2.49)$$

For an ideal gas the partial pressure can be split into two terms, one of which involves the pressure gradient and the other of which involves the concentration gradient. Thereby, Equation (2.49) can be recast as:

$$\begin{pmatrix} N_A \\ N_B \end{pmatrix} = \begin{pmatrix} L_{AA} + L_{AB} & L_{AA} - L_{AB} \\ L_{BA} + L_{BB} & L_{BA} - L_{BB} \end{pmatrix} \begin{pmatrix} -RT \frac{d \ln P}{dz} \\ d \ln \left(\frac{y_A}{y_B} \right) \\ -RT \frac{d \ln \left(\frac{y_A}{y_B} \right)}{dz} \end{pmatrix} \quad (2.50)$$

The total molar flux N is obtained from the summation of the two individual fluxes as:

$$N = (L_{AA} + 2L_{AB} + L_{BB}) \left(-RT \frac{d \ln P}{dz} \right) + (L_{AA} - L_{BB}) \left(-RT \frac{d \ln \left(\frac{y_A}{y_B} \right)}{dz} \right) \quad (2.51)$$

The Onsager reciprocal relations ($L_{AB} = L_{BA}$) from Equation (2.49) have been used in the derivation of the above equation. However, one might notice that Equation (2.50) implies additional Onsager reciprocal relations given by:

$$L_{AA} - L_{AB} = L_{AB} + L_{BB} \quad (2.52)$$

Thereby, Equation (2.51) can be simplified to the following:

$$N = 2L_{AA} \left(-RT \frac{d \ln P}{dz} \right) + 2L_{AB} \left(-RT \frac{d \ln \left(\frac{y_A}{y_B} \right)}{dz} \right) \quad (2.53)$$

In this equation it is clearly shown that total flux through the membrane has two kinds of driving forces; the total pressure gradient and the mole fraction gradient. Therefore, non-equilibrium thermodynamics can incorporate totally different driving forces into one equation for the flux. The diffusion term can be extracted from the following relationship between molar diffusion flux and total flux.

$$J_A^* = N_A - y_A N \quad (2.52)$$

From Equations (2.50) and (2.51), the above equation can be expressed as:

$$J_A^* = \left\{ (1 - 2y_A) L_{AA} + L_{AB} \right\} \left(-RT \frac{d \ln P}{dz} \right) + \left\{ L_{AA} - (1 + 2y_A) L_{AB} \right\} \left(-RT \frac{d \ln \left(\frac{y_A}{y_B} \right)}{dz} \right) \quad (2.53)$$

Up to this point, there is no assumption regarding the flux of species B. Therefore, all the above equations are applicable to any membrane system. Now, let us consider the case of a perfect membrane. Since the species B cannot go through a perfect membrane,

the flux of B at steady-state is zero everywhere. Therefore, the following relationship is found.

$$\frac{L_{BA}}{L_{BB}} = - \left(\frac{d \ln \bar{p}_A}{d \ln \bar{p}_B} \right) \quad (2.54)$$

From the Onsager reciprocal relations the flux of A is rewritten from Equation (2.49) as follows:

$$N_A = -L_{AA} RT \frac{d \ln \bar{p}_A}{dz} + L_{BB} RT \frac{d \ln \bar{p}_B}{dz} \left(\frac{d \ln \bar{p}_B}{d \ln \bar{p}_A} \right) \quad (2.55)$$

The second term of the RHS in the above equation is of particular interest, since it is the expression for the coupling phenomena when species A and B affect each other. A zero flux of B does not necessarily mean a zero concentration gradient of B, since the total flux includes both convective as well as diffusive transport. Thus, the second term might not be negligible. When the coupling phenomenon is ignored, the above equation yields the ordinary gas permeation equation.

A much simpler equation can be derived using Equation (2.50) for a perfect membrane. Equation (2.50) yields the following relationship for the case of a perfect membrane;

$$\frac{L_{AA} - L_{AB}}{L_{AA} - 3L_{AB}} = \frac{d \ln P}{d \ln \left(\frac{y_A}{y_B} \right)} \quad (2.56)$$

The above equation allows the flux equation for species A in the Equation (2.50) to be simplified to yield the following;

$$N_A = L_{BB} \left(-RT \frac{d \ln P}{dz} \right) \quad (2.57)$$

This equation may be useful to determine the phenomenological constants if the total pressure gradient and the flux of species A are measurable.

2.6.6.3 Mass-Average Velocity and Modified Peclet Number

The mass-average velocity is related to the total mass flux, n , as

$$W = \frac{n}{\rho} \quad (2.58)$$

Since the flux of species B is zero, Equation (2.55) along with the ideal gas assumption permit the mass-average velocity to be expressed as:

$$W = -\frac{(RT)^2}{PM} M_A \left\{ L_{AA} \frac{d \ln \bar{p}_A}{dz} - L_{BB} \frac{d \ln \bar{p}_B}{dz} \left(\frac{d \ln \bar{p}_B}{d \ln \bar{p}_A} \right) \right\} \quad (2.59)$$

where \bar{M} is average molecular weight. This equation also shows the effect of the coupling phenomena indicated in Equation (2.55). However, a much simpler but useful expression for the mass-average velocity can be obtained from Equation (2.57) as:

$$W = -\frac{(RT)^2}{PM} M_A L_{BB} \left(\frac{d \ln P}{dz} \right) \quad (2.60)$$

In accordance with this expression for the mass-average velocity, the modified Peclet number is given by

$$Pe_A^M = -\frac{H(RT)^2}{PMD_{AB}} M_A \left\{ L_{AA} \frac{d \ln \bar{p}_A}{dz} - L_{BB} \frac{d \ln \bar{p}_B}{dz} \left(\frac{d \ln \bar{p}_B}{d \ln \bar{p}_A} \right) \right\} \quad (2.61)$$

or

$$Pe_A^M = -\frac{H(RT)^2}{PMD_{AB}} M_A L_{BB} \left(\frac{d \ln P}{dz} \right) \quad (2.62)$$

where H is a characteristic length for diffusion. The above equation implies that convection becomes more significant as an increased total pressure gradient is applied to the membrane system.

2.7 Summary

In this chapter the general approach to construct a well-defined mass-transfer problem was presented. A well-defined mass-transfer problem incorporates both diffusion and convection. The mathematical expression for convection demands a closed mathematical form for the mass-average velocity. The mass-average velocity can be evaluated using the equation-of-continuity and the equation-of-state. By using the equation-of-state the equation-of-continuity was converted from a parabolic partial differential equation to an ordinary differential equation. This is an important manipulation of the equations, since coupled parabolic and hyperbolic PDEs cannot be solved by any currently available numerical algorithms. The resulting equations might look complex; however, they are applicable to any system. Furthermore, by means of an example problem it was shown that ignoring the convective contribution at short contact times can lead to significant errors even at long times.

Generalization of the mass-flux equation using non-equilibrium thermodynamics was also briefly discussed in this chapter. Non-equilibrium thermodynamics is more useful when several different transport phenomena occur simultaneously. Since the driving force in non-equilibrium thermodynamics is much more general than in the Fickian diffusion equation, it can handle coupling effects among the various driving forces was shown via a simple example.

CHAPTER III

DEVELOPMENT OF THE DRY-CASTING MODEL INCORPORATING CONVECTIVE TRANSPORT

3.1 Scope of the Chapter

In Chapter II, the general approach to construct a well-defined mass-transfer problem was presented, incorporating both diffusive and convective contributions into the mass flux correctly. This approach permits description of a mass-transfer process in a given system, considering densification or swelling due to the different density of each species. Dry-casting is one such mass-transfer process where the evaporation of a lighter species leads to densification of the solution. Although Shojaie et al. [29-31] developed the heat and mass-transport model for the dry-cast process, convective transport due to densification in the casting solution was neglected due to lack of a method to construct a well-defined mass-transfer problem. Therefore, in this study, a well-defined mass-transfer model for the formation of a polymeric membrane via the dry-casting process is developed by adding convection to the dry-cast model of Shojaie et al.. Thus, this new model is the first fully-predictive and well-defined model ever developed for the dry-casting process. Experimental verification of this model is essential to prove that the development is robust.

Chapter III is organized as follows. First, an introduction to the dry-cast process is presented. Reviews of prior studies on modeling the dry-cast process and the motivation for this study follow. Then, developments of our model incorporating thermodynamic,

mass transport, energy transport and gas-phase components are shown. Next, the solution methodology and results are presented. Then, experimental corroboration of the predictions obtained from our model is presented. The chapter concludes with a summary.

3.2 Introduction

Dry-casting is the oldest phase-inversion process. In this process, the polymer is dissolved in a solvent or a solvent/nonsolvent mixture and the homogeneous liquid solution is cast on a support. The solvent and the nonsolvent in the polymer solution are allowed to evaporate in an inert atmosphere. Next, the loss of solvent and nonsolvent from initial homogeneous polymer solution leads to formation of a turbid two-phase solution. At this stage, evaporation is accompanied by significant latent heat effect. Then, the solidification follows in which the polymer-rich phase precipitates to form a solid matrix. Depending on the initial conditions of the casting solution, the resulting structure will either be a porous membrane or a nonporous polymer film.

The dry-cast process can be used as a stand-alone casting technique or as a post-processing for another phase-inversion method such as wet-casting. Dry-casting as a stand-alone process has become less popular for fabricating membranes due to concerns about the evaporation of the toxic solvents. Usually the dry-cast process is of particular interest since the evaporation step before immersion into a nonsolvent bath can change the performance of the resulting membrane. Also the slower mass-transfer dynamics in dry-casting are advantageous to researchers interested in manipulating casting conditions to investigate membrane formation processes.

3.3 Review of Prior Studies

The first quantitative model for the dry-casting process was developed by Anderson and Ullman [32], who assumed the casting-solution thickness to be constant as well as semi-infinite with a constant surface concentration. Castellari and Ottani [33] improved upon this model by incorporating three key changes; they considered the casting-solution thickness to be finite and varying with time, as well as having a variable surface concentration. However, they used self-diffusion coefficients instead of binary diffusivities. Moreover, their surface-concentration boundary condition was fitted through experimental data. Krantz et al. [34] improved on Castellari and Ottani's model by incorporating a lumped parameter description of the mass transfer in the ambient gas-phase and also using binary diffusivities, thereby eliminating the need for any adjustable parameters. A slight variation of the Krantz et al. model was proposed by Tsay and McHugh [35], who used an improved equation-of-state for the variable casting solution density. They also considered coupling effects of multicomponent diffusion using non-equilibrium thermodynamics, resulting in a better correlation with experimental data. Surprisingly, none of the above models considered thermal effects during evaporative casting. Tantekin-Ersolmaz [36] was the first to identify that evaporation of solvent (and nonsolvent) during evaporative dry-casting has a significant effect on the mass-transfer characteristics of the process, thereby greatly affecting the final membrane morphology. Shojaie et al. [29–31] incorporated this finding into the first fully predictive coupled heat- and mass-transfer model of dry-casting for binary and ternary casting solutions. Although this was a significant breakthrough, one of the main drawbacks of this fully predictive

model is that it completely neglected the bulk or convective mass and heat flux caused by local densification. This factor can be quite significant in multicomponent systems where all the evaporating species move in the same direction. due Tan et al. [37] attempted to incorporate convection into a comprehensive evaporative casting model. However, their model encountered considerable error owing to effectively using the convection velocity at the interface rather than a velocity that varied throughout the thickness of the casting solution owing to the density gradient. A proper approach to incorporating the convection requires that the convective flux or mass-average velocity be determined based on a variable casting solution density.

3.4 Motivation for This Study

Clearly, no dry-cast model in the literature has been based on well-defined mass-transfer equations. As a result, these models do not successfully incorporate convective transport in the casting solution, although significant densification can occur. In particular, Shojaie et al. found that their diffusion model underpredicted the surface temperature significantly; this possibly could be due to ignoring the convective mass transfer owing to local densification.. Therefore, this study will modify Shojaie et al.'s description of the dry-casting process in order to develop a well-defined mass-transfer model incorporating both convection and diffusion.

3.5 Model Development

3.5.1 System of Interest

The physical system of interest for the current model has been kept identical to that used by Shojaie [29] and Shojaie et al. [30]. It is a simplified laboratory-scale dry-casting process consisting of a standard membrane-casting apparatus that permits spreading the casting solution as a thin film on a glass substrate and exposing it to an ambient gas (air) phase as shown in Figure 3.1. Both the heat and mass transport are assumed to be one-dimensional phenomena. Prior to the initiation of the process, the initial depth and composition of the casting solution are known and each component is assumed to be in phase equilibrium with the ambient gas phase. The process starts with evaporation of the solvent(s) and the nonsolvent(s) from the liquid casting solution into the gas phase, resulting in development of a concentration gradient for each species in the casting solution that is very steep at the liquid-gas interface. The fluxes into the gas phase is expressed in terms of lumped parameters based on the mass-transfer coefficient, the local equilibrium concentration at the liquid/gas interface, and natural convection in the gas phase. Evaporation of the solvent and nonsolvent leads to mass loss and thinning of the casting solution. This changing depth of the casting solution is determined by the instantaneous integral mass balance on the casting solution. In addition, the latent heat effects associated with evaporation of the solvent and nonsolvent cause substantial cooling of the casting solution, which in turn affects the vapor pressure of the evaporating components, thereby significantly altering the evaporative mass fluxes.

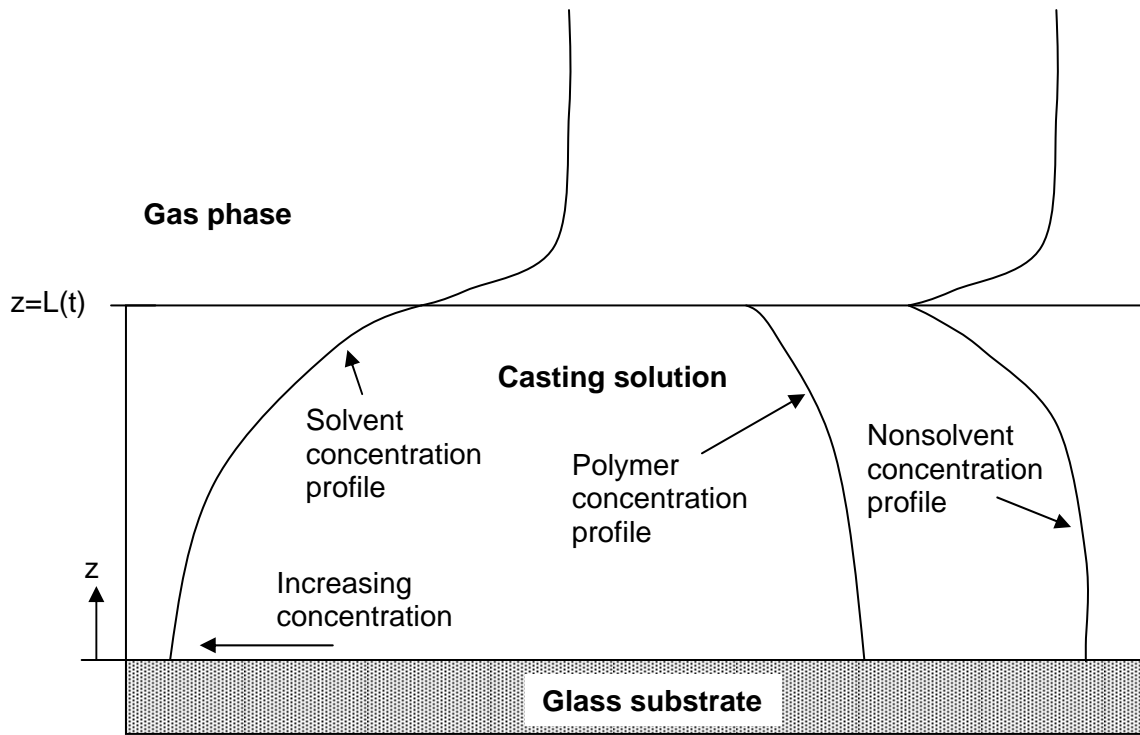


Figure 3.1: Schematic of the dry-cast process for polymeric membrane formation.

3.5.2 Thermodynamic Model

A solution thermodynamic model for the polymeric casting solution model is essential for several reasons. It is required to calculate the chemical potential, activity coefficient, and diffusion coefficient of each species. It is also needed to calculate the bimodal that separates the single and two-phase regions on the ternary phase diagram. In accordance with the Shojaie et al.'s diffusion model, the polymer-solution thermodynamics are described by the Flory-Huggins lattice model. It should be noted that the Flory-Huggins' model assumes zero volume-of-mixing, which is markedly different from assuming a constant overall volume of casting solution. The assumption of zero volume-of-mixing implies that the total volume of the mixture is a summation of the individual component volumes before mixing; therefore it depends on the system concentrations and fluxes. The assumption of a constant mixture volume implies no dependence on of the system concentrations or fluxes.

Shojaie et al. derived equations for the chemical potentials based on the Flory-Huggins lattice model. These equations require the interaction parameters for a specific system. Yilmaz and McHugh [38], Tsay and McHugh [39], and Mulder and Smolders [40] reported the interaction parameters for water (1) / acetone (2), acetone (2) / cellulose acetate (3) and water (1) / cellulose acetate (3), respectively. Details of these equations are given in Shojaie's original work [29].

3.5.3 Mass-Transport Model in Casting Solution

3.5.3.1 Species-Balance Equations

In order to completely describe a ternary system, two independent species-balance equations, typically for the solvent and the nonsolvent, must be solved. These are given by the following:

$$\rho \left(\frac{\partial \omega_1}{\partial t} + W \frac{\partial \omega_1}{\partial z} \right) = - \frac{\partial j_1}{\partial z} \quad (3.1)$$

$$\rho \left(\frac{\partial \omega_2}{\partial t} + W \frac{\partial \omega_2}{\partial z} \right) = - \frac{\partial j_2}{\partial z} \quad (3.2)$$

where ρ is the density of the multicomponent casting solution; ω_i , n_i and j_i are the mass fraction, total mass flux and diffusive mass flux, respectively, of species i ; and W is the mass-average velocity. Note that the second term, containing the mass-average velocity in the lefthand side of the above equations was completely ignored in prior studies [29-36] without any justification. In this study this term will be rigorously incorporated.

In order to complete the description of the model equations, we need appropriate expressions for the unknown variables in equations 3.1 and 3.2. These unknown variables are the density of the multicomponent solution, the mass-average velocity, and the diffusive mass flux for each species.

3.5.3.2 Equation-of-State

The density of the multicomponent casting solution is a variable defined by an equation-of-state. The simplest equation-of-state consistent with the zero volume-of-mixing assumption is the following:

$$\frac{1}{\rho} = \omega_1 \left(\frac{1}{\rho_1^\circ} - \frac{1}{\rho_3^\circ} \right) + \omega_2 \left(\frac{1}{\rho_2^\circ} - \frac{1}{\rho_3^\circ} \right) + \frac{1}{\rho_3^\circ} \quad (3.3)$$

where ρ_i° is the density of pure species i . Note that the zero volume-of-mixing assumption is consistent with the polymer solution thermodynamics (Flory-Huggins model) used in this model. The prior studies of Shojaie et al. [29-31] and Tan et al. [37] assumed a linear relationship between the casting solution density and component weight fractions based on the justification that this weighted arithmetic mean represented the true mixing characteristics of the system incorporating volume-of-mixing effects. However, this claim was not supported by any experimental data available in the literature. These investigators supported their claim by correlating their ternary equation-of-state with the experimental density data for a binary system of cellulose acetate and acetone [41]. Even though the linear relationship correlated well with the binary experimental data, there is no assurance that it will properly account for the presence of the nonsolvent (water). Note that water is a swelling agent for polymers such as cellulose acetate, which could compromise the accuracy of an equation-of-state based on extending binary solution data to a ternary system. Most importantly, using an equation-of-state based on assuming zero volume-of-mixing permits obtaining a closed form algebraic expression for the mass-average velocity and convective mass flux. The linear relationship used in prior studies [29-31, 37] makes the species conservation equation incorporating convection so

complex that it cannot be solved. This undoubtedly is the primary reason why convection has been neglected in the prior studies.

3.5.3.3 Multicomponent Diffusive Flux Equations

The system under consideration is ternary; hence, use of Fick's 1st Law of Diffusion makes it difficult to incorporate the coupling effects of mass-transfer. Shojaie et al. [29] expressed the diffusive material fluxes for the nonsolvent (1) and the solvent (2) using the principles of non-equilibrium thermodynamics based on chemical potential gradients and phenomenological coefficients. The chemical potential gradients can be converted to weight-fraction gradients using the Flory–Huggins model. Thus, the expression for diffusive fluxes in a matrix form is given by the following:

$$J = FX \quad (3.4)$$

where J represents a species' diffusive flux and is defined as $J = \begin{bmatrix} j_1 \\ j_2 \end{bmatrix}$, F represents the

phenomenological coefficients and is defined as $F = \begin{bmatrix} f_1 & g_1 \\ f_2 & g_2 \end{bmatrix}$ and X represents the

driving force and is defined as $X = \begin{bmatrix} \frac{\partial \omega_1}{\partial z} \\ \frac{\partial \omega_2}{\partial z} \end{bmatrix}$

In turn, the phenomenological coefficients are expressed in terms of friction coefficients and mass fractions through the following set of equations:

$$f_1 = \left(\frac{1}{DB - CA} \right) \left(C \frac{\partial \mu_1}{\partial \omega_1} + B \frac{\partial \mu_2}{\partial \omega_1} \right) \quad (3.5)$$

$$f_2 = \left(\frac{1}{DB - CA} \right) \left(D \frac{\partial \mu_1}{\partial \omega_1} + A \frac{\partial \mu_2}{\partial \omega_1} \right) \quad (3.6)$$

$$g_1 = \left(\frac{1}{DB - CA} \right) \left(C \frac{\partial \mu_1}{\partial \omega_2} + B \frac{\partial \mu_2}{\partial \omega_2} \right) \quad (3.7)$$

$$g_2 = \left(\frac{1}{DB - CA} \right) \left(D \frac{\partial \mu_1}{\partial \omega_2} + A \frac{\partial \mu_2}{\partial \omega_2} \right) \quad (3.8)$$

where A, B, C and D are defined as

$$A = \frac{\omega_2 \xi_{12}}{\omega_1 M_2} + \frac{\xi_{13}}{M_3} \left(\frac{1 - \omega_2}{\omega_1} \right) \quad (3.9)$$

$$B = \frac{\xi_{12}}{M_2} - \frac{\xi_{13}}{M_3} \quad (3.10)$$

$$C = \frac{\omega_1 \xi_{12}}{\omega_2 M_1} + \frac{\xi_{23}}{M_3} \left(\frac{1 - \omega_1}{\omega_2} \right) \quad (3.11)$$

$$D = \frac{\xi_{12}}{M_1} - \frac{\xi_{23}}{M_3} \quad (3.12)$$

Here ξ_{ij} is the binary friction coefficient. The relationship between the binary friction coefficients and binary diffusion coefficients is described by Shojaie [29].

3.5.3.4 Mass-Average Velocity

The unique aspect of this study is the development of a dry-cast model incorporating a closed form algebraic equation for the mass-average velocity based on an equation-of-state assuming zero volume-of-mixing that is obtained by combining the continuity equation, the equation for species flux, and the equation-of-state for density as described in Chapter II. The continuity equation is defined as

$$\frac{\partial \rho}{\partial t} = -\frac{\partial(\rho W)}{\partial z} = -\rho \frac{\partial W}{\partial z} - W \frac{\partial \rho}{\partial z} \quad (3.13)$$

Next, the first and third terms in the above equation can be obtained by taking derivatives of equation 3.3 with respect to time and the spatial coordinate, as follows:

$$\frac{\partial \rho}{\partial t} = -\rho^2 \left(\frac{1}{\rho_1^\circ} - \frac{1}{\rho_3^\circ} \right) \frac{\partial \omega_1}{\partial t} - \rho^2 \left(\frac{1}{\rho_2^\circ} - \frac{1}{\rho_3^\circ} \right) \frac{\partial \omega_2}{\partial t} \quad (3.14)$$

$$\frac{\partial \rho}{\partial z} = -\rho^2 \left(\frac{1}{\rho_1^\circ} - \frac{1}{\rho_3^\circ} \right) \frac{\partial \omega_1}{\partial z} - \rho^2 \left(\frac{1}{\rho_2^\circ} - \frac{1}{\rho_3^\circ} \right) \frac{\partial \omega_2}{\partial z} \quad (3.15)$$

Combining equations 3.4 and 3.13–15 yields

$$\frac{\partial W}{\partial z} = -\left(\frac{1}{\rho_1^\circ} - \frac{1}{\rho_3^\circ} \right) \frac{\partial}{\partial z} \left(f_1 \frac{\partial \omega_1}{\partial z} + g_1 \frac{\partial \omega_2}{\partial z} \right) - \left(\frac{1}{\rho_2^\circ} - \frac{1}{\rho_3^\circ} \right) \frac{\partial}{\partial z} \left(f_2 \frac{\partial \omega_1}{\partial z} + g_2 \frac{\partial \omega_2}{\partial z} \right) \quad (3.16)$$

In order to obtain an exact expression for the mass-average velocity, one must integrate equation 3.16, subject to an appropriate boundary condition. For the current system of interest, the presence of an impermeable base under the casting solution implies that at $z = 0$, $\frac{\partial \omega_1}{\partial z} = 0$, $\frac{\partial \omega_2}{\partial z} = 0$ and $W = 0$, yielding the following expression for the mass-

average velocity:

$$W = -\left(\frac{1}{\rho_1^\circ} - \frac{1}{\rho_3^\circ} \right) \left(f_1 \frac{\partial \omega_1}{\partial z} + g_1 \frac{\partial \omega_2}{\partial z} \right) - \left(\frac{1}{\rho_2^\circ} - \frac{1}{\rho_3^\circ} \right) \left(f_2 \frac{\partial \omega_1}{\partial z} + g_2 \frac{\partial \omega_2}{\partial z} \right) \quad (3.17)$$

Note that $\rho_1^\circ < \rho_3^\circ$, $\rho_2^\circ < \rho_3^\circ$, $f_1 < 0$, $g_1 < 0$, $f_2 < 0$, and $g_2 < 0$. This implies that the sign and corresponding direction of the mass-average velocity induced by density changes depend on the sign of the two spatial derivatives of the water and acetone. The gradient of the acetone concentration will always be negative during evaporative casting since acetone is far more volatile than water. The gradient of the water concentration can be

either negative or positive. If both the acetone and water concentration gradients are negative, the mass-average velocity will be negative, thus implying that its direction is downward towards the solid supporting surface. However, the mass-average velocity will be positive if the water concentration gradient is positive and the following condition is satisfied:

$$\begin{aligned} & \left| \left(\frac{1}{\rho_1^\circ} - \frac{1}{\rho_3^\circ} \right) f_1 \frac{\partial \omega_1}{\partial z} + \left(\frac{1}{\rho_2^\circ} - \frac{1}{\rho_3^\circ} \right) f_2 \frac{\partial \omega_1}{\partial z} \right| \\ & > \left| \left(\frac{1}{\rho_1^\circ} - \frac{1}{\rho_3^\circ} \right) g_1 \frac{\partial \omega_2}{\partial z} + \left(\frac{1}{\rho_2^\circ} - \frac{1}{\rho_3^\circ} \right) g_2 \frac{\partial \omega_2}{\partial z} \right| \end{aligned} \quad (3.18)$$

If the inequality in equation 3.18 is satisfied, the mass-average velocity will be positive and upward. Since this arises because of a local increase in the water concentration, it implies a local swelling or decrease in density owing to the fact that $\rho_2^\circ < \rho_3^\circ$.

3.5.3.5 Final Governing Equations

Adding the species-balance equations to the three equations described above (the equation-of-state relationship for the casting solution density, the rigorous expression for diffusive mass flux, and the equation for mass-average velocity) yields a well-defined set of equations that incorporates the salient features of this ternary system of interest. After considerable combination and rearrangement we obtain following forms of the conservation-of-species equations:

$$\begin{aligned} \frac{\partial \omega_1}{\partial t} = & -\frac{1}{\rho} \frac{\partial}{\partial z} \left(f_1 \frac{\partial \omega_1}{\partial z} + g_1 \frac{\partial \omega_2}{\partial z} \right) \\ & + \left[\left(\frac{1}{\rho_1^\circ} - \frac{1}{\rho_3^\circ} \right) \left(f_1 \frac{\partial \omega_1}{\partial z} + g_1 \frac{\partial \omega_2}{\partial z} \right) + \left(\frac{1}{\rho_2^\circ} - \frac{1}{\rho_3^\circ} \right) \left(f_2 \frac{\partial \omega_1}{\partial z} + g_2 \frac{\partial \omega_2}{\partial z} \right) \right] \frac{\partial \omega_1}{\partial z} \end{aligned} \quad (3.19)$$

$$\begin{aligned} \frac{\partial \omega_2}{\partial t} = & -\frac{1}{\rho} \frac{\partial}{\partial z} \left(f_2 \frac{\partial \omega_1}{\partial z} + g_2 \frac{\partial \omega_2}{\partial z} \right) \\ & + \left[\left(\frac{1}{\rho_1^\circ} - \frac{1}{\rho_3^\circ} \right) \left(f_1 \frac{\partial \omega_1}{\partial z} + g_1 \frac{\partial \omega_2}{\partial z} \right) + \left(\frac{1}{\rho_2^\circ} - \frac{1}{\rho_3^\circ} \right) \left(f_2 \frac{\partial \omega_1}{\partial z} + g_2 \frac{\partial \omega_2}{\partial z} \right) \right] \frac{\partial \omega_2}{\partial z} \end{aligned} \quad (3.20)$$

3.5.3.6 Initial and Boundary Conditions

Equations 3.19 and 3.20 are nonlinear second-order partial differential equations requiring one initial condition and two boundary conditions. The initial condition is defined by the known composition of the casting solution at the start of the evaporative casting process:

$$\omega_1 = \omega_1^\circ, \quad \omega_2 = \omega_2^\circ \quad \text{at } t = 0 \quad (3.21)$$

The impermeable glass support implies zero-flux boundary conditions at $z = 0$ as

$$\frac{\partial \omega_1}{\partial z} = 0, \quad \frac{\partial \omega_2}{\partial z} = 0 \quad \text{at } z = 0 \quad (3.22)$$

The boundary conditions at the casting solution/gas interface, $z = L(t)$, can be derived through a combination of instantaneous integral mass balance equations for the individual species and total solution that results in the following equations:

$$\rho_1 \left(\frac{dL}{dt} - W \right) = f_1 \frac{\partial \omega_1}{\partial z} + g_1 \frac{\partial \omega_2}{\partial z} - n_1^G \quad (3.23)$$

$$\rho_2 \left(\frac{dL}{dt} - W \right) = f_2 \frac{\partial \omega_1}{\partial z} + g_2 \frac{\partial \omega_2}{\partial z} - n_2^G \quad (3.24)$$

where n_1^G and n_2^G represent the total flux of species 1 and 2, respectively, in the surrounding gaseous phase.

3.5.3.7 Displacement of the Liquid-Gas Interface of the Casting Solution

In order to complete the description, an equation must be obtained to determine the variable $L(t)$. This is expressed in terms of a coupled ordinary differential equation (ODE) derived via an integral mass balance that Shojaie et al.[29] express in the following form:

$$\begin{aligned} \frac{dL}{dt} = & -\left(\frac{1}{\rho_1^o} - \frac{1}{\rho_3^o}\right) \left(f_1 \frac{\partial \omega_1}{\partial z} + g_1 \frac{\partial \omega_2}{\partial z}\right) \\ & -\left(\frac{1}{\rho_2^o} - \frac{1}{\rho_3^o}\right) \left(f_2 \frac{\partial \omega_1}{\partial z} + g_2 \frac{\partial \omega_2}{\partial z}\right) - \frac{(n_1^G + n_2^G)}{\rho} \end{aligned} \quad (3.25)$$

This ODE requires an initial condition that is given by the initial thickness of the casting solution:

$$L = L^o \quad \text{at} \quad t = 0 \quad (3.26)$$

3.5.4 Energy-Transport Model

3.5.4.1 Energy-Balance Equations

The equation describing the energy transport in the casting solution is

$$\frac{\partial T}{\partial t} + W \frac{\partial T}{\partial z} = \alpha \frac{\partial^2 T}{\partial z^2} \quad (3.27)$$

where the mass-average velocity W is calculated from equation 3.17. Although the glass support does not experience any mass transfer, it serves as a heat reservoir. In the absence of any bulk flow, the heat-transport equation for the glass support is

$$\frac{\partial T_{sub}}{\partial t} = \alpha_{sub} \frac{\partial^2 T_{sub}}{\partial z^2} \quad (3.28)$$

3.5.4.2 Initial and Boundary Conditions

The initial and boundary condition are identical to those used in Shojaie et al.'s development [29] and are given by

$$T = T_{sub} = T^\circ \quad \text{at } t = 0 \quad (3.29)$$

At the liquid–solid interface, the boundary condition for the casting solution is given by

$$T = T_{sub} \quad \text{at } z = 0 \quad (3.30)$$

and that for the glass support is given by

$$K_{sub} \frac{\partial T_{sub}}{\partial z} = K \frac{\partial T}{\partial z} \quad \text{at } z = 0 \quad (3.31)$$

Note that at the liquid/solid interface, the mass–average velocity and the corresponding convective heat-transport term are zero. Also note that, if there is any surface coating (e.g. chromium in Shojaie et al.'s experiments [29]) on the glass plate, the boundary condition of the liquid/solid interface should incorporate the thermal properties of the coating, which is not considered in Shojaie et al.'s model calculation. The bottom of the glass support is insulated, leading to the following boundary condition:

$$\frac{\partial T_{sub}}{\partial z} = 0 \quad \text{at } z = -L_{sub} \quad (3.32)$$

Similar to the formulation used in mass transport, the boundary condition at the liquid–gas interface is obtained from an integral energy balance as

$$\frac{\partial T}{\partial z} = \left(\frac{h^*}{K} \right) (T_a - T) + \left(\frac{\sigma \varepsilon}{K} \right) (T_a^4 - T^4) - \frac{n_1^G \Delta H_1^v}{K} - \frac{n_2^G \Delta H_2^v}{K} \quad \text{at } z = L(t) \quad (3.33)$$

where h^* is the heat-transfer coefficient in the gas phase, T_a is the ambient temperature, σ is the Stefan-Boltzmann constant, ε is the emissivity of the liquid/gas interface, and ΔH_i^v is the molar heat-of-vaporization of species i . Equation 3.33 states that the

conductive heat flux at the liquid/gas interface in the casting solution is equal to the sum of the convective and radiative heat fluxes in the gas phase minus the heat lost to vaporize the two volatile components

3.5.5 Gas-Phase Transport Model

In order to complete the model description, information regarding the heat- and mass-transfer rates into the gas phase is essential. Similar to the pure-diffusion model [29], the gas-phase transport is expressed in terms of a “lumped parameter”. The multicomponent film theory model is used to determine the mass-transfer coefficients corrected for higher fluxes [29, 30]. The complete description and relevant equations can be found in the thesis of Shojaie [29].

3.6 Solution Methodology

The modified ternary transport model equations are solved using a commercially available partial differential equation solver, D03PPF, from the National Algorithms Group, Inc., which uses finite difference methods to solve non-linear parabolic partial differential equations along with coupled ordinary differential equations. The spatial location is normalized by the instantaneous thickness of the casting solution to convert the moving-boundary problem to a fixed-boundary problem. The complete FORTRAN program code is given in Appendix B. For the purpose of comparison, the simulation and numerical conditions were kept identical to those used in Shojaie et al.’s work [29].

3.7 Presentation of Model Results

The most common way to display the concentration change of a ternary system due to mass transfer is to superimpose the instantaneous local compositions onto a ternary phase diagram. The experimental data obtained in this thesis research also will be plotted on ternary diagrams along with the theoretical binodal and spinodal calculated by Shojaie et al. [29]. For further information on ternary diagrams, please refer to Appendix C.

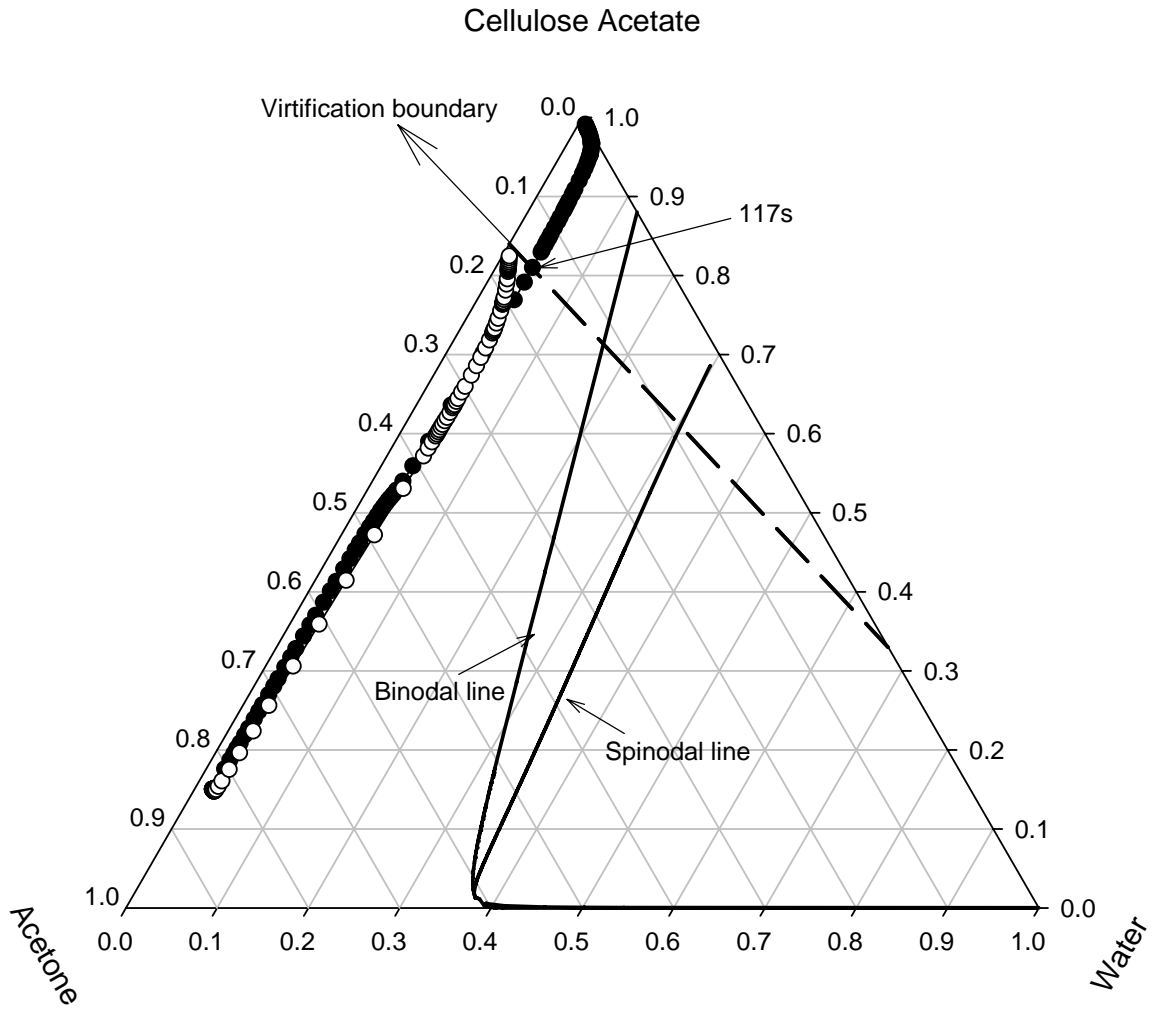
Table 3.1 summarizes the initial conditions for the casting solutions used in this study. Shojaie et al. [29] selected these initial conditions to represent the entire range of possible microstructures for dry-cast polymeric membranes. These three conditions will produce dense polymeric films, symmetric polymeric membranes, and asymmetric polymeric membranes, respectively.

Table 3.1: Summary of Initial Conditions of the Casting Solutions used in the Numerical Solution of the Dry-Casting Model

Casting Solution	Initial Conditions for Casting Solutions
casting solution 1	$\omega_1^\circ = 0.02, \omega_2^\circ = 0.83, L_o = 246\mu m, T_o = 24^\circ C$
casting solution 2	$\omega_1^\circ = 0.10, \omega_2^\circ = 0.75, L_o = 194\mu m, T_o = 23.5^\circ C$
casting solution 3	$\omega_1^\circ = 0.20, \omega_2^\circ = 0.70, L_o = 266\mu m, T_o = 24^\circ C$

In all the subsequent figures black dots (●) and white dots (○) represent the instantaneous composition of the liquid/gas (top) and the liquid/solid (bottom) interface, respectively.

The composition path for casting solution 1 is given in Figure 3.2. As shown in Figure 3.2, the predicted composition path does not cross the binodal into the two-phase region. The concentration profile at the bottom of the casting solution shows that although the acetone concentration decreases, the water concentration does not change appreciably. As a result, the polymer concentration increases greatly, thereby pushing the system towards the vitrification boundary even before it has a chance to cross the binodal and phase-separate. As can be seen from their chemical potential profiles, acetone (Figure 3.4) has a much steeper chemical potential gradient than water (Figure 3.3); this larger driving force for acetone explains its significantly higher rate of evaporation compared to water. The corresponding mass-average velocity profile (Figure 3.5) shows densification starting from the top and spreading through the entire casting solution.



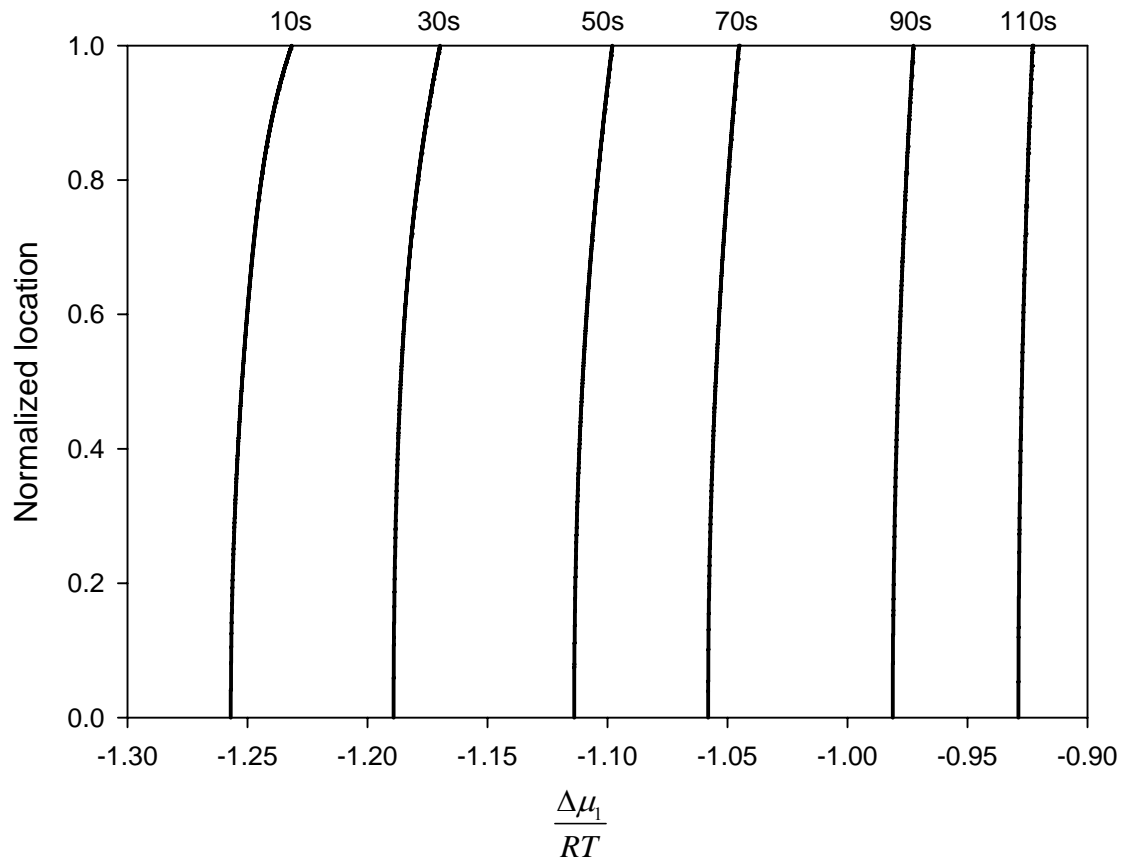


Figure 3.3: Chemical potential profile change of water in the casting solution during the dry-casting process for casting solution 1.

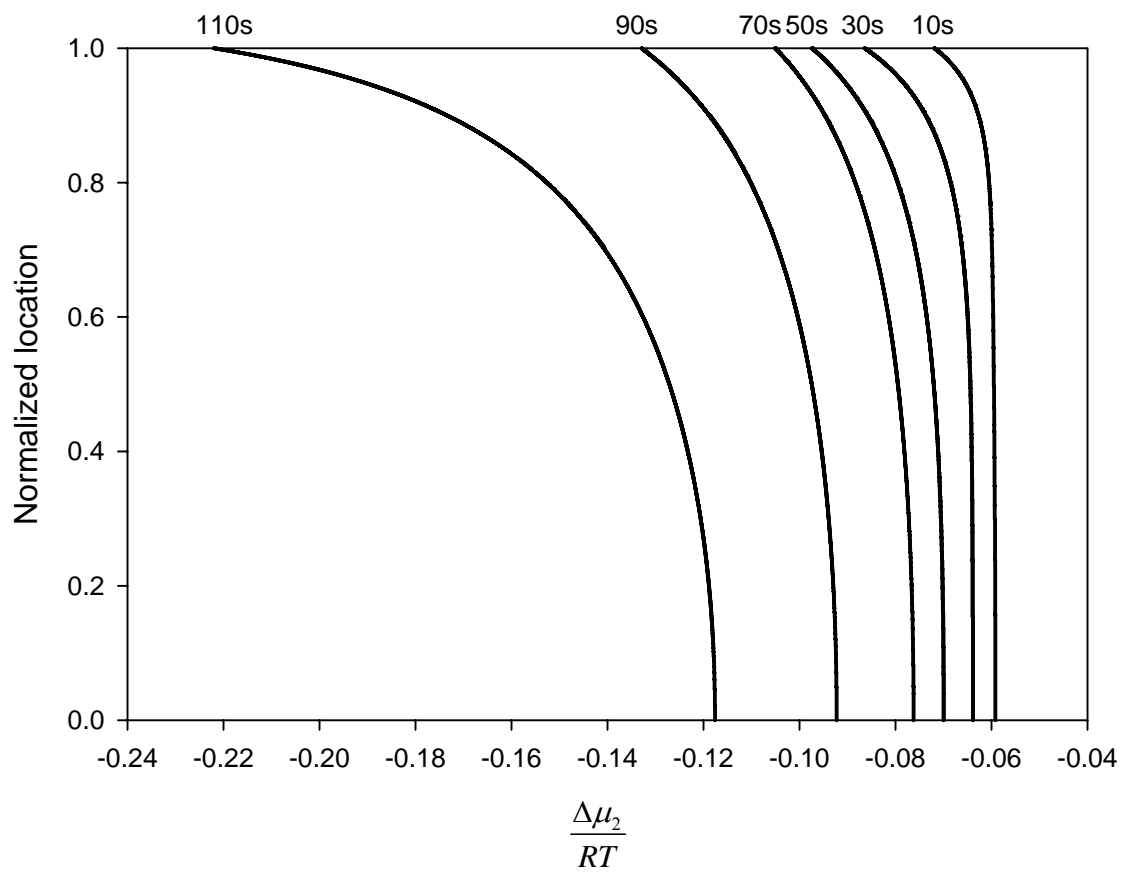


Figure 3.4: Chemical potential profile change of acetone in the casting solution during the dry-casting process for casting solution 1.

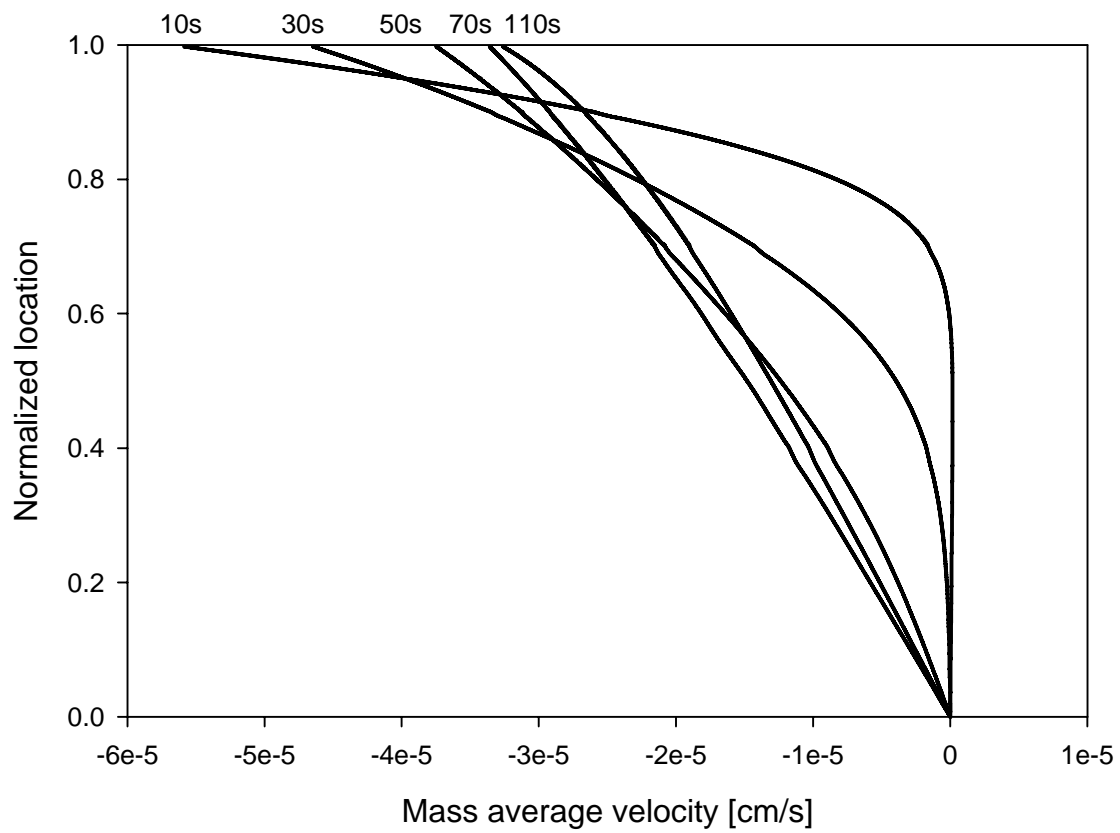


Figure 3.5: Mass-average velocity in the casting solution during the dry-casting process for casting solution 1.

On the other hand, model predictions for casting solution 2 show that it does cross the binodal (Figure 3.6). The concentration profile shows a sharp bend around 23 s, representing a paradigm shift; there is a gradual change in the water concentration while the acetone concentration is kept constant. The binary diffusion coefficient data for the CA–acetone system implies that a sudden change of mobility of molecules due to the gelation occurs when the CA/acetone weight-fraction ratio in the casting solution exceeds 1:1. This prediction agrees well with Reuvers' [43] experimental observation of gelation. Interestingly, the mass-average velocity profile (Figure 3.9) indicates that swelling also occurs in the middle of the casting solution until gelation due to accumulation of polymer at the liquid/gas interface occurs. After 23 s, swelling does not occur anywhere in the casting solution. Furthermore, the chemical potential of water (Figure 3.7) is lower than that of acetone (Figure 3.8) initially. However, after 45 s, water has the higher chemical potential in the entire region of the casting solution. The chemical potential gradient of acetone decreases until 50 s and then increases after that, while the chemical potential gradient of water continues to decrease.

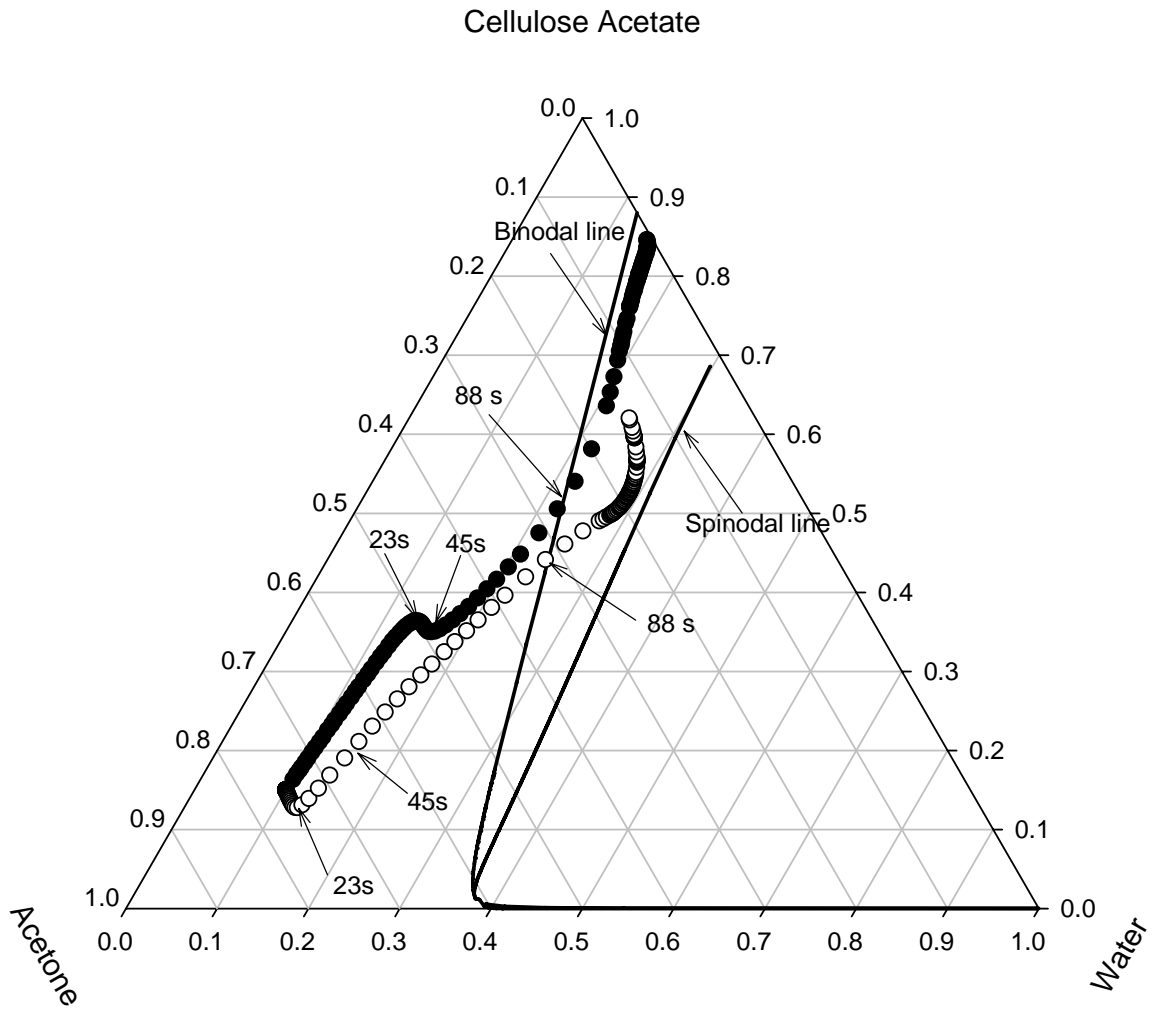


Figure 3.6: Concentration change of liquid-gas interface (●) and solid-liquid interface (○) during the dry-casting membrane-formation process for casting solution 2.

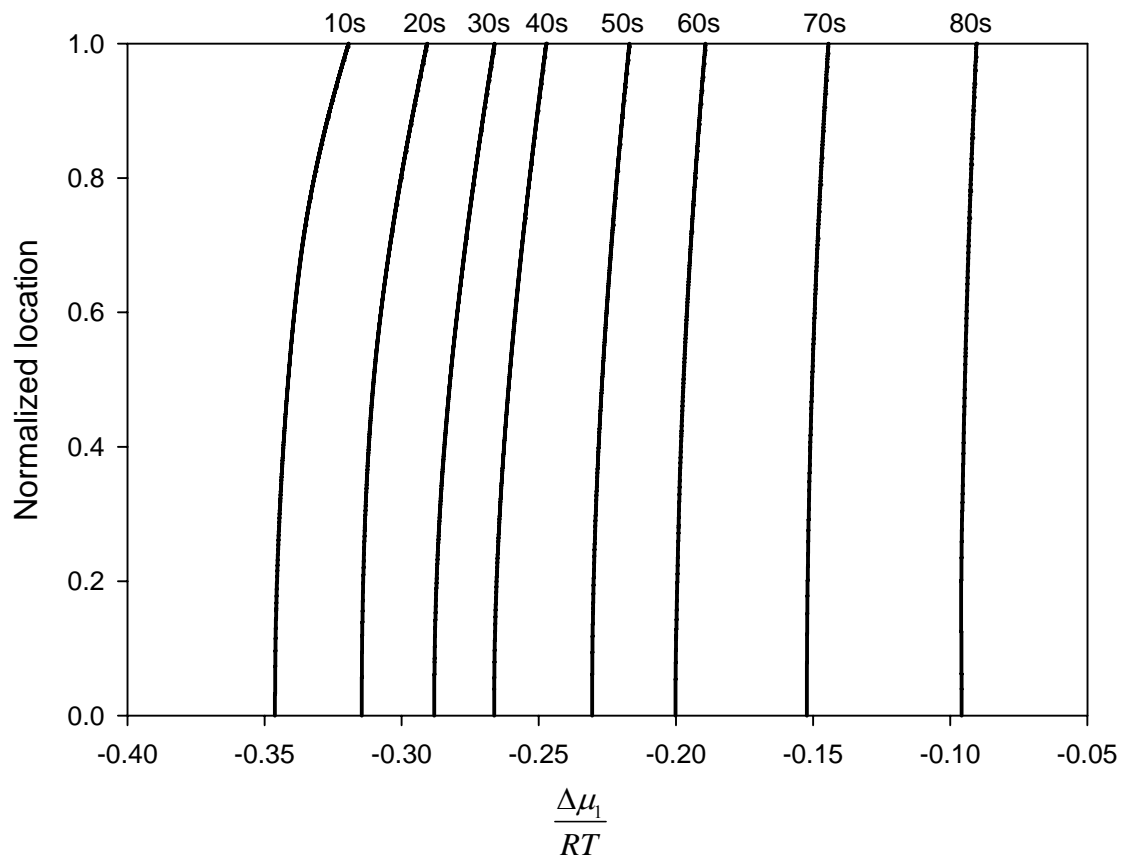


Figure 3.7: Chemical potential profile change of water in the casting solution during the dry-casting process for casting solution 2.

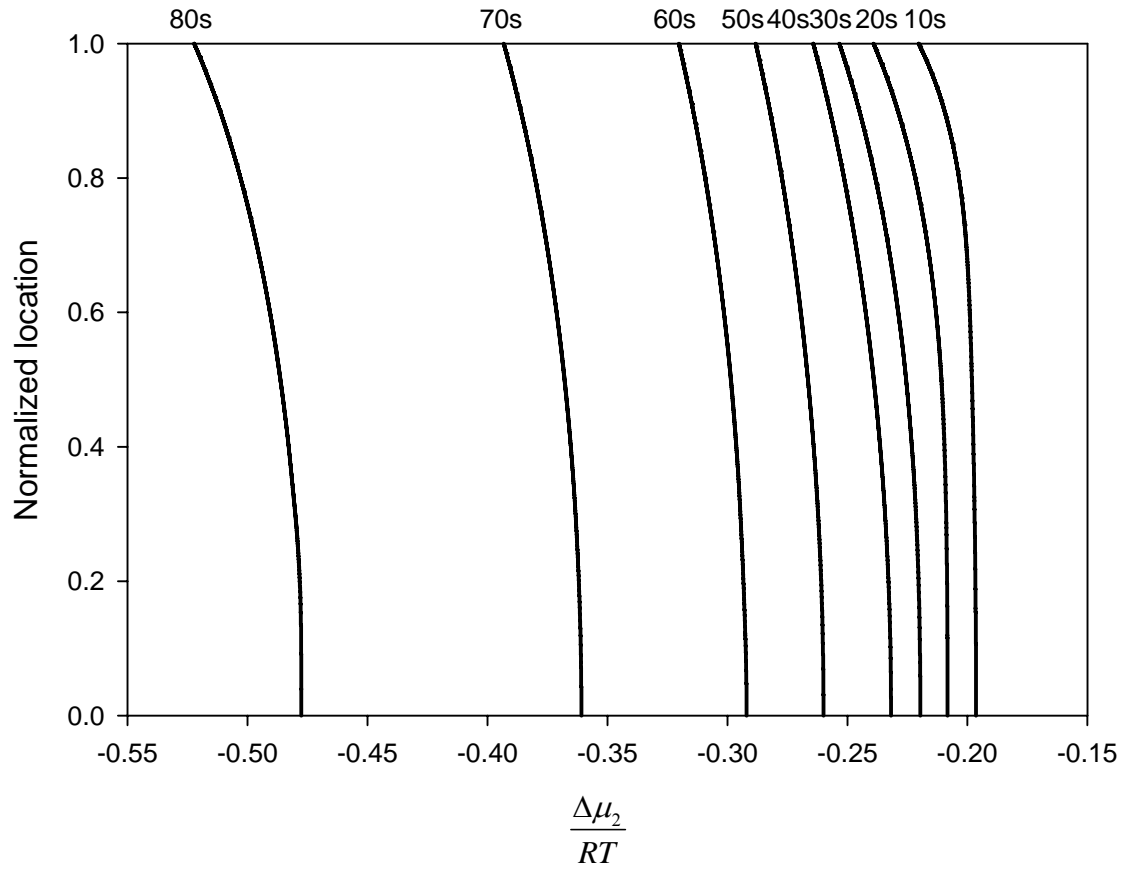


Figure 3.8: Chemical potential profile change of acetone in the casting solution during the dry-casting process for casting solution 2.

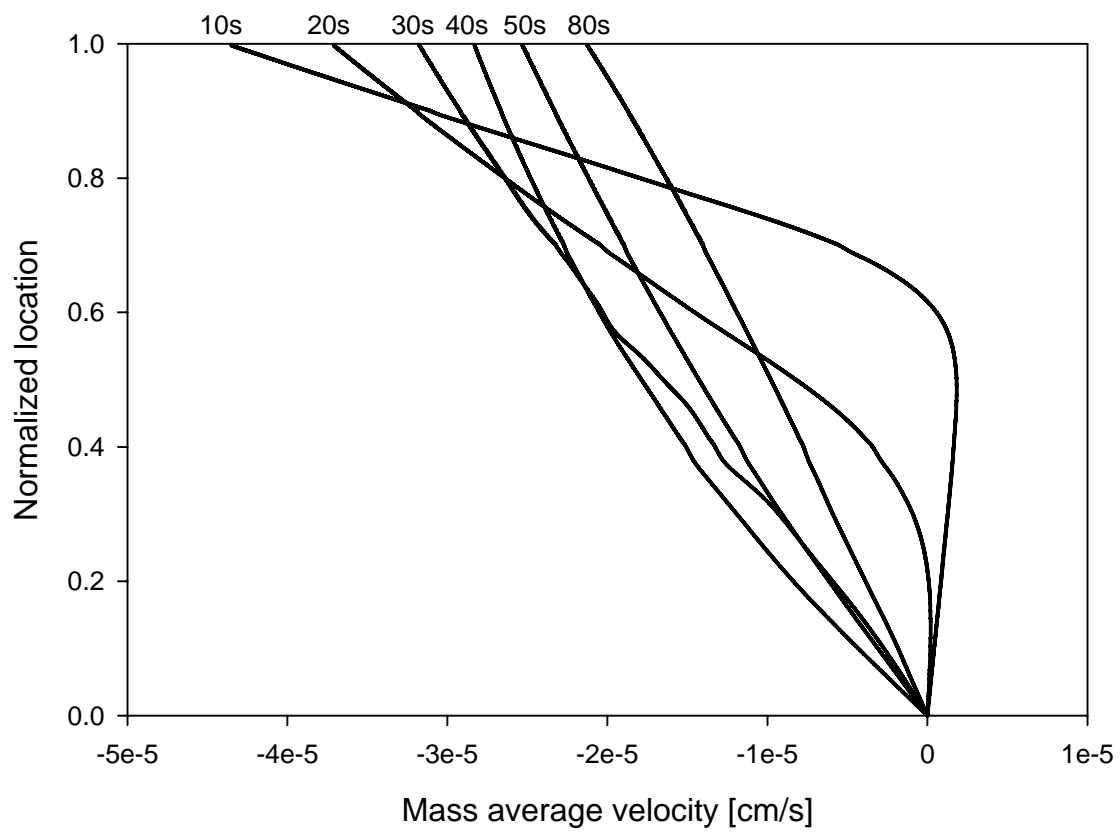


Figure 3.9: Mass-average velocity in the casting solution during the dry-casting process for casting solution 2.

The interfaces for casting solution 3 cross the binodal more quickly than either casting solutions 1 or 2, as shown in Figure 3.10. For casting solution 3 the chemical potential of water (Figure 3.11) is predicted to be higher than that of acetone (Figure 3.12) during the entire dry-casting process. The chemical potential gradients of both acetone and water decrease continuously. Also note that swelling occurs in the middle of casting solution until the CA/acetone ratio approaches 1:1, while the top of the casting solution is densified as shown in Figure 3.13..

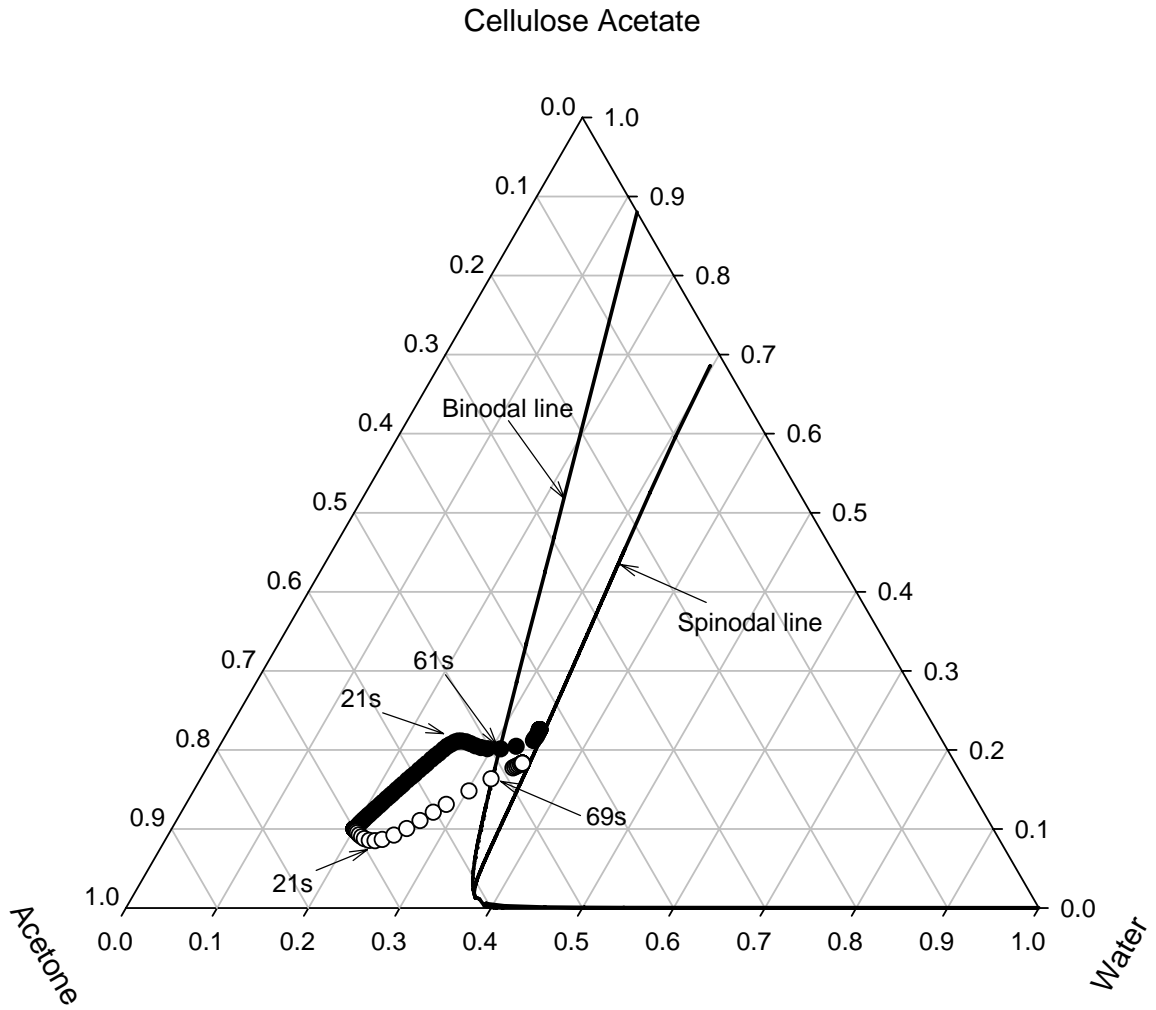


Figure 3.10: Concentration change of liquid-gas interface (●) and solid-liquid interface (○) during the dry-cast membrane formation process for casting solution 3.

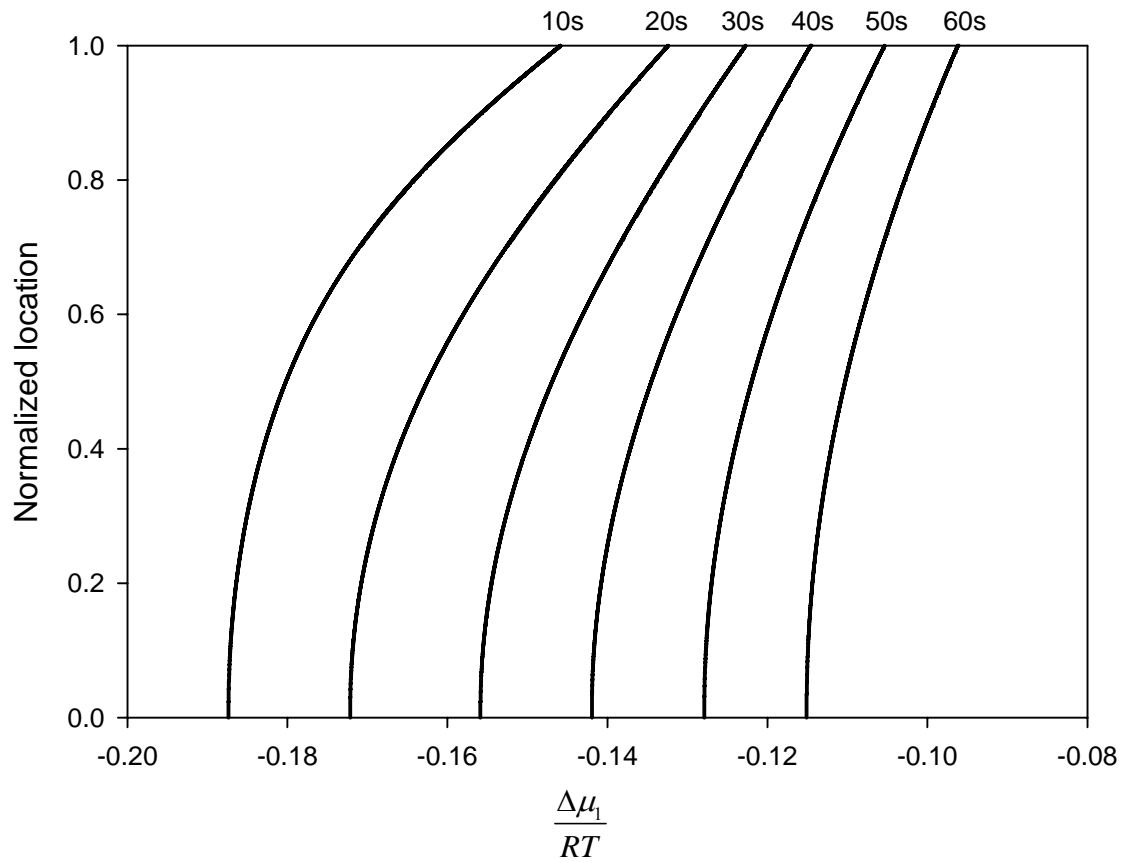


Figure 3.11: Chemical potential profile change of water in the casting solution during dry-casting process for solution 3.

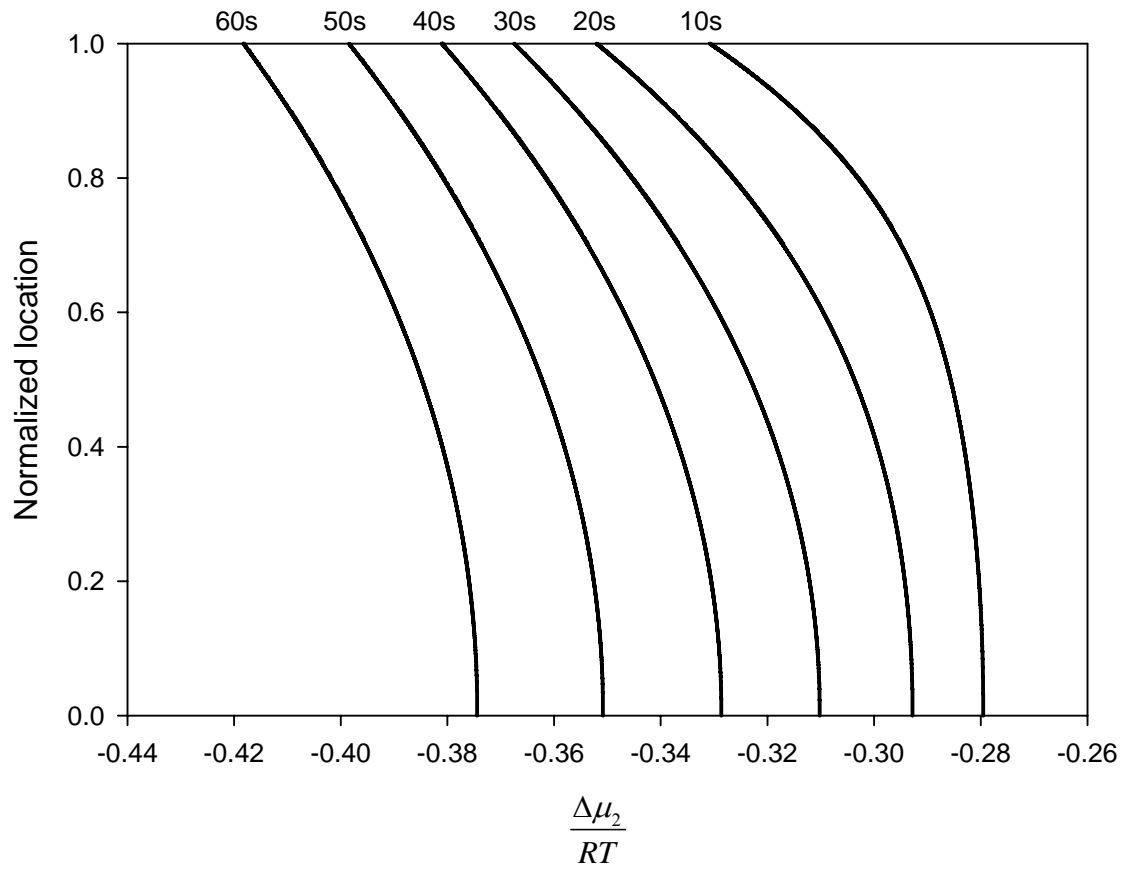


Figure 3.12: Chemical potential profile change of acetone in the casting solution during the dry-casting process for casting solution 3.

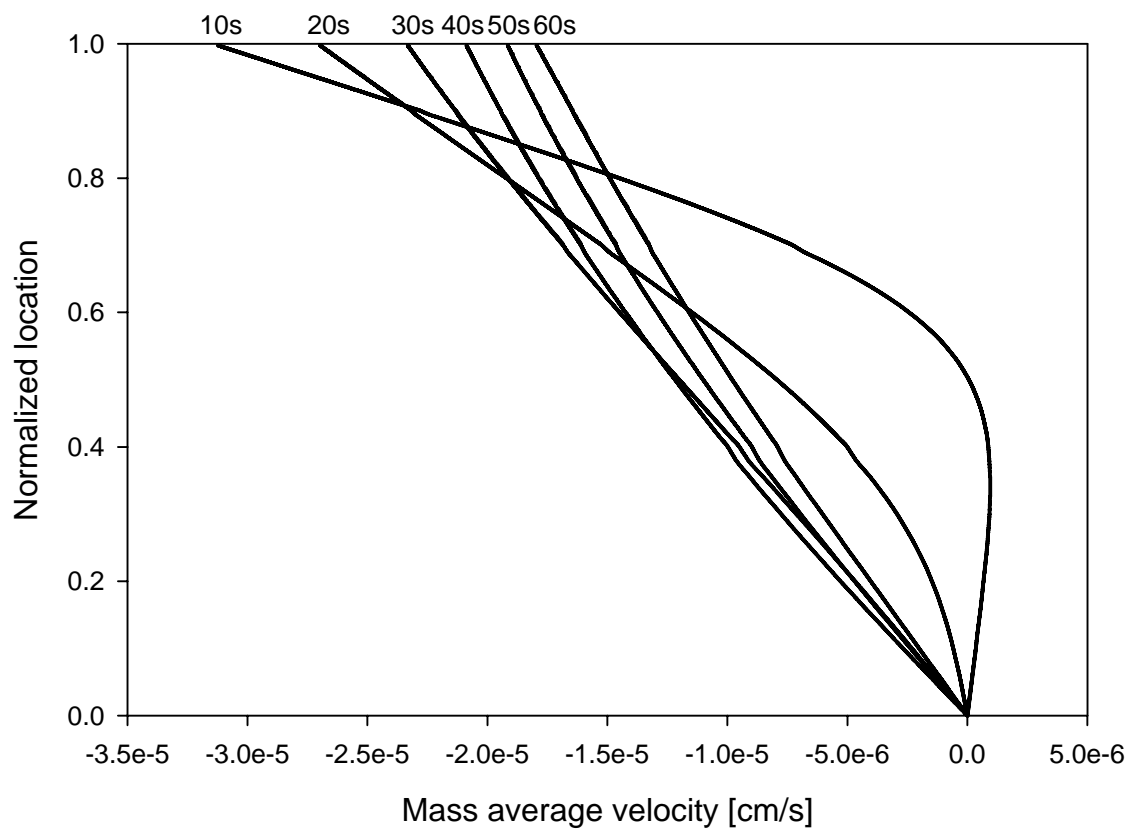


Figure 3.13: Mass-average velocity in the casting solution during the dry-casting process for casting solution 3.

3.8 Discussion of Results

Successful validation of any mathematical model depends on rigorous quantitative corroboration with pertinent experimental data. Shojaie et al. [31] performed sophisticated experimental analysis involving dry-cast membrane formation using various CA/acetone/water systems. In particular, they measured the instantaneous mass and surface temperature of the casting solutions. The detailed description of equipment, measurement techniques and experimental procedures can be found in their 1990 study [31].

3.8.1 Corroboration with Membrane Morphology

To compare the results of the pure-diffusion model of Shojaie et al. and our convection-diffusion model, the composition paths predicted by both models are plotted on the same ternary diagram for each casting solution (Figure 3.14-3.16). Although the composition paths of both models appear quite similar, our convection-diffusion model predicts faster concentration changes. Thus, it takes less time to cross the binodal. This is in accordance with the experimental results on the time of onset for phase separation as discussed in Section 3.8.2.

For casting solution 1 (Figure 3.14), both models show that neither the top (liquid/gas interface) nor bottom (liquid/solid interface) compositions cross the binodal into the two-phase region. Thus, this initial composition is expected to solidify or vitrify rather than phase-separate, resulting in a dense polymeric film instead of a porous membrane. This is verified by the nonporous polymeric film that was obtained by Shojaie et al. [29] using the same initial condition.

In contrast, the composition paths having a higher initial weight fraction of water (casting solutions 2 and 3) cross the binodal into the two-phase region as shown in Figures 3.15 and 3.16. In the experiments an asymmetric structure was obtained using casting solution 2 (Figure 3.15), while with casting solution 3 (Figure 3.16) the resulting membrane structure was symmetric. Shojaie et al. explained that the high concentration gradient of polymer when the composition of the casting solution 3 crosses the binodal results in a denser structure of membrane near the liquid/gas interface side. However, casting solution 2 also has a noticeable concentration gradient of polymer when it crosses the binodal, as shown in Figure 3.16. However, our convection-diffusion model predicts an even larger concentration gap. More importantly, in addition to the larger concentration gap, the liquid-gas interface crosses the binodal before that of the liquid-solid (Figure 3.16). For casting solution 2, Figure 3.15 suggests simultaneous phase separation throughout the entire casting solution. Note that in practice the predictions of both our model and that of Shojaie et al. are valid only until phase separation occurs, because phase separation introduces multi-dimensional transport phenomena that are not incorporated in our model. Also, the phase separation at the liquid/gas interface might affect the transport phenomena. However, one may assume decreasing flux through the phase-separated solid structure to the gas phase. The low flux at the boundary may allow a well-mixed condition of the liquid casting solution below the solidified liquid/gas interface. Thus, the casting solution below the solidified liquid-gas boundary might cross the two-phase boundary as a homogeneous solution, resulting in a symmetric structure of the final membrane. On the other hand, the instantaneous concentration gradient of

polymer in the entire casting solution when it reaches the bimodal as shown in Figure 3.17 explains the asymmetric morphology of the membrane.

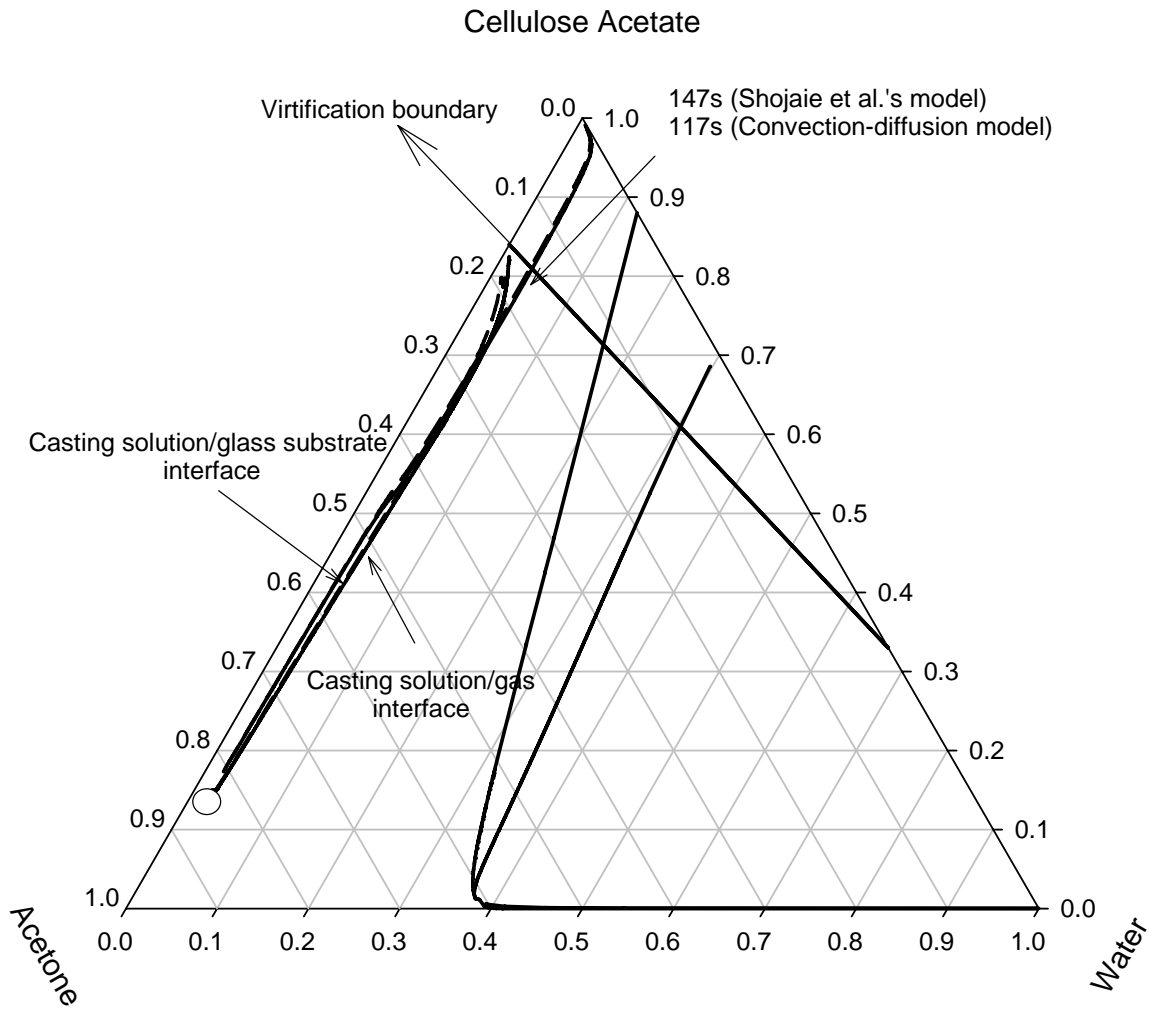


Figure 3.14: Concentration paths for the liquid-gas interface and the solid-liquid interface predicted by the convection-diffusion model (solid lines) and Shojaie et al's diffusion model (dashed line) during the dry-cast membrane formation process for casting solution 1.

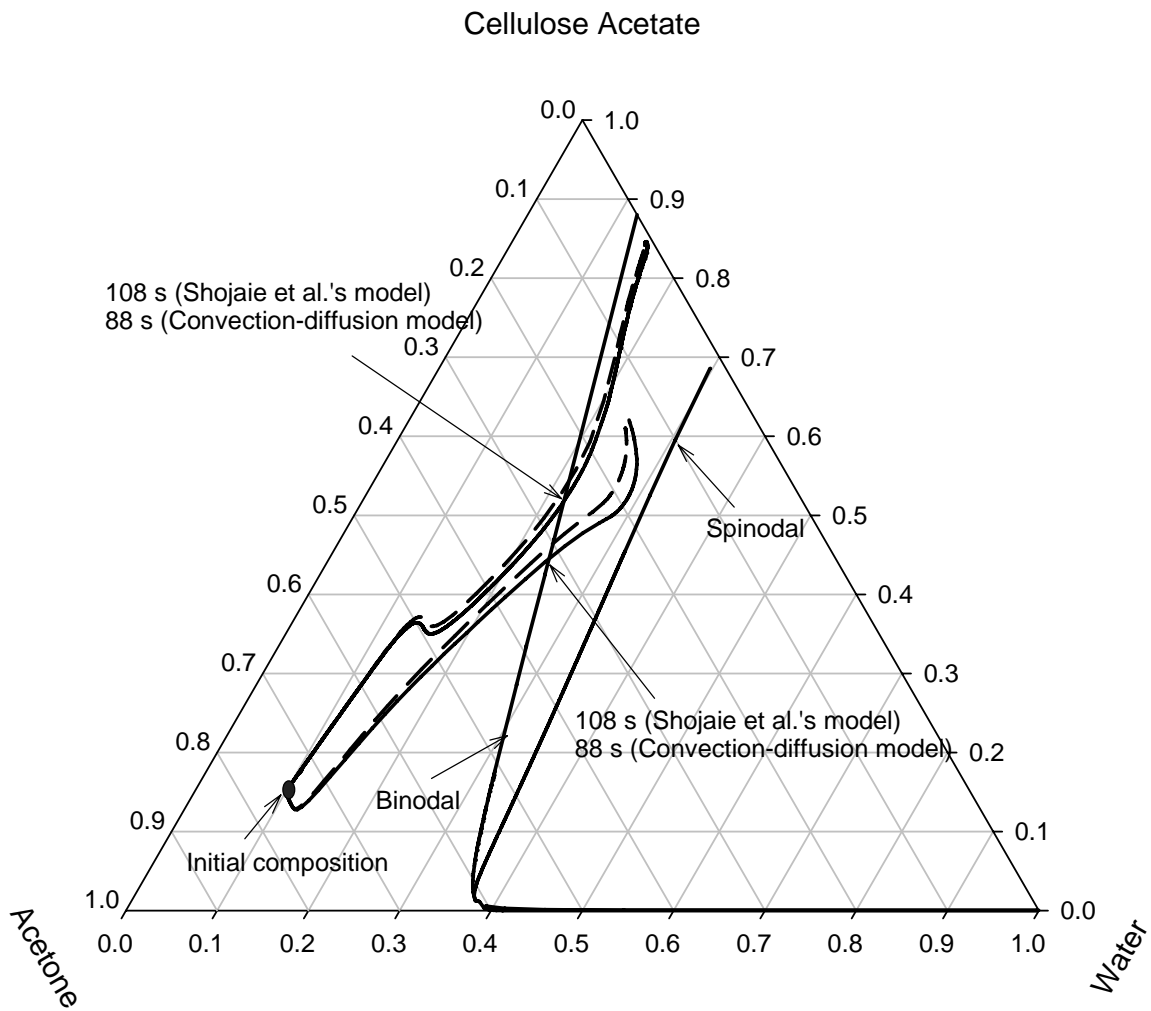


Figure 3.15: Concentration paths for the liquid-gas interface and the solid-liquid interface predicted by the convection-diffusion model (solid lines) and Shojaie et al's diffusion model (dashed line) during the dry-cast membrane formation process for casting solution 2.

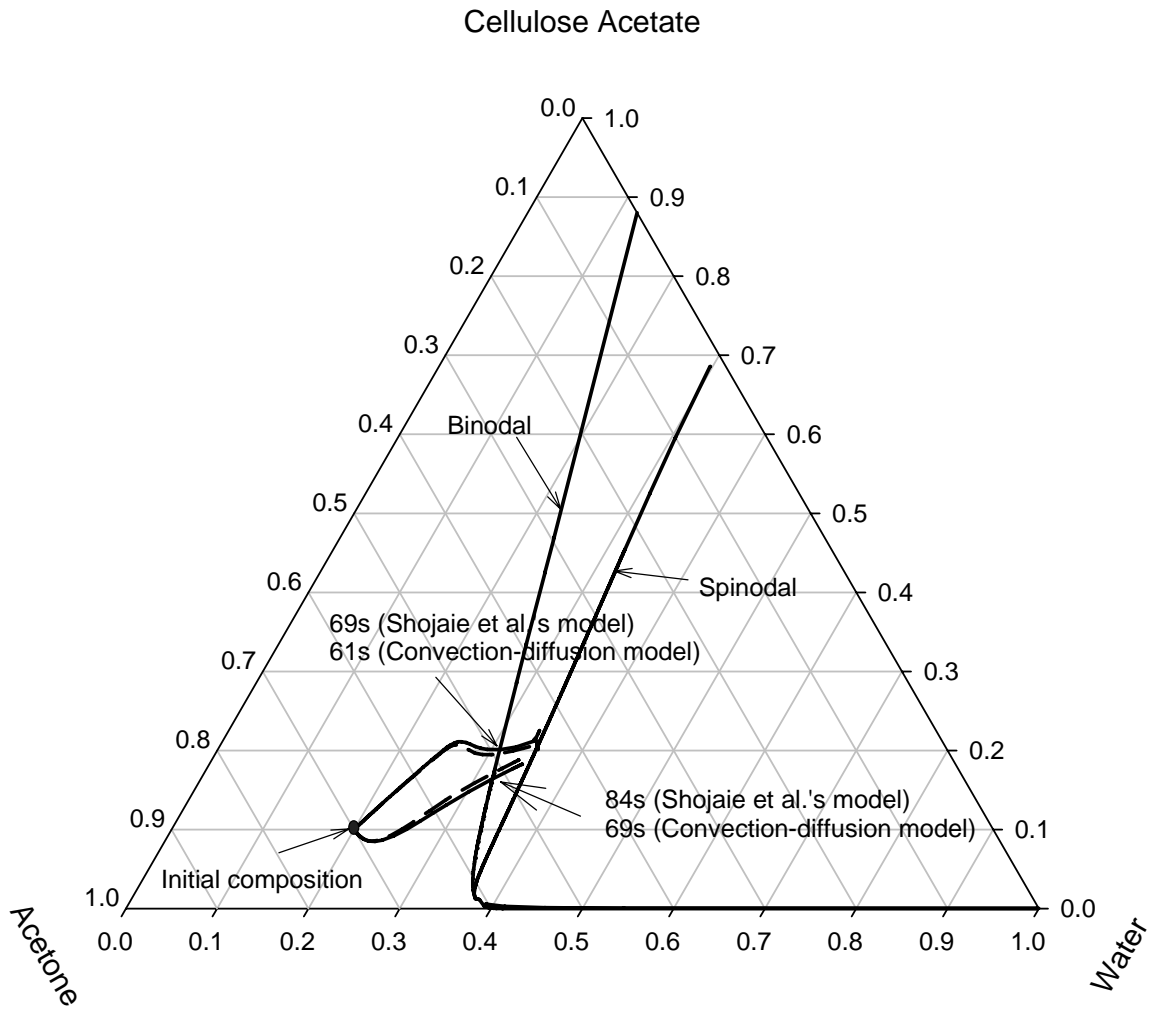


Figure 3.16: Concentration paths for the liquid-gas interface and the solid-liquid interface as predicted by the convection-diffusion model (solid lines) and Shojaie et al.'s diffusion model (dashed line) during the dry-cast membrane formation process for casting solution 3.

3.8.2 Corroboration with Light-Reflection Measurements

Shojaie et al. [31] reported the experimental onset time for phase separation that was determined via light–reflection measurements; the diffraction of the incident light is indicative of droplet formation. Since a droplet must have a certain minimum size to be detectable, the measured is always greater than the actual onset time for demixing. Table 2 summarizes model predictions and the measured onset time for demixing for casting solutions 2 and 3. For both casting solutions the convection-diffusion model predicts faster demixing than observed experimentally, whereas Shojaie’s diffusion model overpredicts the onset time for demixing. Therefore, it is clear that the convection-diffusion model results can predict the onset time for phase separation more accurately.

Shojaie et al.’s experimental data also provide information on the duration of demixing. Casting solution 2 results in a very steep change of the light intensity, thereby indicating an instantaneous phase separation throughout the entire casting solution. The data for casting solution 3 indicate a gradual change in light intensity, indicating that phase separation is a slower process, with different parts of the casting solution phase-separating at different times. These results support our contention that the difference in time for the top and bottom of the casting solution 2 to cross the binodal leads to a symmetric structure in the final membrane, whereas the simultaneous phase-separation such as was observed with casting solution 3 leads to an asymmetric membrane.

Table 3.2: Predicted and measured time for the onset of phase-separation [12]

Initial casting solution	Shojaie's diffusion Model	Convection-diffusion model	Experimental data [31]
2	108 s	88s	90 s
3	69 s	61 s	68 s

3.8.3 Corroboration with Surface Temperature and Total Solution Mass

Shojaie et al. [31] measured the instantaneous solution mass during evaporative casting using a microbalance. Figures 3.17-19 compare the predictions of the new model developed here that incorporates convection and the experimental results of Shojaie et al. [31] for the total casting solution mass as a function of time for casting solutions 1, 2, and 3, respectively. Predictions of the new model for all three representative cases of the casting condition show a good agreement with the experimental instantaneous casting-solution mass data. The prediction for the total solution mass displayed the deviation less than 0.03g from the experimental data for all three cases.

Shojaie et al. [31] used an infrared thermographic imaging camera to measure the temperature of the surface region of the casting solution. It is important to note that this technique does not measure the temperature of the liquid/gas interface, but the average temperature of a thin region (typically a few tens of microns) near the surface [31]. Figures 3.20-22 compare the predictions of the new model developed here that incorporates convection and the experimental results of Shojaie et al. [31] for the temperature of the liquid/gas interface as a function of time for casting solutions 1, 2, and 3, respectively. The maximum deviations of predictions from the measured surface temperature were 3.0 °C for the casting solution 1, 4.2 °C for the casting solution 2, and 3.4 °C for the casting solution 3. Considering that the model of Shojaie et al. [31] underpredicted the surface temperature as much as 7 °C, these are appreciably better results.

Although model predictions agree reasonably well with experimental data, it should be also noted that the underprediction of the surface temperature is consistent with the slight overprediction of mass loss as shown in Figures 3.17-19; larger evaporative mass loss promotes the evaporative cooling more. Shojaie et al. [31] explained these consistent deviations by the fact that the free-convection boundary layer in the gas phase is thicker above the later center of the casting solution. However, the lumped-parameter approach employed in the gas-phase model assumes the boundary-layer thickness average in space. Therefore, the local surface temperature measured above the center of the casting solution might be higher than the instantaneous average surface temperature which model predicts.

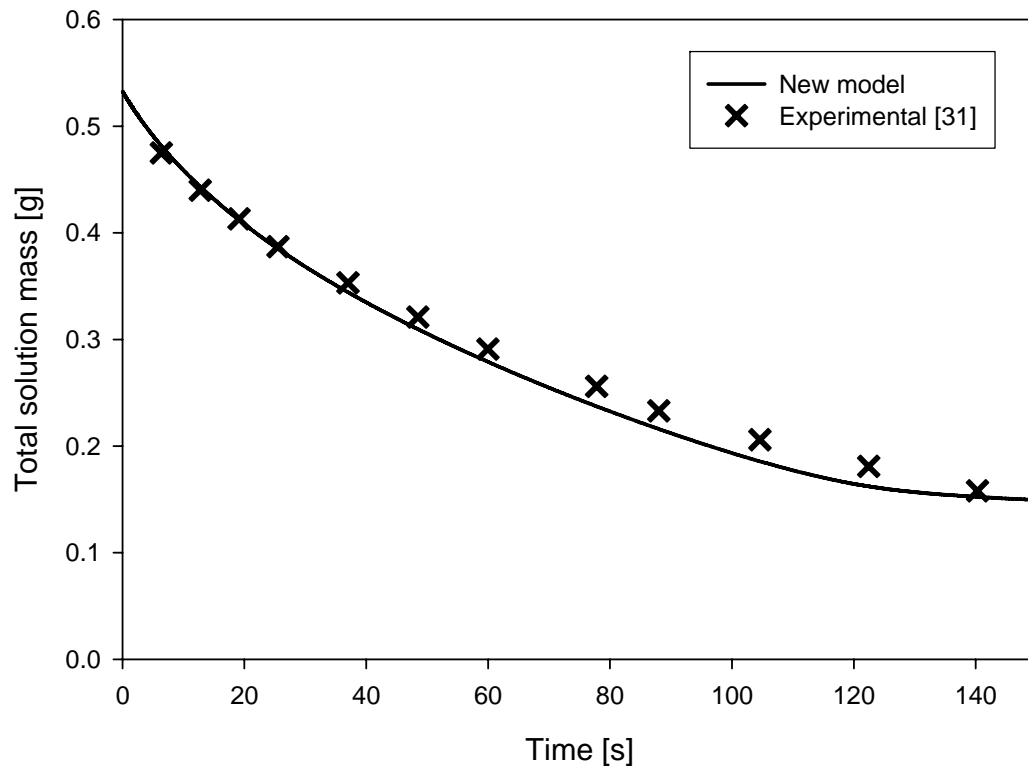


Figure 3.17: Predicted (—) and measured (X) total casting solution mass as a function of time for casting solution 1 in Table 3.1.

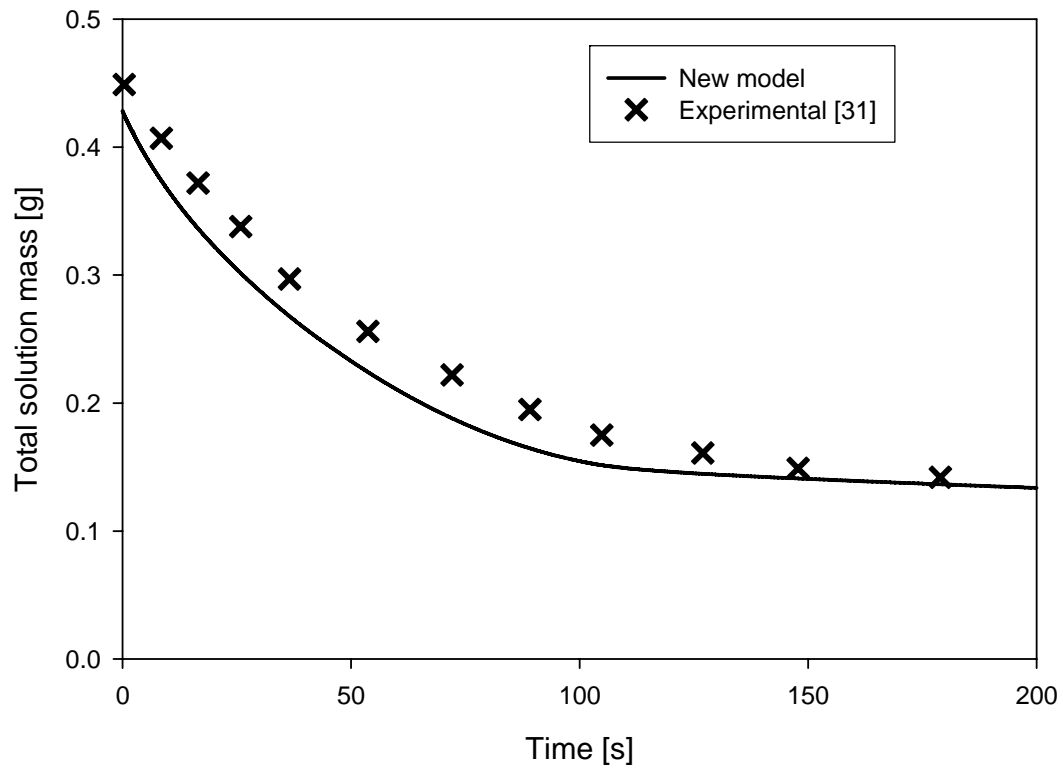


Figure 3.18: Predicted (—) and measured (X) total casting solution mass as a function of time for casting solution 2 in Table 3.1.

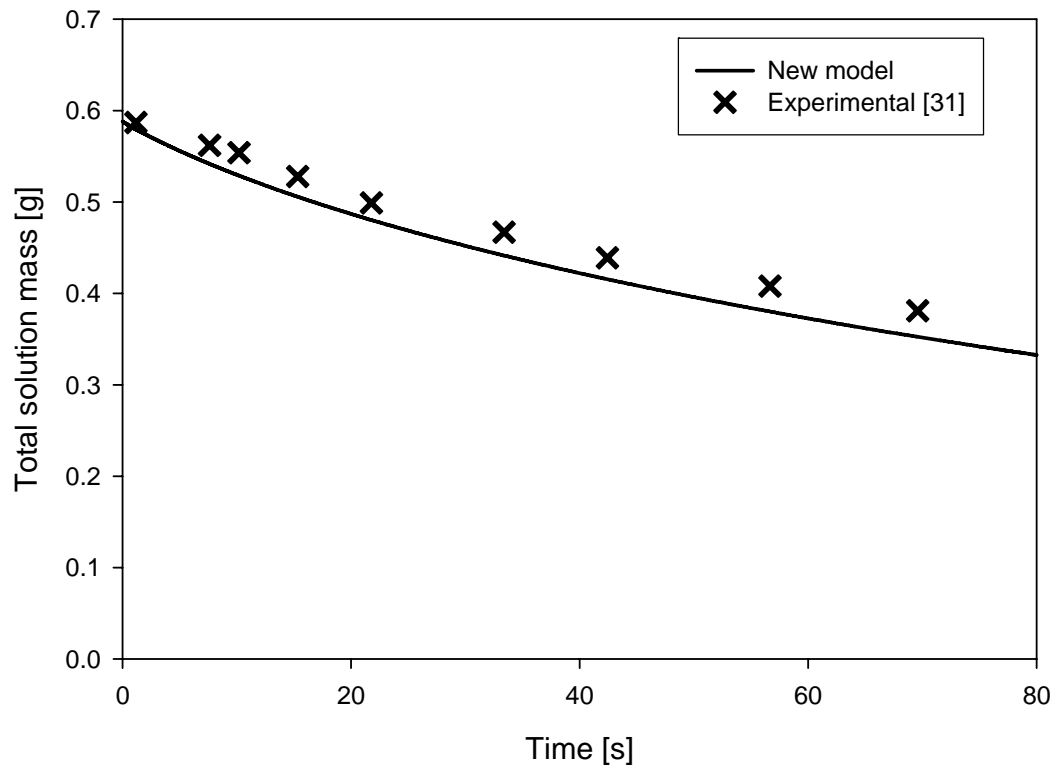


Figure 3.19: Predicted (—) and measured (X) total casting solution mass as a function of time for casting solution 3 in Table 3.1.

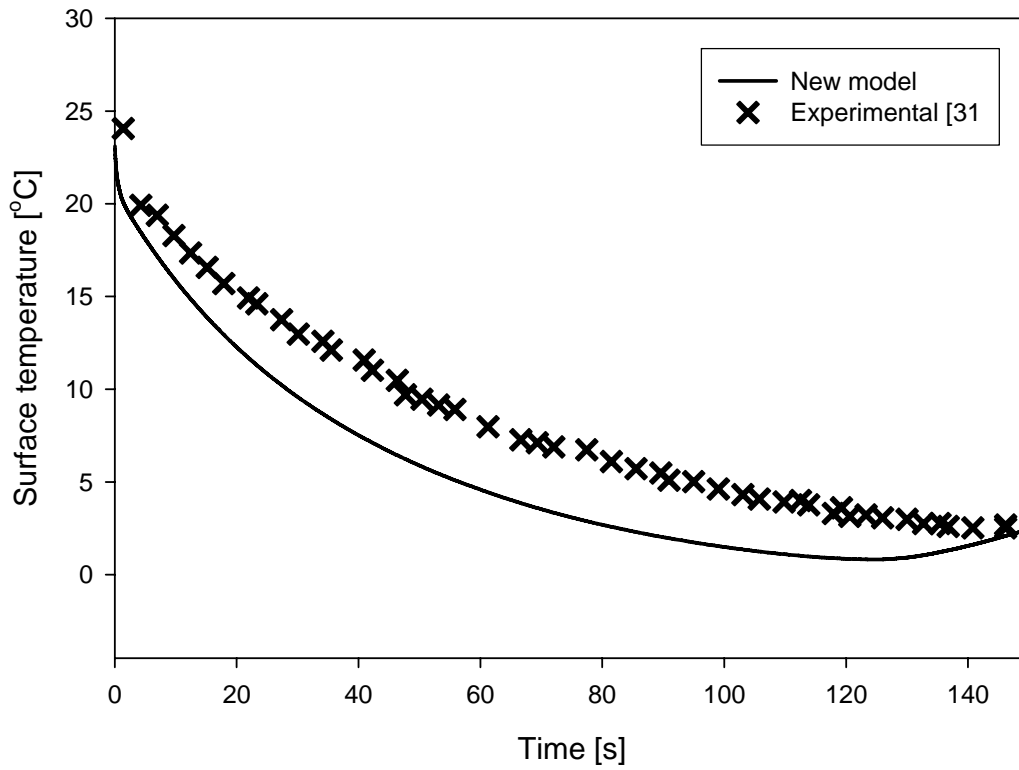


Figure 3.20: Predicted (—) and measured (×) temperature of the liquid/gas interface as a function of time for casting solution 1 in Table 3.1.

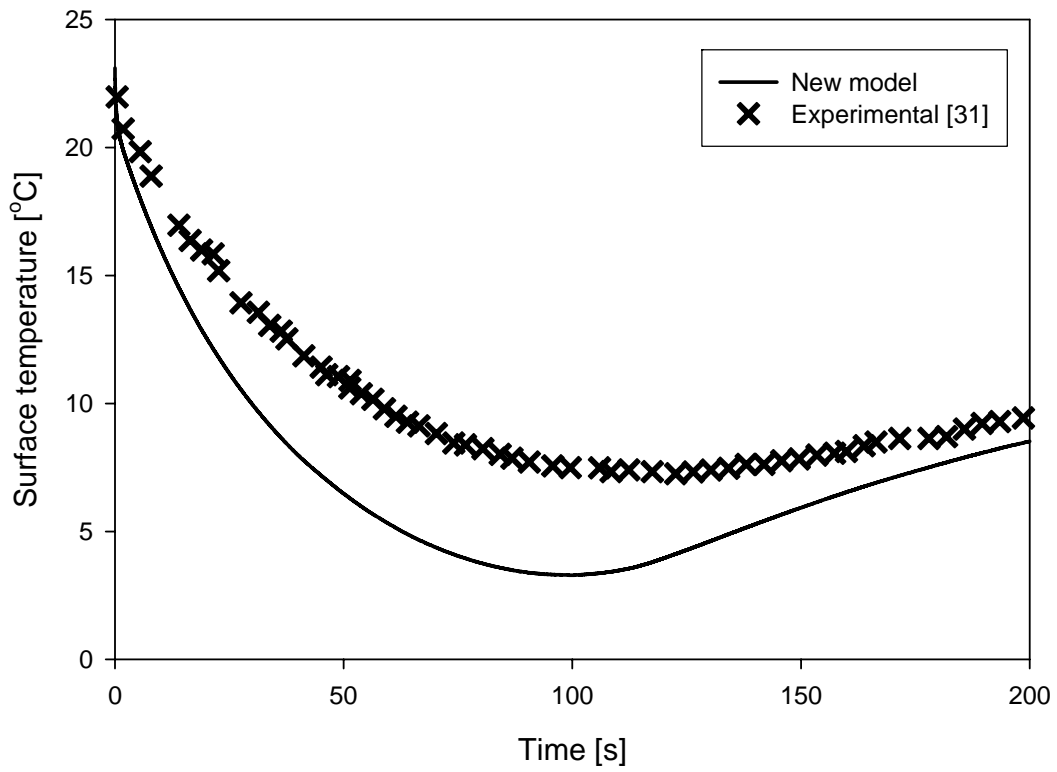


Figure 3.21: Predicted (—) and measured (×) temperature of the liquid/gas interface as a function of time for casting solution 2 in Table 3.1.

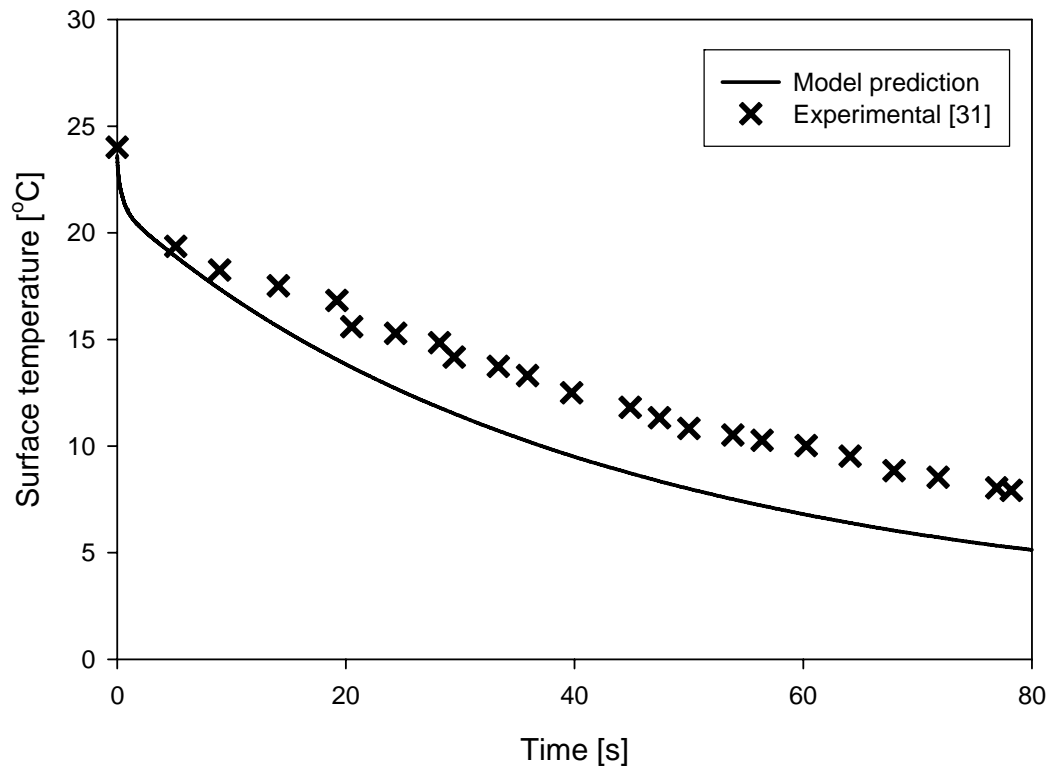


Figure 3.22: Predicted (—) and measured (X) temperature of the liquid/gas interface as a function of time for casting solution 3 in Table 3.1.

3.8.4 Modified Peclet Number

In all the previous dry-casting models discussed, the convective contribution to the mass flux has been neglected. This was explicitly referred to by Shojaie et al. [29, 30] as a ‘low Peclet number’ assumption. However, more accurate terminology would be a ‘low modified Peclet number’, since the convective and the diffusive mass fluxes are parallel. (Refer to Section 2.5.4 of this work.) Since the ternary diffusion coefficient data for the CA/acetone/water system are not available, the modified Peclet number was determined corresponding to the ratio of instantaneous convective and diffusive fluxes. Figure 3.25 shows that the modified Peclet number of acetone at the liquid/gas interface is highest when the casting solution is exposed to air and then decays progressively. The modified Peclet number indicates that neglecting the convective contribution will incur an initial error close to 35%. Also, the modified Peclet number is largest at the top of the casting solution due to the gradients being steepest at the liquid–gas interface. This is precisely where and when the convective mass flux is extremely important since it will have a strong influence on the formation of the functional layer and thereby will dictate the separation characteristics of the resulting membrane. Also, it should be noted that a negative modified Peclet number indicates a progressively denser casting solution due to the evaporation of the lighter components (acetone and water).

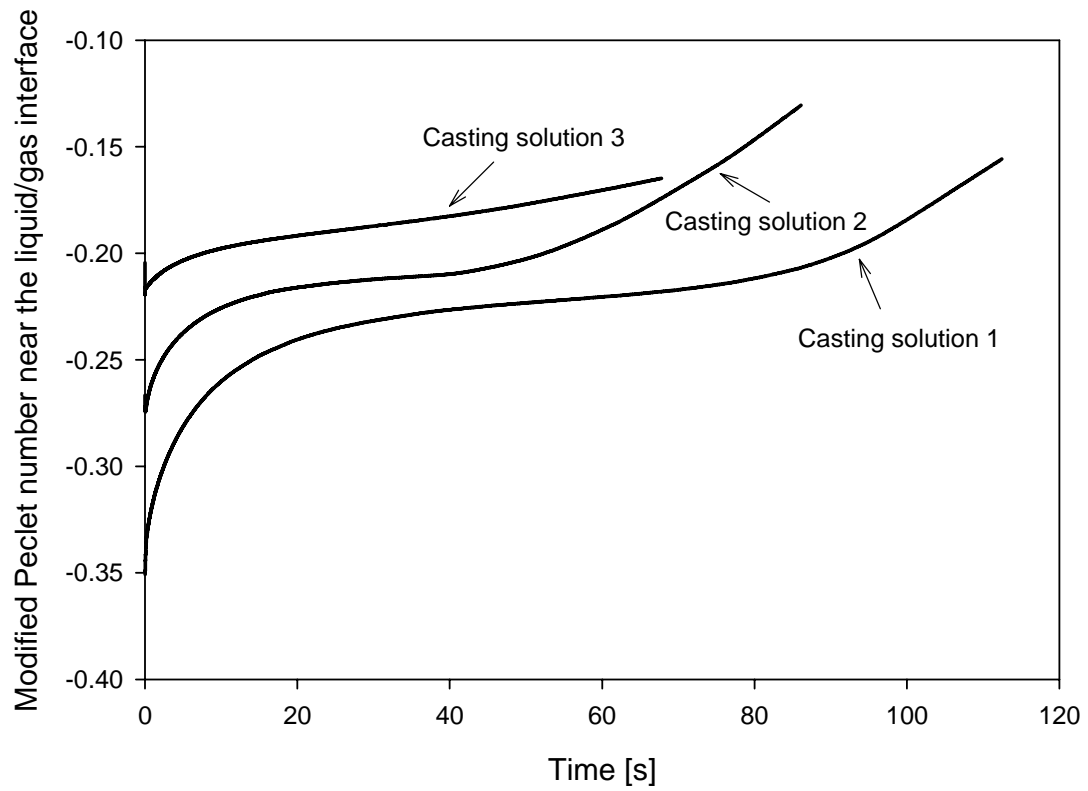


Figure 3.23: Modified Peclet number of acetone near the gas/casting solution interface as a function of time for casting solutions 1, 2, and 3.

3.9 Summary

The mathematical model for dry-casting presented in this chapter is the first model incorporating both convection and diffusion. In our model we combine the equation-of-continuity and the equation-of-state based on a zero volume-of-mixing assumption to obtain an explicit equation of the mass-average velocity for the convection term. Incorporation of this convective contribution in the heat- and mass-transfer model equations makes our model more accurate. The model predictions, particularly for the onset of the phase separation and the surface temperature, show much better agreement with the experimental data than the diffusion model does. This also provides some confidence that this formalism for incorporating the convective mass flux can be used in modeling studies for other membrane formation processes such as the wet-casting process.

CHAPTER IV
DEVELOPMENT OF THE WET-CASTING MODEL INCORPORATING
CONVECTIVE TRANSPORT

4.1 Scope of the Chapter

In this chapter, a wet-casting model incorporating convective transport is presented. The mass-transfer and the thermodynamic models developed for the dry-casting process model can be adapted to a wet-casting process model by consideration of the very rapid mass transfer through the interface between the casting solution and nonsolvent bath. Since the concentration gradient in general will be much steeper for wet-casting, we can expect a larger convective contribution to the mass flux. In this chapter we will establish that a model incorporating the convective contribution yields a more accurate description of effects of the initial casting solution thickness on the wet-casting process. However, it should be noted that our wet-casting model is a fully predictive model and applicable to any ternary casting solution system if the requisite model parameters are known.

The organization of this chapter is as follows. After a short introduction to the wet-casting process, a review of prior modeling studies is presented. The motivation of this study follows. Then, the model development and the solution methodology are presented. Corresponding experimental results are presented and discussed next. A summary is presented at the end of this chapter.

4.2 Introduction

The ‘wet-casting process’, which is also referred as ‘immersion precipitation’, is the most widely used phase-inversion method used by industry for polymeric membrane formation. In the wet-casting process a homogeneous polymer solution is prepared with polymer and solvent (and occasionally nonsolvent) and cast into a thin film or hollow fiber geometry. The cast film or fiber then might be allowed to undergo solvent evaporation for a finite period in a manner similar to the dry-casting process. The film is then immersed in a precipitation bath of nonsolvent that causes rapid mass transfer. Due to the concentration difference, the solvent is transferred from the film to the bath, while the nonsolvent is transferred from the bath to the film. As a result, the local composition at any point changes with the time. However, measuring this local composition as a function of time and position is not possible due to the very rapid change in the small thickness of the casting solution [45]. Therefore, a rigorous model is essential to provide good insight into the influence of various parameters on the structure and performance of a membrane.

4.3 Review of Prior Studies

The first attempt to model the wet-casting process was made by Cohen et al. [46]. Their description of the mass-transfer process was based on a steady-state diffusion model. Several researchers [47, 48] have pointed out that this assumption is not appropriate.

Yilmaz and McHugh [48] improved on this model by using unsteady-state pseudo-binary diffusion formalism. Their governing equations are simplified by assuming zero polymer flux in the casting solution and negligible bath dynamics.

Reuvers et al. [49, 50] further improved on the previous models by coupling the bath dynamics and the diffusion in the casting solution. They utilized the phenomenological approach based on non-equilibrium thermodynamics to describe the coupling effect of diffusion. However, an infinitely thick casting solution is assumed to rationalize the diffusion-only model. The equal flux condition at the interface between the casting solution and coagulation bath in their model is also valid only when the thickness of a casting solution does not change. They further claim that the measured onset time for phase separation shows close agreement with their model prediction. However, since their model assumed that the interfacial composition of the casting solution is already placed on the binodal initially, their model prediction does not predict anything about the onset time for phase separation. However, to validate their approximation of the top boundary condition fixed on the binodal, the phase-separation should start immediately rather than after the relatively longer time (several seconds) detected by their experiments.

Tsay and McHugh [51] improved on Reuvers' model by allowing for a variable interfacial composition with time. However, their model also makes the assumption of equal flux at the interface. Thus, the manner in which the composition at the interface between the casting solution and coagulation bath changes from the initial condition to the being on the binodal was not considered. Their predictions indicated that the polymer concentration decreased and solvent concentration increased at the interface. However,

Kesting [5] reported a strong polymer accumulation at the interface, which occasionally will lead to skin formation at the interface. Furthermore, the final membrane thickness, which is usually thinner than the initial casting solution, indicates that the solvent flux into the coagulation bath is larger than the nonsolvent flux into the casting solution. In turn, solvent molecules near the top interface in the casting solution move much faster than nonsolvent molecules penetrating into the casting solution. Since the diffusivity of the solvent in the nonsolvent bath is much higher than that in the casting solution, solvent molecules have little chance to stay near the interface in the coagulation bath. Thus, it is hard to explain the accumulation of solvent at the both sides of the interface in their model prediction. They also claim that the volume-average velocity should be zero at any location in a casting solution; thereby, there is no convective contribution. However, this is valid only when the pure densities of all the species are the same. Details on the volume-average velocity are given in Appendix C.

Radovanovic et al. [52, 53] showed that the description of diffusion in the bath given by Reuvers is in error and proposed a modified version of the model. With their diffusion model and experimental results, they showed that the structure of a polysulfone membrane strongly depends on the onset time of demixing.

Cheng et al. [54] further modified Reuvers' model by allowing for a finite thickness for the casting solution. Although an advanced numerical method is used in their calculations, their neglect of the convective contribution results in no densification of the casting solution, regardless of the densities of the exchanging components used in the process.

Recently, Fernandes et al. [55] presented a simple mathematical model using the Fickian diffusion equation to describe the wet-casting process. In spite of utilizing their advanced numerical calculation method, their model is too simplified since it neglects the coupling effects of diffusion and assumes an ideal solution.

4.4 Motivation for this Study

The very high accumulation of polymer observed experimentally near the interface and the very fast mass-transfer dynamics imply a potentially very large contribution of convection due to densification in the wet-casting process. Also the change in the casting-solution thickness is strongly associated with densification and convection. Therefore, an accurate wet-casting model must incorporate both diffusive and convective contributions, especially when studying the effect of the initial casting-solution thickness.

The morphology of the upper surface of a membrane is determined by the interfacial concentration at the time of phase separation. In prior models, the interfacial local equilibrium concentration is calculated assuming no change in the thickness of the casting solution, thus completely ignoring the interfacial composition change from the initial composition to the binodal. A better description of this process is needed to understand the formation of the top functional layer that controls the permselectivity properties of the final membrane.

4.5 Model Development

4.5.1 System of Interest

The target system for the simulation is an idealized mass-transfer model of the wet-casting process as shown in Figure 4.1. This involves casting a ternary polymer solution having uniform initial thickness L_0 into an infinitely thick pure nonsolvent bath. The casting solution is assumed to be homogeneous before the initiation of the wet-casting process.

At time $t = 0$, the species in both the casting solution and the coagulation bath begin to move corresponding to their respective driving forces. The mass transfer is assumed to be one-dimensional both to simplify the model and to represent typical commercial wet-casting conditions. The solvent loss along with nonsolvent gain in the casting solution leads to a change in the local composition as well as the instantaneous thickness of the casting solution, $L(t)$. The pure nonsolvent coagulation bath also starts absorbing solvent from the casting solution. Since the polymer solubility in a nonsolvent bath is very low, the movement of a polymer molecule into the nonsolvent bath is negligible. However, it should be noted that polymer molecules can move in the casting solution. To calculate the interfacial fluxes, one needs to know the local concentrations at the both sides of the interface. The most reasonable assumption for the upper interface is that the transferring components are in local thermodynamic equilibrium. If polymer cannot diffuse into the bath, the coagulation bath will always be at most a binary solution of nonsolvent and solvent. Under this condition, it is necessary to demand that the chemical potentials of only one of the three components in the casting solution be equal

at the upper interface. Note that non-ideal solution behavior in both phases should be considered in this equilibrium condition. Surprisingly, all previous studies in the literature have ignored the process whereby the concentration of the upper interface changes from the initial non-equilibrium composition to some equilibrium value on the binodal.

As the mass transfer proceeds, the local compositions in the casting solution and in the nonsolvent bath change. Eventually, the local composition at the casting solution / nonsolvent bath interface will reach the binodal. After this moment until vitrification or phase separation occurs, the local equilibrium concentration at the interface can be calculated by a tie line from the Flory-Huggins lattice model.

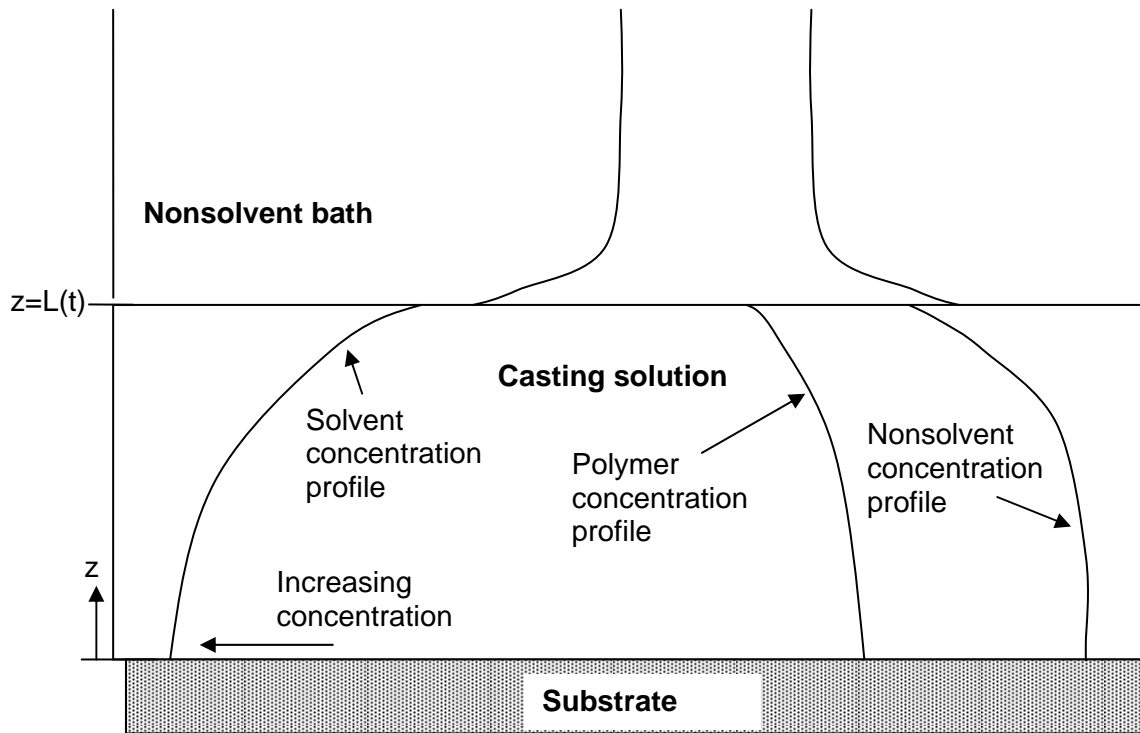


Figure 4.1: Schematic representation of wet-casting process for membrane formation.

4.5.2 Thermodynamic Model

The need for a thermodynamic model is discussed in the previous chapter. The thermodynamic model developed for the dry-casting process based on Flory-Huggins theory is also valid for the wet-casting process.

4.5.3 Mass-Transport Model in Casting Solution

4.5.3.1 Governing Equations

This study considers a ternary casting solution that is composed of nonsolvent (1), solvent (2), and polymer (3). Since the same ternary system is used in the dry-casting model, equations 3.18 and 3.19 are also suitable for the final governing mass-transport equations for the wet-cast model.

4.5.3.2 Initial and Boundary conditions

The homogeneous composition of the casting solution before the process begins dictates the following initial condition:

$$\omega_1 = \omega_1^{\circ}, \quad \omega_2 = \omega_2^{\circ} \quad \text{at} \quad t = 0 \quad (4.1)$$

Since there is an impermeable support at the bottom of the casting solution, the boundary condition at $z = 0$ is

$$\frac{\partial \omega_1}{\partial z} = 0, \quad \frac{\partial \omega_2}{\partial z} = 0 \quad \text{at} \quad z = 0 \quad (4.2)$$

In order to determine the boundary conditions at $z = L(t)$, the density of the nonsolvent bath must be considered in the wet-casting model since the overall mass densities of the two liquid phases are similar, although the density of the ambient gas of which the mass

density is much less than that of the casting solution was ignored in the dry-casting model. Furthermore, the nonsolvent bath can swell by absorbing solvent with a lower density. Considering the density variation of a nonsolvent bath, An overall mass balance for the nonsolvent that incorporates the effect of possible density variation in the coagulation bath is given by the following:

$$\frac{d}{dt} \int_{z=0}^{z=L(t)} \rho_1 dz + \frac{d}{dt} \int_{z=L(t)}^{z=\infty} \rho_1^B dz = 0 \quad (4.3)$$

Here and elsewhere in this thesis, the superscript B indicates a property in the nonsolvent bath. The first and second term in the above equation represent the accumulation of mass in the casting solution and nonsolvent bath, respectively. The overall conservation-of-mass dictates that sum of these two terms is zero. Applications of Leibnitz rule-of-differentiation to both terms yields

$$\int_{z=0}^{z=L(t)} \left(\frac{d\rho_1}{dt} \right) dz + \rho_1 \Big|_{z=L(t)} \frac{dL}{dt} + \int_{z=L(t)}^{z=\infty} \left(\frac{d\rho_1^B}{dt} \right) dz - \rho_1^B \Big|_{z=L(t)} \frac{dL}{dt} = 0 \quad (4.4)$$

Simplifying the above using the conservation-of-species equation (equation 2.4) for the nonsolvent then results in the following equation:

$$\frac{dL}{dt} = \left(\frac{n_1 - n_1^B}{\rho_1 - \rho_1^B} \right) \Big|_{z=L(t)} \quad (4.5)$$

The flux of nonsolvent in the casting solution is the sum of diffusive and convective contributions as follows:

$$n_1 = j_1 + \omega_1 \rho W \quad (4.6)$$

Combining equations (3.4), (3.17) and (4.6) yields

$$n_1 = \left\{ 1 - \rho \omega_1 \left(\frac{1}{\rho_1^\circ} - \frac{1}{\rho_3^\circ} \right) \right\} \left(f_1 \frac{\partial \omega_1}{\partial z} + g_1 \frac{\partial \omega_2}{\partial z} \right) - \rho \omega_1 \left(\frac{1}{\rho_2^\circ} - \frac{1}{\rho_3^\circ} \right) \left(f_2 \frac{\partial \omega_1}{\partial z} + g_2 \frac{\partial \omega_2}{\partial z} \right) \quad (4.7)$$

From Equations (4.5) and (4.7) the following boundary condition at $z = L(t)$ for nonsolvent can be obtained.

$$\begin{aligned} (\rho_1 - \rho_1^B) \frac{dL}{dt} = & \left\{ 1 - \rho \omega_1 \left(\frac{1}{\rho_1^\circ} - \frac{1}{\rho_3^\circ} \right) \right\} \left(f_1 \frac{\partial \omega_1}{\partial z} + g_1 \frac{\partial \omega_2}{\partial z} \right) \\ & - \rho \omega_1 \left(\frac{1}{\rho_2^\circ} - \frac{1}{\rho_3^\circ} \right) \left(f_2 \frac{\partial \omega_1}{\partial z} + g_2 \frac{\partial \omega_2}{\partial z} \right) - n_1^B \end{aligned} \quad (4.7)$$

A similar development leads to the boundary condition at $z = L(t)$ for the solvent:

$$\begin{aligned} (\rho_2 - \rho_2^B) \frac{dL}{dt} = & -\rho \omega_2 \left(\frac{1}{\rho_1^\circ} - \frac{1}{\rho_3^\circ} \right) \left(f_1 \frac{\partial \omega_1}{\partial z} + g_1 \frac{\partial \omega_2}{\partial z} \right) \\ & + \left\{ 1 - \rho \omega_2 \left(\frac{1}{\rho_2^\circ} - \frac{1}{\rho_3^\circ} \right) \right\} \left(f_2 \frac{\partial \omega_1}{\partial z} + g_2 \frac{\partial \omega_2}{\partial z} \right) - n_2^B \end{aligned} \quad (4.8)$$

4.5.3.3 Displacement of the Casting Solution/Nonsolvent Bath Interface

The boundary conditions described in the previous section require the interfacial displacement velocity, $\frac{dL}{dt}$. Applying the Leibnitz rule-of-differentiation to the total mass-balance equation yields

$$\frac{dL}{dt} = \left. \left\{ \frac{\rho W - (n_1^B + n_2^B)}{\rho - \rho^B} \right\} \right|_{z=L(t)} \quad (4.9)$$

From equations (3.4), (3.17), and (4.9) the following ordinary differential equation is obtained for locating the position of the interface:

$$\begin{aligned}
(\rho - \rho^B) \Big|_{z=L(t)} \frac{dL}{dt} = & - \left\{ \rho \left(\frac{1}{\rho_1^\circ} - \frac{1}{\rho_3^\circ} \right) \left(f_1 \frac{\partial \omega_1}{\partial z} + g_1 \frac{\partial \omega_2}{\partial z} \right) \right\} \Big|_{z=L(t)} \\
& - \left\{ \rho \left(\frac{1}{\rho_2^\circ} - \frac{1}{\rho_3^\circ} \right) \left(f_2 \frac{\partial \omega_1}{\partial z} + g_2 \frac{\partial \omega_2}{\partial z} \right) \right\} \Big|_{z=L(t)} - (n_1^B + n_2^B) \Big|_{z=L(t)}
\end{aligned} \tag{4.10}$$

The initial condition for this equation is the initial thickness of a casting solution:

$$L = L^\circ \quad \text{at} \quad t = 0 \tag{4.11}$$

4.5.4 Mass-Transport Model in the Nonsolvent Bath

In this study polymer transport into the nonsolvent bath is neglected. As Tsay and McHugh [49] have pointed out, this assumption implies a discontinuity in the polymer concentration at the upper interface. This phenomenon can be explained thermodynamically. Figure 4.2 shows the binodal determined via Flory-Huggins Theory by Shojaie et al. [29] for the water (1)/acetone (2)/cellulose acetate (3) system. Tie lines connect the two phases in thermodynamic equilibrium. The two phases are distinguished by their relative polymer concentrations and hence are referred to as the polymer-rich and polymer-lean phases. Inside the casting solution, a polymer-lean phase is responsible for the formation of a pore in the final membrane. At the casting solution/coagulation bath interface, the local equilibrium assumption demands that the coagulation bath have a composition corresponding to the polymer-lean phase in the casting solution. The assumption of no polymer in the coagulation bath is rationalized by the fact that any point on the polymer-lean side of the bimodal for the CA/acetone/water system has negligible polymer as shown in Figure 4.2. Also, note that a discontinuity in the concentration at the interface does not violate solution thermodynamics. On the contrary, it is clear that any corresponding polymer-lean and polymer-rich phases result in a discontinuity in the

concentration at the interface between them. (See Figure 4.2.) However, in all cases the chemical potential should be continuous to satisfy local thermodynamic equilibrium.

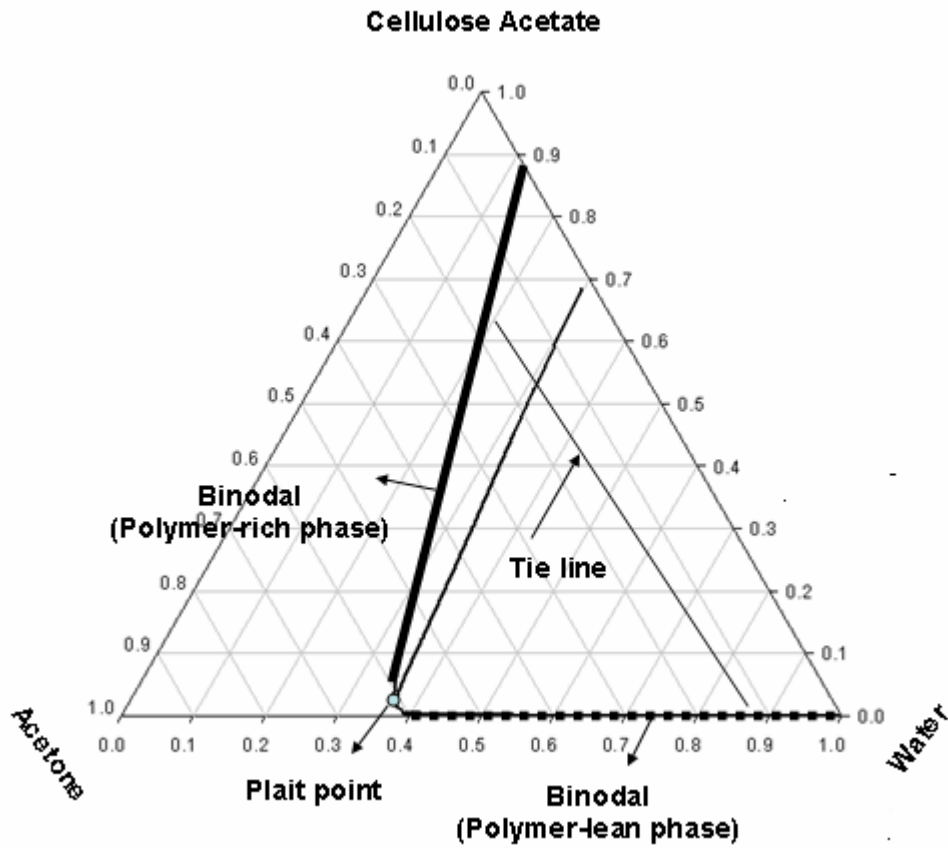


Figure 4.2: Phase diagram of the water (1)/ acetone (2)/cellulose acetate (3) system in which the concentration has a discontinuity at the interface between the polymer-rich and polymer-lean phases in equilibrium.

By assuming no polymer in the nonsolvent bath, the mass transfer in the coagulation bath is described via the binary convection-diffusion model in equation (2.30). The flux equation for nonsolvent (1) can be obtained by combining equations (2.21), (2.23), and (2.29) to obtain

$$n_1^B = (\rho^B)^2 \left(\frac{1}{\rho_1^\circ} - \frac{1}{\rho_2^\circ} \right) D_{12} \frac{\partial \omega_1^B}{\partial z} \quad (4.12)$$

The difficulty in using equation (4.12) with the equations for the casting solution is that the thickness of nonsolvent bath is much greater than that of the casting solution; that is, the casting solution is only a few hundred microns thick, whereas the water bath is several centimeters thick. The numerical solver, D03PPF in the NAG® FORTRAN library uses the finite difference method in which two connected systems must have the same number of calculation points. It has difficulty handling this type of problem owing to the vastly different length scales in the casting solution and the coagulation bath. This compromises the accuracy of the predictions for the nonsolvent bath. However, the main focus of this study is to construct and solve the equations for the casting solution during the wet-casting process. The information required from the equations for the nonsolvent bath is the fluxes of the nonsolvent and solvent at the interface. Therefore, we obtained an approximate analytical solution for the flux of nonsolvent by the following procedure. First, the boundary-layer thickness was determined using penetration theory as

$$\delta = \sqrt{D_{12}t} \quad (4.13)$$

Then, the weight-fraction gradient at the interface was calculated from the boundary-layer thickness and the following analytical solution for binary mass-transfer in the absence of convective transport:

$$\left. \frac{\partial \omega_1^B}{\partial z} \right|_{z=L(t)} = -\frac{\omega_1^{Bo}}{\delta} + \sum_{n=1}^{\infty} \left\{ \left(\frac{2\omega_1^{Bo}}{\delta} \right) \exp\left(-\frac{D_{12}n^2\pi^2t}{\delta^2} \right) \right\} \quad (4.13)$$

where ω_1^{Bo} is the initial weight fraction. Finally, the weight-fraction gradient value was put into the interfacial flux equation (4.12). The solvent (2) flux was calculated by a similar procedure, knowing that the summation of the two weight-fraction gradients is zero for a binary system. Although the weight-fraction gradient was calculated without considering a convective contribution, the convection-diffusion equation, equation (4.12) yields a better solution for the flux than a diffusion-only equation. Also, if the maximum density difference between the nonsolvent and solvent in the coagulation bath is much smaller than that in the casting solution, the convective contribution in a nonsolvent bath will be correspondingly much smaller than that in a casting solution. For this reason ignoring the convective contribution in the coagulation bath is a reasonable assumption. For example, the densities of water, acetone, and cellulose acetate are 1.0, 0.78 and 1.31 g/cm³, respectively. For this system the maximum density variation in the nonsolvent bath is approximately half the density variation in the casting solution.

The binary diffusion coefficient for water (1)/acetone (2) in the nonsolvent bath was calculated by the following equation fitted to the experimental data in [56]:

$$D_{12} = 0.0002\omega_2^4 - 0.0002\omega_2^3 + 0.0002\omega_2^2 - 6.0 \times 10^{-5}\omega_2^4 + 10^{-5} \quad (4.14)$$

Figure 4.3 shows the diffusion coefficient data and the fitting curve.

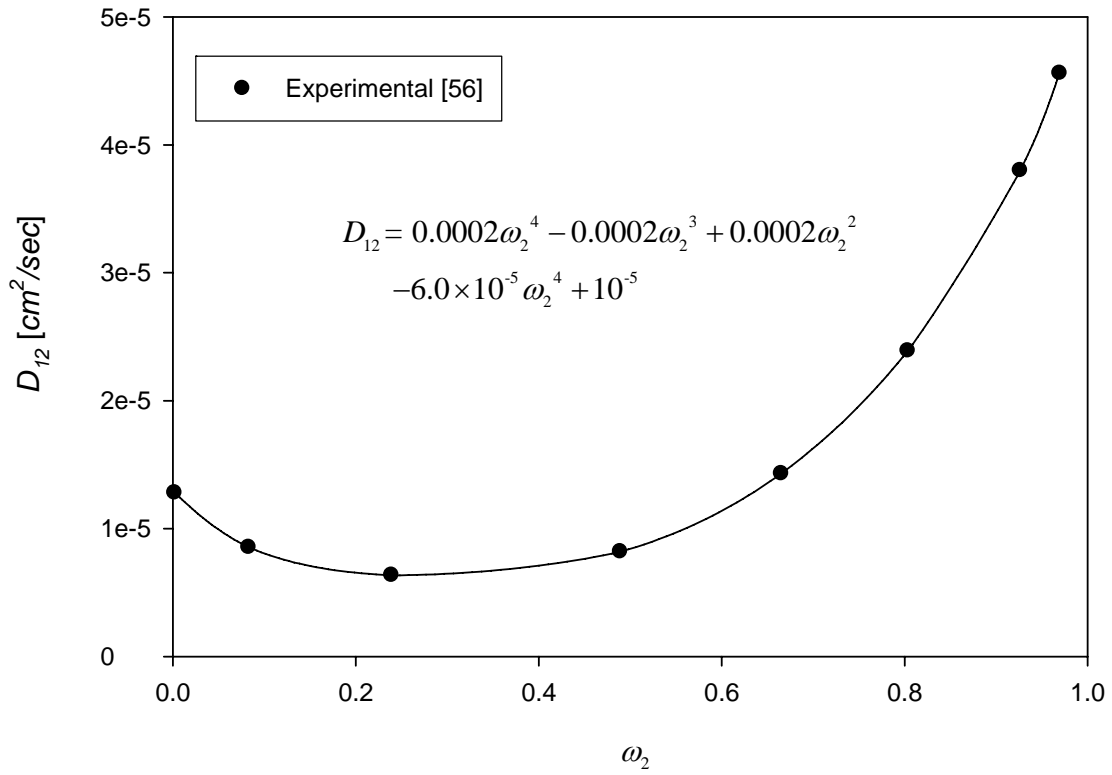


Figure 4.3: Polynomial fit to the binary diffusion coefficient data for the water (1)/acetone (2) system.

4.5.5 Interfacial Local Equilibrium Concentration

Thermodynamic equilibrium is defined as a state in which there is no tendency to change on a macroscopic scale [57]. The chemical potential provides the following criterion for equilibrium between two phases denoted by *I* and *II*:

$$\mu_i^I = \mu_i^{II} \quad \text{for } i = 1, 2, \dots, N \quad (4.15)$$

As mentioned earlier in this chapter, to comply with the local equilibrium condition at the interface and with the assumption of no polymer in the nonsolvent bath (local pseudo-equilibrium), only one independent chemical potential equation needs to be satisfied:

$$x_2^B \gamma_2^B = \exp\left(\frac{\Delta\mu_2}{RT}\right) \quad (4.16)$$

where x_2^B and γ_2^B are a local equilibrium mole fraction and activity coefficient of the solvent in the nonsolvent bath, respectively. The chemical potential in the casting solution can be calculated using the Flory-Huggins model. However, if the Flory-Huggins model is also applied to calculate the equilibrium composition in the coagulation bath corresponding to a stable casting solution, the interfacial compositions on both sides satisfying all three chemical potential equations are the same, thus violating the assumption of no polymer in the bath. Although it would be better to use a consistent thermodynamic model for both systems, since the nonsolvent bath is essentially a solvent/nonsolvent mixture, an alternative thermodynamic model suitable for a non-ideal and non-polymeric system will be used to calculate the activity coefficients in the nonsolvent bath. Therefore, in this study, the activity of the solvent in the bath for equation 4.16 was calculated by the following NRTL (Non-Random Two-Liquids) model equation with the experimental parameters suggested in the literature [58-61].

$$\ln(\gamma_2^B) = (x_1^B)^2 \left[1.065 \left(\frac{0.566}{x_1^B + 0.566x_2^B} \right)^2 + \left(\frac{0.686}{(x_1^B + 0.340x_2^B)^2} \right) \right] \quad (4.17)$$

After the interfacial composition of the casting solution reaches the binodal, the tie lines from the Flory-Huggins model can be used to calculate the interfacial local equilibrium composition on the bath side without violating the assumption of no polymer in the bath. The tie lines from Flory-Huggins model were fitted to the following auxiliary equation with a range of acetone weight-fraction from 0.4 to 0.15:

$$\omega_2^B = \omega_2 + 0.171(0.35 - \omega_2) + 0.09 \quad (4.18)$$

The tie lines for 25 °C were obtained from Shojaie's work [29].

4.6 Solution Methodology

The solution for the wet-casting model equations as a function of time and space was calculated with the same PDE solver used for the dry-casting model in the previous chapter. The equations for a fixed coordinate system were obtained by normalizing the instantaneous thickness of the casting solution in a manner similar to that used for the dry-casting model equations. Since the interfacial fluxes for the wet-casting process were expected to be much larger than those for the dry-casting process, it was assumed that at short contact times they would result in very steep concentration gradients confined to a thin region. Thus, this study places 100 of the total 131 numerical calculation points in the top one micron of the casting solution in order to increase the accuracy in this critical region.

It should be noted that no study in the literature focuses on the effect of the initial casting solution thickness on the model predictions. A model that allows for both

convective and diffusive mass transfer should predict the effect of the initial casting solution thickness more accurately than prior models that ignored convective transport. Thus, the simulation focused on the effect of the initial thickness. The same weight fraction was used for the initial composition for all simulations: water (1)/acetone (2)/cellulose acetate (3) = 0/0.15/0.85 (weight fraction). The nonsolvent bath was assumed to be pure water initially. All other physical parameters not specified in this thesis, such as the density and molecular weight of the pure species, are the same as used in Shojaie's work [29].

4.7 Presentation and Discussion of Results

4.7.1 Local Pseudo-equilibrium

This segment of the wet-casting process simulation involves describing the path by which concentration of the interfacial region changes from the initial casting solution composition to a point on the binodal. Again, the local pseudo-equilibrium interfacial compositions of the casting solution and the nonsolvent bath were obtained by the Flory-Huggins model and the NRTL model, respectively.

Figure 4.4 shows the composition change of the upper interface during the very early part of the wet-casting process. The results from two different initial thicknesses ($75 \mu m$ and $125 \mu m$) were identical, as shown in this figure. In very short time, approximately 3.3×10^{-10} seconds, the predicted composition of the upper interface reached the binodal. For both cases changes in the compositions were predicted only in top $0.05 \mu m$ of the casting solution. These results indicate that the process to reach a true

interfacial local equilibrium occurs extremely quickly and occurs only within a thin interfacially region corresponding to the local equilibrium concept.

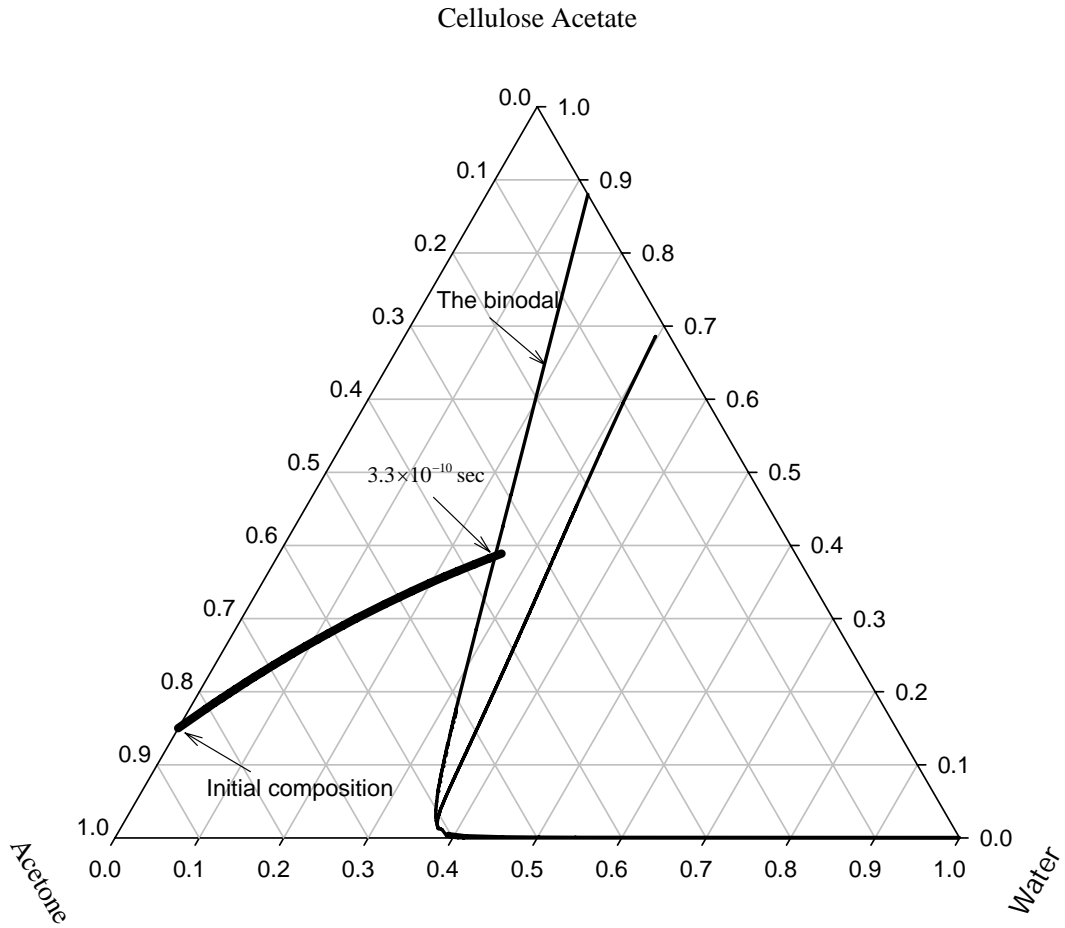


Figure 4.4: Composition change of the upper interface during wet-casting of a ternary solution of water/acetone/cellulose acetate (0, 0.15, 0.85 mass fraction). Initial casting solution thicknesses of $75 \mu\text{m}$ and $125 \mu\text{m}$ gave identical results.

4.7.2 Local Equilibrium

After the top composition of the casting solution reaches the binodal, the true local equilibrium composition that satisfies the chemical potential equations for all three species can be calculated from the tie lines using the Flory-Huggins model. Figure 4.5 shows the rapid change in the composition at the upper interface for both initial casting solution thicknesses studied ($75 \mu m$ and $125 \mu m$) until the the vitrification boundary was reached. Composition change was predicted only in the top $0.05 \mu m$; the bulk of the casting solution did not change during this process as was observed for the pseudo-equilibrium process discussed in previous section. These results imply that the upper interface of the casting solution vitrified or solidified even before a change of composition occurred in the bulk of the casting solution. Also note that the upper interface composition closely follows the binodal toward the upper apex corresponding to pure cellulose acetate. As discussed earlier, the prediction of Tsay and McHugh's diffusion model [39] is not supported by the higher diffusivity of acetone ($10^{-17} \sim 10^{-5} cm^2 / s$ [32, 54 and 55]) relative to that of water ($10^{-5} cm^2 / s$ [44 and 62]) in the presence of cellulose acetate. However, the depletion of acetone at the interface predicted by our convection-diffusion model is more reasonable. The model predictions also imply that vitrification or the glass transition, rather than phase separation, occurs at the upper interface of the casting solution.

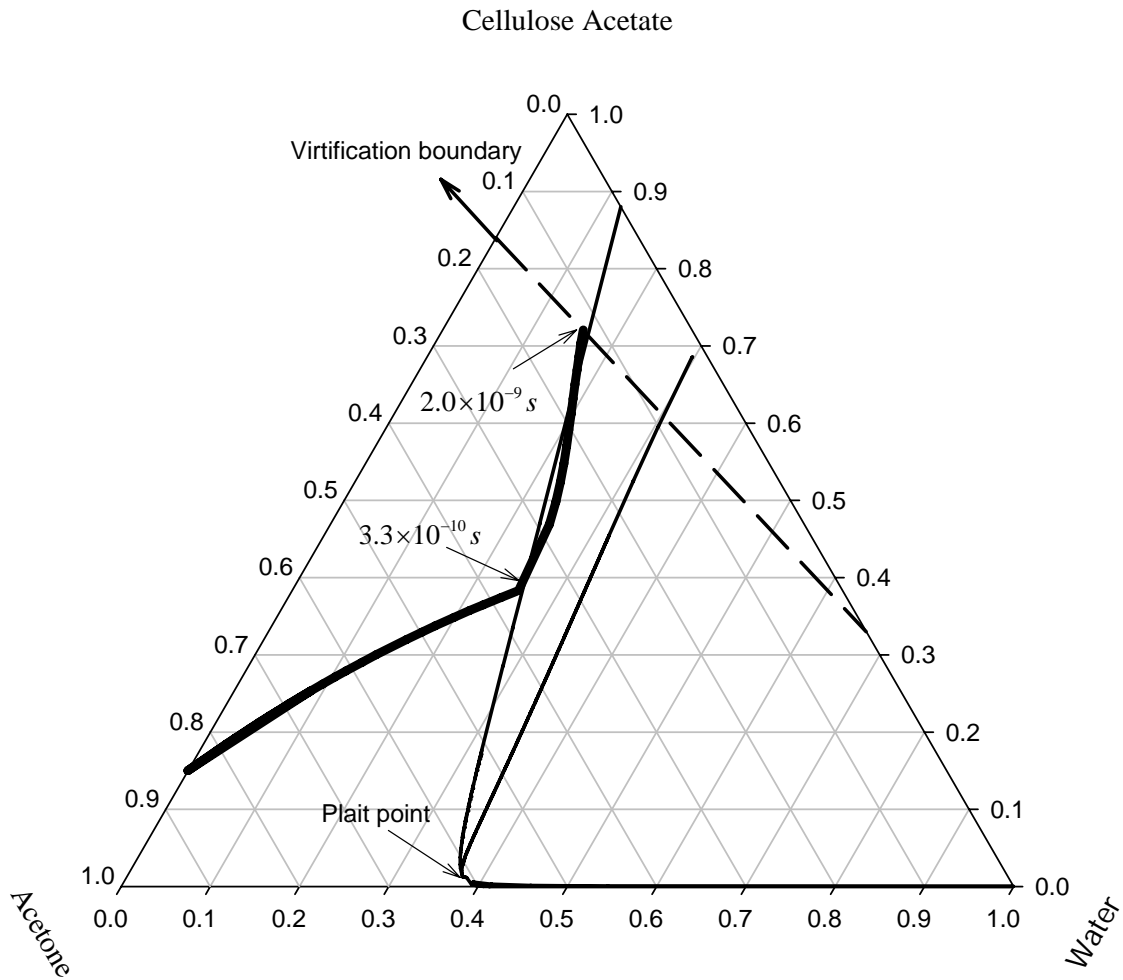


Figure 4.5: Composition change of the upper interface during wet-casting of a ternary solution of water/acetone/cellulose acetate (0, 0.15, 0.85 mass fraction). The initial casting solution thicknesses are $75 \mu m$ and $125 \mu m$. The composition changes on the binodal (from $3.3 \times 10^{-10} \text{ sec}$ to $2.0 \times 10^{-9} \text{ sec}$) were calculated using the tie-lines from the Flory-Huggins model. The composition trajectory for contact times less than $3.3 \times 10^{-10} \text{ sec}$ in Figure 4.4 is also shown here.

4.7.3 Extended Simulation after Vitrification on Interface

Vitrification is synonymous with glass transition or amorphous solidification. In statistical mechanical terms, solidification is the transition from the liquid or rubbery state to the state in which molecules possess only vibrational motion, losing their transitional and rotational modes [63]. Generally, polymers can be amorphous or crystalline, depending on the absence or presence of long-range order of the molecules, respectively. Gelation or viscosity transition, is different in that viscosity above 10^6 cp is the criterion [64, 65], while vitrification is determined by the glass-transition temperature. The glass-transition compositions of a water (1)/acetone (2)/cellulose acetate (3) system at a given temperature were calculated by Prakash [44] based on the Kelley-Bueche theory [66] and experimental data [67]. The vitrification boundary shown in the ternary phase diagrams is based on a system at 25°C .

After the top composition reaches the vitrification boundary, the polymer solution at this location can be considered to be a solid. Strictly speaking, the flux through the solidified interface depends on its structure, that is, its porosity and pore size. To simplify the model calculations and to obtain the maximum benefit from the model, the predictions were extended by assuming that the solidified very thin top layer maintains all the properties of the liquid state and that its composition remains fixed on the vitrification boundary. For calculations with the PDE solver, the casting solution was divided into 130 small sections, each with the same thickness, to maintain consistent accuracy in the entire system.

4.7.3.1 Convection-Diffusion Model Results

In this section the predictions of the improved wet-casting model are presented. The implications of these results then are discussed.

Figure 4.6 shows the composition at each point in the casting solution extending from the upper casting solution/water bath interface to the bottom substrate boundary as a function of contact time for a casting solution with an initial thickness of $75 \mu\text{m}$. After 3.4 seconds, the composition of the entire casting solution is on the binodal; moreover, no compositions are predicted to be in the two-phase region. Figure 4.7 and Figure 4.8 show the corresponding chemical potential changes with time. The thickness of the casting solution changes markedly initially and then decreases more slowly until it reaches approximately $64 \mu\text{m}$ as shown in Figure 4.9. The fluxes through the casting solution/water-bath interface also reach a maximum initially and then asymptotically decrease to zero with time as shown in Figure 4.10. Note that the negative flux of water indicates that it penetrates into the casting solution. The penetration of the denser species (water) and the elimination of the lighter species (acetone) result in densification of the casting solution. The corresponding mass-average velocity profiles in Figure 4.11 reflect this densification. The dramatic change in the shape of the mass-average velocity profile occurs when the acetone/polymer ratio is about one. In the dry-casting model results the concentration profile also showed a pronounced change when the ratio was about one. The steep decrease in the diffusion coefficient might explain this phenomenon for the wet-casting process as well. Figure 4.12 shows the corresponding modified Peclet number near the casting solution/water-bath interface. As described earlier, the modified Peclet number is the ratio of the convective to the diffusive contributions to the mass

flux. The modified Peclet number results indicate that the initial convective contribution is 65 times greater than the diffusive contribution. Therefore, neglecting the convective contribution as has been done in all prior models can result in serious inaccuracies in the predictions.

For an initial casting solution thickness of $125\ \mu\text{m}$ the model predictions for composition at each point in the casting solution are shown in Figure 4.13. The composition in the top $7\ \mu\text{m}$ crosses the binodal after 1 second, which implies that the top $7\ \mu\text{m}$ region of the casting solution enters the metastable region nearly instantaneously, unlike the casting solution having an initial thickness of $75\ \mu\text{m}$. Furthermore, it takes 7.5 seconds for the entire casting solution to cross the binodal, which is much longer than predicted for the $75\ \mu\text{m}$ thickness. Therefore, even with identical initial casting solution compositions, the effect of the initial thickness is significant. Having a substantial portion of the casting solution in the metastable region could result in a different membrane morphology. The corresponding chemical potentials of the water and acetone in the casting solution are shown in Figures 4.14 and 4.15, respectively. As shown in Figure 4.16, the thickness decreases to about $107\ \mu\text{m}$. Figure 4.17 shows that the fluxes through the top interface decline with time. The mass-average velocity profile displays a marked change in shape when the acetone/cellulose acetate ratio reaches one as shown in Figure 4.18. The corresponding modified Peclet number also indicates that the convective contribution is more than 60 times greater than the diffusive contribution.

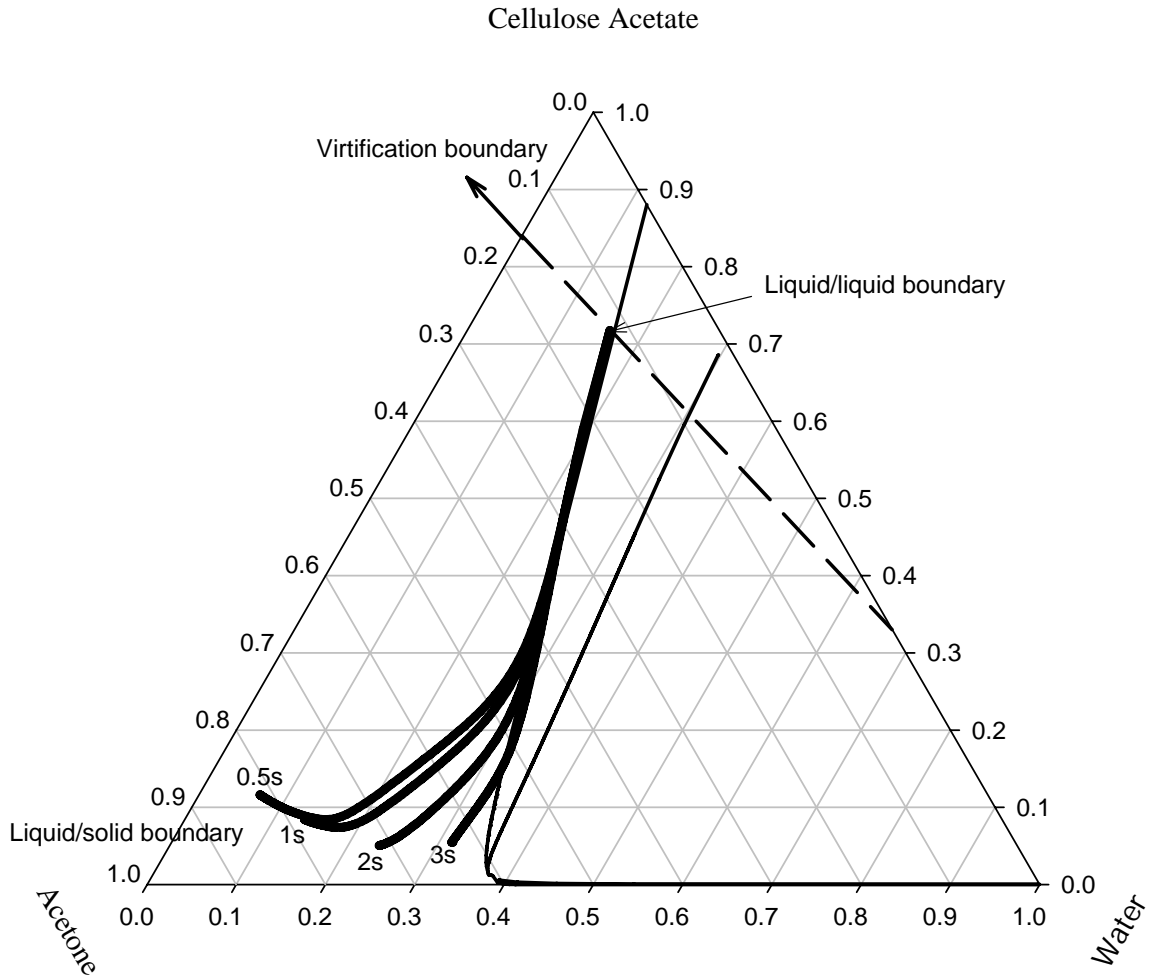


Figure 4.6: Composition changes for a membrane wet-cast from a ternary solution of water/acetone /cellulose acetate (0/0.15/0.85 mass fraction) having an initial solution thickness of $75 \mu\text{m}$. Each curve shows the composition from the lower substrate to the upper interface for a different time after immersion.

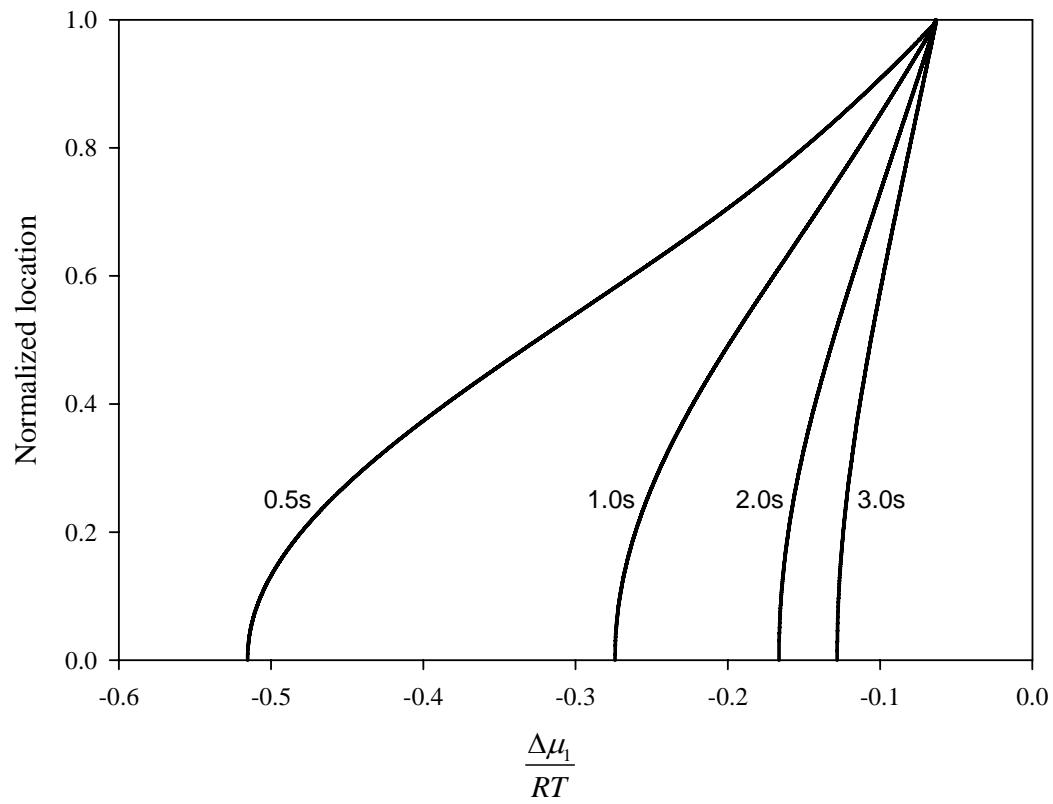


Figure 4.7: Chemical potential profiles for water for a membrane wet-cast from a ternary solution water/acetone /cellulose acetate (0/0.15/0.85 mass fraction) having an initial solution thickness of $75 \mu m$.

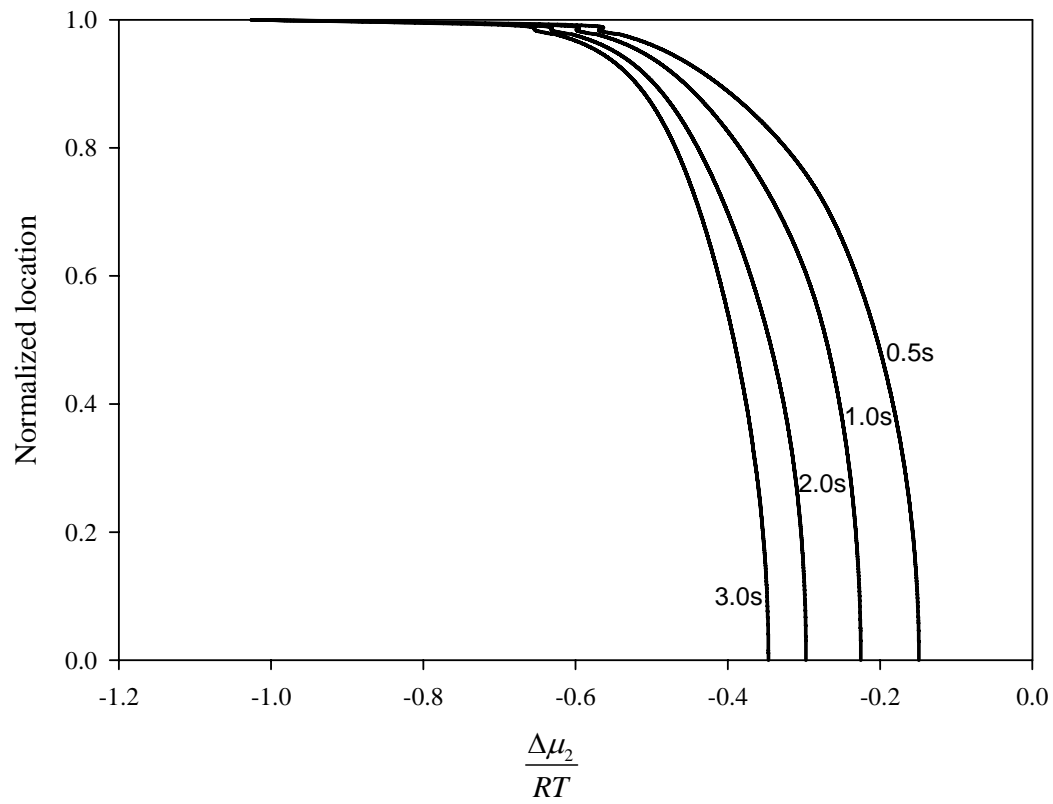


Figure 4.8: Chemical potential profiles for acetone for a membrane wet-cast from a ternary solution water/acetone /cellulose acetate (0/0.15/0.85 mass fraction) having an initial solution thickness of $75 \mu m$.

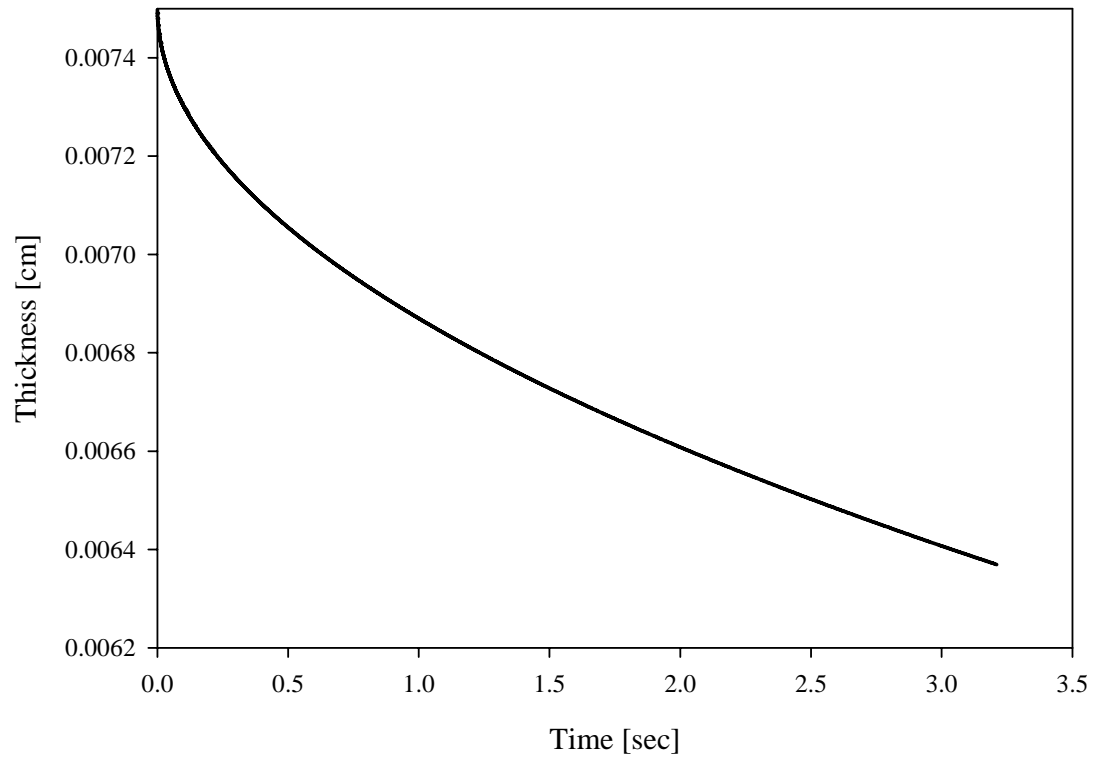


Figure 4.9: Thickness change for a for a membrane wet-cast from a ternary solution water/acetone /cellulose acetate (0/0.15/0.85 mass fraction) having an initial solution thickness of $75 \mu m$.

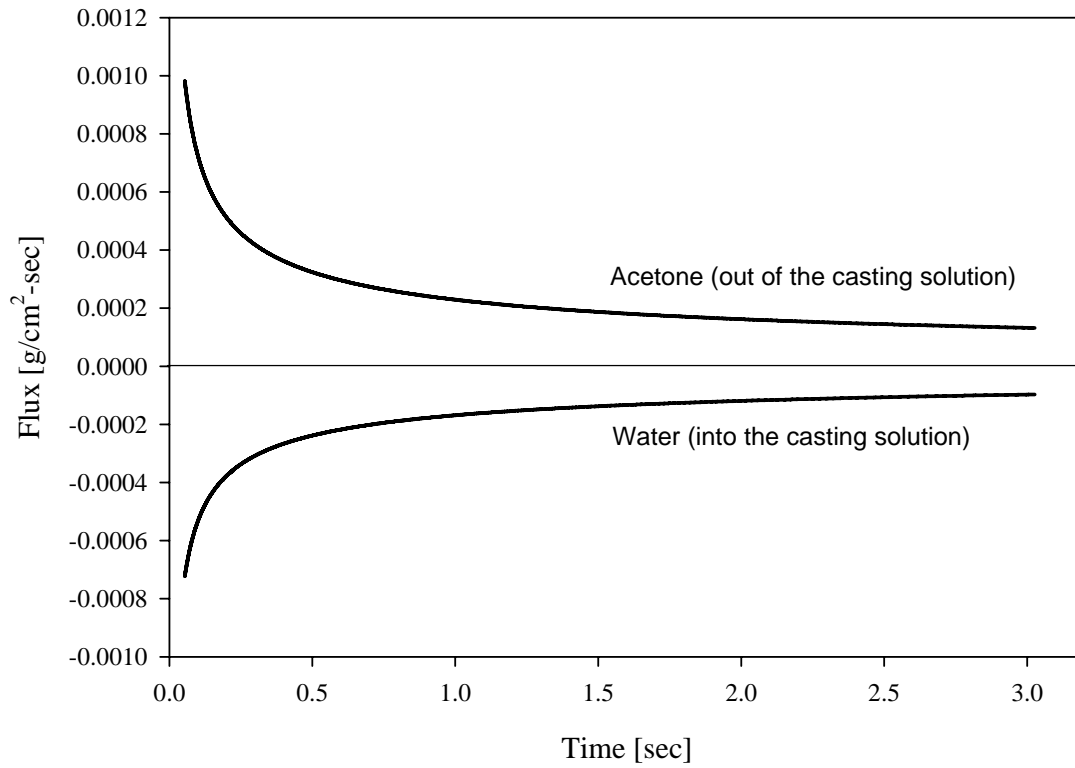


Figure 4.10: Flux change at the upper interface for a for a membrane wet-cast from a ternary solution water/acetone /cellulose acetate (0/0.15/0.85 mass fraction) having an initial solution thickness of $75 \mu m$.

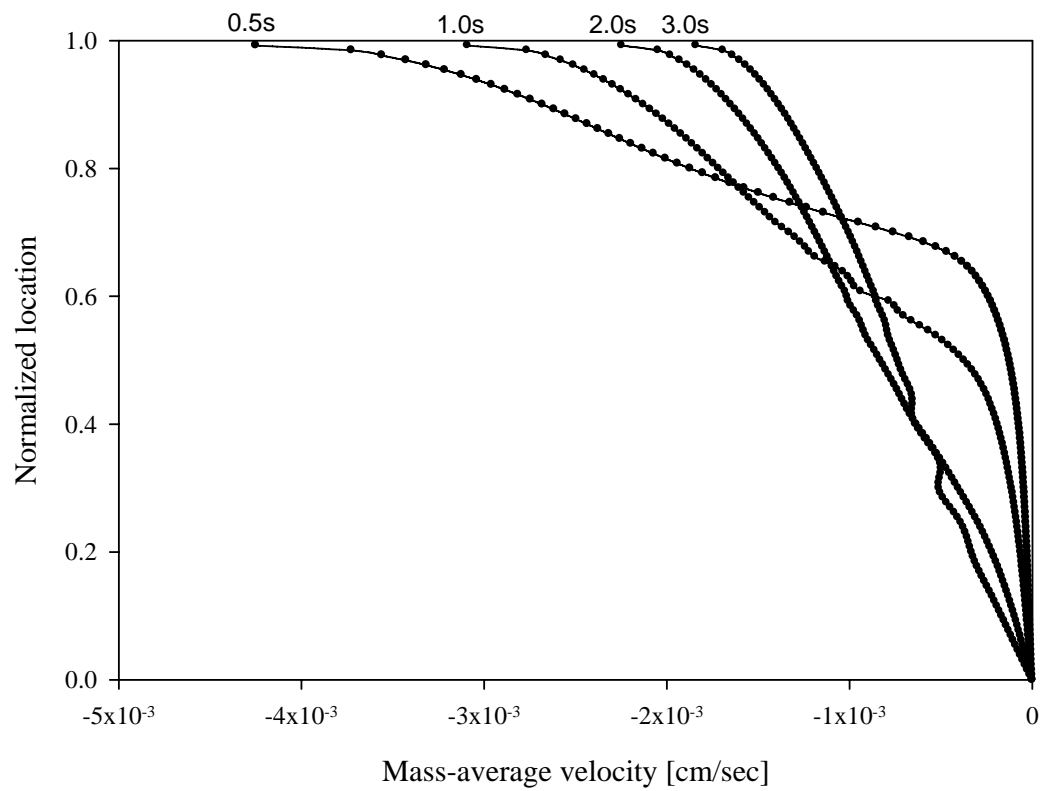


Figure 4.11: Mass-average velocity profiles for a for a membrane wet-cast from a ternary solution water/acetone /cellulose acetate (0/0.15/0.85 mass fraction) having an initial solution thickness of $75 \mu m$.

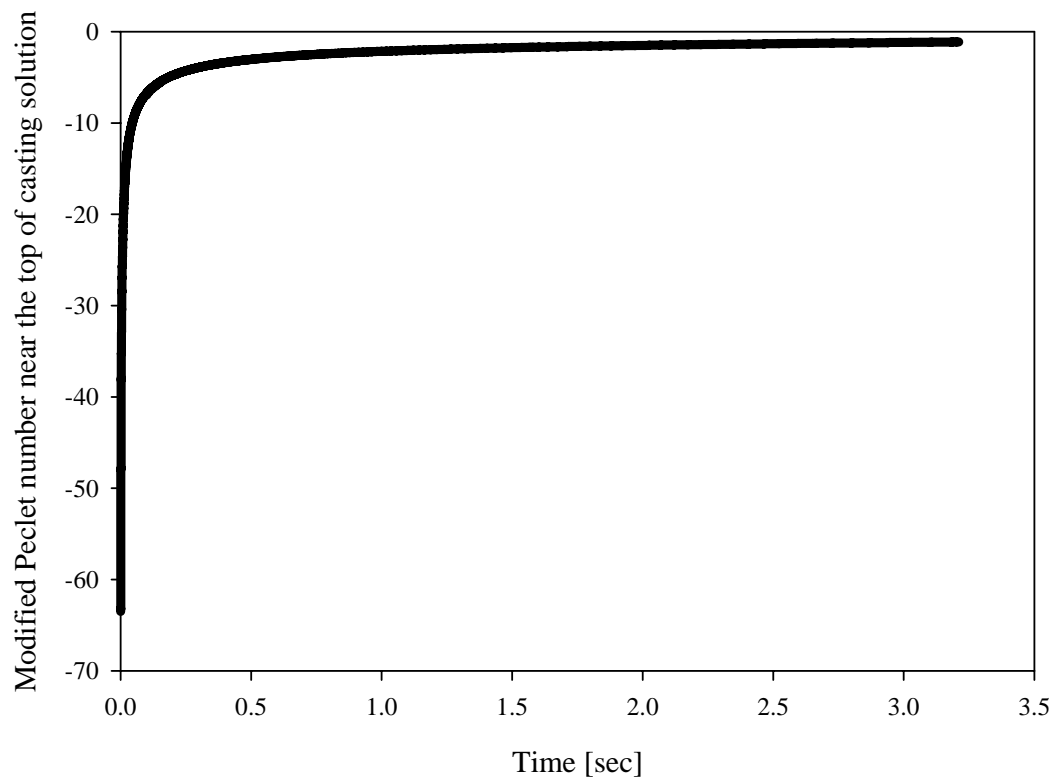


Figure 4.12: Modified Peclet number profiles for a for a membrane wet-cast from a ternary solution water/acetone /cellulose acetate (0/0.15/0.85 mass fraction) having an initial solution thickness of $75 \mu m$.

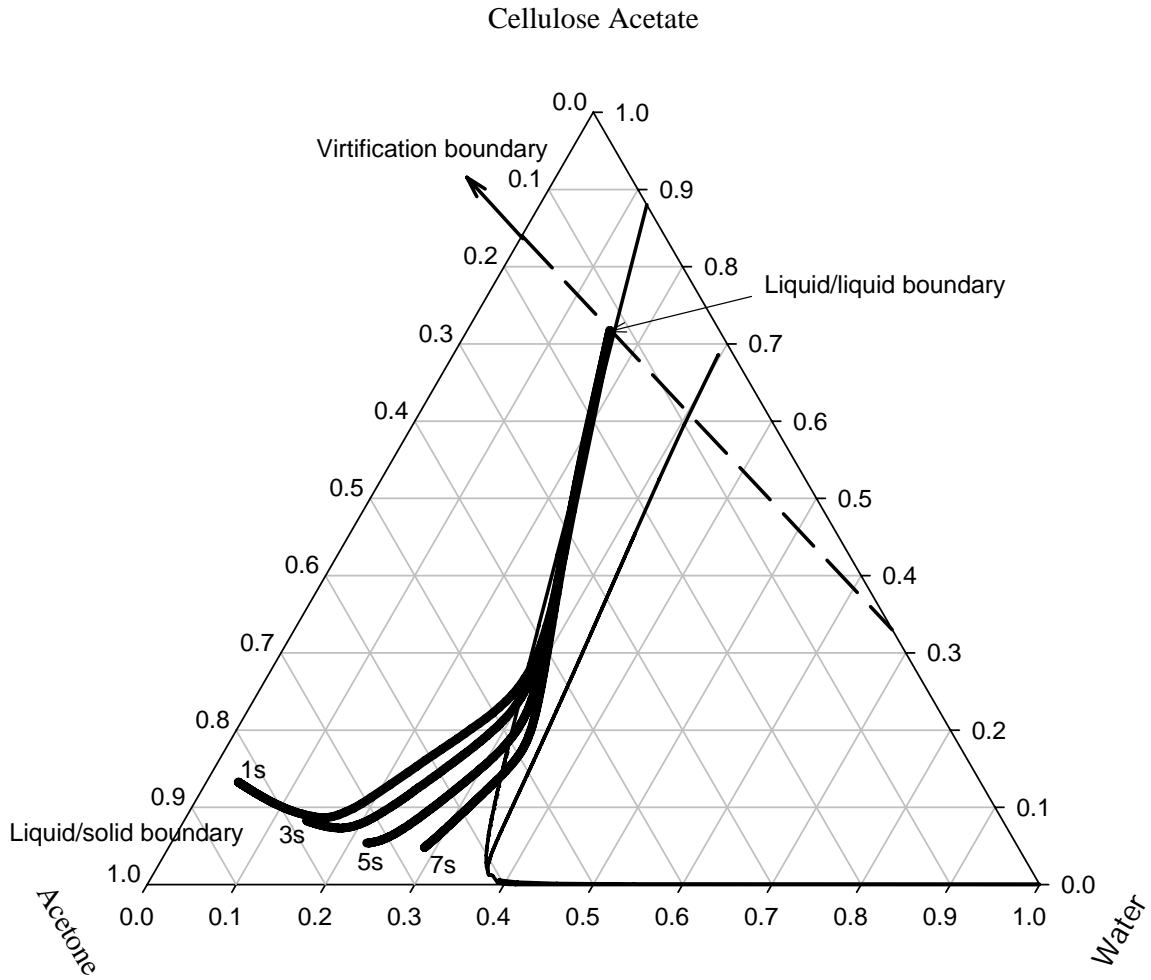


Figure 4.13: Composition changes for a membrane wet-cast from a ternary solution of water/acetone /cellulose acetate (0/0.15/0.85 mass fraction) having an initial solution thickness of $125 \mu\text{m}$. Each curve shows the composition from the lower substrate to the upper interface for a different time after immersion.

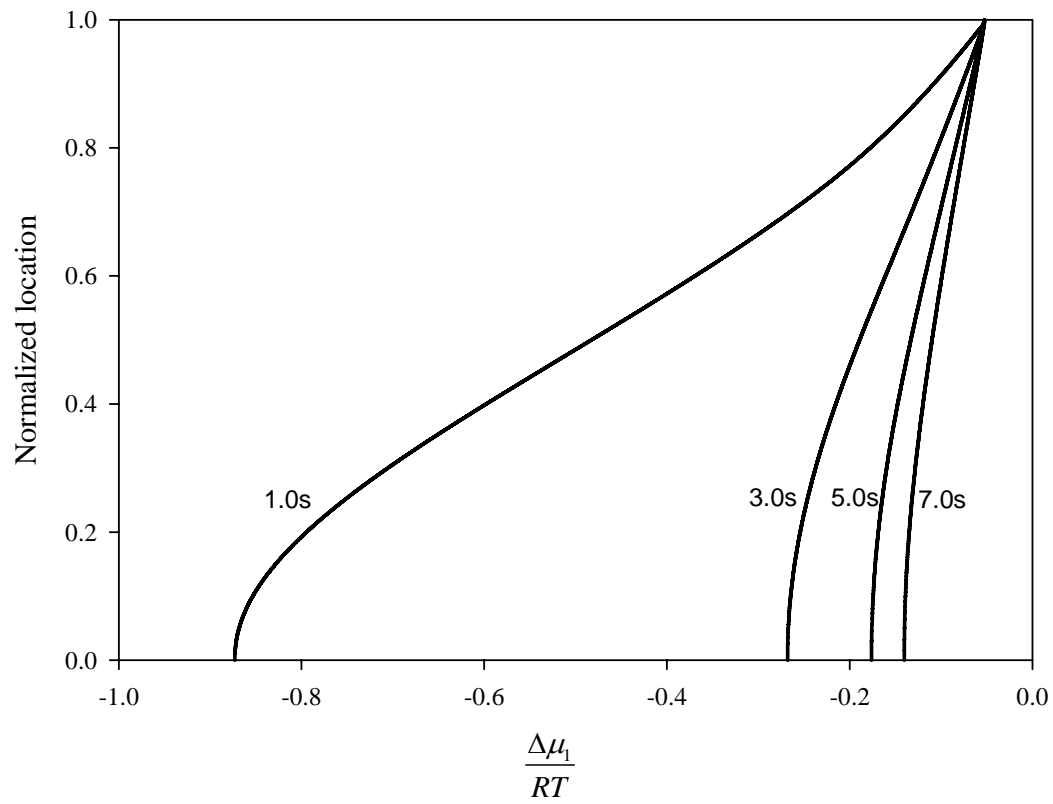


Figure 4.14: Chemical potential profiles for water for a membrane wet-cast from a ternary solution water/acetone /cellulose acetate (0/0.15/0.85 mass fraction) having an initial solution thickness of $125 \mu m$.

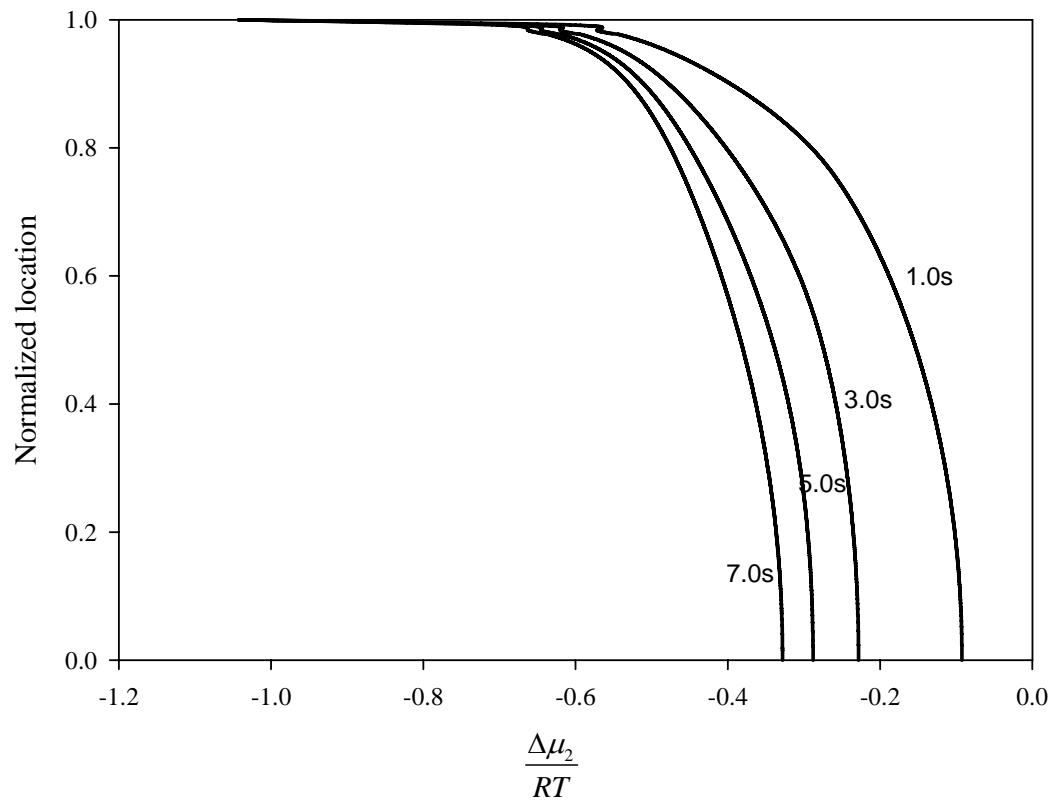


Figure 4.15: Chemical potential profiles for acetone for a membrane wet-cast from a ternary solution water/acetone /cellulose acetate (0/0.15/0.85 mass fraction) having an initial solution thickness of $125 \mu m$.

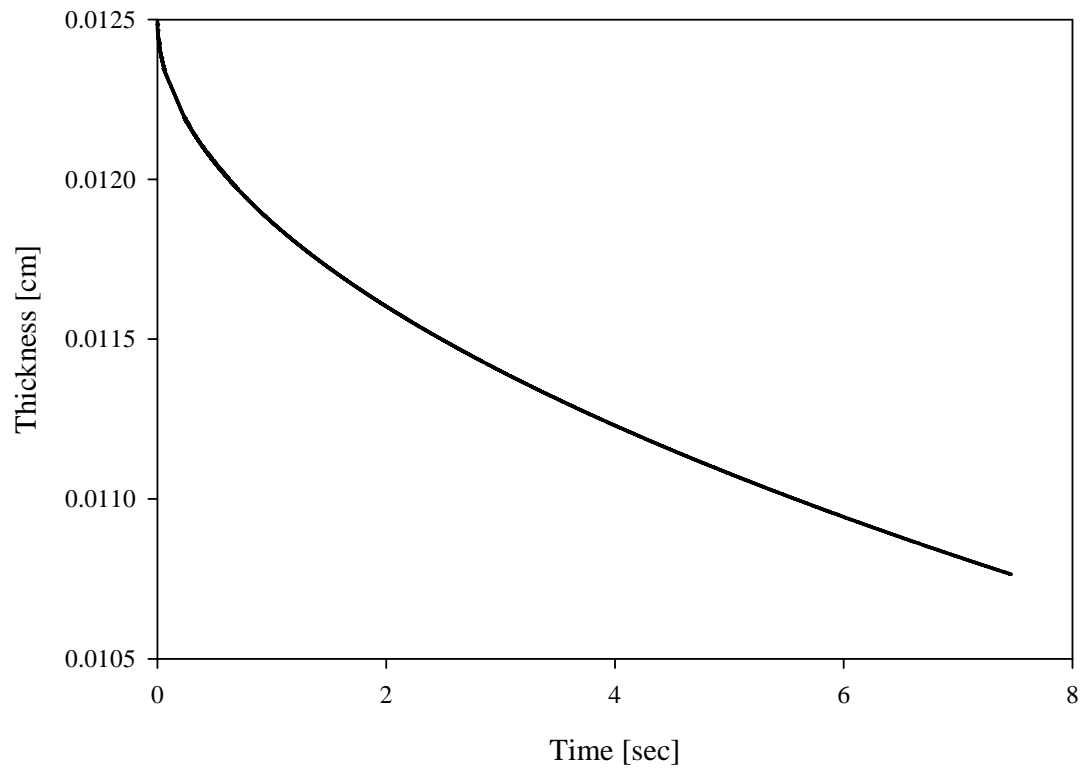


Figure 4.16: Thickness change for a membrane wet-cast from a ternary solution water/acetone /cellulose acetate (0/0.15/0.85 mass fraction) having an initial solution thickness of $125 \mu m$.

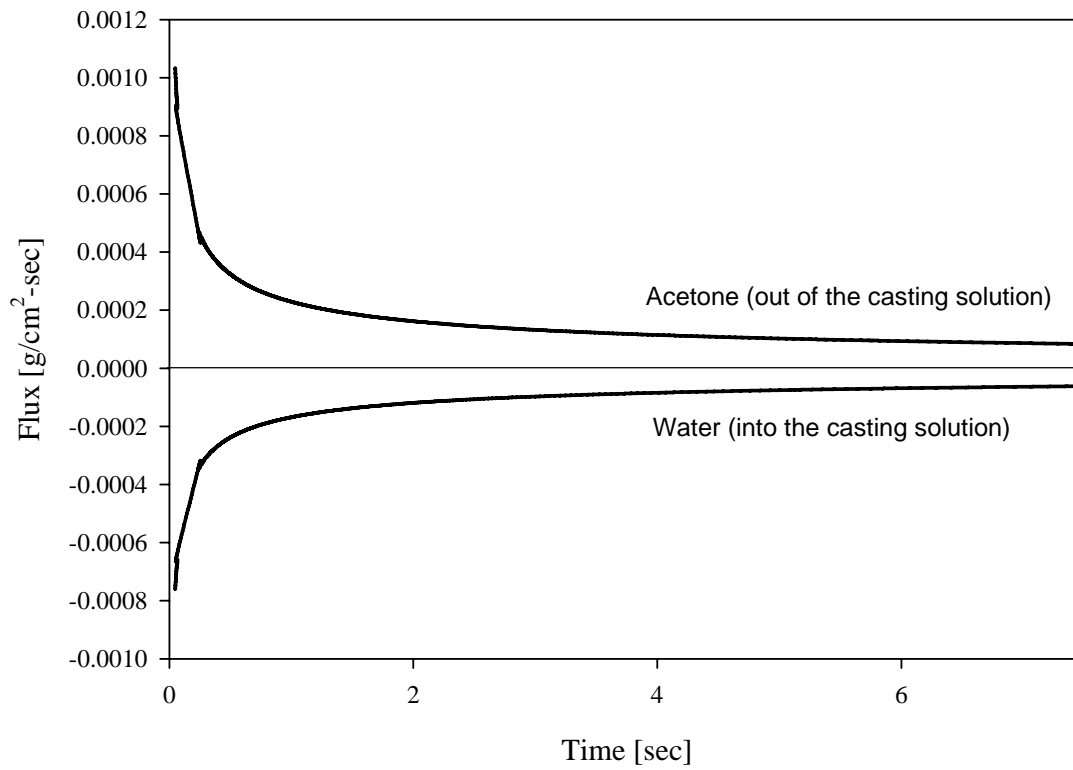


Figure 4.17: Flux change at the upper interface for a membrane wet-cast from a ternary solution water/acetone /cellulose acetate (0/0.15/0.85 mass fraction) having an initial solution thickness of $125 \mu\text{m}$.

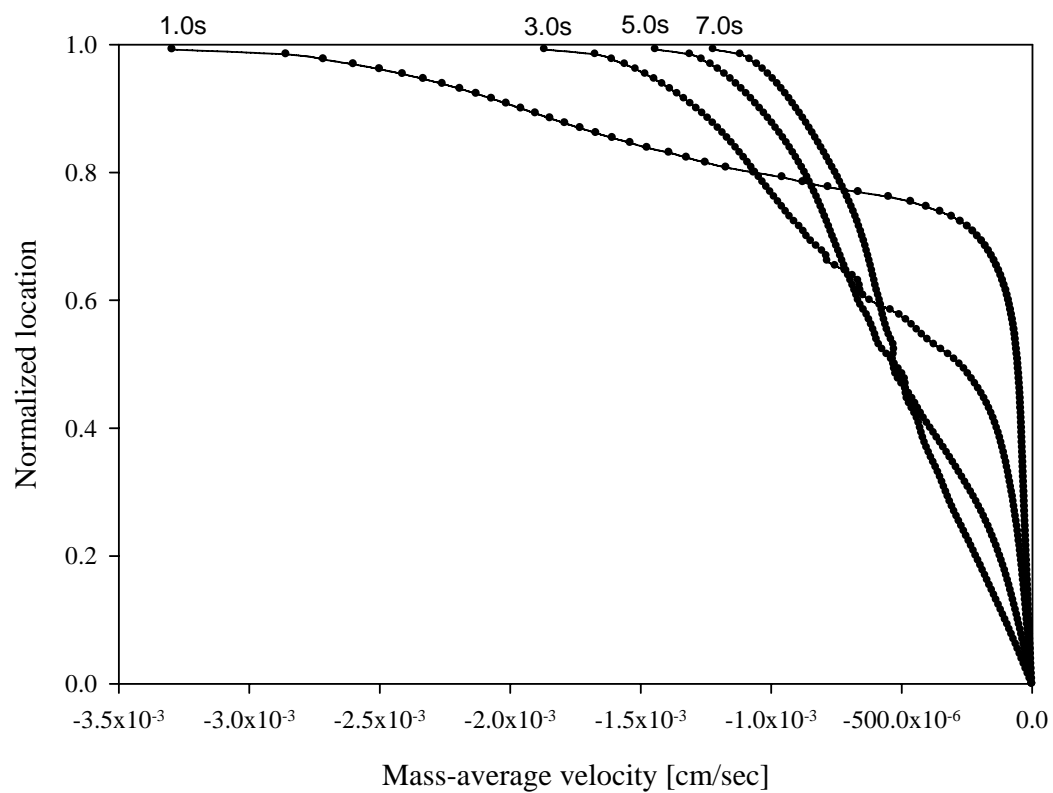


Figure 4.18: Mass-average velocity profiles for a for a membrane wet-cast from a ternary solution water/acetone /cellulose acetate (0/0.15/0.85 mass fraction) having an initial solution thickness of $125 \mu m$.

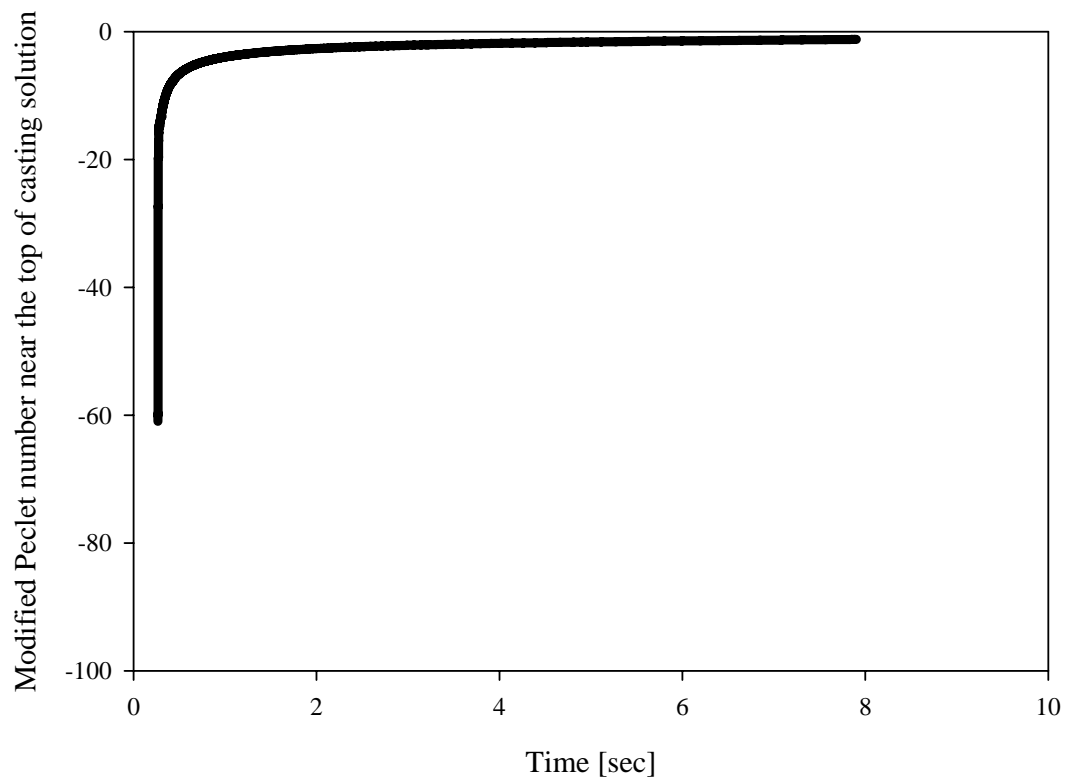


Figure 4.19: Modified Peclet number profiles for a for a membrane wet-cast from a ternary solution water/acetone /cellulose acetate (0/0.15/0.85 mass fraction) having an initial solution thickness of $125 \mu m$.

4.7.3.2 Diffusion-only Model Results

In the previous section the modified Peclet numbers calculated for initial casting solution thicknesses of $75\ \mu\text{m}$ and $125\ \mu\text{m}$ proved that the convective contribution to the mass flux must be included in the mass-transfer model. For comparison the extended model results from the model that allows for only diffusive transfer in the absence of convection are presented in this section.

If the convective contribution to the mass flux is ignored, the boundary condition at the upper interface in combination with binary diffusion in the coagulation bath implies that the mass fluxes of the two transferring component are equal; this is referred to as “equi-mass” mass transfer. The pure diffusion model then result in the predictions for the local composition at specified times after immersion for an initial casting solution thickness of $75\ \mu\text{m}$.shown in Figure 4.20. Since equi-mass mass transfer is implied when convection is ignored, the instantaneous fluxes of water and acetone at the upper interface are equal in magnitude but opposite in direction as shown in Figure 4.21. The equi-mass limitation in combination with ignoring densification effects implies that the casting solution thickness remains constant as shown in Figure 4.22..

A much more significant difference in the concentration profile is observed when for an initial casting-solution thickness of $125\ \mu\text{m}$. For this thickness, the mass-transfer model incorporating convection predicts the presence of a metastable region in the casting solution. This phenomenon is not predicted by the model that ignores convective mass transfer as is shown in Figure 4.23. Figures 4.24 and 4.25 also show typical flux and thickness changes during an equi-mass mass-transfer process. Therefore, it can be

concluded that neglecting the convective contribution to the mass flux in model for the wet-casting process leads to significant error.

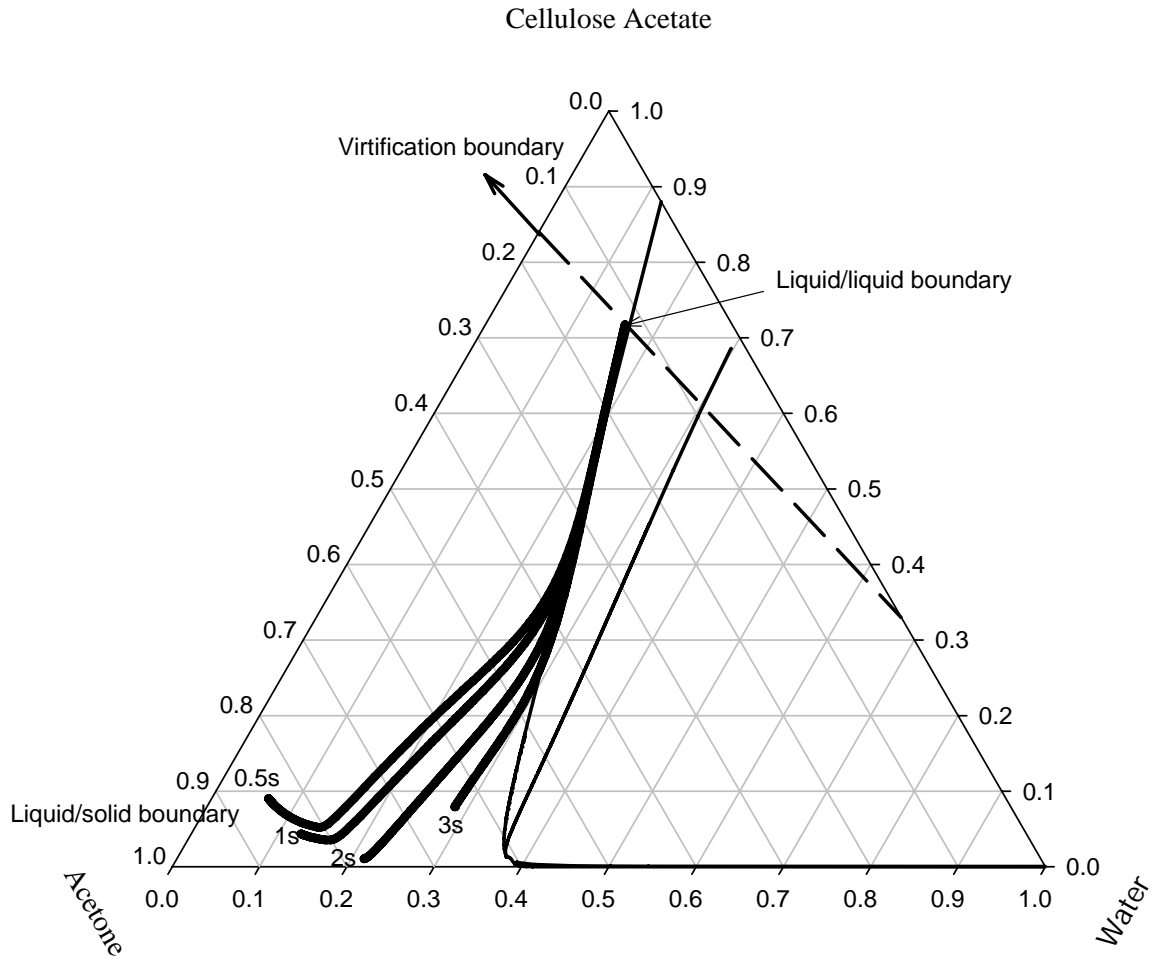


Figure 4.20: Model predictions when convection is ignored: Composition changes for a membrane wet-cast from a ternary solution of water/acetone /cellulose acetate (0/0.15/0.85 mass fraction) having an initial solution thickness of $75 \mu m$. Each curve shows the composition from the lower substrate to the upper interface for a different time after immersion.

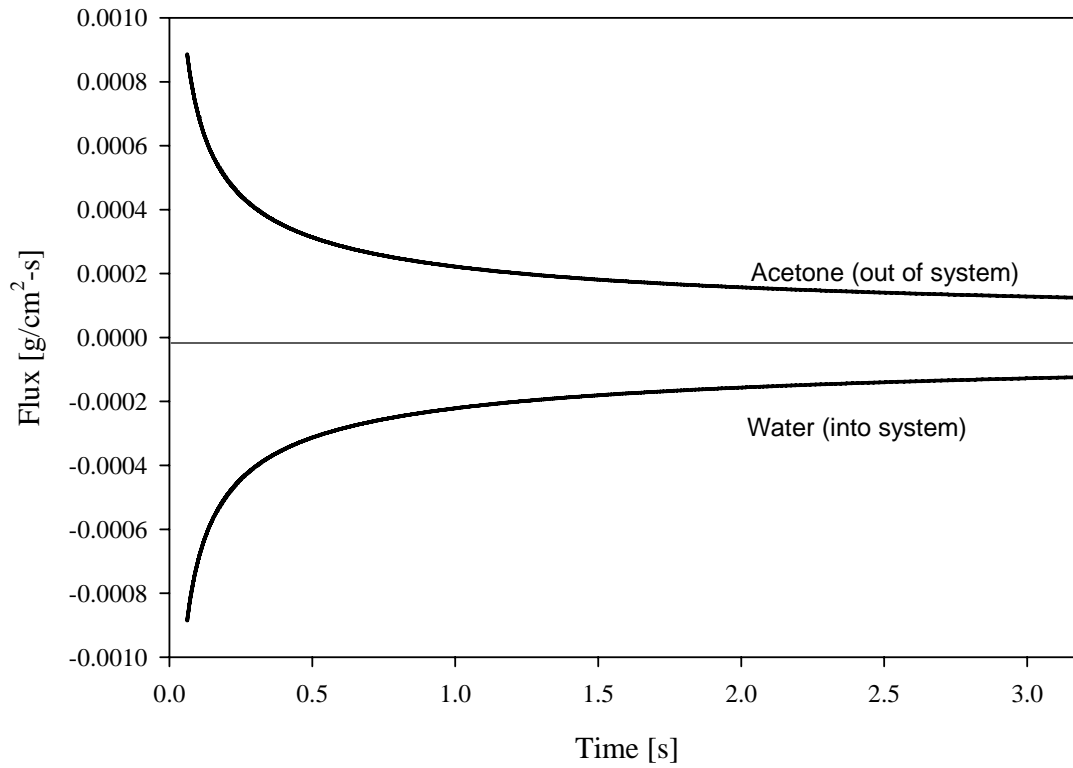


Figure 4.21: Model predictions when convection is ignored: Flux change at the upper interface for a membrane wet-cast from a ternary solution of water/acetone/cellulose acetate (0/0.15/0.85 mass fraction) having an initial solution thickness of $75 \mu\text{m}$

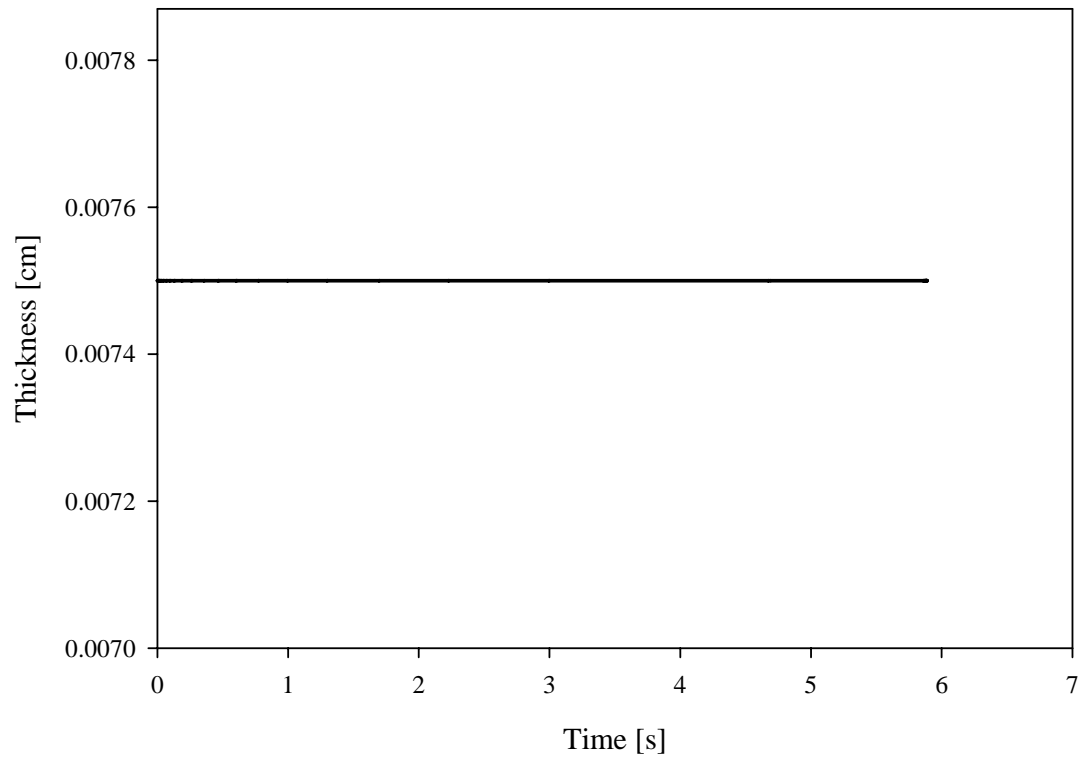


Figure 4.22: Model predictions when convection is ignored: Thickness change for a membrane wet-cast from a ternary solution of water/acetone /cellulose acetate (0/0.15/0.85 mass fraction) having an initial solution thickness of $75 \mu m$

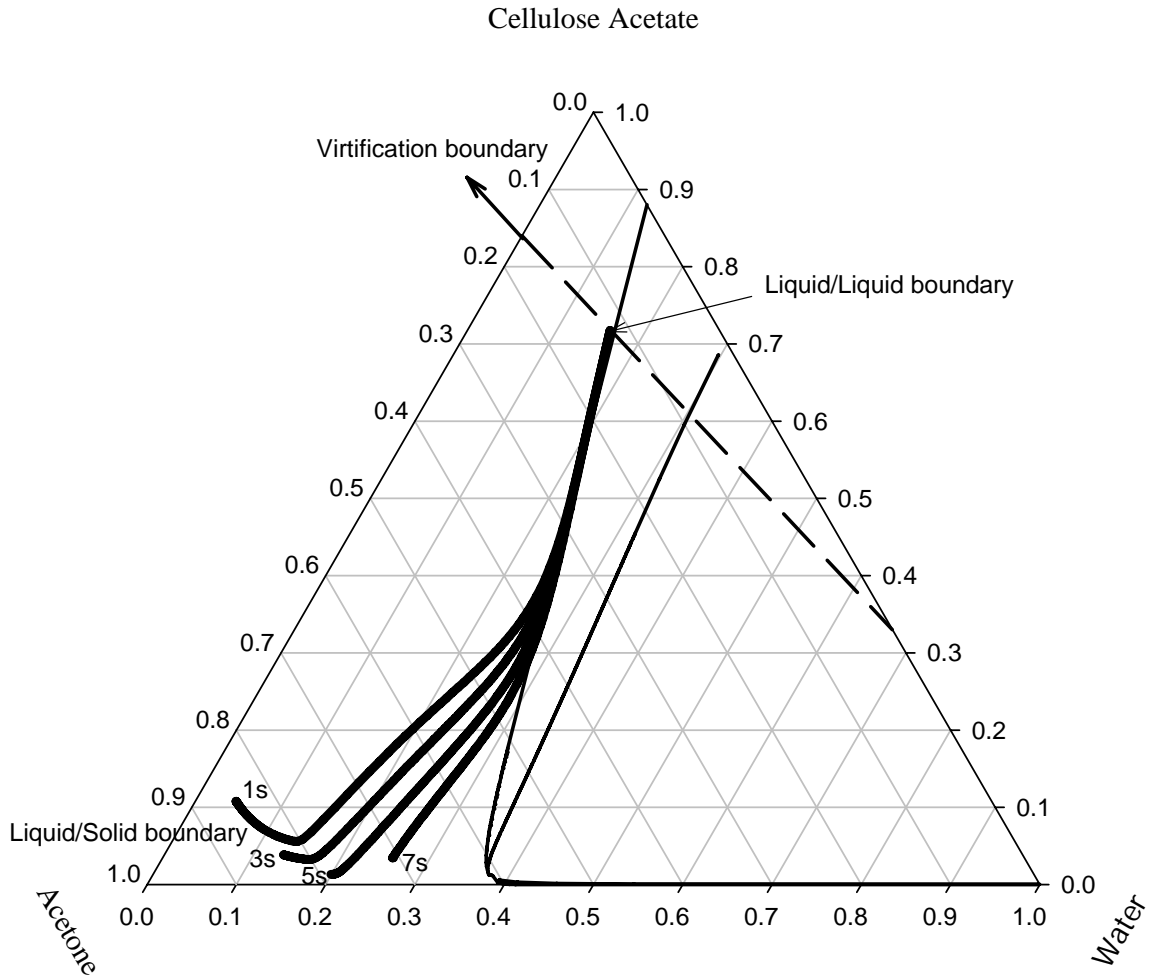


Figure 4.23: Model predictions when convection is ignored: Composition changes for a membrane wet-cast from a ternary solution of water/acetone /cellulose acetate (0/0.15/0.85 mass fraction) having an initial solution thickness of $125 \mu m$. Each curve shows the composition from the lower substrate to the upper interface for a different time after immersion.

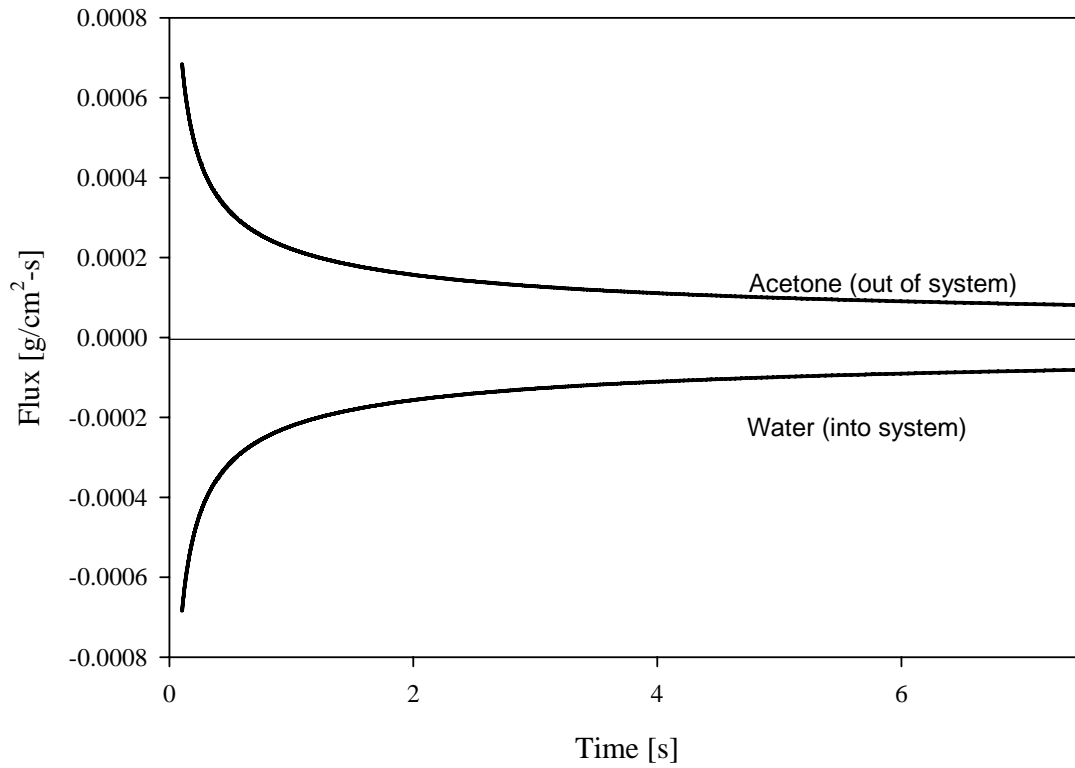


Figure 4.24: Model predictions when convection is ignored: Flux change at the upper interface for a membrane wet-cast from a ternary solution of water/acetone/cellulose acetate (0/0.15/0.85 mass fraction) having an initial solution thickness of $125 \mu\text{m}$

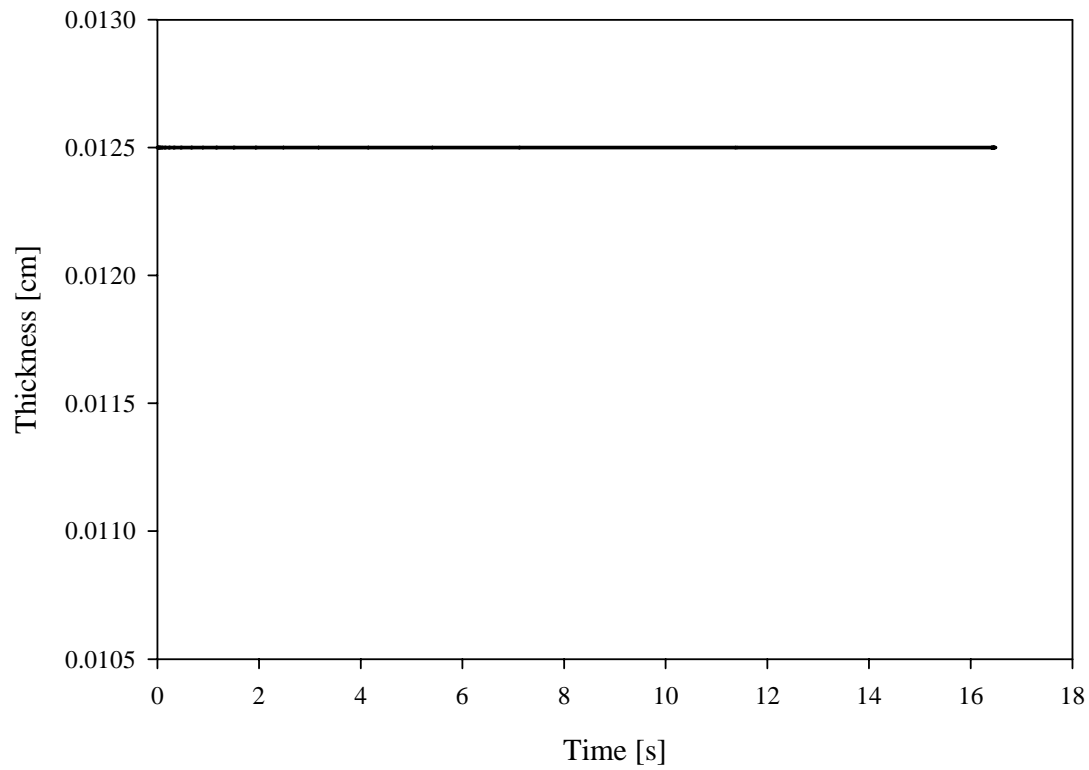


Figure 4.25: Model predictions when convection is ignored: Thickness change for a membrane wet-cast from a ternary solution of water/acetone /cellulose acetate (0/0.15/0.85 mass fraction) having an initial solution thickness of $125 \mu m$.

4.8 Summary

An improved model for the wet-casting process was developed and solved numerically in this chapter. This improved model correctly incorporates both the convective and diffusive contributions to the mass-transfer flux. Therefore, the effect of local densification during the wet-casting process can be accounted for in the model equations. The numerical solution of the model equations was divided into three time segments. The first segment used the local pseudo-equilibrium assumption at the moving upper interface that combined the NRTL model for the bath side and the Flory-Huggins model for the casting solution side. The resulting description of the very rapid composition changes near the upper interface of the casting solution satisfied the local equilibrium concept. The second segment used the Flory-Huggins model for both sides of the interface. This predicted very rapid polymer accumulation at the upper interface that result in vitrification. The composition changes at the upper interface for the first and second segments were not affected by the initial thickness of the casting solution. The simulation then was extended to the third segment by assuming a fixed upper interface composition on the vitrification boundary. The model predictions for two initial casting-solution thicknesses of 75 and 125 μm resulted in markedly different composition profiles. The thicker initial casting solution led to the formation of a thick metastable region near the upper interface, whereas there was no metastable region predicted for the thinner initial casting solution. This significant difference was not predicted by the model that allowed for only diffusive mass transfer in the absence of convection. Indeed, the modified Peclet number indicated that the convective contribution was much larger than the diffusion contribution for short times after immersion in the coagulation bath.

Therefore, this new model that incorporate convective mass transfer provides more accurate predictions of the effect of the initial casting solution thickness on the composition change during the wet-casting process.

CHAPTER V

MACROVOID FORMATION MECHANISM

5.1 Scope of Chapter

A rigorous mathematical model can be utilized not only to predict experimental results but also to explain phenomena that are otherwise difficult to study, particularly experimentally. In this chapter, the fundamental mechanism for macrovoid formation is investigated utilizing both experimental data as well as the developed wet-casting model that incorporates both the convective and diffusive mass transport. The final membrane morphology is extremely sensitive to the casting conditions, thus requiring a precise experimental design. The usual batch processes used in the laboratory involve complex three-dimensional free convection, while even the continuous industrial process has a simpler well-developed boundary condition. To create a laboratory batch process ensuring the one-dimensional mass transfer in our wet-casting model presented in the previous chapter, we used a low-gravity environment and a specialized membrane-casting apparatus for our experimental study. Experiments were also conducted incorporating surfactant in the coagulation bath to assess the effect of coalescence on the macrovoid formation.

This chapter is organized in the following manner. First, the theoretical background for nucleation and growth, spinodal decomposition, coalescence and macrovoid formation is presented. This is followed by a literature review of the proposed macrovoid-formation hypotheses and of the phenomenological approaches for

macrovoid formation mechanism and of membrane casting in low gravity. Experimental design of materials and methods are then discussed with special emphasis on the design and operation of a novel membrane casting apparatus and data collection in a low-gravity environment on a NASA KC-135A parabolic flight research aircraft. Finally, the results are presented and discussed.

5.2 Introduction

5.2.1 Nucleation and Growth (NG) and Spinodal Decomposition (SD)

Porous polymeric membranes formed by phase-inversion methods are the result of phase separation of a homogenous one-phase polymer solution into polymer-rich and polymer-lean phases, which eventually become the solid polymeric matrix and pores, respectively. The phase-separation mechanisms for polymer solutions are crystallization, gelation, and liquid-liquid demixing; this research studies macrovoid growth, which involves a liquid-liquid demixing phenomenon. Liquid-liquid demixing has two pathways: nucleation and growth (NG) and spinodal decomposition (SD) [45, 68].

The nucleation and growth (NG) process was recognized by Josiah Willard Gibbs in the late 1800s as one of the two classes of phase change that occur in an infinitesimal nucleus of material with the thermodynamic properties approaching a more stable state; in NG, the metastable phase becomes stable by the formation of phase-separated nuclei. Uhlmann and Chalmers [69] have shown that the change of the Gibbs free energy during the NG process reaches a maximum when the growing nucleus approaches a certain size as shown in Figure 5.1, implying that the nascent nucleus must overcome an energy

barrier in order to grow larger than the critical size, R_c . A nucleus of critical size can grow spontaneously in order to decrease its Gibbs free energy. NG can be expected when a thermodynamically stable system slowly enters the metastable region between the binodal and the spinodal on the equilibrium phase diagram [70]. The thermodynamics and kinetics of NG show that the droplet size increases with time, while the composition of polymer-lean phase remains approximately constant [71-73].

The second type of phase change is spinodal decomposition (SD), in which local composition fluctuations spread rapidly throughout the entire volume of the casting solution. Cahn and Hilliard [71] showed that the energy barrier to grow a nucleus approaches zero as the unstable region on the phase diagram is approached. Therefore, fast quenching into the unstable region leads to spontaneous growth of phase-separated nuclei. Near the plait point, SD can take place even with slow transition of the composition into the two-phase region. In particular, Nunes and Inoue [70] reported that SD results in high interconnectivity of the pores in the resulting membranes.

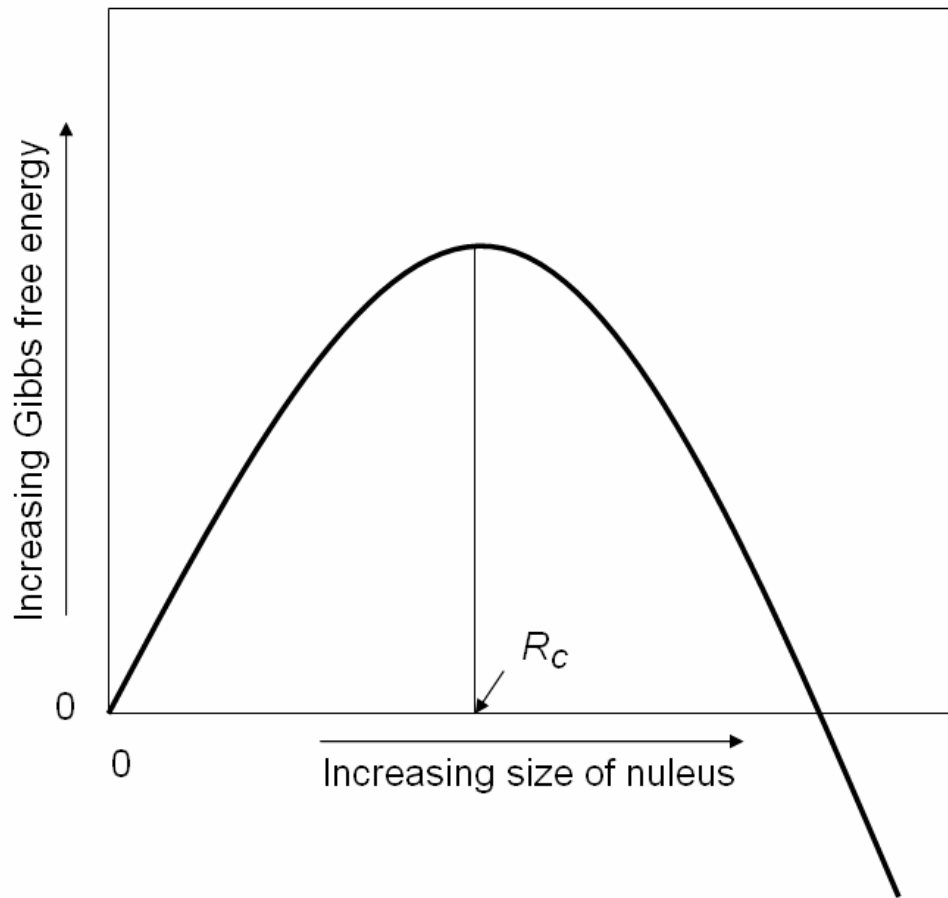


Figure 5.1: Schematic representation of Gibbs free energy as a function of the size of the nucleus.

5.2.2 Coalescence

Coarsening processes occur to minimize the interfacial free energy and have been widely studied for various polymer systems [70, 74-78]. Coalescence is the coarsening process in which dispersed microdroplets interact and combine to form larger droplets and eventually a continuous phase. Coalescence may also take place in conjunction with Ostwald ripening, in which the small droplets dissolve in the continuous matrix and re-precipitate on the larger drops [72]. There are several driving forces for coalescence, including Brownian motion of microdroplets, gravity, and Van-der-Waals attraction. For non-polymeric systems, the droplet growth mechanism via coalescence and Ostwald ripening processes is known to follow the power law:

$$\langle a \rangle \sim Kt^\xi \quad (5.1)$$

where $\langle a \rangle$, K and ξ are the mean radius of the droplets, the prefactor and the growth exponent, respectively. The growth exponent for non-polymer systems is approximately 0.33 [79]. However, McGuire et al. [78] observed appreciably faster coarsening in a polymer solution, with the growth exponent as low as 0.22. Martula et al. [79] showed that the viscosity is too high and the droplet size too large to allow Brownian motion, so one cannot expect many coalescence events to occur. In addition, the diffusion coefficient is too low for Ostwald ripening to explain the observed growth of the droplets. Hence, McGuire et al. [80] proposed a “coalescence-induced coalescence” model to account for these observations; their model was later improved by Martula et al. [79]. In this model rapid coalescence in polymer systems is explained by shape relaxation effects. Figure 5.2 shows their schematic representation of the flow fields that created a peanut-shaped composite droplet by coalescence. These flow fields caused coalescence events in

their vicinity by disturbing the nearby droplets. Martula et al. [79] showed that the model simulation agreed well with the experimental data.

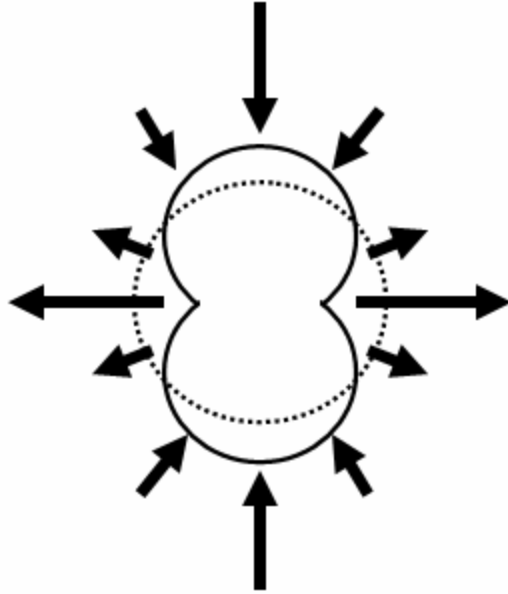


Figure 5.2: Schematic representation of the flow field created by shape relaxation of two small coalescing droplets (peanut-shaped solid line). The coalescence results in the round shape of the single large droplet (dotted line).

5.2.3 Macrovoid Pores (MV)

Macrovoid pores or macrovoids (MVs) are large open cavities, typically 5-100 μm in diameter, interspersed among the smaller (0.5–2 μm) sponge-like pores in the porous sublayer beneath the skin of the membrane [81]. Figure 5.3 shows a cross-sectional view of an asymmetric cellulose-acetate membrane that contains a large number of typical macrovoids. Application of a moderate pressure difference across macrovoid-containing membranes often leads to compaction (collapse of the porous sublayer) and possibly to skin rupture [5]. Compaction can cause a large reduction in the flux through the membrane. Skin rupture also results in a loss of permselectivity of the membrane, since all the components can simply flow through the large holes in the skin. Understandably, macrovoids are extremely undesirable in phase-inversion membranes used in chemical separation applications. Therefore, substantial research has been focused in this area. One of the approaches is to try to understand the macrovoid-formation process. Deeper understanding of the macrovoid-formation process will facilitate robust optimization of the membrane-formation process and avoiding macrovoid generation. The other approach is to develop recipes based on detailed experimental analysis and observations to avoid or minimize macrovoid formation.

Although macrovoids are highly undesirable for membranes, as described above, they can be useful in several specialized applications. For example, recent research has shown that macrovoid-containing membranes may be used for transdermal and osmotic drug delivery [14–15]. They also may be used for specialized ultrafiltration applications to separate colloid-size molecules from smaller ones. They may also be used as a support layer in composite membranes [16]. A process for making polyvinyl chloride membranes

containing large pores as a vapor permeable medium has been patented [17] and used by The B. F. Goodrich Company to make industrial screen-printing products. The application of macrovoids in miniature bioreactors has also been suggested [18]. It is evident from the above application areas that it is necessary to know how to control the occurrence, size, and shape of macrovoids, rather than simply to investigate methods to eliminate them.

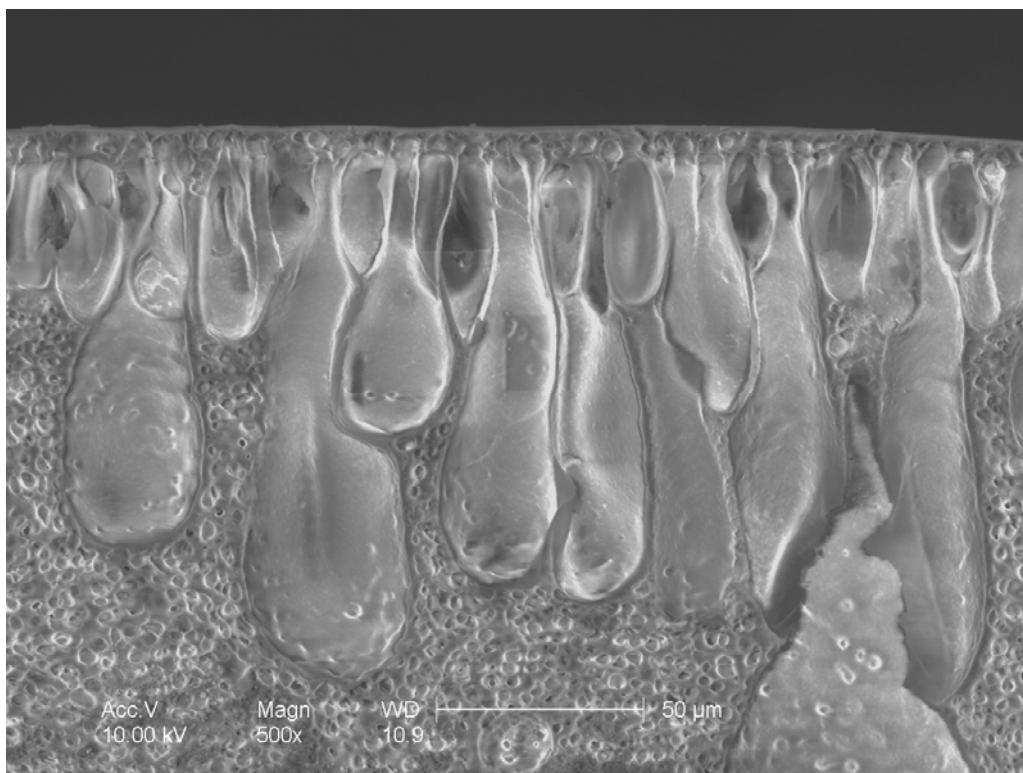


Figure 5.3: Environmental scanning electron micrograph (ESEM) of typical macrovoids in the cross-section of a cellulose-acetate membrane.

5.3 Review of Prior Studies

5.3.1 Hypotheses for Macrovoid-Formation Mechanism

As has been already stated, the mechanism of MV growth is still open to debate. More than a dozen mechanisms for MV growth have been proposed in the literature. These can be categorized into five major classes: (1) surface tension-driven instability at the casting solution/nonsolvent bath interface; (2) selective nonsolvent penetration at this interface; (3) diffusion between the growing macrovoid and the surrounding casting solution; (4) solutocapillary convection-aided mass transfer between the macrovoid and casting solution; and (5) enhanced coalescence of droplets in the supersaturated casting solution.

Matz [85] was the first to conduct an in-depth study of the macrovoid formation mechanism in membranes. In his work the initiation of macrovoids was explained by zero surface tension at the casting solution/nonsolvent bath interface, based on the observation of convective cells at that interface. Subsequent solvent diffusion into the microdroplets was hypothesized to be the growth mechanism of MVs. However, this hypothesis cannot explain the occurrence of MVs in dry-casting membranes or those in wet-casting membranes initiating well below the top surface.

Frommer and Messalem [86] claimed that surface tension gradients along the casting solution/nonsolvent bath interface induced Marangoni convection near the membrane surface, which is the main factor in mass transfer of nonsolvent across the interface, thereby forming macrovoids. The supporting evidence for this hypothesis comes from a direct observation of the convective flow at the interface and in the

macrovoid itself. However, a highly viscous polymeric system precludes the possibility for macrovoid growth via a Marangoni instability mechanism, so this hypothesis does not completely explain MV formation.

Strathmann et al. [87] believed that the rupture of the skin at the nascent membrane/immersion bath interface initiates macrovoids. They asserted that the shrinkage stress in the solidified polymer caused by syneresis cannot always be relieved by polymer molecule relaxation, due to the rapid nature of the precipitation process, thus leading to skin rupture. Once macrovoids have been initiated via skin rupture, their growth occurs due to shrinkage of the polymer matrix, which in turn causes drainage of freshly precipitated polymer from the bottom of the macrovoids to outside the macrovoids. However, one of the major drawbacks for this hypothesis is the lack of indication of syneresis cracks at the membrane surface.

Stevens et al. [88] also claimed that Marangoni instability, as described by Sterling and Scriven [89], is responsible for macrovoid formation. By performing a linear stability analysis, they showed that the small perturbations of surface tension at the interface between the casting solution and the nonsolvent bath could grow, thereby leading to instability and cellular convection. They hypothesized that if the surface-tension gradients at the interface were sufficiently large, the interfacial stress caused by the convection cells could lead to the rupture of the interface and to macrovoid initiation. They further hypothesized that the subsequent macrovoid growth was caused by the flow of nonsolvent from the bath into the nascent membrane. However, this hypothesis cannot account for the macrovoids observed below the top surface of the membrane and also for the formation of macrovoids in dry-cast membranes.

Broens et al. [90] agreed with Strathmann's hypothesis that the penetration of nonsolvent through 'cracks' on the skin is responsible for the initiation of MV growth. They also believed that the observed faster penetration rate of MVs as compared to the speed of the demixing front indicates that the diffusive flux of solvent into nascent MVs is responsible for the formation of MVs. They rationalized this diffusive flux with a lower Gibbs free energy by mixing solvent and nonsolvent. However, this hypothesis cannot explain the occurrence of MVs far away from the top skin. Also, no indication of cracks on the skin has been found yet.

Reuvers et al. [50] and Smolders et al. [91] proposed a hypothesis for the macrovoid formation in wet-cast membranes that has become widely accepted because it adequately explains all the observations made on the effects of various physical parameters and experimental conditions on macrovoid formation. This hypothesis is mainly based on the observation that macrovoids are formed only when the onset time of demixing in the polymer solution is below a certain critical value (instantaneous demixing). They proposed that the formation of macrovoids initiates via liquid-liquid demixing through spinodal decomposition just beneath the top surface of the casting solution. In this hypothesis the macrovoids grow downward into the casting solution, assisted by molecular diffusion from the surrounding casting solution. However, the molecular diffusion is not rapid enough in these viscous polymer solutions to permit macrovoid growth on such short time scales. Indeed, typical molecular diffusion coefficients in polymer casting solutions range from 10^{-17} to 10^{-5} cm^2/s , as compared to 10^{-5} cm^2/s for ordinary liquids. Furthermore, experimental observations showed normal pores surrounding the MVs with skin [90-100], indicating that a nucleation and

growth (NG) process (rather than SD) prevails in this layer. Their diffusion model results [50] also do not appear to support their hypothesis because spinodal decomposition cannot occur in the middle of the metastable region.

Shojaie et al. [31] proposed the solutocapillary convection-aided diffusion mechanism. In this hypothesis they agreed with Reuvers' assertion that the macrovoids initiate through the nucleation of the polymer-lean phase and grow in systems that exhibit instantaneous demixing at the surface of the casting solution. However, they pointed out that the growth by diffusion only, as hypothesized by Reuvers cannot account for the rapid growth of macrovoids (as little as 2-5 seconds). They believed surface tension-driven convection enhanced the propagation of MVs.

Pekny et al. [92] also proposed the growth mechanism by the solutocapillary convection-aided diffusion. They further asserted that the concentration gradient between macrovoids and the bulk solution is not favorable for the macrovoid growth, as opposed to both Shojaie's and Reuvers' hypotheses. Thus, they proposed a three-layer model composed of a demixing front, a supersaturated solution region and the bulk casting solution. By introducing the supersaturated layer they successfully accounted for the growth of macrovoids. The existence of a supersaturated layer in membrane-forming casting solutions had already been supported by Strathmann et al. [87]. However, the lack of an appropriate mathematical model to describe the wet-casting process prevented validation of this hypothesis.

Recently, Prakash [42] proposed a hypothesis similar to that of Strathmann et al. [81]. However, he argued that the rupture of the surface can occur not only at the demixing front, but also anywhere in the polymer framework. Based on his experimental

results and the Shojaie et al.'s dry-casting model prediction, he concluded that gelation provides an unstable condition in the casting solution beneath the gelled interface, although he did not explain how gelation could induce an unstable condition in the casting solution underneath the skin. He further hypothesized that the surface ruptures of the polymer-lean phase nuclei could cause coalescence of droplets grown by diffusion; coarsening following coalescence would cause the surface of the MV to become smooth. To validate his hypothesis, he carried out time-sectioning cryo-SEM experiments permitting visualization of coalescence and coarsening. Although his experiments are focused on the dry-casting process, his hypothesis is also applicable to the wet-casting process. However, an appropriate wet-casting model is needed to support the claim proposed in this hypothesis, i.e., the presence of gelation before the phase separation.

5.3.2 Phenomenological Approach to Macrovoid Formation

Optical microscopy has been the most popular device to study demixing and MV formation. These studies visualize the macrovoid formation process by placing the casting solution between two thin plates of glass. After several drops of nonsolvent are introduced between these plates using capillary action, the formation of the MV is observed with the help of optical microscopy. The demixed region appears opaque due to scattering of visible light. Matz [85] observed the rapid initial growth of MVs using this technique.

Frommer and Messalem [86] found that a rapid liquid-liquid demixing induces MV formation, corroborating similar experimental observations by Strathmann et al. [87], Broens et al. [90] and Broens et al. [93]. The opposite results were reported only by

Kang et al. [94]. Frommer and Messalem further found that the speed of the demixing front is proportional to the square-root of time, which has subsequently been rediscovered in many other research studies [90, 95, and 96]. These results led Frommer and Messalem to conclude that demixing is controlled by the diffusion of nonsolvent from the coagulation bath.

Ray et al. [97] observed MV growth in a water/acetone/cellulose-acetate system undergoing the wet-casting process using an experimental technique similar to that of Matz. They found that the addition of surfactant into the coagulation bath increased the MV growth rate. However, the surfactant concentration used in his study was much higher than the critical micelle concentration, causing the formation of micelles in their experimental membranes.

Wang et al. [98] also observed that the speed of the demixing front is proportional to the square-root of time. They argued that the variation of the MV size with the solvent/nonsolvent ratio in the coagulation bath supported the diffusion mechanism, as proposed by Reuvers et al. [50]. However, their SEM results showed a distorted shape of the MV, indicating the presence of the experimentally undesirable forced convective flow.

Konagurthu [81] investigated MV growth in the dry-casting process using optical microscopy. He showed that decreasing the evaporation rate can eliminate MVs in the final membrane and suggested that a decrease in the water concentration gradient in the casting solution reduces the driving force for solutocapillary convection. He also found that the addition of surfactant decreases both the lateral spacing and the size of MVs.

Prakash [42] used time-sectioning cryogenic scanning electron microscopy to observe the MV growth. He found that MVs can grow only in a bi-continuous region, but

not in the region where droplets are dispersed in a polymer matrix. From these results, he concluded that coalescence is involved in MV growth.

Vogrin et al. [99] showed that the MV growth strongly depends on the thickness of the initial casting solution. Morphological studies have revealed that a thicker initial casting solution encourages MV formation. They hypothesized that the thickness of a casting solution might be related to the thickness of the layer where macrovoid formation can occur in the casting solution. However, no evidence supporting this relationship has yet been found.

Recently, Pekny et al. [100] used video microscopy to show that neither diffusion nor solutocapillary convection-aided diffusion can account for a rapid initial growth of MVs. They claimed that the penetration of tracer particles from the coagulation bath into MVs indicated the occurrence of coalescence.

5.3.3 Membrane Casting in Low Gravity

To the best of our knowledge, there has been no attempt to utilize low gravity for the formation of polymeric membranes via the wet-casting process. However, several studies of the dry-cast membrane formation process in low gravity are found in the literature. McGinniss et al. [101] were the first group to study the dry-cast membrane formation in low gravity. A vacuum pump was used to absorb the solvent from the casting solutions in a sounding rocket, in the KC-135A parabolic flight research aircraft, and in the Space Shuttle. They showed that lower gravity leads to higher porosity of the final membrane, indicating the potentially strong influence of gravity on the mass-transfer coefficient in the gas phase. However, no analysis of the effects of changes

in the gravitational force field on the mass-transfer coefficient was presented in this study. Moreover, using a vacuum to cause solvent transfer from the casting solution could be very disruptive and could result in a lack of reproducibility.

Pekny et al. [92, 102] and Khare et al. [103] both utilized the KC-135A parabolic flight research aircraft to create low gravity environments to fabricate cellulose acetate membranes via the dry-casting process. In both studies a new design of the casting apparatus was used to create less disruptive conditions of the membrane casting process than the vacuum evaporation used in the prior study. There was some improvement, but the MV shapes produced in their studies were still slightly distorted, indicating the presence of undesirable external convective force. Pekny et al. and Khare et al. showed that the linear number-density and size of macrovoids were significantly greater in low gravity than in normal gravity due to the effect of buoyancy. They also claimed that their results could not be explained by Reuvers' diffusive growth hypothesis.

5.4 Motivation for This Study

For more than a decade, the ability to control macrovoid pores has been extremely limited because the physics of the MV formation process has been poorly understood. Although there are more than a dozen hypotheses regarding the formation mechanism of MVs, none of these models could successfully explain all observed phenomena in MV formation due to the lack of a rigorous model as well as the limited experimental approaches for the wet-casting process. The model presented in the previous chapter incorporating both the convective and diffusive contributions can provide significant

insight into the macrovoid-formation process, providing a more description than any other model in the literature.

The goal of this section of the study is to test three distinct hypotheses that have been put forth to explain macrovoid formation: (1) Diffusion is the only process playing a key role in the formation of MVs in polymeric membranes (diffusion mechanism); (2) Membrane morphology is strongly influenced by solutocapillary convection effects that are masked by gravitational body forces in normal gravity (solutocapillary convection-aided mechanism); and (3) Coalescence of polymer-lean phase droplets in the liquid casting solution leads to MVs (coalescence mechanism).

Low-gravity experiments are essential for this research in order to study the possible effect gravity might have on solutocapillary convection and free convection. Such experiments conducted by Pekny et al. already have established the dominant role of buoyancy forces in suppressing macrovoid growth in the dry-casting process. Low-gravity conditions eliminate any buoyancy force, thus permitting study of the role of solutocapillary convection in MV growth. In addition, free convection is negligible in low gravity. Therefore, performing the study in low gravity provides an experimental environment corresponding to the conditions accounted for in the developed wet-casting model.

5.5 Experimental Design

5.5.1 Materials

The water/acetone/cellulose acetate system was chosen as a representative wet-casting system in order to use the model presentation presented in the previous chapter for the analysis of experimental results.

Cellulose acetate (Eastman, acetyl 39.69 weight %) was dehumidified at 70 °C for more than 24 hours before mixing with acetone (Pharmco, HPLC-UV grade) to prepare the casting solution. Water (Fischer, HPLC grade) was processed to eliminate any dissolved gases using an electronic stirrer and a vacuum pump. The casting solution was homogenized for at least 8 hours. All experiments were performed within 12 hours of the preparation of a homogenous casting solution.

5.5.2 Parabolic flight research aircraft (KC-135A)

There are three possible ways to simulate a low-gravity environment on earth. One is a ‘free fall’, which requires an initial high altitude for a free-falling elevator that has the ability to provide low-gravity for at least several seconds and also a method to stop the whole system before it crashes at the bottom. A low-gravity environment can also be simulated via rapid centrifugal motion. The third and most popular method is using a parabolic airplane flight (Figure 5.4). NASA provides this with their KC-135A aircraft. This aircraft flies in a series of parabolic maneuvers that provide short periods (25-30 sec) of near-zero gravity in the cabin followed by a high-gravity pullout. To

accomplish successful experiments on this airplane, the time limitation of low gravity should be considered in the experimental design.

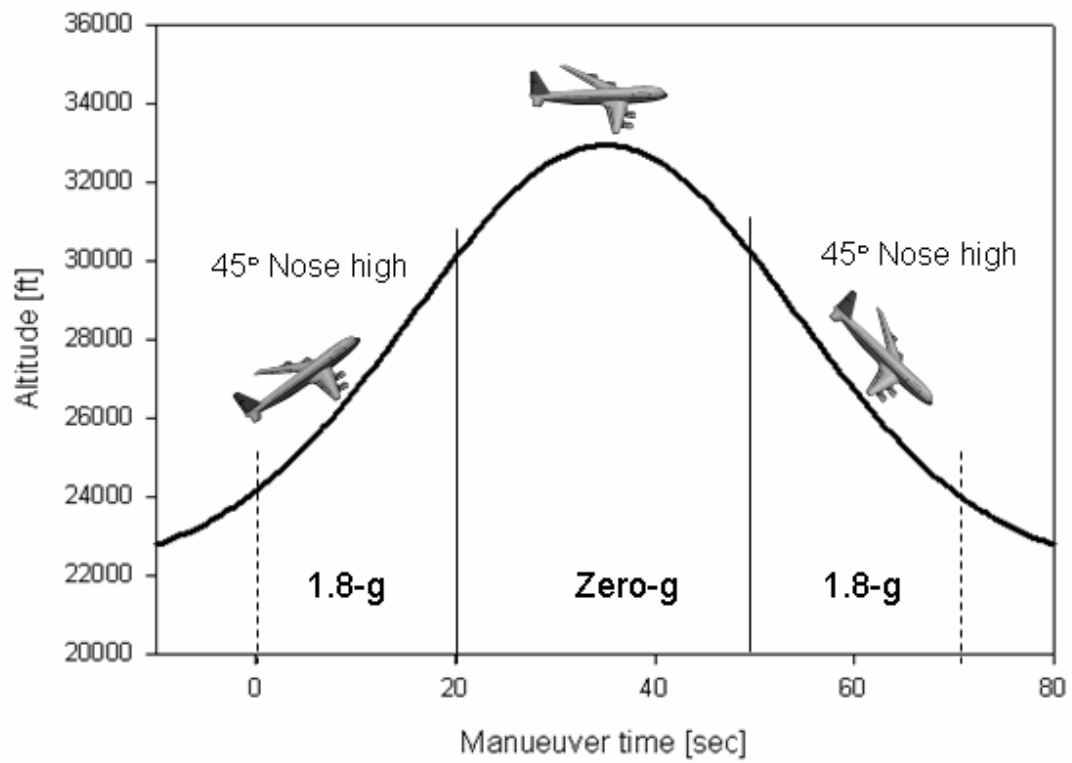


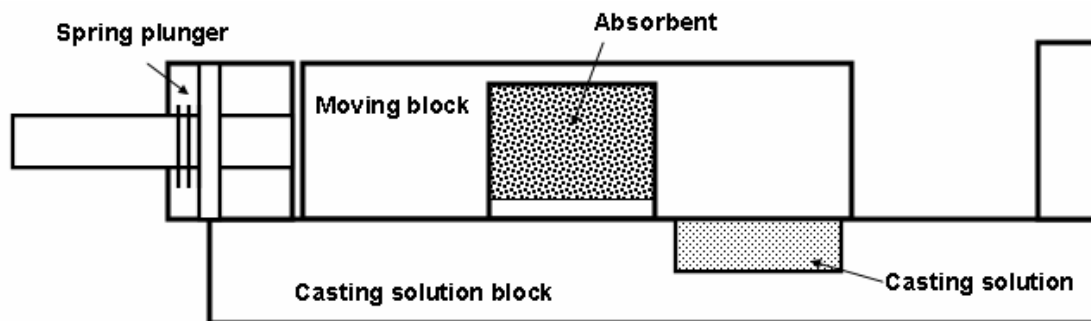
Figure 5.4: Schematic representation of parabolic flight of NASA-KC135A.

5.5.3 Membrane Casting Apparatus (MCA)

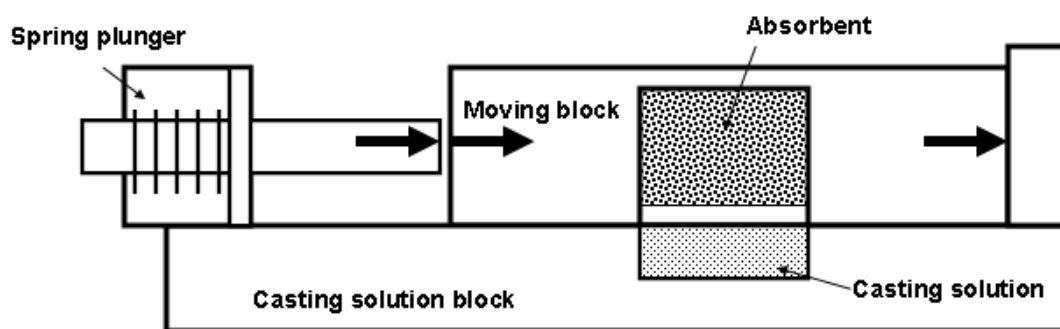
5.5.3.1 Design Requirements

Most of the commercial wet-cast membranes are manufactured by simply continuously drawing the casting solution through a nonsolvent bath. However, in the absence of gravity, this simple process needs further consideration, since there is no force holding the casting solution and nonsolvent bath inside the apparatus. The requirements of a membrane casting apparatus (MCA) in low gravity are that all chemicals should be encapsulated and that this apparatus should be able to cast a membrane on a controlled time-scale.

Pekny et al. [92, 102] and Khare et al. [103] used a spring plunger-driven membrane-casting apparatus for the dry-casting process in low gravity, as illustrated in Figure 5.5. The lower or casting solution block of the membrane-casting apparatus consists of six 150 μm deep wells. The upper or moving block contains activated carbon blocks of comparable size and shape. The membrane is cast by moving the casting wells directly under the absorbent. A spring plunger pushes the moving block (which has casting wells) until it hits the side wall. Although this novel membrane-casting apparatus (MCA) enabled them to make membranes under different gravitational conditions, the membranes formed had a distorted morphology indicating the presence of an undesirable forced convection that was probably introduced by viscous drag and/or by the collision between the wall and the moving block. Therefore, the preliminary experimental and modeling studies were conducted to identify the origin of the undesirable forced convection and to find a way to avoid it.



(a)



(b)

Figure 5.5: Membrane-casting apparatus used by Pekny et al [92, 102] and Khare [103]:

(a) Before moving the absorbent block and (b) after moving the absorbent block.

5.5.3.2 Preliminary Experiments and Results

The test apparatus, made of polycarbonate vapor-polished to improve its optical clarity after machining, was used to observe the convective fluid motion of the casting solution. A glycerin/water (70/30 volume%) solution was used as a substitute for an acetone/water/cellulose-acetate solution because acetone can chemically decrease the optical clarity of the polycarbonate testing apparatus. The density of the glycerin/water solution is approximately 1.1 g/cc and its viscosity is about 600cp, making it much less viscous than the casting solution used in the later parts of this MV study. Note that the density of the casting solution reaches 1 million cp when gelation occurs (cellulose acetate/acetone = 0.5/0.5, weight fraction). Therefore, this preliminary experiment uses a condition in which much more convective motion can occur than the viscous drag in the casting solution. To visualize the motion of fluid particles, dye (bromothymol blue) was applied at the top of the casting slit. The casting slit aspect ratio can be manipulated by injecting a variable amount of pure glycerin into the slit before the glycerin/water solution is placed into the cell. The pure glycerin acts as a virtual block of solid since its viscosity is much higher (800cp). Figure 5.6 shows the slit filled with dye, the glycerin/water solution and pure glycerin. The tested aspect ratios were 1:1, 1:3, 1:5 and 1:13 (width:depth). When the sliding block or glass slide covering the slit was moved horizontally, there was no observable indication of the convective motion for all tested width:depth aspect ratios, although some degree of vertical diffusive motion of dye was observed. Then, experiments with aluminum powder instead of dye in order to minimize the vertical diffusion also showed that viscous drag cannot create an undesirable forced convection in the casting process.

However, the effect of convection caused by mechanical disturbance was found to be significant in experiments focused on the effect of impact using the same testing apparatus. In the first set of these experiments simulating Pekny et al.'s MCA [92 and 102], the upper moving block was quickly pushed all the way across the top of the glycerin/water mixture until impacting against an obstacle beyond the slit of the testing apparatus, in order to determine if the impact caused any disturbance in the glycerin/water solution. The disturbance of the glycerin/water mixture was detected by the distorted vertical diffusion of the dye or aluminum powder. The second set of experiments, without collision against the obstacle, showed a shorter and undistorted vertical diffusion of dye. These results indicate that the mechanical impact was the cause of the undesirable forced convection, which then disturbed the flow in the casting solution and distorted the shape of MVs in Pekny et al.'s experiments.

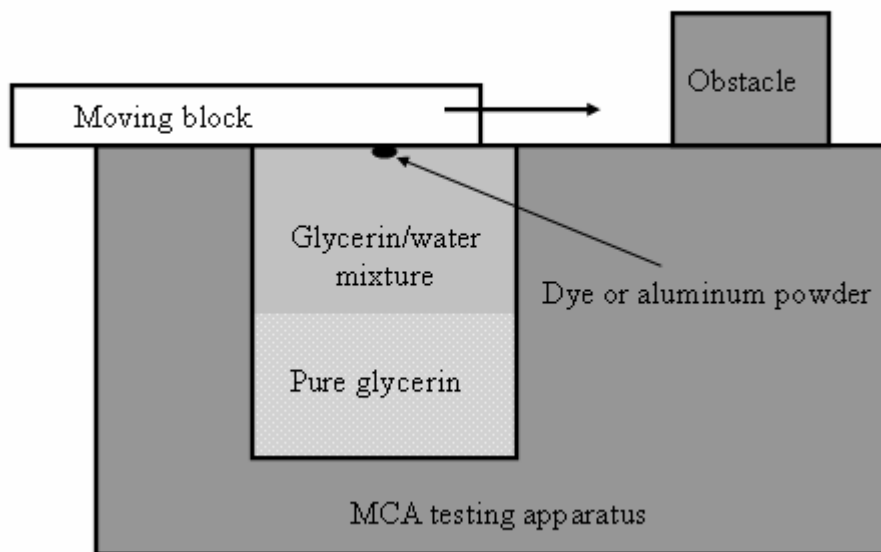


Figure 5.6: Schematic of MCA (membrane casting apparatus) testing apparatus filled with dye or aluminum powder, the glycerin/water mixture, and pure glycerin to visualize the effects of viscous drag.

5.5.3.3 Preliminary Flow Simulations and Results

In order to verify the experimental results, flow simulations were performed using a commercial fluid mechanics program, FIDEP (v8.52). The simulated aspect ratios were 1:2, 1:3, and 40:1 (width:depth) . The speed of the moving block was assumed to be 4 cm/s. The viscosity and density of the casting solution were maintained at 1000cp and 1g/cm³, respectively. The simulation results for each aspect ratio are shown in Figures 5.7, 5.8, and 5.9. It should be noted that the results are represented by dimensionless groups corresponding to time and velocity. The dimensional values of time and velocity are related to the each dimensionless value as:

$$t = 0.025 \times t^* \quad (5.2)$$

$$U_x = 4 \times U_x^* \quad (5.3)$$

The dimensional velocity parallel to the direction of the moving block (u_x) reaches a maximum at the middle of the top of the casting solution well. This velocity represents maximum convective movement of fluid due to viscous drag. If this convection velocity is appreciably less than the diffusion velocity of any species in the casting solution, then the disturbance due to viscous drag is negligible. In order to calculate the diffusion velocity, the species flux is approximated by the following equation:

$$N_A = c_A \bar{v}_A \approx D_{AB} \frac{\Delta c_A}{\Delta x} \approx D_{AB} \frac{c_A}{\Delta x} \quad (5.4)$$

Therefore, the approximate diffusion velocity is

$$\bar{v}_A = \frac{D_{AB}}{\Delta x} \quad (5.5)$$

Using the penetration theory, the characteristic length for diffusion can be calculated with the following equation:

$$\Delta x = \sqrt{D_{AB}t_c} \quad (5.6)$$

Combining Equations (5.5) and (5.6) yields

$$\bar{v}_A = \sqrt{\frac{D_{AB}}{t_c}} \quad (5.7)$$

where, t_c is the observation time. The minimum diffusion velocity of acetone inside the casting solution was obtained using the minimum diffusion coefficient, $D_{AB} = 10^{-17} \text{ cm}^2/\text{s}$. Then, the minimum diffusion velocity was compared with the convection velocity at that point in time. A summary of these results is given in Table 5.1. According to these results, even with a 40:1 aspect ratio of the casting solution, the convection effect induced by viscous drag will be negligible after 6.25×10^{-4} seconds since even the minimum diffusion velocity is 6.7 times larger than the maximum convection velocity. These results imply that the convection is damped out very quickly and thus difficult to observe in the experiments presented in the previous section. Therefore, the simulation results support the experimental results that the effect of viscous drag is negligible in the wet-casting process.

Table 5.1: Summary of the convective velocity due to viscous drag and the diffusion velocity.

Dimension [cm] $\times 10^{-1}$		Observation time [s]	Velocity [cm/s] $\times 10^{-7}$	
width	depth		Convection	Diffusion
1	2	6.25×10^{-4}	1.7480×10^{-3}	1.2649
1	3	6.25×10^{-4}	1.2350×10^{-2}	1.2649
40	1	6.25×10^{-4}	1.8600×10^{-1}	1.2649

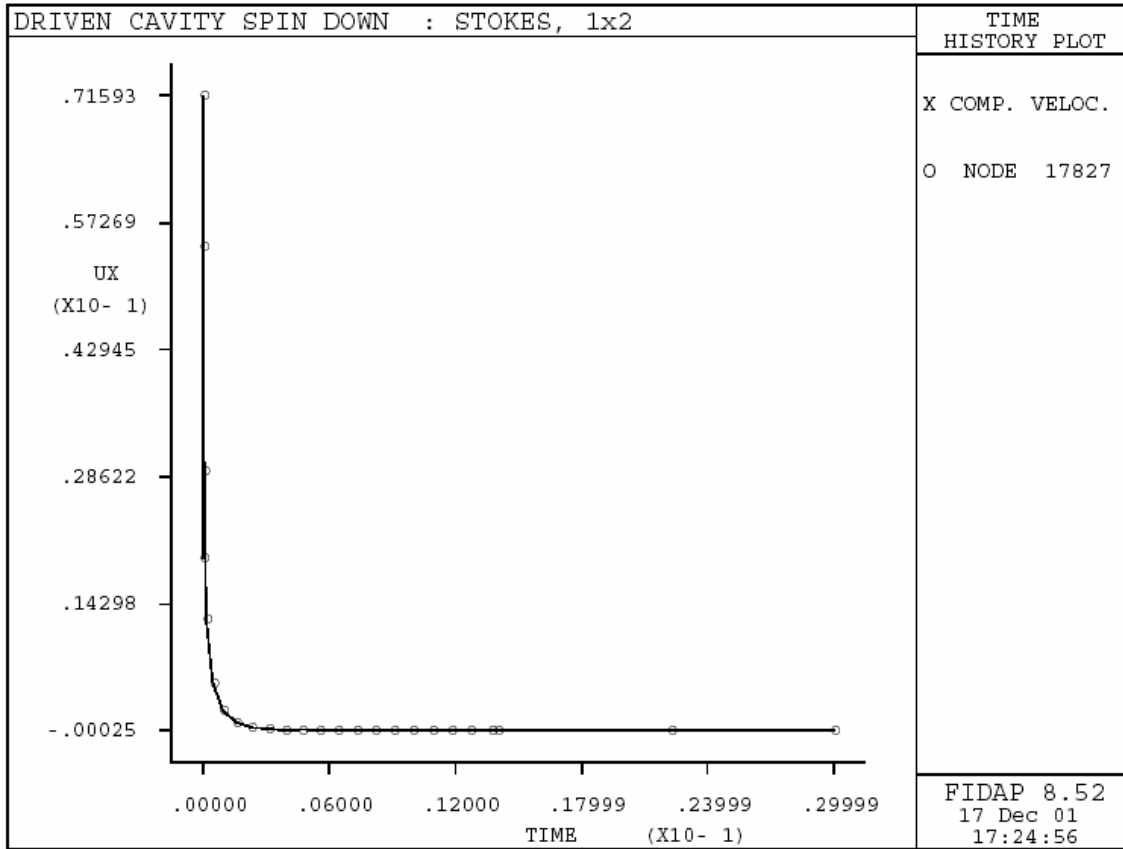


Figure 5.7: Dimensionless parallel velocity change with dimensionless time at the top of the casting-solution well having aspect ratio = 1:2 (width:depth).

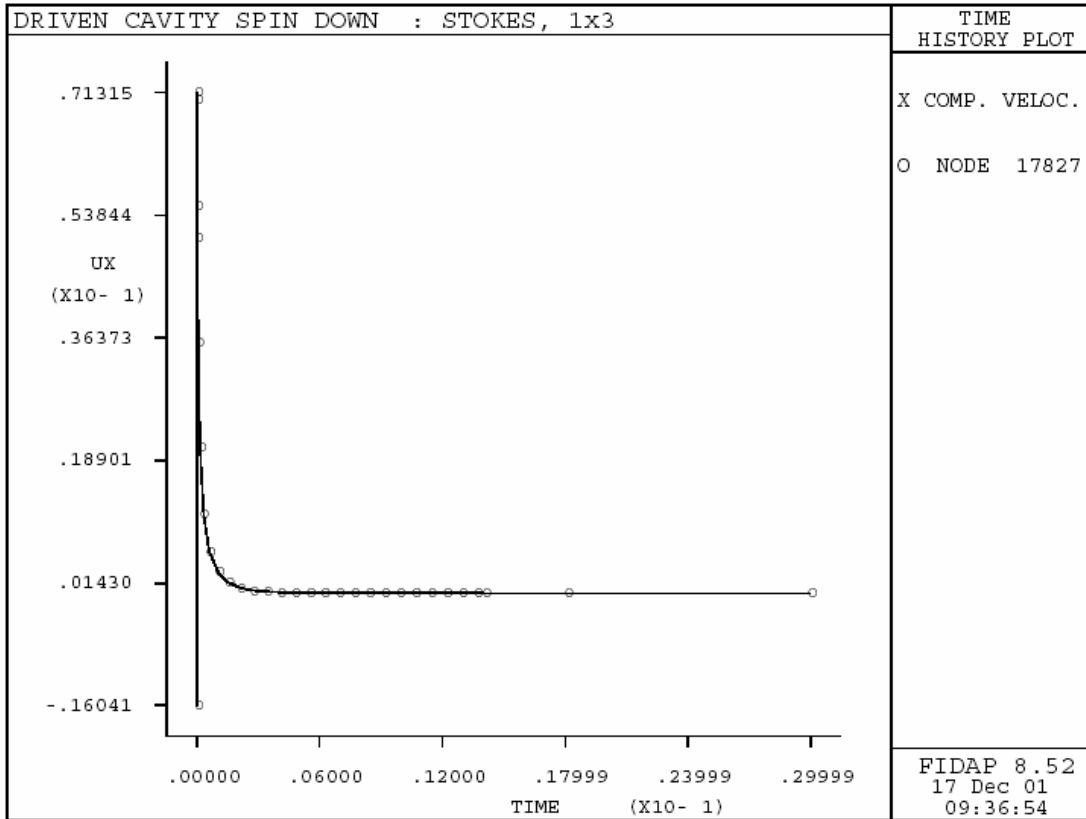


Figure 5.8: Dimensionless parallel velocity change with dimensionless time at the top of the casting-solution well having aspect ratio = 1:3 (width:depth).

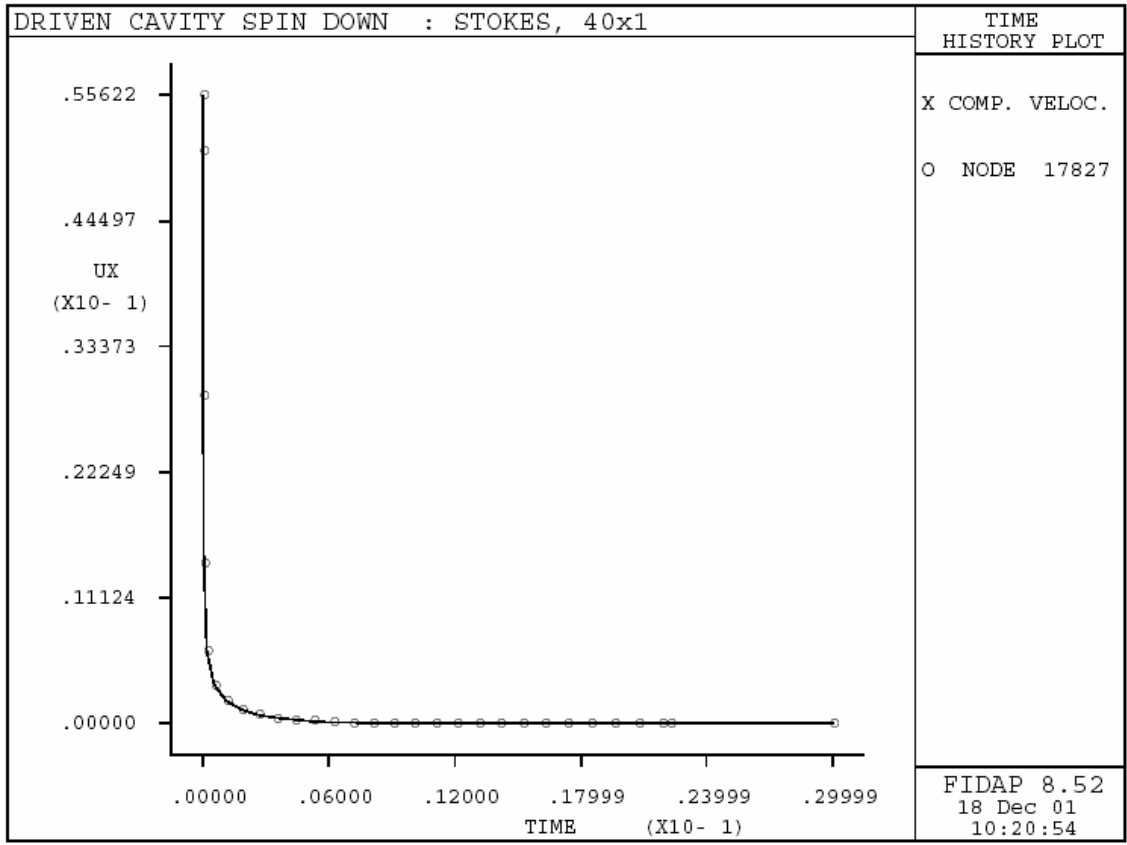


Figure 5.9: Dimensionless parallel velocity change with dimensionless time at the top of the casting-solution well having aspect ratio = 40:1 (width:depth).

5.5.3.4 Novel Membrane Casting Apparatus

Both experimental and flow simulation results showed that the undesirable forced convection observed in Pekny et al.'s study was due to the mechanical impact induced by the spring-loaded plunger mechanism of their MCA. Therefore, this mechanism for low-gravity experiments was replaced with a cam-driven mechanism for our study in order to avoid distortion of the MVs in the final membrane. Since the cam-driven mechanism pushes the moving block at a lower speed, the size of the casting solution well in our MCA was made smaller (2 mm×30 mm) so that the entire top area of the casting solution could contact with the nonsolvent bath simultaneously. Considering that a typical macrovoid is less than 100 μm, this size of well is sufficient to study MV formation.

In addition, there were several changes of the design of MCA to accommodate the wet-casting process in low gravity. The moving (upper) block and the casting (lower) block were precisely machined in order to prevent any leakage of liquids without using any glue or sealant between the two plates. Both plates were made of Delrin® (polyoxymethylene), which has good mechanical and optical properties. Since adhesion of a cellulose-acetate membrane to Delrin® can cause undesirable damage of the final membranes when they are removed from the MCA for further analysis, the bottom of the casting-solution well was made of non-stick anodized aluminum. The anodized aluminum bottom was designed to be adjustable in order to manipulate the depth of the well and therefore the initial thickness of the casting solution for experiments

Figure 5.10 shows a schematic side view of the new MCA. During the preparation step, the location of anodized aluminum block in each casting-solution well was adjusted for the initial casting-solution thickness using screws or thin spacer bars. The depths of

the casting-solution wells were rechecked with a micrometer. Then the casting solution and water were injected into each well using syringes. This step was completed 30 minutes before takeoff. Inside the KC-135A aircraft, the MCAs were placed on a metal support and connected to the light-reflectometry apparatus. As soon as low gravity was achieved, the cam was rotated to initiate the wet-casting process as shown in Figure 5.10 (b). After 25 seconds, the moving bock was advanced using the cam to completely cover the top of the well so that the final membrane could be stored safely.

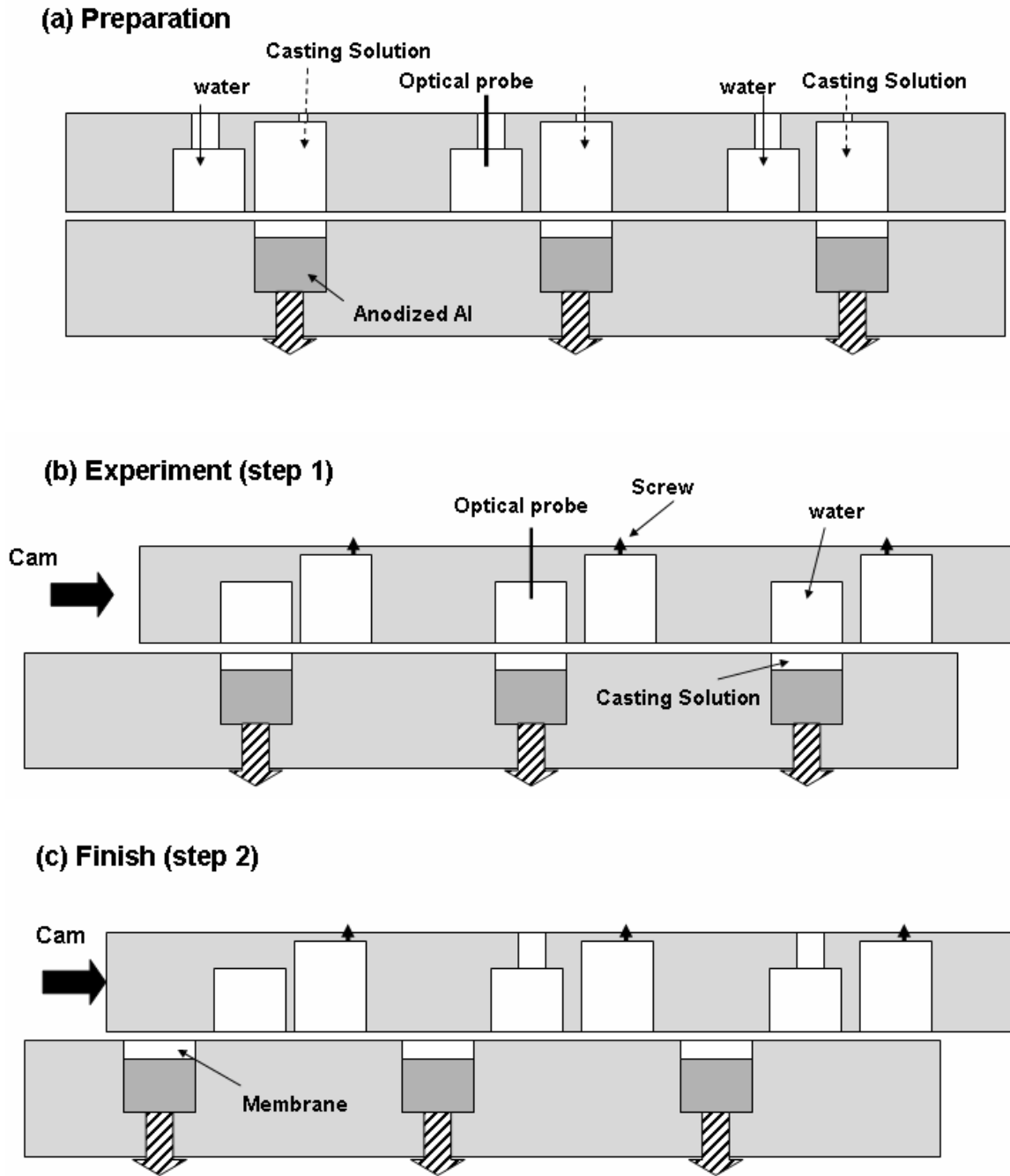
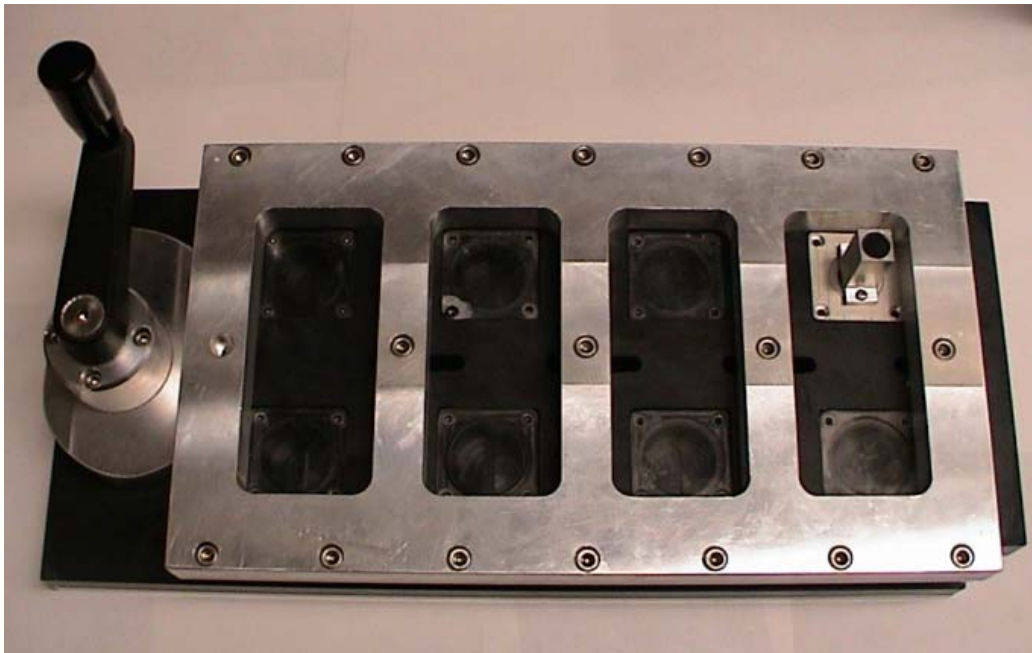
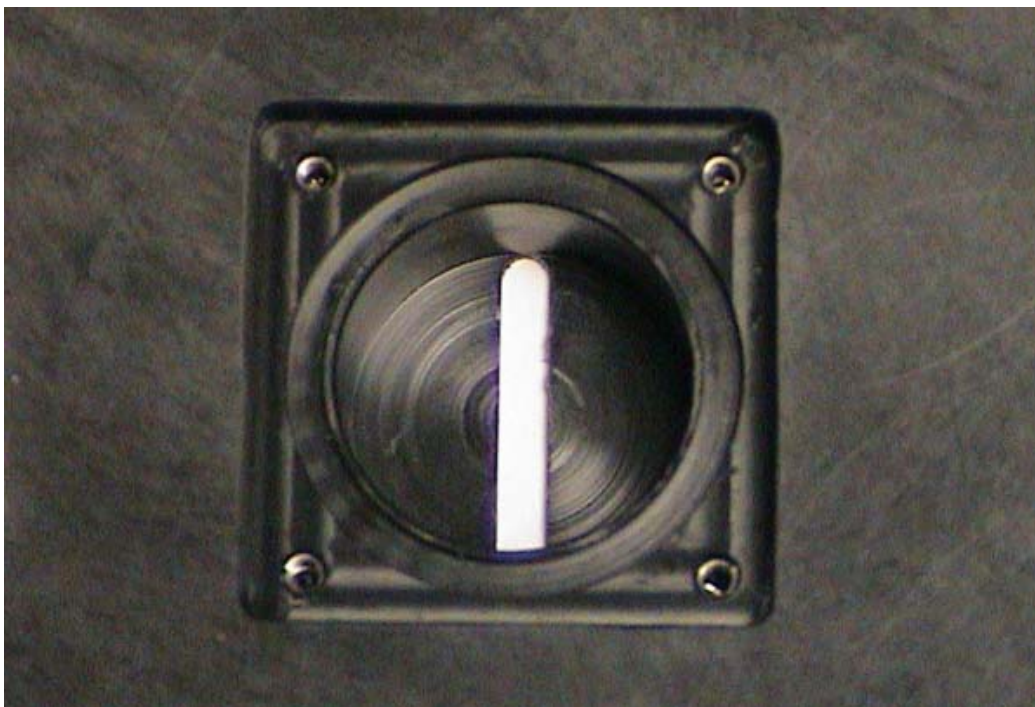


Figure 5.10: Schematic side view of the new membrane casting apparatus for low gravity in the three experimental stages: (a) setup; (b) membrane formation; and (c) storage of the membrane.



(a)



(b)

Figure 5.11: Photograph of (a) the new membrane casting apparatus (MCA) and (b) nonsolvent chamber in the moving block of the MCA.

5.5.4 Light-Reflection Measurement

As discussed in Chapter 3.8.2, scattered visible light from the phase-separated microdroplets can be used for real-time measurements of the onset time for phase separation [104]. A light-reflection apparatus (Oriel Model 77501) composed of a laser source, a bifurcated fiberoptic cable and a photodiode was attached to the MCA. The laser light has a wavelength of 600~670 nm. The light-intensity data are measured every 0.5 seconds and stored in a laptop computer.

5.5.5 Surfactant-Induced Membrane Formation

According to the coalescence hypothesis for the macrovoid-growth mechanism, reduction of the surface energy of the dispersed microdroplets should lower the driving force for coalescence events. Therefore, the presence of surfactant below its critical micelle concentration in the casting solution should lead to significantly different morphology of MVs and the final membrane. To test this hypothesis, Triton X-100 (polyoxyethylene iso-octyl phenyl ether, critical micelle concentration = 40ppm) was used in this study.

5.6 Presentation of Experimental Results

All membrane morphologies shown in this section were fabricated using the new MCA. The initial casting solution composition (water/acetone/water = 0/0.85/0.15, weight fraction) was kept identical for all the experiments. Initial thicknesses were $75 \pm 2 \mu\text{m}$ and $125 \pm 3 \mu\text{m}$ to ensure complete formation of membranes within 30 seconds,

which is the duration of low gravity in the KC-135A aircraft. For the surfactant-induced experiments, water with 20ppm of Triton X-100 was placed in the nonsolvent bath chamber of the MCA. Subsequently, morphological analysis was carried out on uncoated frozen membrane samples using an environmental scanning electron microscope (ESEM, FEI/Philips XL30 FEM ESEM).

Figure 5.12 shows a representative environmental scanning electron micrograph of the cross-sectional view of a membrane cast under low gravity with an initial thickness of $75\mu\text{m}$. The final membrane morphology shows a nearly symmetric structure except for a few larger pores beneath the very thin skin. The corresponding light intensity data in Figure 5.13 show an immediate drop of intensity, indicating very rapid phase-separation or glassification. Indeed, this change of light intensity was detected in all experiments regardless of the thickness of the casting solution, the magnitude of the gravitational acceleration, and the presence or absence of surfactant in the water bath. Figure 5.14 is a membrane morphology cast under low gravity using a water bath containing surfactant and the same casting solution used for the membrane described in Figure 5.12. The presence of surfactant in the water bath made only a slight difference in the structure of the final membrane when the initial thickness of the casting solution was $75\mu\text{m}$. However, a closer look revealed that the structure of the membrane formed with surfactant in the water bath did not have the larger pores that were present in the corresponding surfactant-free coagulation bath experiments. Under normal gravity without surfactant, the casting solution formed a membrane with pores dispersed in a dense polymeric matrix, as shown in Figure 5.16. Under high gravity, the same initial casting solution produced a significantly thinner dense polymer film.

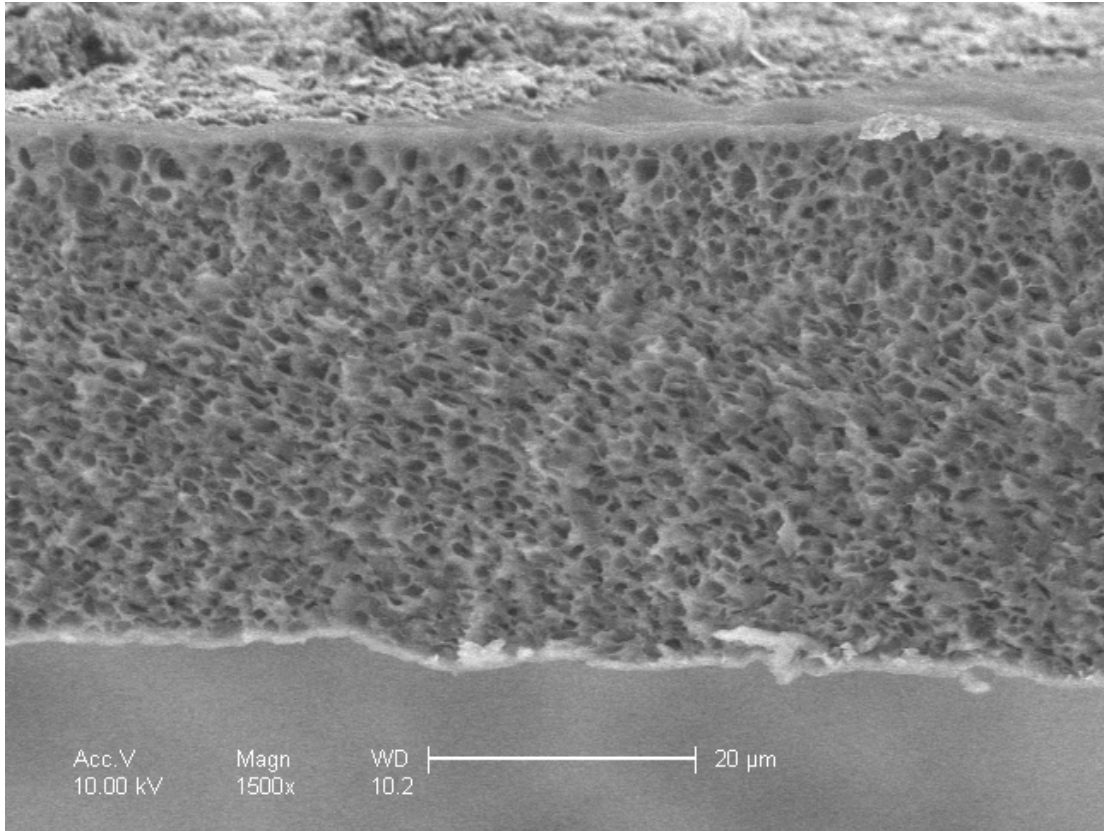


Figure 5.12: Environmental scanning electron micrograph of a membrane cast from a ternary water/acetone/cellulose-acetate solution with a pure water bath in low gravity. The initial water and acetone mass fractions and film thickness are $\omega_1^\circ = 0$, $\omega_2^\circ = 0.15$, and $L_o = 75\mu\text{m}$, respectively.

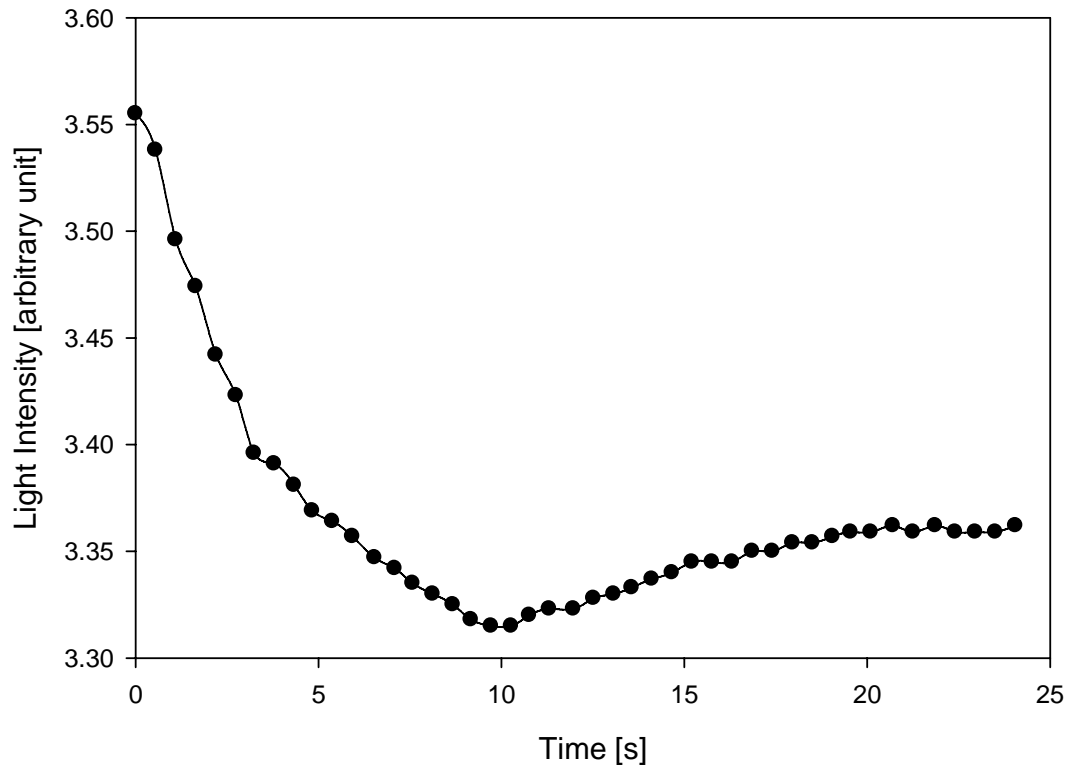


Figure 5.13: Light intensity data for cellulose-acetate membrane formation corresponding to the initial casting condition used for Figure 5.12.

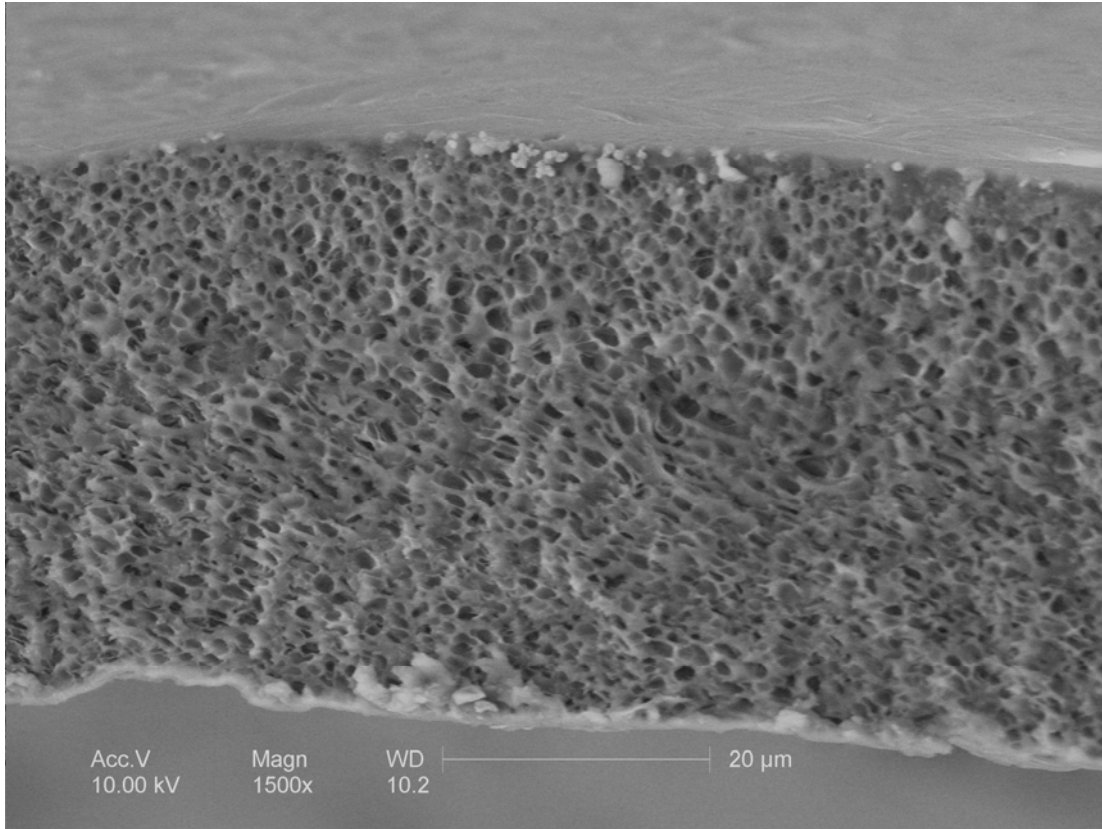


Figure 5.14: Environmental scanning electron micrograph of a membrane cast from a ternary water/acetone/cellulose-acetate solution with a water/surfactant (20 ppm) bath in low gravity. The initial water and acetone mass fractions and film thickness are $\omega_1^0 = 0$, $\omega_2^0 = 0.15$, and $L_0 = 75\mu\text{m}$, respectively.

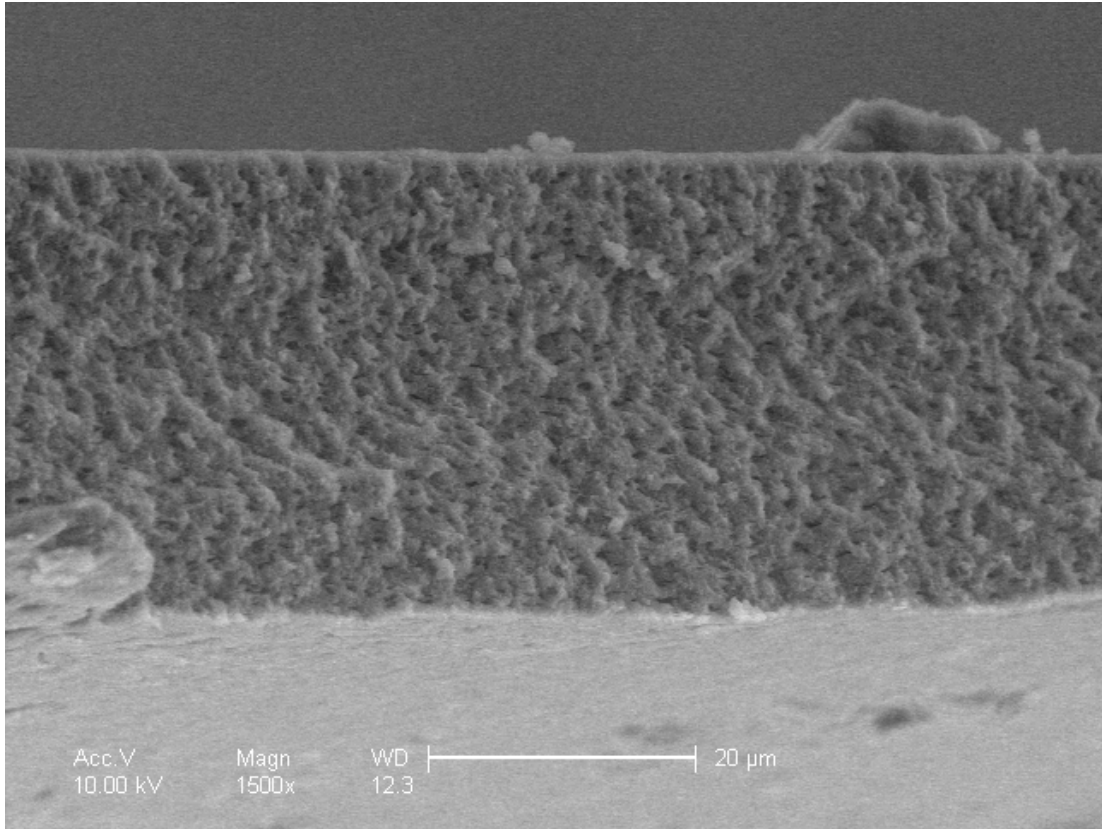


Figure 5.15: Environmental Scanning micrograph of a membrane cast from a ternary water/acetone/cellulose-acetate solution with a pure water bath in normal gravity. The initial water and acetone mass fractions and film thickness are $\omega_1^\circ = 0$, $\omega_2^\circ = 0.15$, and $L_\circ = 75\mu\text{m}$, respectively.

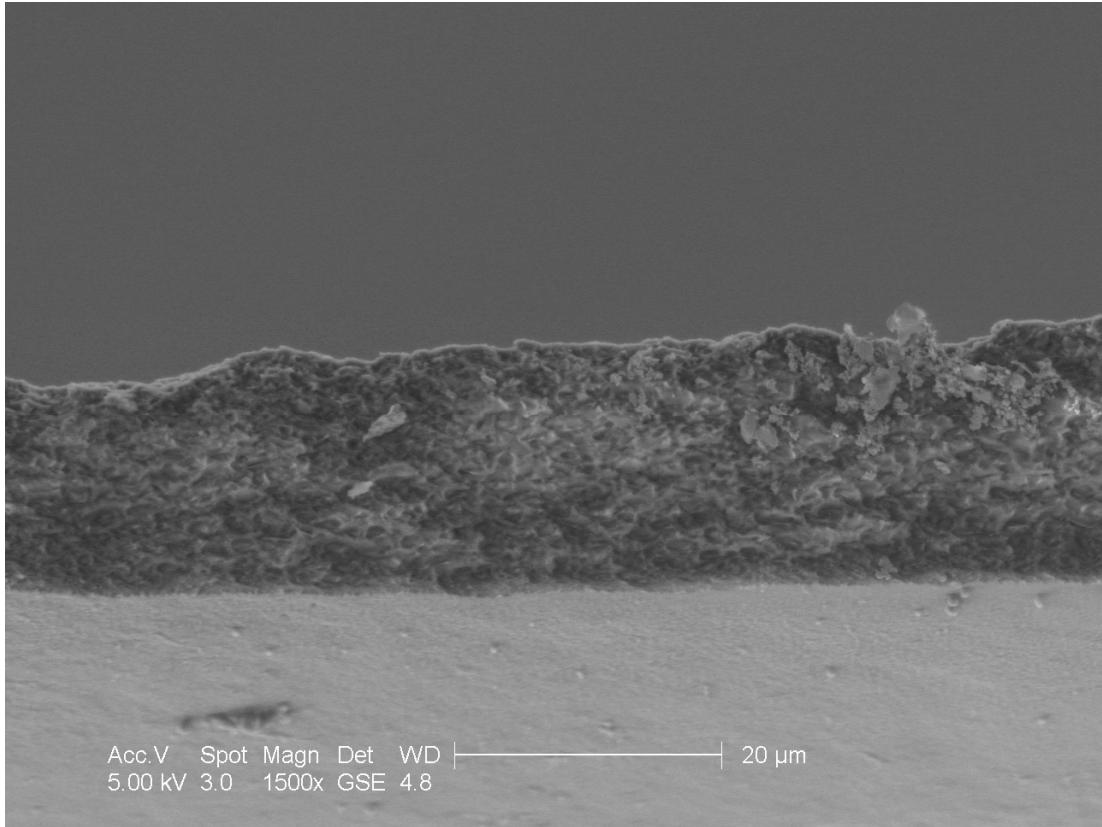


Figure 5.16: Environmental Scanning micrograph of a membrane cast from a ternary water/acetone/cellulose-acetate solution with a pure water bath in high gravity. The initial water and acetone mass fractions and film thickness are $\omega_1^\circ = 0$, $\omega_2^\circ = 0.15$, and $L_s = 75\mu\text{m}$, respectively.

Increasing the initial thickness from $75\mu\text{m}$ to $125\mu\text{m}$ resulted in a remarkably different membrane structure. Using the same pure water bath and casting solution, a $125\mu\text{m}$ initial thickness produced a membrane with MVs just beneath the top skin, with large voids near the bottom, as shown in Figure 5.17. Figure 5.18 shows the corresponding light intensity data, indicating immediate solidification. Interestingly, when surfactant was present in the water bath, smaller but more numerous MVs formed at the top of the membrane, and there were large voids at the bottom surrounded by MV-like pores, as shown in Figure 5.19. These huge voids at the bottom with surrounding MV-like pores did not occur when membranes were formed under normal gravity, but normal MVs were present, as seen in Figure 5.20. Under high gravity, no MVs were formed, as shown in Figure 5.12. When the initial thickness was increased to $500\mu\text{m}$ even under normal gravity conditions, there were large voids at the bottom as well as MVs at the top.

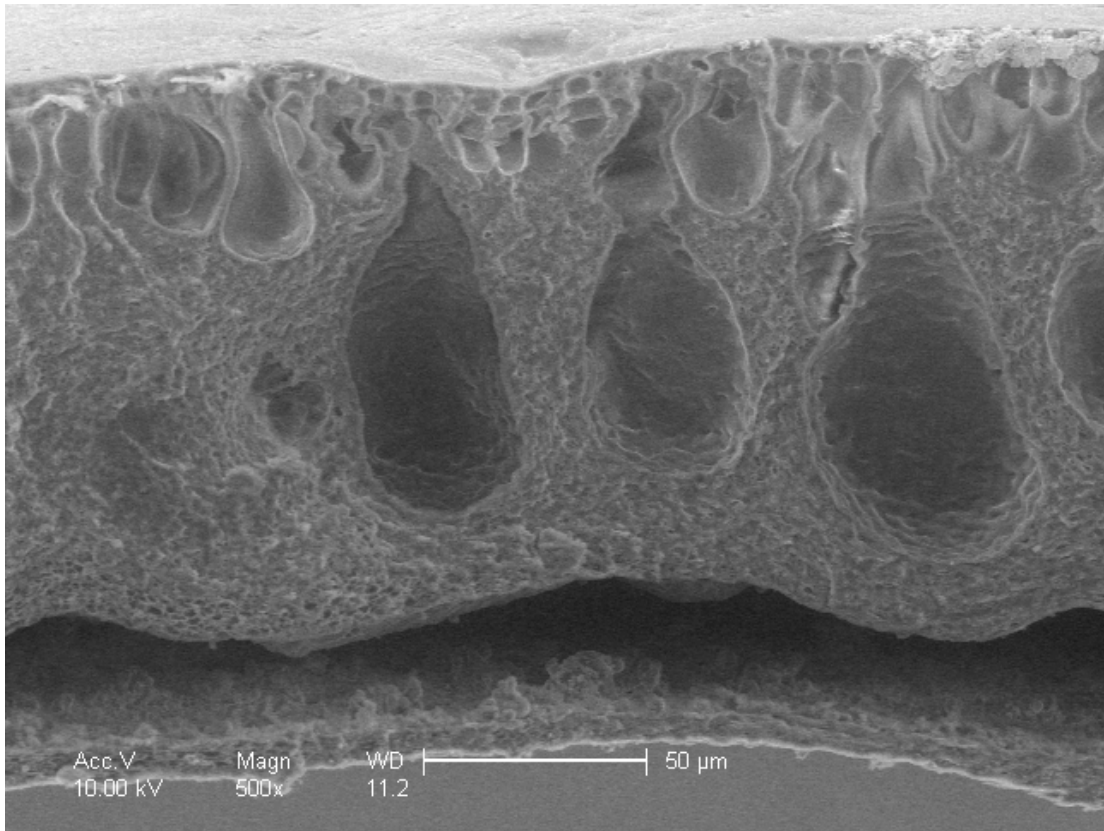


Figure 5.17: Environmental Scanning micrograph of a membrane cast from a ternary water/acetone/cellulose acetate solution with a pure water bath in low gravity. The initial water and acetone mass fractions, film thickness are $\omega_1^o = 0$, $\omega_2^o = 0.15$, and $L_o = 125\mu\text{m}$, respectively.

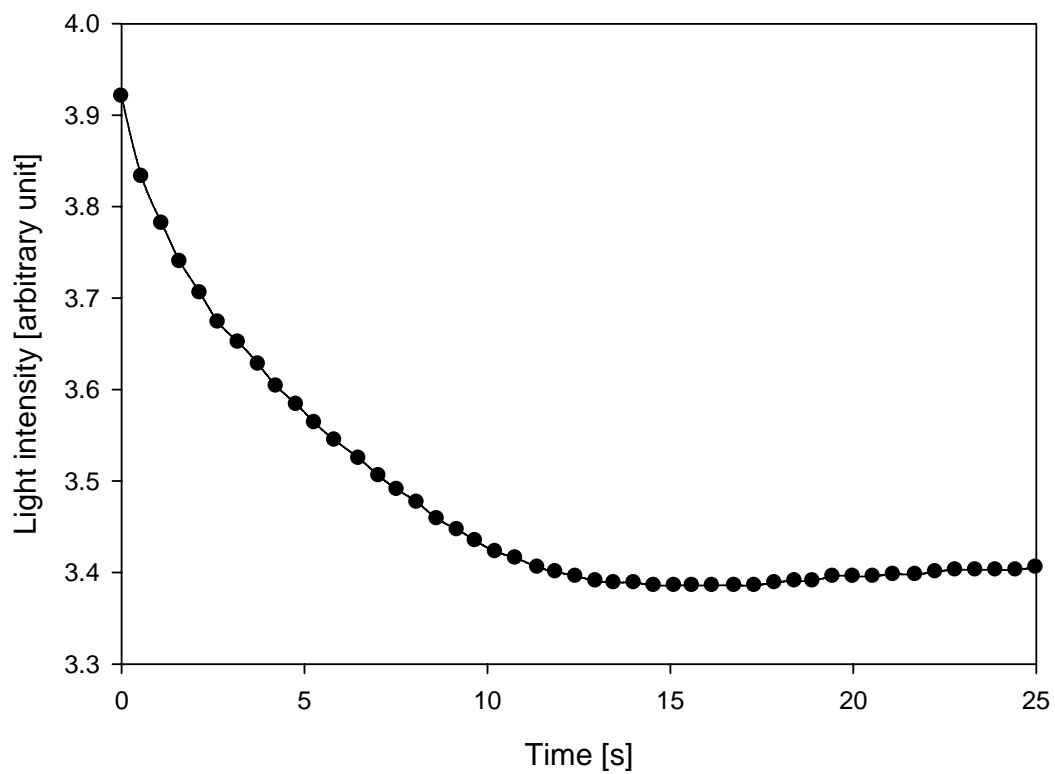


Figure 5.18: Light intensity data for cellulose-acetate membrane formation corresponding to the initial casting condition of Figure 5.17.

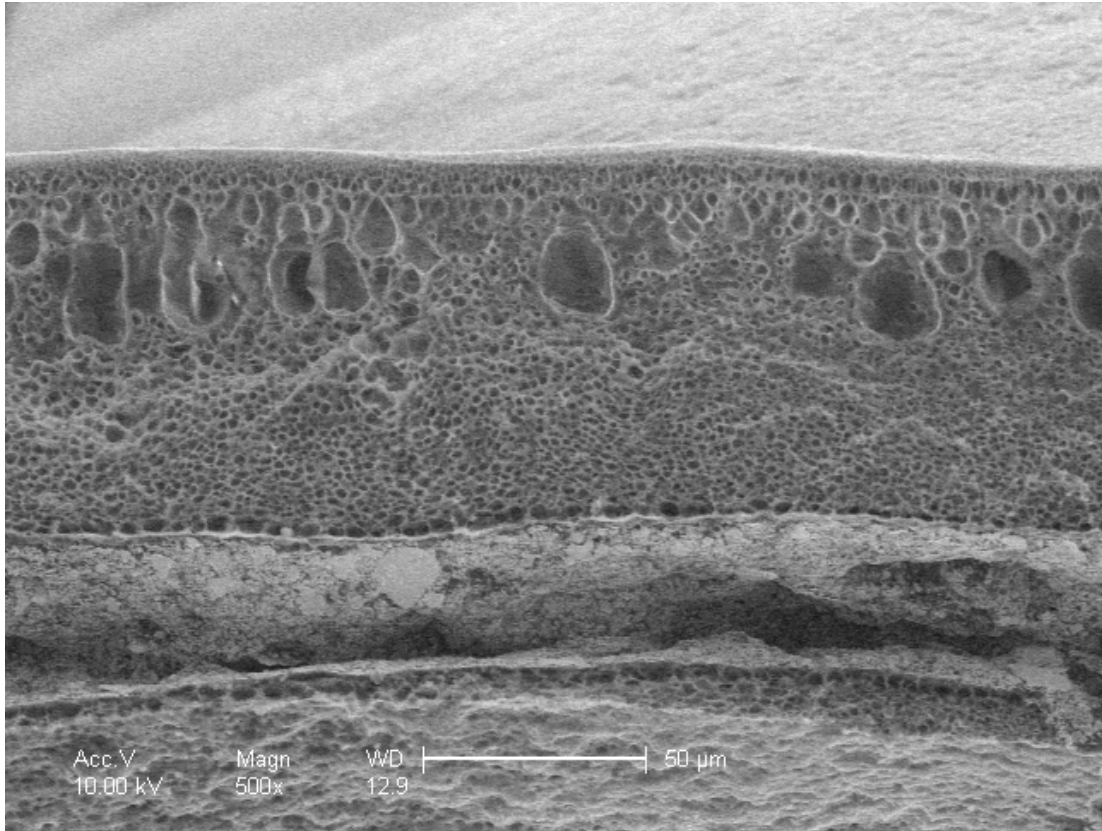


Figure 5.19: Environmental Scanning micrograph of a membrane cast from a ternary water/acetone/cellulose-acetate solution with a water / surfactant (20ppm) bath in low gravity. The initial water and acetone mass fractions, film thickness are $\omega_1^\circ = 0$, $\omega_2^\circ = 0.15$, and $L_o = 125\mu\text{m}$, respectively.

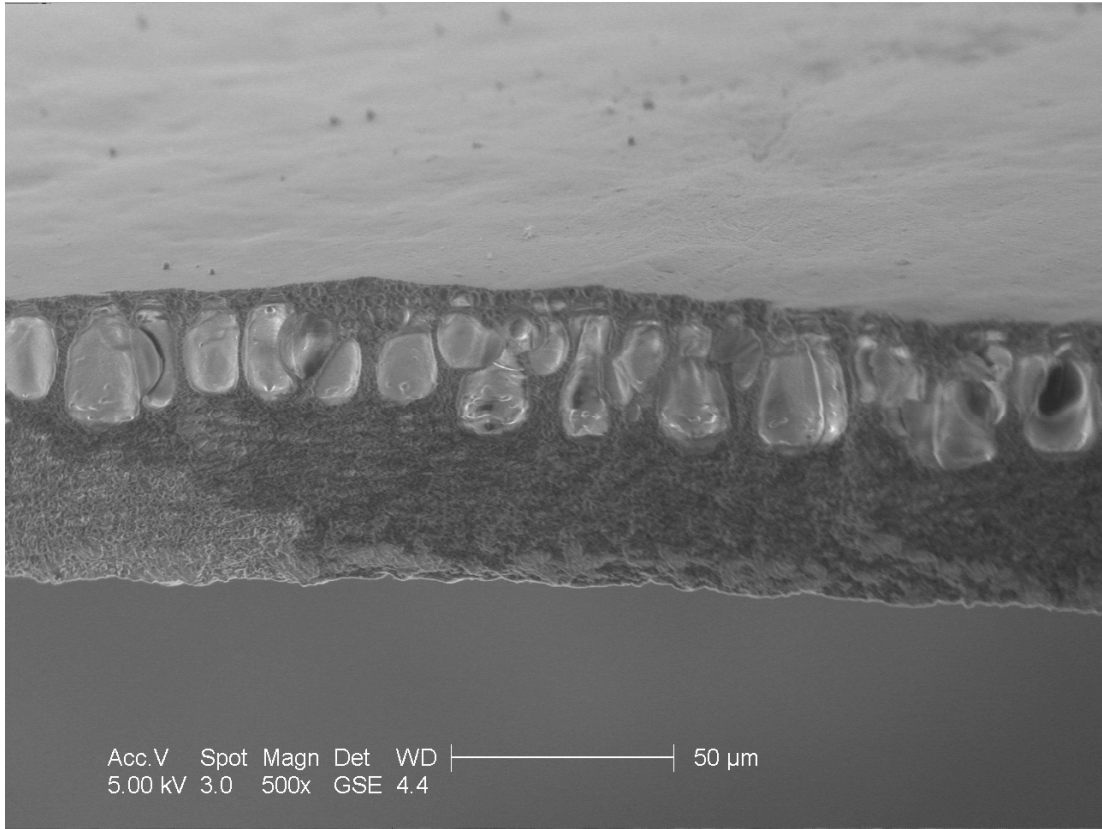


Figure 5.20: Environmental Scanning micrograph of a membrane cast from a ternary water/acetone/cellulose-acetate solution with a pure water bath in normal gravity. The initial water and acetone mass fractions, film thickness are $\omega_1^\circ = 0$, $\omega_2^\circ = 0.15$, and $L_0 = 125\mu\text{m}$, respectively.

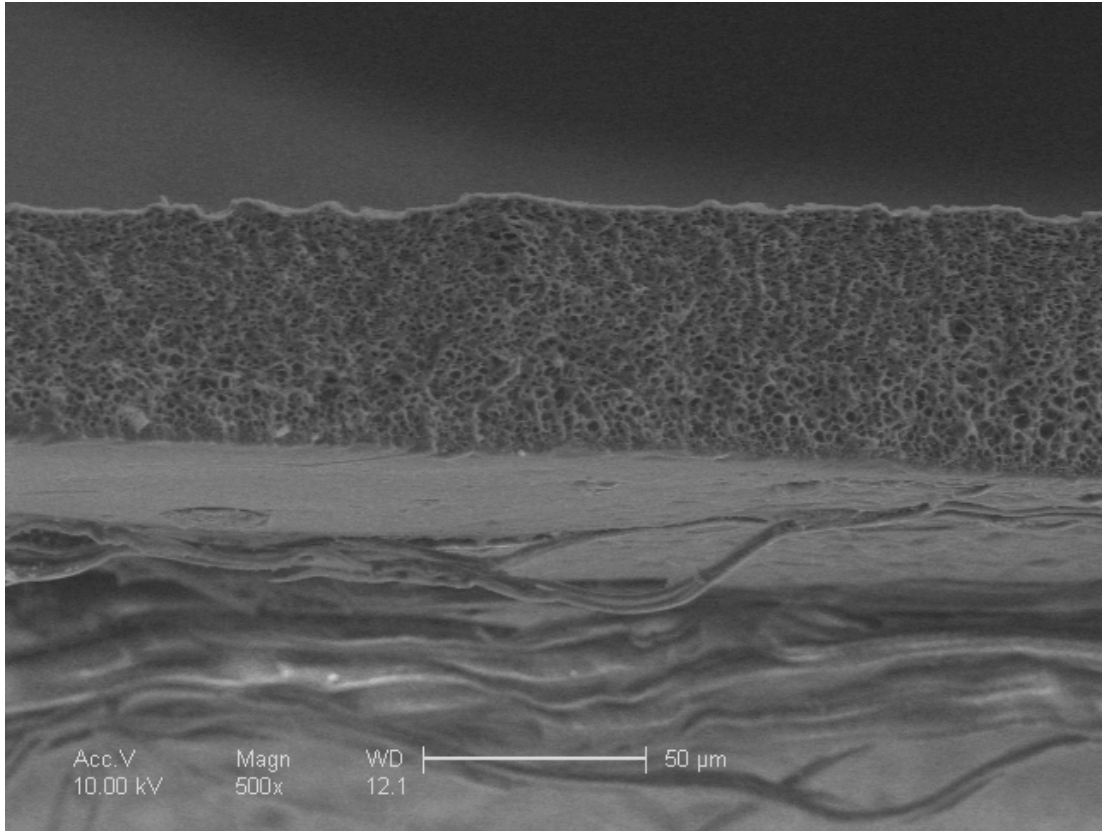


Figure 5.21: Environmental Scanning micrograph of a membrane cast from a ternary water/acetone/cellulose-acetate solution with a pure water bath in high gravity. The initial water and acetone mass fractions, film thickness are $\omega_1^\circ = 0$, $\omega_2^\circ = 0.15$, and $L_0 = 125\mu\text{m}$, respectively.

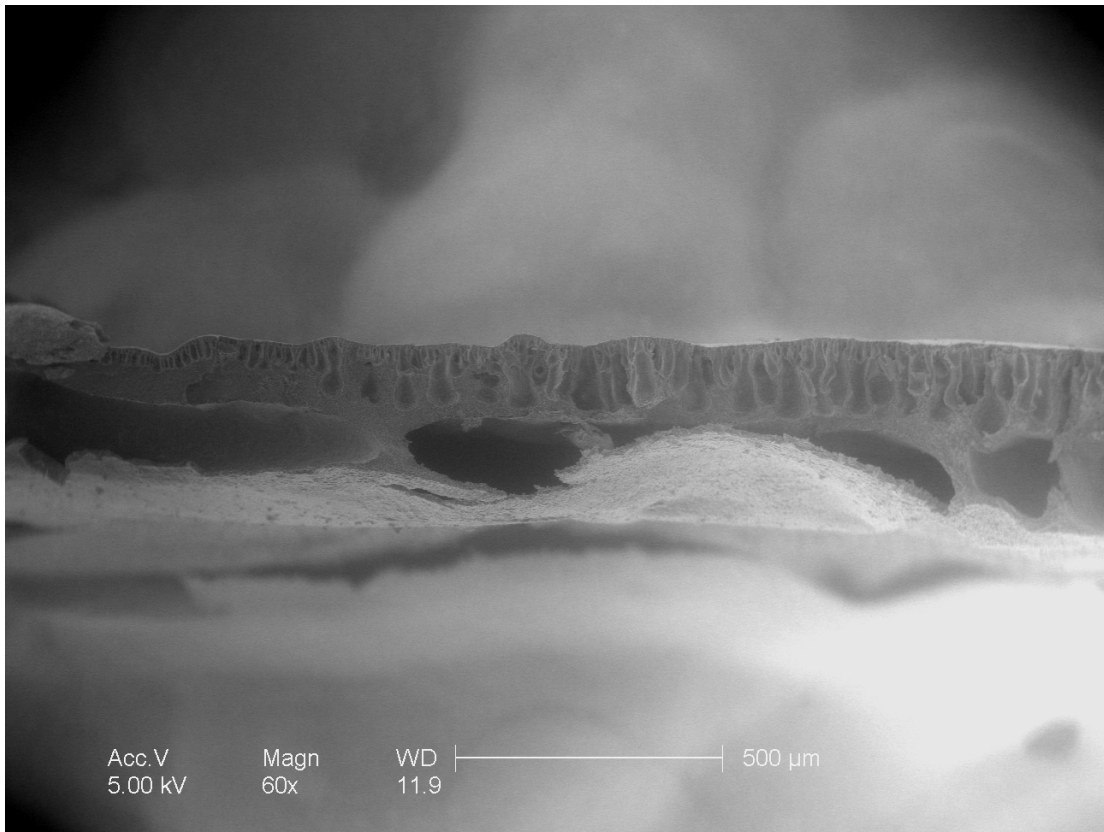


Figure 5.22: Environmental Scanning micrograph of a membrane cast from a ternary water/acetone/cellulose-acetate solution with a pure water bath in normal gravity. The initial water and acetone mass fractions, film thickness are $\omega_1^o = 0$, $\omega_2^o = 0.15$, and $L_o = 500\mu\text{m}$, respectively.

5.7 Discussion of Results

5.7.1 Elimination of Undesirable Convection

The membrane casting apparatus (MCA) was designed to eliminate undesirable mechanical disturbances in the casting solution in order to obtain conditions comparable to those used in the model developed in the previous chapter. As shown in Figures 5.17, 5.19, 5.20, and 5.22, MVs formed with the new MCA are more-or-less axis-symmetric, indicating one-dimensional mass-transfer.

5.7.2 Corroboration with Model Predictions

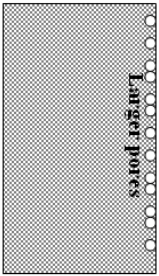
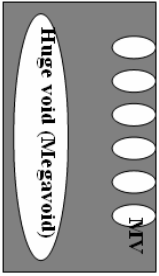
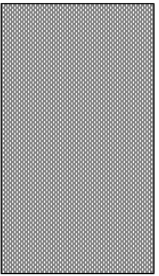
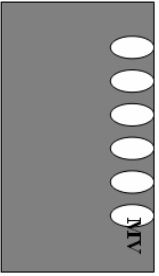
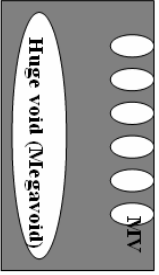


The wet-casting model presented in the previous chapter predicted the formation of a vitrified skin on the top of the casting solution at 2.0×10^{-9} seconds. This is confirmed by the light-intensity data that indicate immediate solidification in all experiments. Also, observation of the morphology of the final membranes by ESEM shows the presence of a thin skin at the top regardless of initial thickness (Figures 5.12 and 5.17). Permeation tests also revealed the presence of dense skin.

The markedly different morphology of the membranes as shown in Figures 5.12 and 5.17 is induced only by variation of the initial solution thickness. Results of the experiments performed under normal gravity indicate that the initial thickness of the casting solution has systematic effects on the MV formation tendency: A thicker initial casting solution enhances MV formation, as shown in Figures 5.14, 5.20 and 5.22. This systematic change is represented schematically in Table 5.2. The effect of the initial thickness of the casting solution has also been reported by Vogrin et al.[99]. Furthermore,

our wet-casting model predicted a systematic change of composition in the casting solution as a function of initial thickness. Figure 5.23 shows the collective result for different initial thicknesses. Clearly, the top region penetrates further into the binodal as the initial thickness of the casting solution increases. The casting solution in this top region is in a metastable state. According to Strathmann et al., "... polymer systems in the two-phase region are often slow to separate into different phases and metastable states are common, especially when a polymer network is rapidly precipitated" [87]. The thickness of this metastable region is predicted to be $10\ \mu\text{m}$ when the initial casting solution thickness is $125\ \mu\text{m}$. It should be further noted that this $10\ \mu\text{m}$ -thick region becomes a metastable state simultaneously. From both experimental and modeling results, it can be concluded that the presence of a thick metastable region is required for MV growth. These results are consistent with the coalescence mechanism. In the metastable region polymer-lean phase microdroplets can grow by nucleation and growth (NG). If this metastable region is thick enough, coalescence of the droplets leads to the formation of large pores like MVs. If the metastable region is thin, normal pores are formed because the coalescence events are limited by the boundaries of the smaller region. However, the diffusion mechanism requires the opposite condition, i.e., a thick metastable region, for MV growth. MV growth in the diffusion mechanism is explained by diffusion of acetone from the stable casting solution into the thin unstable region. If this Reuvers' diffusion mechanism is correct, a thinner unstable region should be a better condition for MV growth.[50]. In addition, our model predicts that spinodal decomposition is impossible since it needs an unstable condition, not a metastable condition. The model prediction also does not support the solutocapillary convection-aided mechanism, since at the top of

casting solution the concentration of water is lower; therefore, there is lower surface energy in the top region of the casting solution.

Table 5.2: Summary of systematic change of the wet-cast membrane structure formed with the studied initial thicknesses and gravity conditions. The darker color of the membrane represents a denser or less porous structure of the membrane

Gravity	Initial thickness of casting solution		
	75 μm	125 μm	500 μm
0 (Low)			
1 (Normal)			
2 (High)			

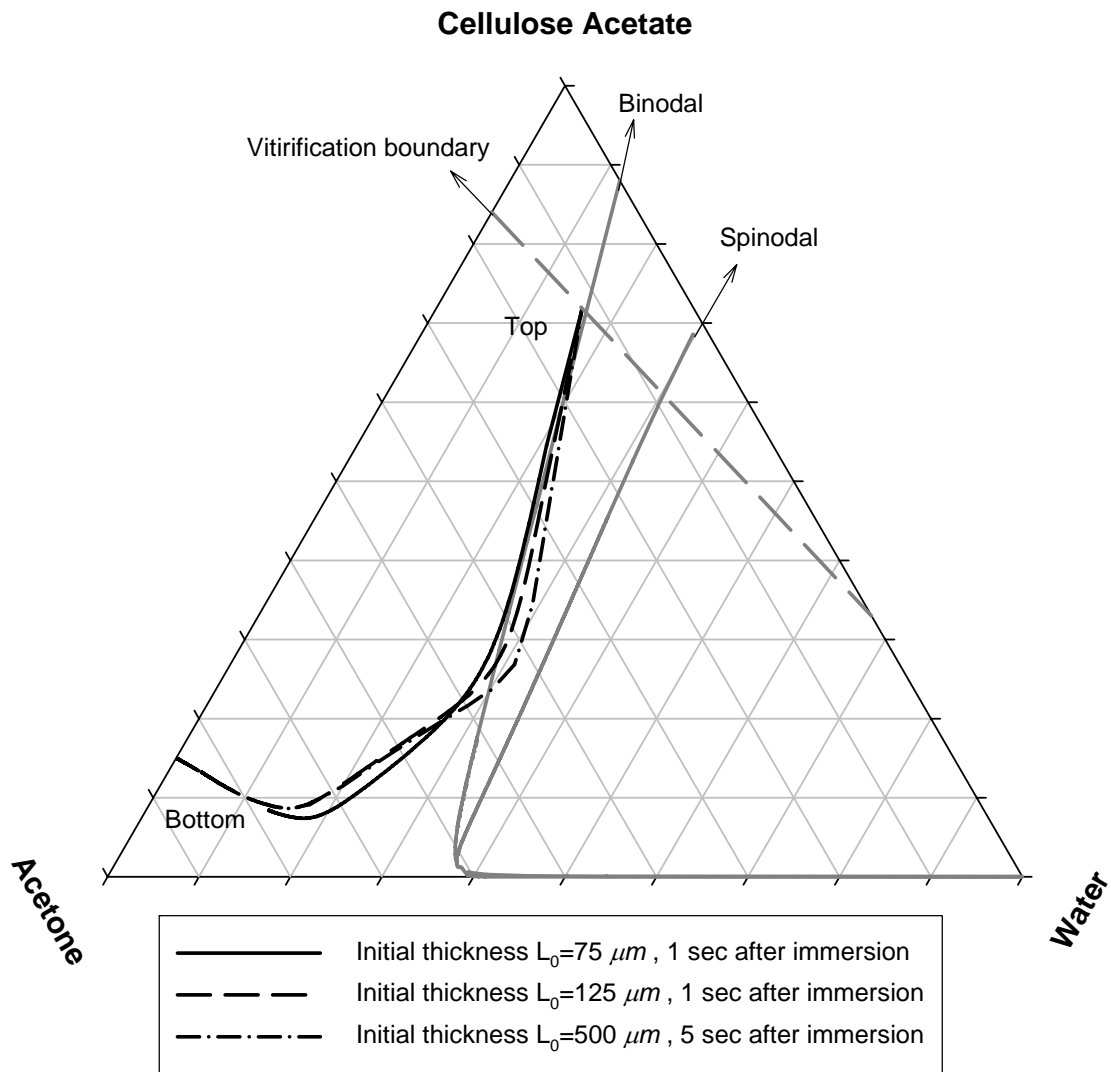


Figure 5.23: Composition profiles from the top to the bottom of the casting solution depending on initial thickness predicted by our wet-casting model using the same initial composition of casting solution of water/acetone/cellulose-acetate = 0/0.15/0.85 (mass fraction).

5.7.3 Effects of Gravity

The presence of gravity creates free convection due to the density difference among species. This free convection results in a rising plume of water near the vertical mid-plane of the water layer and descending plumes near the two walls of the slit. This free convection aids the acetone leaving the casting solution but retards water entering the casting solution. Resulting concentration profile will be shifted to the left-hand side of the ternary phase diagram and therefore, formation of the metastable region will be inhibited. Therefore, the noticeable difference in size of the MVs, as shown in Figures 5.17 and 5.20, is a consistent result with the tendency of MV formation in the metastable region as discussed in the previous section. Under high gravity, MVs formed in the thick casting solution could not survive (Figure 5.21) and in the thin casting solution, even the normal pores were reduced in size (Figure 5.16). These results may imply that MVs and normal pores have the same mechanism of formation through coalescence. The diffusion-only mechanism cannot account for this systemic change of morphology with gravity. On the contrary, if the diffusion-only mechanism is valid, MV formation should be encouraged under high gravity due to the faster mass exchange at the top interface of the casting solution; this is opposite to our experimental observations. Larger size of MVs in low gravity may also support the solutocapillary convection-aided mechanism since, in the absence of a buoyancy force, the penetration of MVs would be enhanced by solutocapillary convection. However, Peckny [92] already showed that the buoyancy force would be insignificant with respect to the very high viscous drag force due to the very high viscosity of the casting solution. Furthermore, our model predicted a lower concentration of water near the top of the casting solution than that in the middle of

metastable region when MV grows. Solutocapillary convection cannot explain MV growth in this condition.

5.7.4 Surfactant-Induced Macrovoid Formation

If MVs are a result of coalescence of a large number of microdroplets, the presence of surfactant should act to mitigate coalescence, thereby resulting in membranes with smaller but more macrovoids. Figures 5.17 and 5.19 show that the number of macrovoids is significantly increased and their size is decreased when surfactant (Triton X-100) is present in the coagulation bath. However, the normal pores seen in Figure 5.19 are larger and increased in number compared to those shown in Figure 5.17. These results suggest that high surface energy of normal pores leads to coalescence into MVs, as displayed in Figure 5.17, consistent with the coalescence mechanism. In addition, it should be noted that a large void near the bottom of membrane is surrounded by many small MVs when surfactant is added to the water bath (Figure 5.19). To distinguish these from macrovoids (MVs), these very large voids are henceforth referred to as “megavoids”. Indeed, the presence of megavoids has not been reported anywhere in the literature. A magnified image of a megavoid surface is shown in Figure 5.24. The presence of small MVs surrounding megavoids might indicate that megavoids also have same formation mechanism as MVs. When diffusion opposite to the concentration gradient occurs in spinodal decomposition (referred as ‘undiffusion’ in some literature), one would expect instantaneous demixing in the whole system, so spinodal decomposition should suppress formation of any other pores near a megavoid. The

solutocapillary convection-aided mechanism also cannot explain the increasing number of MVs when the surface energy is lower.

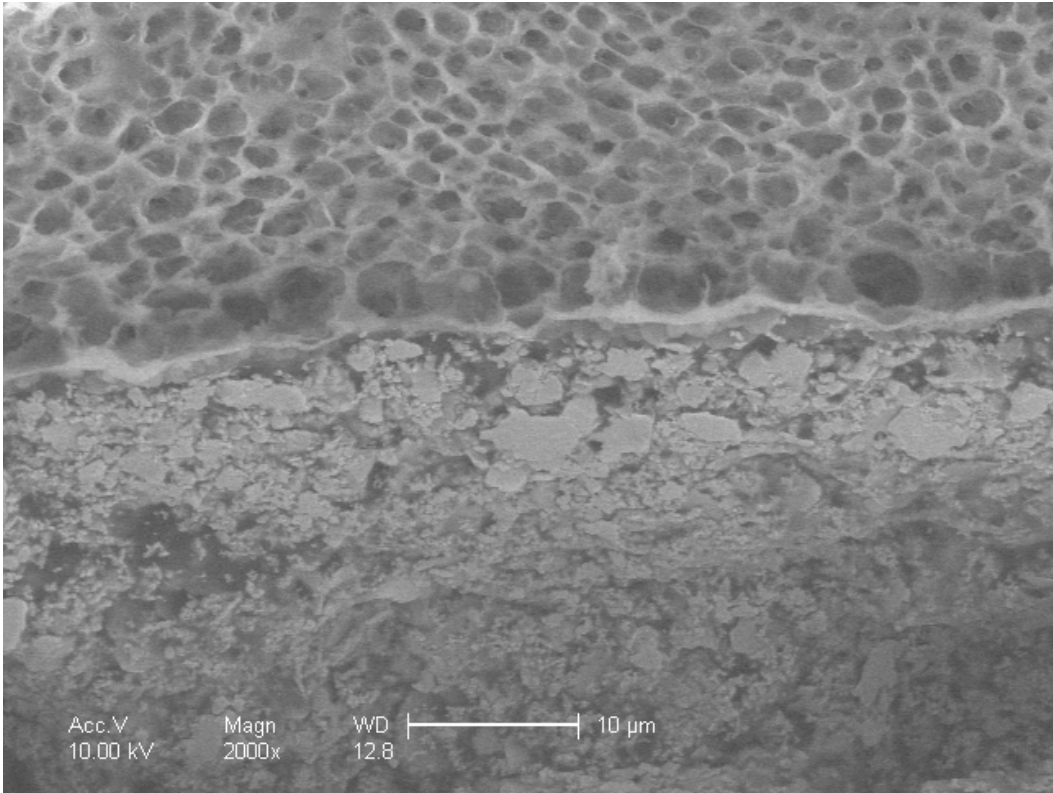


Figure 5.24: Magnified view showing the MV-like pores surrounding a huge void (megavoid) that is located at the bottom of the membrane shown in Figure 5.19.

5.7.5 Coalescence-Induced Coalescence Macrovoid Formation Mechanism

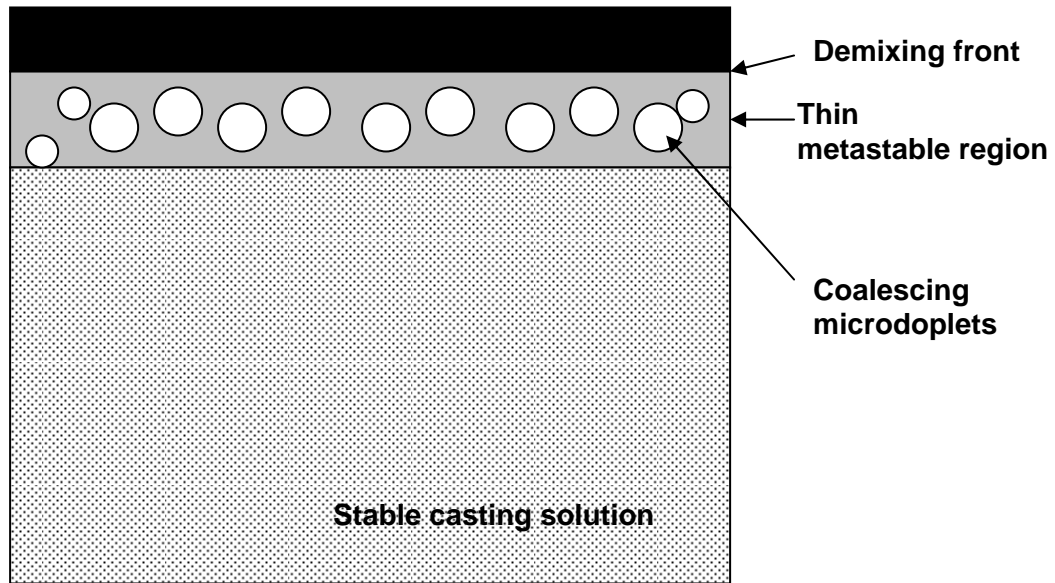
In the previous sections it has been shown that coalescence is the primary mechanism for macrovoid growth. This section will present the coalescence-induced coalescence (CIC) mechanism, which can explain the rapid growth of MVs in conjunction with recent findings of Martula et al. [79] and McGuire et al. [80].

As soon as a casting solution is immersed into the nonsolvent, phase-separation or vitrification occurs at the casting solution/nonsolvent bath interface. This vitrification accompanies a significant decrease of the amount of flux through the interface. Our wet-casting model also predicts an extremely fast composition change at the interface but relatively slow composition change in the casting solution after vitrification. A small but continuous flux through the interface creates a metastable region beneath the skin. In the metastable region, numerous polymer-lean-phase microdroplets are formed because of the natural tendency of the system to lower its Gibbs free energy. Subsequently, the metastable region becomes supersaturated by the formation of numerous microdroplets. These microdroplets have a small volume and a large surface area, and their high surface energy forces them to undergo coalescence, forming larger droplets with relatively smaller surface area and smaller surface energy. If the metastable region is thick enough, the resulting droplets can become quite large (Figure 5.26). The coalescence process is much faster initially because the smaller droplets are more strongly affected by the flow fields created by neighboring coalescence events (coalescence-induced coalescence). This fast initial growth of MVs has been observed in previous studies [42, 81, 85, 92, and 100]. If the polymer concentration is high and the demixing front moves slowly, shape relaxation effects result in macrovoids developing a skin. The shape of an MV is affected

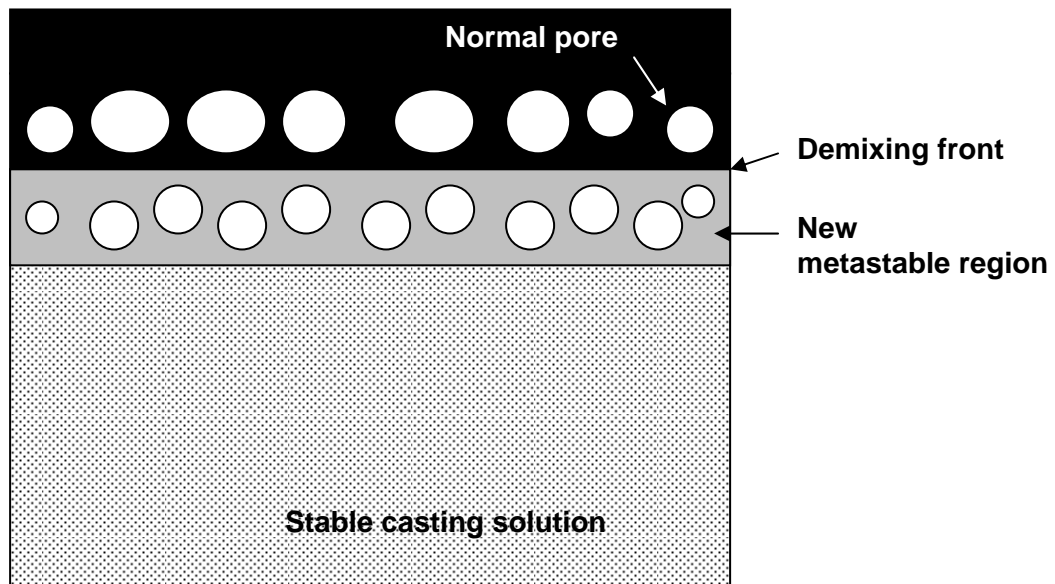
by the solidification of the casting solution, the degree of supersaturation, and the viscosity; the diameter of the MV can expand more in its lower part, where the viscosity and polymer concentration are lower, thus changing to a teardrop shape. Figure 5.23 shows the very steep gradients of viscosity and polymer concentration through the cross-section of casting solution from the top to the bottom. In addition, the composition profile in the metastable region shown in Figure 5.23 implies that the degree of supersaturation will be higher in the middle section of the metastable region. Thus, typical MVs observed in many studies [5, 85, 87, 90, 91, 93-99] have a teardrop shape, as shown in Figure 5.27.

In summary, the CIC mechanism requires a thick metastable region supersaturated by numerous droplets that have a high surface energy. A metastable region, which does not satisfy all of the above conditions, will produce normal pores in the final membrane. There are several ways to manipulate the conditions for MV formation. First, a thicker initial casting solution promotes MV formation by creating a thicker metastable region with a higher degree of supersaturation, as shown in Figure 5.23. Dense skin formation also helps form a thicker metastable region, since the lower flux through the dense skin allows a thicker region to maintain the metastable state. However, if the flux is too low initially, the demixing front will move downward too quickly, decreasing the thickness of the metastable region, not allowing enough time for coalescence of the droplets. Thus, the resulting membrane will not have any MVs, as shown in Smolder et al.'s study using a very high solvent concentration in the initial coagulation bath [91]. The very low initial flux in dry-casting also explains why MVs are rare in dry-cast membranes. However, the thick metastable region does not necessarily

form near the top of the casting solution. If the demixing front moves more slowly after the initial phase separation at the top, a thick metastable region can exist even near the bottom of casting solution. Thus, both the megavoids observed in this study and the very few MVs formed by the dry-casting process [92 and 102] are located at the bottom of the final membranes. Coalescence events in a region with very low polymer concentration (such as the region near the bottom of the casting solution shown in Figure 5.23) can result in the formation of a huge void. Finally, high surface energy promotes coalescence and thereby MV formation. It is well-known that MVs prevail when the casting process involves water, which has very high surface energy. If a surfactant concentration below CMC is added to the system to lower the surface energy, coalescence will be limited and the resulting membrane will have smaller but more numerous MVs, as shown in Figure 5.19. Therefore, the CIC mechanism can explain all the general trends of MV formation.

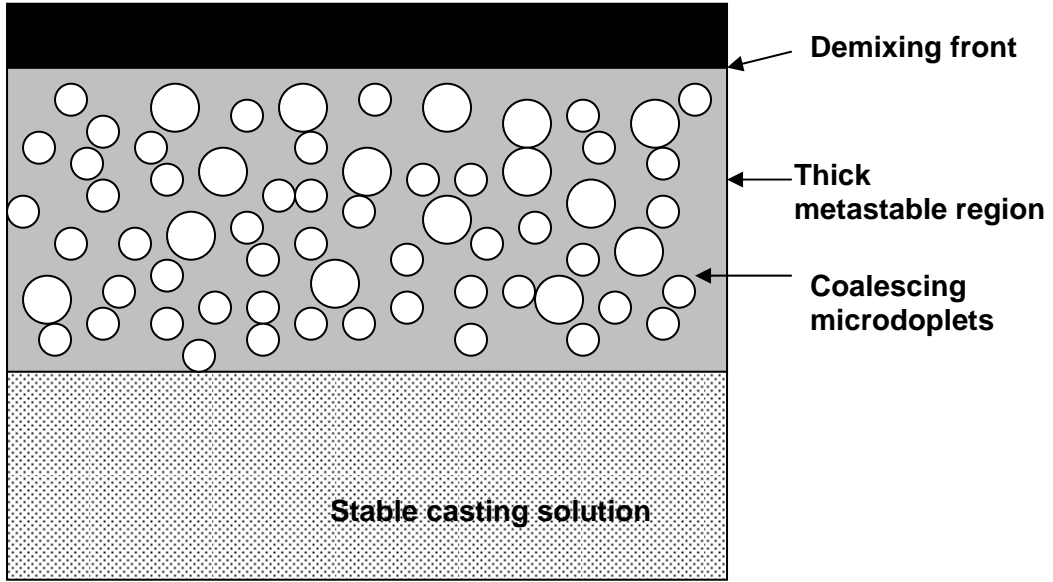


(a)

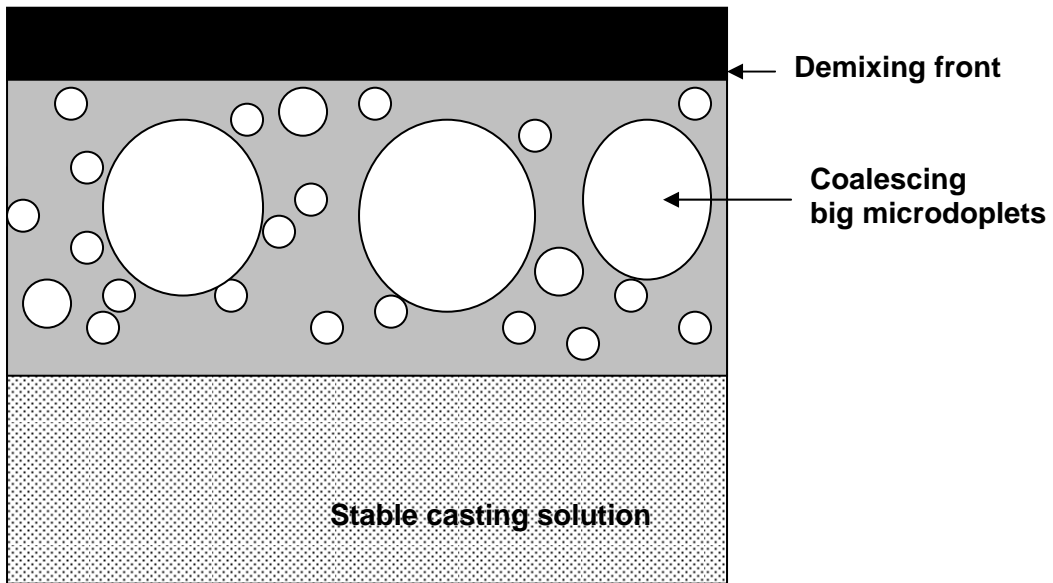


(b)

Figure 5.25: Schematic representation of normal pore formation from a thin metastable region: (a) formation of the thin metastable region (b) formation of normal pores and a new metastable region.



(a)



(b)

Figure 5.26: Schematic representation of initial MV formation from a thick metastable region: (a) formation of the thick metastable region (b) formation of nascent MVs.

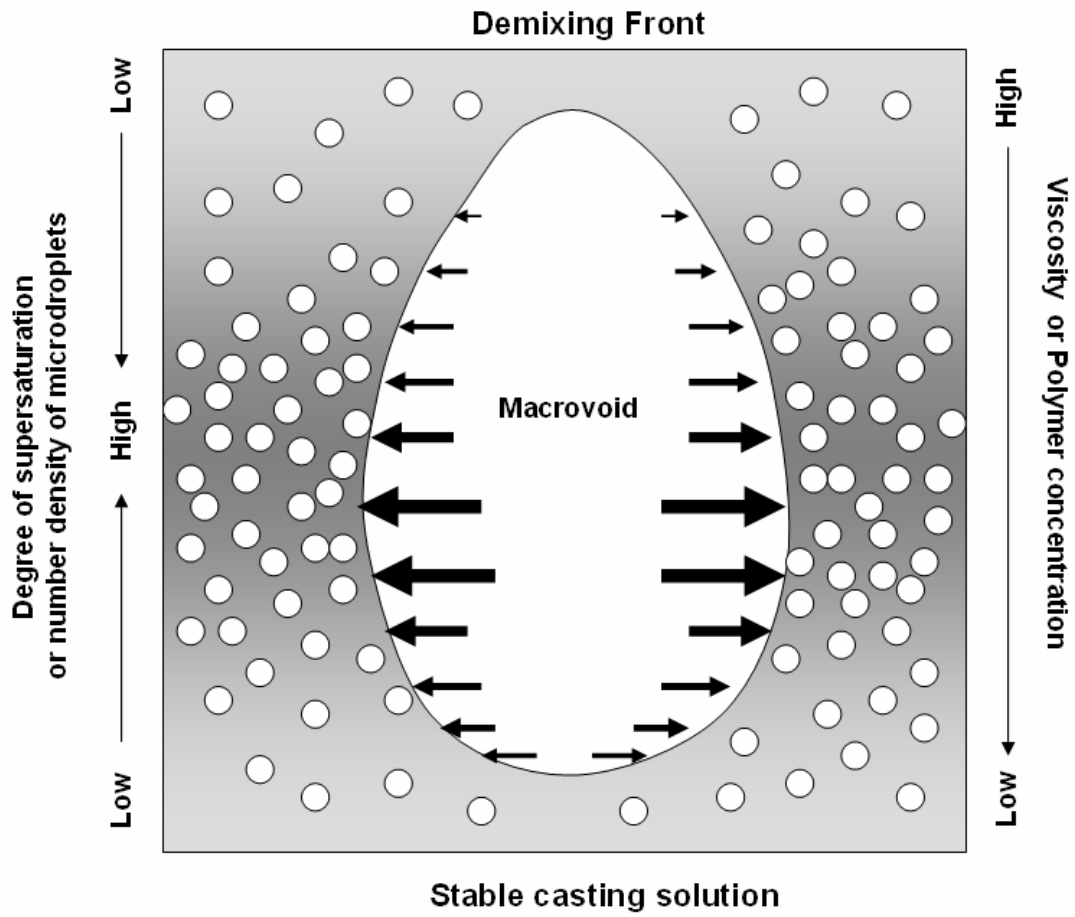


Figure 5.27: Schematic representation of MV growth in a metastable region. The arrows inside the macrovoid represent the spatial expansion rate of the MV.

5.8 Summary

In this chapter, the coalescence-induced coalescence macrovoid formation mechanism was presented and tested by experimental results and model predictions. To eliminate complex free convection effects in experiments, a low gravity environment was used with a novel membrane casting apparatus (MCA). This MCA was specifically fabricated to avoid mechanical disturbance to the nascent membrane during the wet-casting process. Low-gravity experiments revealed that a thicker initial casting solution promotes MV formation. The wet-casting model incorporating convection due to density gradients predicted that a thicker initial thickness of the casting solution promotes the formation of a thick metastable region in the casting solution. Lowering of surface energy by the addition of surfactants results in smaller but more numerous MVs, suggesting that MVs originate from coalescence of the numerous small droplets. Fast initial growth of macrovoids can be explained by the coalescence-induced coalescence model. All the general trends of MV growth and the occurrence of huge voids (megavoid) can be explained by the CIC mechanism.

CHAPTER VI

CONCLUSIONS AND RECOMMENDATIONS

6.1 Scope of Chapter

The principal conclusions emanating from this thesis are summarized in this chapter. First, specific conclusions regarding convective transport are presented. This is followed by conclusions from the development of the dry-casting model and the wet-casting model. Conclusions regarding the macrovoid formation mechanism are presented next. Finally, recommendations for future modeling and experimental studies are presented.

6.2 Conclusions

6.2.1 Convective Transport

- A general procedure to construct well-defined mass-transfer equations incorporating diffusion and convection was developed.

- The equation-of-continuity in conjunction with the equation-of-state provides an explicit equation for the mass-average velocity and the corresponding convective flux.

- Difficulties in dealing with coupled hyperbolic and parabolic PDE equations can be avoided by manipulating the equation-of-continuity with the equation-of-state.
- The convective contribution in the mass-transfer model depends on the local densification or swelling as well as on the presence of external forces, including the gravitational force.
- The sign (positive or negative) of mass-average velocity determines the local densification or swelling, depending on the location of the origin of the coordinate system.
- Even without any external force, the convective contribution to mass transfer can exist due to the diffusive mass-transport; however, conduction in heat transfer cannot cause heat convection.
- The diffusion-only model results in larger error in predicting the concentration profile and the thickness change as the difference among pure densities increases.
- The modified Peclet number depends on the rate of densification or swelling. If densification or swelling in a system occurs very rapidly, both the modified Peclet number and the convective contribution are large.

- Nonequilibrium thermodynamics is useful to describe the coupling effects in multicomponent mass transfer as well as to deal with multiple driving forces, not just concentration gradients.

6.2.2 Dry-Casting Model

- The approach to building a well-defined mass-transfer equation produced a dry-casting model incorporating both convection and diffusion.
- The results of the new convection-diffusion model for the onset time for phase separation were more accurate than the pure diffusion model results, based on the light-reflection intensity measurement.
- The gradual change of the light intensity observed in Shojaie's dry-casting experiments [31] supported our hypothesis that phase separation at the top of the casting solution allows a well-mixed condition in the liquid casting solution, resulting in the formation of a symmetric membrane.
- The new dry-casting convection-diffusion model accurately predicts the surface temperature of the casting solution in evaporative casting, in contrast to the pure diffusion model that underpredicts it.

- The new dry-casting model predicts the swelling of the casting solution in the region near the casting solution/glass substrate interface before gelation as well as the densification of the casting solution near the casting solution/ambient gas interface due to the increased polymer concentration at the top of the casting solution.
- The modified Peclet number determined from the new model indicates that neglecting the convective contribution can cause an initial error of close to 35%. Also, the modified Peclet number is largest at the top of the casting solution due to the steepest gradients being at the liquid–gas interface.

6.2.3 Wet-Casting Model

- A comprehensive wet-casting process model was developed to incorporate diffusion and convection due to local densification or swelling and to describe the effects of the initial casting solution thickness variation on the casting process.
- By combining the assumption of no polymer in the bath and the local equilibrium assumption (local pseudo-equilibrium assumption), the new wet-casting model predicts the top of the casting solution will reach the binodal in 10^{-9} seconds. All previous models in the literature assumed the initial top composition of the casting solution was on the binodal; however, this is not valid for a convection-diffusion process.

- The new wet-casting model, which uses the local equilibrium assumption after the top composition of the casting solution reaches the binodal, predicts that the top of the casting solution vitrifies or solidifies even before a change of composition has occurred in the bath of the casting solution below.
- Extended simulation assuming a fixed top composition at the vitrification boundary shows the clear effect of the initial thickness of the casting solution on the formation of a metastable layer near the casting solution/coagulation bath interface.
- The composition of the entire casting solution, for the CA/acetone/water system with an initial composition and an initial thickness of $75\ \mu\text{m}$, was on the binodal after 3.4 seconds; moreover, none of the casting solution had crossed over the binodal into the two-phase region.
- Increasing the initial thickness of the casting solution for the CA/acetone/water system to $125\ \mu\text{m}$ with the same initial composition resulted in the top $7\ \mu\text{m}$ crossing the binodal after 1 second; this implies that the top $7\ \mu\text{m}$ of the casting solution enters the metastable state simultaneously.
- The modified Peclet number shows that convection in the wet-cast process for the CA/acetone/water system is about 30% of diffusion initially.

6.2.4 Macrovoid Formation Mechanism

- A new membrane casting apparatus (MCA) was developed and successfully adapted to membrane formation experiments under various gravitational force fields while ensuring one-dimensional mass transfer.
- The preliminary experimental and simulation studies prove that the spring-plunger-driven mechanism used in Pekny et al.'s research [102] was responsible for the macrovoid distortion they observed. Therefore, a cam-driven mechanism was used in designing a new MCA.
- Macrovoids (MVs) formed with the new MCA were more-or-less axis-symmetric which implies one-dimensional mass-transfer.
- The wet-casting process in low gravity, using an initial casting solution with 75 μm thickness and an initial pure water bath, produced a skinned cellulose-acetate membrane with a nearly uniform pore structure without any macrovoids.

- The wet-casting process in high gravity, using an initial casting solution with 75 μm thickness and an initial pure water bath, produced a dense cellulose-acetate film with a few dispersed pores.
- The wet-casting process in low gravity, using an initial casting solution with 125 μm thickness and an initial pure water bath, produced a skinned cellulose-acetate membrane with macrovoids near the top surface and a very large void (megavoid) in the bulk.
- The wet-casting process in normal gravity, using an initial casting solution with 125 μm thickness and an initial pure water bath, produced a skinned cellulose-acetate membrane with macrovoids near the top surface, without any megavoid in the bulk.
- The wet-casting process in high gravity, using an initial casting solution with 125 μm thickness and an initial pure water bath, produced a skinned cellulose-acetate membrane with normal pores but neither macrovoids nor megavoid.
- The wet-casting process in low gravity, using an initial casting solution with 125 μm thickness and an initial water/surfactant bath, produced a skinned cellulose-acetate membrane with smaller but more numerous macrovoids near the top surface and a megavoid surrounded by large MV-like pores in the bulk.

- Real-time light-reflection data showed that the demixing of the casting solution occurred instantaneously, regardless of the thickness of the casting solution, the gravity or the presence or absence of surfactant in the water bath for the CA/acetone/water system.
- MVs were formed in the final membrane only when the wet-casting model predicted the presence of a metastable region in the casting solution for the CA/acetone/water system.
- The coalescence-induced-coalescence mechanism for MV formation is consistent with all the experimental and modeling results of this thesis.
- The coalescence-induced coalescence mechanism implies that the formation of MVs requires the presence of a thick metastable region supersaturated by numerous microdroplets.
- The coalescence-induced-coalescence mechanism can explain the formation of the megavoid observed near the bottom of a membrane a well-mixed metastable region is formed near the bottom of the casting solution.

6.3 Recommendations

- The zero volume-of-mixing assumption is used for all model calculation since it results in the simplest closed form of equation for the mass-average velocity. For further generalization of mass-transfer equations, the volume-of-mixing effects should be considered.
- The general mass-transfer equation presented in this thesis is obtained assuming an isothermal condition. The equation-of-state for a more general system should be expressed as a function of temperature as well as of composition.
- The ternary phase diagrams used in this thesis assumed a system with a constant temperature of 25°C . When a casting solution has significant temperature change, ternary phase diagrams as a function of temperature would provide more accurate results.
- All the experimental results and modeling in this thesis can be easily extended to other phase-inversion processes such as the thermal-cast, polymer-assisted and vapor-induced processes.
- The modeling in this thesis should be extended to geometrics such as hollow fiber and tubular membranes.

- Most commercial membranes are made via a continuous rather than a batch process. The modeling work in this thesis should be extended to a two-dimensional mass-transfer model to describe a continuous membrane-casting process.
- Predictions from both the dry- and the wet-casting models presented in this thesis are valid until phase separation starts. Two- or three-dimensional phase separation combined with the mass-transfer model developed in this study would provide much more useful information to optimize the membrane-fabrication recipe. In particular, the flux change due to solidification in the casting solution should be considered.
- The new wet-casting model incorporates an approximate analytic solution for the diffusion-convection mass-transfer equation for the nonsolvent bath. For better accuracy a PDE for the nonsolvent bath should be incorporated into the equations for the casting solution side..
- The new wet-casting model assumes low gravity. In normal or high gravity, free convection effects should be considered. However, the lumped parameter approach for wet-casting mass-transfer problems implicitly assumes equimolar counter diffusion due to the limitations of the analogy between heat transfer and mass transfer. Therefore, an approach to consider both free convection and

convection due to densification or swelling should be developed as the first step in a model for the wet-casting process in normal or high gravity.

- Modeling and experimental studies in this thesis were focused on the water/acetone/cellulose-acetate casting solution and a water/acetone nonsolvent bath. However, our model should be tested on other casting solution-nonsolvent bath systems.
- This thesis focuses on the effect of the initial thickness in the wet-casting process. However, the new model is also applicable to study the effects of other initial conditions, such as the compositions of the casting solution and the bath.
- In this study the onset time for phase separation in the wet-casting process was measured by light reflection. Other noninvasive real-time measurement techniques might provide more information on the casting process such as the duration of phase separation and thickness change.
- The wet-casting model was developed assuming isothermal conditions. However, some polymer solution-nonsolvent bath systems can have a significant heat-of-mixing. The thermodynamic model and the heat-transfer model should be modified to describe such systems.

- The new wet-casting process model predicted MV growth in a thick metastable region using the coalescence-induced-coalescence mechanism. Two- or three-dimensional simulation in the predicted metastable condition might reveal more information about the dynamics of MV formation.

BIBLIOGRAPHY

- [1] Market reports: membrane desalination equipment., *Filtration Industry Analysis*, (2003, November) pp. 14.
- [2] Growth expected for MBR market., *Membrane Technology*, (2005, February) pp. 4.
- [3] US membrane separation technology markets analyzed., *Membrane Technology*, (2002, September) pp. 10.
- [4] Loeb, S. and Sourirajan, S., Sea water demineralization by means of an osmotic membrane. *Adv. Chem. Ser.*, 38, (1962) 117.
- [5] Kesting, R. E., *Synthetic Polymeric Membranes – A structural Perspective* (2nd ed.). Wiley: New York (1986).
- [6] Hadamard, J., Sur les problèmes aux dérivées partielles et leur signification physique. *Princeton University Bulletin*, 49 (1902).
- [7] *Well-posed problem* (n.d.) Retrieved July, 1, 2005 from http://en.wikipedia.org/wiki/Well-posed_problem.
- [8] Deen, W. M., *Analysis of Transport Phenomena*, Oxford University Press, New York, (1998).
- [9] Kuiken, G. D. C., *Laminar-turbulent transition : IUTAM Symposium, Sendai/Japan, September 5-9*, Springer-Verlag, New York, (1995).
- [10] Welty J. R., Wicks C. E. , Wilson C. E., Rorrer G. *Fundamentals of Momentum, Heat and Mass Transfer*, John Wiley & Sons, New York, (2001).

- [11] Eckert E. R. G., Sakamoto H., Simon T. W. The heat/mass transfer analogy factor, Nu/Sh , for boundary layers on turbine blade profiles. *Intl. J. Heat. Mass Trans.*, 44, (2001) 1223.
- [12] Bird B. R., Stewart W. E., Lightfoot E. N. *Transport phenomena*, John Wiley & sons, New York, (1960).
- [13] Mikhailov, M. D., and Ozisik, M. N., *Unified Analysis and Solutions of Heat and Mass Diffusion*, Dover, Mineola, (1984).
- [14] Driessen B. J., Dohner J. L., A finite element–boundary element method for advection–diffusion problems with variable advective fields and infinite domains. *Int. J. of Heat and Mass Trans.* 44 (2002) 2183–2191.
- [15] Qui, Z. H, Wrobel, L. C., Power H., Numerical solution of convective–diffusion problems at high Peclet number using boundary elements, *Int. J. Numer. Methods Engrg.* 41 (1998) 899–914
- [16] A. Matsumura and T. Nishida, The initial value problem for the equations of motion of compressible and heat conductive fluids, *Comm. Math. Phys.* 89 (1983) 445–464.
- [17] E. Feireisl and H. Petzeltová, On the Existence of Globally Defined Weak Solutions to the Navier–Stokes Equations, *J. Mathematical Fluid Mechanics* 3 (2001) 358–392
- [18] R. V. Mises, H. Geiringer and G.S.S. Ludford, *Mathematical theory of compressible fluid flow*, Academic press, New York, (1958).
- [19] Cussler, E. L., *Diffusion : mass transfer in fluid systems*, 2nd ed. Cambridge University Press, New York, (1997).

- [20] Belfiore, L. A., *Transport Phenomena for Chemical Reactor Design*, John Wiley & Sons, New York, (2003).
- [21] Hirschfelder, J. O., Curtiss, C.F., and Bird, R. B., *Molecular Theory of Gases and Liquids*, John Wiley & Sons, New York, (1964).
- [22] Welty, J. R., Wicks, C. E., and Wilson, R. E., *Fundamentals of Momentum, Heat and Mass Transfer*, 3rd ed., John Wiley & Sons, New York, (1984).
- [23] deGroot, S. R., *Thermodynamics of Irreversible Processes*, North-Holland, Amsterdam, (1951).
- [24] Sherwood, T. K., Pigford, R. L., and Wilke, C. R., *Mass Transfer*, McGraw-Hill, New York, (1975).
- [25] Bardow, A., Marquardt, W., Göke, V., Koss, H. -J., and Lucas, K., Model-based measurement of diffusion using Raman spectroscopy, *AIChE J.* 49 (2003) 323–334
- [26] Unger, J., Kroner, A., and Marquardt, W., Structural-Analysis of Differential-Algebraic Equation Systems Theory and Applications, *Comput. Chem. Eng.*, 19 (1995) 867
- [27] Bhattacharya S., and Hwang, S. -T., ‘Concentration polarization, separation factor, and Peclet number in membrane processes,’ *J. Mem. Sci.* 132 (1997) 73.
- [28] Hwang, S. -T., ‘Nonequilibrium Thermodynamics of Membrane Transport,’ *AIChE J.* 50 (2004) 862
- [29] Shojaie, S. S., Polymeric Dense Films and Membranes via the Dry-Cast Phase Inversion Process: Modeling, Casting, and Morphological Studies, Ph.D. Dissertation, University of Colorado, Boulder, CO, (1992).

- [30] Shojaie, S. S., Krantz W. B., and Greenberg, A. R., Dense polymer film and membrane formation via the dry-cast process: Part I. Model development, *J. Membrane Sci.*, 94 (1994) 255.
- [31] Shojaie, S. S., Krantz, W. B., and Greenberg, A. R., Dense polymer film and membrane formation via the dry-cast process: Part II. Model validation and morphological studies, *J. Membrane Sci.*, 94 (1994) 281.
- [32] Anderson, J. E., and Ulmann, R., Mathematical analysis of factors influencing the skin thickness of asymmetric reverse osmosis membranes, *J. Appl. Phys.*, 44 (1973) 4303.
- [33] Castellari, C., and Ottani, S., Preparation of reverse osmosis membranes. A numerical analysis of asymmetric membrane formation by solvent evaporation from cellulose acetate casting solutions, *J. Membrane Sci.*, 9 (1981) 29.
- [34] Krantz, W. B., Ray, R. J., Sani, R. L., and Gleason, K. J., Theoretical study of the transport processes occurring during the evaporation step in asymmetric membrane casting, *J. Membrane Sci.*, 29 (1986) 11.
- [35] Tsay C. S., and McHugh, A. J., Mass transfer dynamics of the evaporation step in membrane formation by phase inversion, *J. Membrane Sci.*, 64 (1991) 81.
- [36] Tantekin-Ersolmaz, S. B., The evaporation step in asymmetric membrane formation: Modeling, gravimetric / inframetric and morphology studies, PhD dissertation, University of Colorado, Boulder, Colorado, (1990).
- [37] Tan, L., Krantz, W. B., Greenberg, A. R., and Sani, R. L., Studies of convective transport in evaporative casting of dense polymer films, *J. Membrane Sci.*, 108 (1995) 245.

- [38] Yilmaz, L. and McHugh, A. J., Analysis of nonsolvent-solvent-polymer phase diagram and their relevance to membrane formation modeling, *J. Appl. Polym. Sci.*, 31, (1986) 997-1018
- [39] Tsay, C. S. and McHugh, A. J., Mass transfer modeling of asymmetric membrane formation by phase inversion, *J. Polym. Sci. Polym. Phys.*, 28, (1990), 1327-1365.
- [40] Mulder, M. H. V. and Smolders, C. A., On the mechanism of separation of ethanol / water mixtures by pervaporation I. Calculations of concentration profiles, *J. Membrane Sci.*, 17, (1984), 289-301.
- [41] Bikales, N., M., and Segal, L., *High polymers. Volume V: Cellulose acetate and cellulose derivatives, Part IV*, Wiley-Interscience, New York (1971).
- [42] Prakash, S., The origin of microstructure in phase inversion casting of membranes: snapshots of the transient from time-sectioning cryo-SEM, Ph.D. Dissertation, University of Minnesota, Minnesota (2001).
- [43] Reuvers, A. J., Altena, F. W., and Smolders, C. A., Demixing and gelation behavior of ternary cellulose acetate solutions, *J. Polymer Sci. Part B: Polymer Physics*, 24 (1986) 793.
- [44] Park, G. S., Radioactive studies of diffusion in polymer systems, *Trans. Farad. Soc.*, 57 (1961) 18.
- [45] Mulder, M., *Basic Principles of Membrane Technology*, Kluwer Academic Publishers, The Netherlands, (1997).
- [46] Cohen, C., Tanny, G. B., and Prager, S., Diffusion-controlled formation of porous structures in ternary polymer system, *J. Polym. Sci. Polym. Phys. Ed.*, 17, (1979) 477-489.

- [47] Wijmans, J. G., Altena, G. W., and Smolders, C. A., Diffusion during the immersion precipitation process, *J. Polym. Sci. Polym. Phys. Ed.*, 22, (1984) 519-524.
- [48] McHugh, A. J. and Yilmaz, L., The diffusion equations for polymer membrane formation in ternary systems, *J. Polym. Sci. Polym. Phys. Ed.*, 23, (1985), 1271-1274.
- [49] Reuvers, A. J., Berg, J.W.A., and Smolders, C. A., Formation of membranes by means of immersion precipitation – Part I. A model to describe mass transfer during immersion precipitation, *J. Mem. Sci.*, 34 (1987) 45-65
- [50] Reuvers, A. J., Berg, J.W.A., and Smolders, C. A., Formation of membranes by means of immersion precipitation – Part II. The mechanism of formation of membranes prepared from the system cellulose acetate-acetone-water, *J. Mem. Sci.*, 34 (1987) 67-86
- [51] Tsay, C. S. and McHugh, A. J., Mass transfer modeling of asymmetric membrane formation by phase inversion, *J. Polym. Sci. Polym. Phys.*, 28, (1990),1327-1365.
- [52] Radovanovic, P., Thiel, S. W., and Hwang, S. T., Formation of asymmetric polysulfone membranes by immersion precipitation. Part I. Modeling mass transport during gelation, *J. Mem. Sci.*, 65 (1992) 213-229
- [53] Radovanovic, P., Thiel, S. W., and Hwang, S. T., Formation of asymmetric polysulfone membranes by immersion precipitation. Part II. The effects of casting solution and gelation bath compositions on membrane structure and skin formation, *J. Mem. Sci.*, 65 (1992) 231-246

- [54] Cheng, L. P., Soh, Y. S., Dwan, A. H., and Gryte, C. C., An improved model for mass transfer during the formation of polymeric membranes by the immersion-precipitation process, *J. Poly. Sci. part B*, 32 (1994) 1413-1425
- [55] Fernandes, G. R., Pinto, J. C., and Nobrega, R., Modeling and simulation of the phase-inversion process during membrane preparation, *J. Poly. Sci.*, 82 (2001) 3026-2051
- [56] Anderson, D. K., Hall, J. R., and Babb, A. L., "Mutual diffusion in non-ideal binary liquid mixture," *J. Phys. Chem.*, 62, (1958), 404-409.
- [57] Smith, V. M., Van Ness, H. C., and Abbott, M. M., *Introduction to chemical engineering thermodynamics*, 5th ed. McGraw-Hill, Singapore, (1996), 34.
- [58] Gmehling, J., and Onken, U., *Chemistry data series: Vol 1. Vapor liquid equilibrium data collection*, DECHEMA, New York, (1988), 153
- [59] Loehe, J. R., Van Ness, H. C., and Abbott, M. M. Excess thermodynamic functions for ternary systems. 7. Total pressure data and GE for acetone/1,4-dioxane/water at 50.degree.C, *J. Chem. Eng. Data* 26 (1981), 178.
- [60] Polednová, J. and Wichterle, I., Vapour-liquid equilibrium in the acetone-water system at 101.325 kPa, *Fluid Phase Equilibria* 17, (1984), 115.
- [61] Othmer, D. F. and Morley, F. R., Composition of Vapors from Boiling Binary Solutions, *Ind. Eng. Chem.*, 38 (1946), 751.
- [62] Singer, S. J., On the concentration dependence of the rates of sedimentation and diffusion of macromolecules in solution. Preliminary, *J. Chem. Phys.*, 15, (1947) 341.
- [63] McQuarrie, D. A., *Statistical Mechanics*, Harper Collins, New York, NY, (1976)

- [64] Zeman, L. and Fraser T., Formation of air-cast cellulose acetate membranes. Part I. Study of macrovoid formation, *J. Membrane. Sci.* 84 (1993) 93.
- [65] Zeman, L. and Fraser T., Formation of air-cast cellulose acetate membranes. Part II. Kinetics of demixing and macrovoid growth, *J. Membrane. Sci.*, 87 (1994) 267.
- [66] Kelley, F. N., and Bueche, F., Viscosity and glass transition relations for polymer-diluent systems, *J. Polym. Sci.*, 50, (1961), 549.
- [67] Frdors, R. F., A universal reduced glass transition temperature for liquids, *J. Polym. Sci. : Polym. Letters Ed.*, 17, (1979), 719.
- [68] Olabisi, O., Robeson, L. M., and Shaw, M. T., *Polymer-polymer miscibility*, Academic Press, New York, (1979).
- [69] Uhlmann, D. R., and Chalmers, B., The energetics of nucleation, *I&EC*, 57, (1965), 19-31.
- [70] Nunes, S. P., and Inoue, T. Evidence of spinodal decomposition and nucleation and growth mechanisms during membrane formation, *J. Membrane Sci.*, 111, (1996) 93-103.
- [71] Cahn, J. W., and Hilliard, J. E., Free energy of a nonuniform system. III. Nucleation in a two-component incompressible fluid, *J. Chem. Phys.*, 31, (1959), 688-699.
- [72] Lifshitz, I. M., and Sloyozov, V. V., The kinetics of precipitation from supersaturated solid solution, *J. Phys. Chem. Solid*, 19 (1961), 35.
- [73] Cumming, A., Wiltzius, P., and Bates, F. S., Nucleation and growth of monodisperse droplets in a binary-fluid system, *Phys. Rev. Let.*, 65, (1990), 863.

- [74] Song, S.-W., and Torkelson, J. M., Coarsening effects on the formation of microporous membranes produced via thermally induced phase separation of polystyrene-cyclohexanol solutions, 98, (1995), 209.
- [75] Song, S.-W., and Torkelson, J. M., Coarsening Effects on Microstructure Formation in Isopycnic Polymer Solutions and Membranes Produced via Thermally Induced Phase Separation, *Macromolecules*, 27, (1994), 6389.
- [76] Aubert, J. H., Structural coarsening of demixed polymer solutions, *Macromolecules*, 23, (1990), 1446.
- [77] Lal, J. and Bansil, R., Light-scattering study of kinetics of spinodal decomposition in a polymer solution, *Macromolecules*, 24, (1991), 290.
- [78] McGuire, K. S., Laxminarayan, A., and Lloyd, D. R., Kinetics of droplet growth in liquid-liquid phase separation of polymer-diluent systems: experimental results, *Polymer*, 36, (1995), 4951.
- [79] Martula D. S., Hasegawa, T., Lloyd D. R., and Bonnecaze, R. T., Coalescence-induced coalescence of inviscid droplets in a viscous fluid, *J. Colloid Interface Sci.*, 232, (2000), 241.
- [80] McGuire, K. S., Laxminarayan, A., Martula D. S., and Lloyd, D. R., Kinetics of Droplet Growth in Liquid-Liquid Phase Separation of Polymer-Diluent Systems: Model Development, *J. Colloid Interface Sci.*, 182, (1996), 46.
- [81] Konagurthu, S., Macrovoids in dry-cast polymeric membranes: growth mechanisms, non-invasive detection, and effects on performance. Ph.D. Dissertation. University of Colorado, Boulder (1998)

- [82] Herbig, S. H., Carinal, J. R., Korsmeyer, R. W. and Smith, K. L., Asymmetric membrane tablet coating for osmotic drug delivery, *J. Control. Release*, 35 (1995) 127-136
- [83] Wang, D. M., Lin, F. C., Chen, L. Y., and Lai, J. Y., Application of asymmetric TPC membranes to transdermal delivery of mitroglycerin, *J. Control Release*, 50 (1998) 187-195
- [84] Kobylak, Method for making breathable polyvinyl chloride films., U.S. patent #3644259 (1972)
- [85] Matz, R. The structure of cellulose acetate membranes I. The development of porous structure in anisotropic membranes, *Desalination*, 10 (1972) 1-15
- [86] Frommer, M. A. and Messalem R. M. Mechanism of membrane formation. IV. Convective flows and large void formation during membrane precipitation. *Ind. Chem. Prod. Res. Develop.*, 12 (1973) 328-333
- [87] Strathmann, H., Kock, K. and Amar, P., The formation mechanism of asymmetric membranes. *Desalination*, 16 (1975) 179-203
- [88] Stevens, W. E., Dunn, C. S., Petty, C. A., Surface tension induced cavitation in polymeric membranes during gelation, Paper presented at the 73rd Annual AIChE meeting, Chicago (1980).
- [89] Sternling, C. V. and Scriven, L. E., Interfacial turbulence: hydrodynamic instability and the Marangoni effect, *AIChE Journal*, 5 (1959) 514-523.
- [90] Broens, L., Altena, F. W., Smolders, C. A., and Koenhen, D.M., Membrane formation – diffusion induced demixing processes in ternary phase separation phenomena., *Desalination*, 32 (1980) 33-45.

- [91] Smolder, C.A., Reuvers, A.J., Boom, R. M., and Wienk, I. M., Microstructures in phase-inversion membranes. Part 1. Formation of macrovoids, *J. Membrane Sci.*, 73 (1992), 259.
- [92] Pekny, M. R., Influence of solutocapillary convection on macrovoid defect formation in dry-cast polymeric membrane, M.S. Thesis. University of Colorado, Boulder (1996)
- [93] Broens, L., Koenhen, D. M., and Smolders, C. A., On the mechanism of formation of asymmetric ultra- and hyper-filtration membranes, *Desalination*, 22 (1977) 199.
- [94] Kang, Y. S., Kim H. J., and Kim, U. Y., Asymmetric membrane formation via immersion precipitation method. Part I. Kinetic effect, *J. Membrane Sci.*, 60, (1987) 219.
- [95] Yao, C. W., Burford, R. P., Fane, A. G., and Fell, C.D.J., Effect of coagulation conditions on structure and properties of membranes from aliphatic polyamides, *J. Membrane Sci.*, 38, (1988), 113.
- [96] Koenhen, D. M., Mulder, M. H. V., and Smolders, C. A., Phase separation phenomena during the formation of asymmetric membranes, *J. Polym. Sci.* 21, (1977), 199.
- [97] Ray, R. J., Krantz, W. B., and Sani, R. L., Linear stability theory model for finger formation in asymmetric membranes, *J. Membrane Sci.*, 23, (1985), 155.
- [98] Wang, D., Lin, F., Wu, T., and Lai, J., Formation mechanism of the macrovoids induced by surfactant additives, *J. Membrane Sci.* 142 (1998) 191-204.
- [99] Vogrin, N, Stropnik, C., Musil, V., and Brumen, M., The wet phase separation: the effect of cast solution thickness on the appearance of macrovoids in the membrane

forming ternary cellulose acetate/acetone/water system, *J. Membrane Sci.* 207 (2002) 139.

[100] Pekny, M. R., Zartman J., Krants, W. B., Greenberg, A. R., and Todd, P., Flow-visualization during macrovoid pore formation in dry-cast cellulose acetate membranes, *J. Membrane Sci.*, 211, (2003), 71.

[101] McGuinniss, V. D., and Whitmore, R. S., Preparation and analysis of thin polysulfone films under high and low gravitational field environments, *J. Mem. Sci.*, 98 (1995) 27-47.

[102] Pekny, M. R., Greenberg, A. R., Khare, V. P., Zartman J., Krants, W. B., and Todd, P., Macrovoid pore formation in dry-cast cellulose acetate membranes: buoyancy studies, *J. Membrane Sci.* 205, (2002), 11.

[103] Khare, V. P., Greenberg, A. R., Zartman J., Krants, W. B., and Todd, P., Macrovoid growth during polymer membrane casting, *Desalination*, 145, (2002), 17.

[104] Nasr, A. M., Characterization of polymer films for optical applications, *Polymer Testing*, 21 (2002) 303-306.

APPENDIX A

EVAPORATION PROGRAM

The FORTRAN code developed to solve the unsteady-state evaporation equation incorporating convection is given below. This code uses the commercial PDE solver, NAG®.

```
PROGRAM ADVCTION3
CCCCCCCCCCCCCCCCCCCCCCCCCCCCCCCCCCCCCCCCCCCCCCCCCCCCCCCCCCCC
C
C    UNSTEADY-STATE EVAPORATION PROBLEM
C        1) Original Fick's 1st law
C        2) Binary mixture of liquid solution
C        3) Negligible evaporation of 2 to gas phase
C        4) Constant diffusion coefficient (DAB)
C        5) Constant thermodynamic partition coefficient (=1)
C        6) Constant mass transfer coefficient in gas phase (FLX1)
C        7) Constant density of pure 1 and 2 (DNSTY1 and DNSTY2)
C        8) Zero-volume of mixing or zero excess volume
C
CCCCCCCCCCCCCCCCCCCCCCCCCCCCCCCCCCCCCCCCCCCCCCCCCCCCCCCCCCCC
    IMPLICIT DOUBLE PRECISION (A-H , O-Z)
    IMPLICIT INTEGER (I-N)

    PARAMETER (NPTS=131, M=0,NXI=1,NV=1,NCODE=NV)
    PARAMETER (NXFIX=0, NPDE=1)
    PARAMETER (NWKRES=NPDE*(3*NPDE+6*NXI+NPTS+15)+NXI+NCODE+
$       7*NPTS+NXFIX+2+9000)
    PARAMETER (NEQN=NPDE*NPTS+NCODE)
    PARAMETER (NIW=25*NEQN+25+NXFIX+900000)
    PARAMETER (LENODE=(6+5)*NEQN+50)
    PARAMETER (NW=4*NEQN+11*NEQN/2+1+NWKRES+LENODE+20000)
    PARAMETER (PI = 3.14159265359)

    DOUBLE PRECISION Y(NEQN), X(NEQN), RTOL(NEQN), ATOL(NEQN),
$       XI(1), XBK(11), XFIX(1), IW(NIW), W(NW), Y2(NEQN)
    DOUBLE PRECISION DOMG(130,3)

    INTEGER ITERATION
    INTEGER ITASK

    LOGICAL THETA
```

```
DOUBLE PRECISION ALGOPT(30)
CHARACTER*1 LAOPT
INTEGER NRMESH,IPMINF
REAL DXMESH,TRMESH,XRATIO,CONST
```

```
CHARACTER*1 NORM
```

```
EXTERNAL UVINIT, ODEDEF, PDEDEF, BNDARY, D03PPF, D03PCL
```

```
COMMON /DEVICE/ lconc1, lconc2, ldomg1, ladv, lerr, llt, ltop, lpe
COMMON /CONST/ DAB, OMG1IN, FLMIN, DNSTY1, DNSTY2
COMMON /CTOR/ RHO, DNSF
COMMON /FLX/ FLX1, K
COMMON /GRDOMG/ GDU(130,3)
```

```
theta = .false.
neq = neqn
nnpts = npts
norm = 'A'
```

C Define output files

```
lconc1 = 1      !D03PPF solution
lconc2 = 2      !DUMMY:Analytic solution
lerr = 3        !DUMMY:Difference between two solutions
llt = 4         !ODE solution (thickness)
ldomg1 = 7     !Mass concentration gradient of 1
ladv = 8        !Mass average velocity
ltop = 9        !top concentration
lpe = 10       !modified peclet number
```

```
open (lconc1, file='conc1.8dat', status='new')
open (lconc2, file='conc2.8dat', status='new')
open (lerr, file='err.8dat', status='new')
open (llt, file='llt.8dat', status='new')
open (ldomg1, file='ldomg.8dat', status='new')
open (ladv, file='ladv.8dat', status='new')
open (ltop, file='top.8dat', status='new')
open (lpe, file='pe.8dat', status='new')
```

C..... Initial conditions for the problem (CGS unit)

```
C      OMG1IN = 5.0D-01      !Initial mass fraction
      OMG1IN = 1.0D-8
      FLMIN = 1.0D-01      !Thickness of system
      DAB = 1.0D-04        !Diffusion coefficient
      DNSTY1 = 0.8D0        !Density of pure 1
      DNSTY2 = 1.0D0        !Density of pure 2
C      FLX1 = 1.0D-02      !Mass transfer coefficient of A to the gas phase
      FLX1 = 1.0D-8

      DNSF = 1.0D0/DNSTY1 - 1.0D0/DNSTY2
```

```
WRITE(LCONC1,13) OMG1IN, FLMIN, DAB, FLX1,DNSTY1
```

```

        WRITE(LLT,14)
        WRITE(LTOP,15)
        WRITE(LPE,16)
13      FORMAT('THE INPUT VALUES ',/, 'OMG1IN =',F10.6/, 'FLMIN =',F10.6/, 'DAB
=,F10.6/, 'FLX1 =',F10.6/, 'DNSTY1 =',F10.6, 2(2X,A1))
14      FORMAT(2X,'TIME[S]', 2X,'THICKNESS[CM]', 1X)
15      FORMAT(2X,'TIME[S]', 2X,'OMG1_AT_TOP', 1X)
16      FORMAT(2X,'TIME[S]', 2X,'MODIFIED_PE_NEAR_TOP', 1X)

C.....  Start NAG initialization
C        NPDE = 4 ! turned into a parameter
        NPDEM = NPDE

        ITASK = 2

        DO 26 I=1,30
          ALGOPT(I)=0.0D0
26      CONTINUE
        ALGOPT(4)=2.0D0 !don't do the Petzold test.
        ALGOPT(29)=0.5
        ALGOPT(30)=1D-300

        LAOPT='S' !use the sparse matrix routines

C.....  Define the mesh positions in the array X(I)
        X(1) = 0.0D0
        XBK(1) = 0.0D0
        DX1047 = 1.0D0/ DBLE(130.0D0)

C        NPTS = 131 and uniform mesh
        PRINT*,' NPTS = ', NPTS
        DO 1047 J=2, 130
1047    X(J) = X(J-1) + DX1047

        X(NPTS) = 1.0D0
        NPTSM = NPTS

        XI(1) = 1.0D0

C....  Initialize GDU(J,1) which contains a normalized location.
        DO 2005 J=1, NPTS-1 !Dimension of GDU1 should be changed accordingly.
          GDU(J,1) = 0.0D0
2005    CONTINUE

        REMESH = .FALSE.
        MAXNPT = NNPTS
        T = 0.0D0

        ITIME = 1

        NRMESH = 0
        DXMESH = 0.0
        TRMESH = 1.0
        IPMINF = 0
        XRATIO = 1.5

```

```

CONST = 2.0/(NNPTS-1)

NMOSS = 2
SENS = 0.0D0
IRET = 0

C..... Set convergence criterion
DO 52 I = 1,NEQ
RTOL(I) = 1.0D-9
52 ATOL(I) = 1.0D-9
ITOL = 1

NEQMAX = NEQ + 1

WRITE(LCONC1,*) TFINAL, NPTS, ATOL(1), MAXORD

JSPARS = 0

T = 0.0D0

TOUT = 0.0D0
LNO = 0
LINO = 1

DO 9999 IT=1, 2000
TOUT = T + 1.0D0

IFAIL = -1

write (*,*) NPDE,M,T,TOUT,NNPTS,NEQN
ITERATION=ITERATION+1
write (*,*) ITERATION
write (*,*) "Entering d03ppf..."
CALL D03PPF(NPDE,M,T,TOUT,PDEDEF,BNDARY,UVINIT,Y,
$ NNPTS,X,NV,ODEDEF,NXI,XI,NEQN,RTOL,ATOL,
$ ITOL,NORM,LAOPT,ALGOPT,REMESH,NXFIX,XFIX,
$ NRMESH,DXMESH,TRMESH,IPMINF,XRATIO,CONST,
$ D03PCL,W,NW,IW,NIW,ITASK,ITRACE,IND,IFAIL)

PRINT*, "Time=", T
write (*,*) "Leaving d03ppf..."

C..... Calculate and write out the component mass fraction gradients
C..... Convert the dimensionless mass frac grad to dimensional grad
DO 2004 J=1, NPTS-1
DOMG(J,1) = GDU(J,1)*Y(NEQ)
DOMG(J,2) = GDU(J,2)/Y(NEQ)
DOMG(J,3) = GDU(J,3)/Y(NEQ)
2004 CONTINUE

C.... Calculate modified Peclet number at the top
PECLET = DOMG(NPTS-1,3)*Y(NEQ)/DAB

C... Write out solutions
WRITE(LDOMG1,2008) T, Y(NEQ)

```

```

WRITE(LDOMG1,2007) (DOMG(J,2), J=1, NPTS-1)
WRITE(LADV,2010) T, Y(NEQ)
WRITE(LADV,2009) (DOMG(J,3), J=1, NPTS-1)
WRITE(LPE, 2020) T, PECLET
WRITE(lconc1,250) T
WRITE(LCONC1,200) (Y(J), J=1, NPTS)
WRITE(ltop,230) T, Y(NPTS)
WRITE(ilt,220) T, Y(NEQ)

9999  CONTINUE

250  FORMAT('TIME(s) ',F15.9)
200  FORMAT(6(F12.8,1X))
220  FORMAT(F15.9, 4X, F17.12)
230  FORMAT(F15.9, 4X, F12.8)
2007 FORMAT(6(F19.8,1X))
2008 FORMAT('TIME(s) ',2(F15.9, 2X))
2009 FORMAT(6(F19.8,1X))
2010 FORMAT('TIME(s) ',2(F15.9, 2X))
2020 FORMAT(2(F15.9, 2X))

CLOSE(LCONC1, STATUS='KEEP')
CLOSE(LCONC2, STATUS='KEEP')
CLOSE(LERR, STATUS='KEEP')
CLOSE(ilt, STATUS='KEEP')
CLOSE(ltop, status='keep')
CLOSE(ldomg1, status='keep')
CLOSE(ladv, status='keep')
CLOSE(lpe, status='keep')

STOP
END

C.....          ***** USER SUBROUTINES *****

C*****
C*              SUBROUTINE UVINIT                      *
C*  This subroutine initializes the pdes.                *
C*****

SUBROUTINE UVINIT(NPDE, NPTS,NXI, X, XI, U, NV,V)
IMPLICIT DOUBLE PRECISION (A-H , O-Z)
IMPLICIT INTEGER (I-N)
DOUBLE PRECISION X(NPTS), U(NPDE,NPTS)

c
DOUBLE PRECISION V(NV)

COMMON /CONST/ DAB, OMG1IN, FLMIN, DNSTY1, DNSTY2

DO 10 I = 1,NPTS
U(1,I) = OMG1IN
10  CONTINUE

V(1) = FLMIN

```

RETURN
END

```
C*****
C*          SUBROUTINE PDEDEF          *
C*    The pdes are defined in this subroutine.          *
C*****

SUBROUTINE PDEDEF (NPDE,T,X,U,DUDX,NV,V,VDOT,C,Q,RR,IRES)

IMPLICIT DOUBLE PRECISION (A-H , O-Z)
IMPLICIT INTEGER (I-N)
DOUBLE PRECISION U(NPDE), DUDX(NPDE),
$      C(NPDE,NPDE), Q(NPDE), RR(NPDE), V(NV), VDOT(NV)

COMMON /CONST/ DAB, OMG1IN, FLMIN, DNSTY1, DNSTY2
COMMON /FCTOR/ RHO, DNSF
COMMON /GRDOMG/ GDU(130,3)

RHO = 1.0D0 / (U(1)*DNSF + (1.0D0/DNSTY2))
DIM1 = (RHO**2.0D0)/DNSTY2

C.....  Component (1)
C(1,1) = RHO*(V(1)**2.0D0)/DAB
Q(1)  = (RHO*DIM1*DNSF*DUDX(1) - (RHO*V(1)*X/DAB)*VDOT(1))*DUDX(1)
RR(1) = DIM1*DUDX(1)

CCCCCCCCCCCCCCCCCCCCCCCCCCCCCCCCCCCCCCCCCCCCCCCCCCCCCCCCCCCC
C      Store the mass fr. grad and location
CCCCCCCCCCCCCCCCCCCCCCCCCCCCCCCCCCCCCCCCCCCCCCCCCCCCCCCCCCCC

C....      Count empty space in GDUs
ICNT = 0
DO 2001 J=1, 130
    IF (GDU(J,1) .EQ. 0.0D0) THEN
        ICNT = ICNT + 1
    ENDIF
2001  CONTINUE

C...      If there is any empty space in GDUs, then fill it with mass fr. grad and location.
IF (ICNT .GT. 0) THEN
    DO 2018 J=1,130
        IF (GDU(J,1) .EQ. X) THEN
            ICNT=ICNT+1
        ENDIF
2018  CONTINUE
        GDU(130-ICNT+1,1) = X
        GDU(130-ICNT+1,2) = DUDX(1)
        GDU(130-ICNT+1,3) = DIM1*DNSF*DAB*DUDX(1)/V(1)
    ENDIF

C...      If there is no empty space in GDUs, then find the location and fill it with fr. grad.
IF (ICNT .EQ. 0) THEN
    DO 2002 J=1,130
```

```

                IF (GDU(J,1) .EQ. X) THEN
                    GDU(J,2) = DUDX(1)
                    GDU(J,3) = DIM1*DNSF*DAB*DUDX(1)/V(1)
                ENDIF
2002          CONTINUE
            ENDIF

            RETURN
            END

C*****
C*          SUBROUTINE BNDARY                      *
C*    The boundary conditions are defined in this subroutine.      *
C*****

$          SUBROUTINE BNDARY(NPDE,T,U,UX,NV,V,VDOT,
            IBND,BBETA,GAMA,IRES)

            IMPLICIT DOUBLE PRECISION (A-H , O-Z)
            IMPLICIT INTEGER (I-N)
            DOUBLE PRECISION BBETA(NPDE), GAMA(NPDE), U(NPDE), UX(NPDE)
$            ,V(1), VDOT(1)

            INTEGER IBND

            COMMON /CONST/ DAB, OMG1IN, FLMIN, DNSTY1, DNSTY2
            COMMON /FCTOR/ RHO, DNSF
            COMMON /FLX/ FLX1, K

            RHO = 1.0D0 / (U(1)*DNSF + (1.0D0/DNSTY2))
            DIM1 = RHO/DNSTY2

            IF (IBND .EQ. 0) THEN

C                BBETA(1) = 0.0D0
                GAMA(1) = UX(1)
                GAMA(1) = U(1) - 0.1D0

            ELSE

                BBETA(1) = (DAB/V(1))*DIM1
                GAMA(1) = 0.0D0 - FLX1*U(1) - RHO * U(1) * VDOT(1)
            ENDIF
            RETURN
            END

C*****
C*          SUBROUTINE ODEDEF                      *
C*    The ode coupled at the interface is defined in this      *
C*    subroutine.                                             *
C*****

$          SUBROUTINE ODEDEF (NPDE,T,NV,V,VDOT,NXI,XI,UI,UXI,RI,
            UTI,UTXI,VRES,IRES)

```



```

IMPLICIT DOUBLE PRECISION (A-H , O-Z)
IMPLICIT INTEGER (I-N)
DOUBLE PRECISION XI(NXI), UI(NPDE,NXI), UXI(NPDE,NXI),
$      RI(NPDE,NXI), UTI(NPDE,NXI), UTXI(NPDE,NXI), VRES(NV),
$      V(NV), VDOT(NV)

COMMON /CONST/ DAB, OMG1IN, FLMIN, DNSTY1, DNSTY2
COMMON /CTOR/ RHO, DNSF
COMMON /FLX/ FLX1, K

RHO = 1.0D0 / (UI(1,1)*DNSF + (1.0D0/DNSTY2))
DIM1 = (RHO**2.0D0)/DNSTY2

IF(IRES.EQ.-1) THEN
    VRES(1) = - VDOT(1)
ELSE
    VRES(1) = 0.0D0 - VDOT(1) - FLX1*UI(1,1)/RHO +
(DAB/V(1))*DIM1*DNSF*UXI(1,1)
ENDIF

RETURN
END

```

APPENDIX B

DRY-CASTING MASS-TRANSPORT PROGRAM

The FORTRAN code developed to solve the dry-casting mass-transfer equation incorporating convection is presented below. This code uses the commercial PDE solver, NAG®.

```
PROGRAM DRYCAST
  IMPLICIT DOUBLE PRECISION (A-H , O-Z)
  IMPLICIT INTEGER (I-N)

  PARAMETER (NPTS=131, M=0,NXI=1,NV=1,NCODE=NV)
  PARAMETER (NXFIX=0,NPDE=4)
C   PARAMETER (NWKRES=NPDE*(3*NPDE*NPTS+21)+7*(NPTS+NXFIX+3))
  PARAMETER (NWKRES=NPDE*(3*NPDE+6*NXI+NPTS+15)+NXI+NCODE+
$       7*NPTS+NXFIX+2+9000)
  PARAMETER (NEQN=NPDE*NPTS+NCODE)
  PARAMETER (NIW=25*NEQN+25+NXFIX+90000)
  PARAMETER (LENODE=(6+5)*NEQN+50)
C   PARAMETER (NW=NEQN*NEQN+NEQN+NWKRES+LENODE)
  PARAMETER (NW=4*NEQN+11*NEQN/2+1+NWKRES+LENODE+20000)

  DOUBLE PRECISION Y(NEQN), X(NEQN), RTOL(NEQN), ATOL(NEQN),
$       XI(1), XBK(11), DX(9000), XFIX(1), IW(NIW), W(NW),
$       SOL(1000,10), CHP1(NEQN), CHP2(NEQN), DST(2)
  DOUBLE PRECISION LAMBDA

  INTEGER ITERATION
  INTEGER INFORM(14+NEQN)
  INTEGER ITASK

  LOGICAL THETA
  DOUBLE PRECISION ALGOPT(30)
  CHARACTER*1 LAOPT
  INTEGER NRMESH,IPMINF
  REAL DXMESH,TRMESH,XRATIO,CONST

  CHARACTER*16 ZID
  CHARACTER*1 TISO, BINRY
```

CHARACTER*1 NORM

```
EXTERNAL UVINIT,ODEDEF,PDEDEF,BNDARY,SPDEF1,D03PPF,MONITR,
$   D03PCL

COMMON /SDEV2/ ITRACE, IDEV
COMMON /DEVICE/ LCONC1, LCONC2, LRHO1, LRHO2, LLT, LDMU,
$   LMASS, LTEM, LSURFT, LSUB, LGEL, LWARN, LFLX
$   , LCONT, LCONB, LCONGR, LTEMGR, LCHMP1, LCHMP2, LDIF, LADV, LPEN,
LPENT
COMMON /CONST/ RH01, RH02, RH03, RH013, RH023, SV1, SV2
$   , SV3, WM1, WM2, WM3, WMAIR, V1, V2, V3, R, V12, V21
$   , V13, V23, ETA, LAMBDA, GAMMA, ALPHA, BETA, FUJDO
$   , FUJA, FUJB, G
C
COMMON /GLSPAR/ TCONGL, RHOGLS, CPGLS, SUBTHK, WPLATE, ALFSUB
COMMON /PLYPAR/ TCONPS, CPPS, EPSLON, SIGMA
COMMON /GASPAR/ TCONGS, VISGAS
COMMON /SCALES/ RHOSC, DIF1SC, DIF2SC,SOLLSC, SUBLSC, TIMESC,
$   VELSC, TEMPSC, F1SC, F2SC, G1SC, G2SC, HEATSC, FLX1SC, FLX2SC
$   ,OMG1SC, OMG2SC
COMMON /INPUTS/ OMG1IN, OMG2IN, YK1, TEMPIN, TEMAMB
$   , FLMIN, GELTIM, PTOT
COMMON /CHARA/ TISO, BINRY
COMMON /BLK1/ RHOINT, C1MASI, C2MASI, C3MASI, DX, JCT,
$   KCT, AREA, NPTSM, NPDEM
COMMON /GRDOMG/ GDU1(130,3), GDU2(130,3)
COMMON /DEVICE2/ LADVL

theta = .false.
neq = neqn
nnpts = npts
norm = 'A'

kct  = 0
jct  = 0

lconc1 = 1
lconc2 = 2
lrho1  = 3
lrho2  = 4

lmass = 7
litem  = 8
lsurft = 9
lsub   = 10
lgel   = 11
lwarn  = 12
lflx   = 13
llt    = 14
lcont  = 15
lconb  = 16
lcongr = 17
ltemgr = 18
lchmp1 = 19
lchmp2 = 20
```

```

ldif = 21
ldmu = 22
ladv = 23
lpen= 24
lpent = 25
ladvl = 27

itrace = 1
idev = 6

open (lconc1, file='conc1.8dat', status='new')
open (lconc2, file='conc2.8dat', status='new')
C open (lrho1, file='rho1.dat', status='new')
C open (lrho2, file='rho2.dat', status='new')
open (llt, file='lstar.8dat', status='new')
open (lmass, file='mass.8dat', status='new')
open (ltem, file='temp.8dat', status='new')
open (lsurft, file='surft.8dat', status='new')
open (lsub, file='subt.8dat', status='new')
open (lgel, file='gel.8dat', status='new')
open (lwarn, file='err.8dat', status='new')
open (lflx, file='flx.8dat', status='new')
open (lcont, file='topc.8dat', status='new')
open (lconb, file='botc.8dat', status='new')
open (lcongr, file='gradc.8dat', status='new')
open (ltemgr, file='gradt.8dat', status='new')
open (lchmp1, file='chemp1.8dat', status='new')
open (lchmp2, file='chemp2.8dat', status='new')
open (ldif, file='diff.8dat', status='new')
open (ldmu, file='dmudo.8dat', status='new')
open (ladv, file='adv.8dat', status='new')
open (lpen, file='pe.8dat', status='new')
open (lpent, file='pet.8dat', status='new')
open (ladvl, file='advl.8dat', status='new')

C..... The time increment at which the control is returned to the main
C program. The smaller this time step the smaller the error.
TINC = 3.00D0
TFINAL = 300.0

C..... If this is a binary and/or isothermal run
BINRY = 'N'
TISO = 'N'

C..... Initial conditions for the problem
IF(BINRY .EQ. 'Y') THEN
C..... Experiment identification number
ZID = 'B000000.000.00.0'

OMG1IN = 1.0D-13
YK1 = 0.0D0
OMG2IN = 0.870D0
FLMIN = 0.026600
TEMPIN = 296.15D0
PTOT = 760.0
SUBTHK = 0.122

```

```

C          SUBTHK = 0.465
          GELTIM = 0.4D0
          PRINT*,' This is a binary run. '
ELSE
C.....  Experiment identification number
        ZID = "T091092.600.15.3"

          OMG1IN = 0.20D0
          OMG2IN = 0.70D0
          YK1  = 0.000000011D0
          FLMIN = 0.0266D0
          TEMPIN = 297.15D0
          PTOT  = 632.0
C          PTOT = 760
C.....  Ambient temperature, usually the same as initial temp
          TEMAMB = TEMPIN
          SUBTHK = 0.122
          GELTIM = 0.4D0
          PRINT*,' This is a ternary run. '
ENDIF

C.....  Initialize the constants specific to the system of interest
        CALL CONSTS

        write(LDMU,1060)
        write(LLT,1070)
        write(LMASS,1080)
        write(LSURFT,1090)
        write(LSUB,1095)
        write(LFLX,1100)
        write(LCONT,1110)
        write(LCONB,1120)
        write(LCONGR,1130)
        write(LTEMGR,1140)
        write(LCONC1,550) ZID
        write(LCONC1,13) OMG1IN, OMG2IN, FLMIN, TEMPIN, YK1,
$          TISO, BINRY
13  FORMAT('THE INPUT VALUES ', 5(F10.6,1X),2(2X,A1))

        WRITE(lpen,91)
        WRITE(lpent,92)
        WRITE(ladv,93)
        WRITE(ladv1,94)
91  FORMAT(2X, 'TIME(S)', 2X, 'Pe#_for_Mass', 2X, 'Thickness(cm)')
92  FORMAT(2X, 'TIME(S)', 2X, 'Pe#_for_Heat', 2X, 'Thickness(cm)')
93  FORMAT(2X, 'Mass_average_velocity')
94  FORMAT(2X, 'Location_matrix_for_mass_average_velocity')

        WRITE(LCONC1,*) RHOSC, DIF1SC, DIF2SC, SOLLSC, SUBLSC,
$          TIMES, TEMPSC, F1SC, F2SC, G1SC, G2SC, HEATSC,
$          FLX1SC, FLX2SC, OMG1SC, OMG2SC

        WRITE(LDIF,103)
103  FORMAT('TIME(S)', 5X, ' DIMENSIONAL F1, F2, G1, G2')

```

```

C..... Calculate the initial mass of nonsolvent(NS)(1), solvent(S)(2),
C        and polymer(P)(3).
        RHOINT = RH01*OMG1IN + RH02*OMG2IN + RH03*(1.D0-OMG1IN-OMG2IN)
        C1MASI = RHOINT*OMG1IN*AREA*FLMIN
        C2MASI = RHOINT*OMG2IN*AREA*FLMIN
        C3MASI = RHOINT*(1.0D0 - OMG1IN - OMG2IN)*AREA*FLMIN

```

```

C..... Start SPRINT initialization
C        NPDE = 4 ! turned into a parameter
        NPDEM = NPDE

```

```

C..... M = geometry (0 = planar, 1 = cylindrical, 2 = spherical)
C        M = 0 turned into a parameter

```

```
ITASK = 2
```

```

        DO 16 I=1,30
            ALGOPT(I)=0.0D0
16 CONTINUE
        ALGOPT(4)=2.0D0 !don't do the Petzold test.
        ALGOPT(29)=0.5
        ALGOPT(30)=1D-300

```

```
LAOPT='S' !use the sparse matrix routines
```

```

C..... Define the mesh positions in the array X(I)
        X(1) = 0.0D0
        XBK(1) = 0.0D0
        DX25 = 1.0D0 / DBLE(25.0D0)
        DX50 = 1.0D0 / DBLE(50.0D0)
        DX100 = 1.0D0 / DBLE(100.0D0)
        DX200 = 1.0D0 / DBLE(200.0D0)
        DX400 = 1.0D0 / DBLE(400.0D0)
        DX800 = 1.0D0 / DBLE(800.0D0)
        DX1600 = 1.0D0 / DBLE(1600.0D0)

```

```

        ncase = 2
        IF(NCASE .EQ. 2) THEN
c npts=131
            DO 5 J=2,21
5                X(J) = X(J-1) + DX50

            DO 6 J = 22, 51
6                X(J) = X(J-1) + DX100

            DO 7 J = 52, 91
7                X(J) = X(J-1) + DX200

            DO 8 J = 92, 130
8                X(J) = X(J-1) + DX400
                PRINT*, ' NPTS = ', NPTS
            ENDIF

```

```
IF(NCASE .EQ. 6) THEN
```

```

C          npts = 80
c          npts = 5
          PRINT*, 'NPTS = ', NPTS
          DXXP = 1.0D0 / DBLE(NPTS-1)
          DO 650 J = 2, NPTS
650        X(J) = X(J-1) + DXXP
          ENDIF
        IF(NCASE .EQ. 4) THEN
C npts=191
          PRINT *, 'NPTS = ', NPTS
          DO 55 j=2,21
55         X(J) = X(J-1) + DX50

          DO 66 J = 22, 51
66         X(J) = X(J-1) + DX100

          DO 77 J = 52, 91
77         X(J) = X(J-1) + DX200

          DO 88 J = 92, 111
88         X(J) = X(J-1) + DX400

          DO 89 J = 112, 190
89         X(J) = X(J-1) + DX1600
          ENDIF

        IF(NCASE .EQ. 3) THEN
C          NPTS = 261
          PRINT*, 'NPTS = ', NPTS
          DO 1 J = 2, 41
1          X(J) = X(J-1) + DX100

          DO 2 J = 42, 101
2          X(J) = X(J-1) + DX200

          DO 3 J = 102, 181
3          X(J) = X(J-1) + DX400

          DO 4 J = 182, 260
4          X(J) = X(J-1) + DX800
          ENDIF

        IF(NCASE .EQ. 5) THEN
C          NPTS = 521
          PRINT*, 'NPTS = ', NPTS
          DO 555 J = 2, 81
555       X(J) = X(J-1) + DX200

          DO 666 J = 82, 201
666       X(J) = X(J-1) + DX400

          DO 777 J = 202, 361
777       X(J) = X(J-1) + DX800

          DO 888 J = 362, 520
888       X(J) = X(J-1) + DX1600

```

ENDIF

```
      X(NPTS) = 1.0D0
      NPTSM  = NPTS

C....  GDU(J,1) contains a normalized location.
      DO 2005 J=1, NPTS-1 !Dimension of GDU1 and GDU2 should be changed accordingly.
      GDU1(J,1) = 0.0D0
      GDU2(J,1) = 0.0D0
2005   CONTINUE

C.....  Transfer x values into the DX for use in subroutine MONITR
      DO 41 KP = 1 , NPTS
      WRITE(LCONC1,57) X(KP)
      WRITE(LCONC2,57) X(KP)
      WRITE(LCHMP1,57) X(KP)
      WRITE(LCHMP2,57) X(KP)
C      WRITE(LTEM,57) X(KP)
41     DX(KP) = X(KP)
57     FORMAT(F20.15)

C.....  Coupled O.D.E. at the solution/air interface (moving boundary)
C      NV   = 1 turned into a parameter
C      NXI  = 1 turned into a parameter
      XI(1) = 1.0D0
C      NCODE=NV Turned into a parameter

      REMESH = .FALSE.
      MAXNPT = NNPTS
      T      = 0.0D0
C      IBAND =
      ITIME = 1

      NRMESH = 0
      DXMESH = 0.0
      TRMESH = 1.0
      IPMINF = 0
      XRATIO = 1.5
      CONST = 2.0/(NNPTS-1)

      NMOSS = 2
      SENS = 0.0D0
      IRET = 0

C.....  Set convergence criterion
      DO 52 I = 1,NEQ
      RTOL(I) = 2E-4
52     ATOL(I) = 2E-4
      ITOL = 1

      DO 99 I = 1 , 14
99     INFORM(I) = 0
      INFORM(2) = 1
      INFORM(3) = 1
```



```

INFORM(4) = 9000
C   SNORM = 'L2NORM'
    NEQMAX = NEQ + 1

    WRITE(LCONC1,*) TFINAL, NPTS, ATOL(1), MAXORD

C..... Write the initial conc and mass fractions of components 1 & 2
    WRITE(LCONC1,250) T*TIMESC, Y(NEQ)*SOLLSC
    WRITE(LCONC1,200) (Y(J)*OMG1SC, J=1, NEQ-1, NPDE)
C   WRITE(LRHO1,250) T*TIMESC, Y(NEQ)*SOLLSC
C   WRITE(LRHO1,200) (RHOACT(J), J=1, NEQ-1, NPDE)

    WRITE(LCONC2,250) T*TIMESC, Y(NEQ)*SOLLSC
    WRITE(LCONC2,200) (Y(J)*OMG2SC, J=2, NEQ-1, NPDE)
C   WRITE(LRHO2,250) T*TIMESC, Y(NEQ)*SOLLSC
C   WRITE(LRHO2,200) (RHOACT(J), J=2, NEQ-1, NPDE)

C..... Write out the initial chemical potentials for components 1 & 2
    WRITE(LCHMP1,250) T*TIMESC, Y(NEQ)*SOLLSC
    WRITE(LCHMP2,250) T*TIMESC, Y(NEQ)*SOLLSC
    DO 603 K = 1, NPTS
        DST(1) = OMG1IN/OMG1SC
        DST(2) = OMG2IN/OMG2SC
        CALL CHEMPT (0.0, 2, DST, 4, XNONSL, XSOLV)
        CHP1(K) = XNONSL
        CHP2(K) = XSOLV
603  CONTINUE
    WRITE(LCHMP1,200) (CHP1(J), J=1, NPTS)
    WRITE(LCHMP2,200) (CHP2(J), J=1, NPTS)

C..... Write the initial temperature in the polymer solution
    WRITE(LTEM,250) T*TIMESC, Y(NEQ)*SOLLSC
    WRITE(LTEM,201) (Y(J)*TEMPSC-273.15, J = 3, NEQ-1, NPDE)
    JSPARS = 0

C   Nondimensionize the final time
    TFIN = TFINAL / TIMESC
    TOUT = 0.0
    LNO = 0
    LINO = 1
54  TOUT = T + TINC/TIMESC
C 54  TOUT = TOUT + TINC/TIMESC

    write (*,*) NPDE,M,T,TOUT,NNPTS,NEQN
    ITERATION=ITERATION+1
    write (*,*) ITERATION
    write (*,*) "Entering d03ppf..."
    CALL D03PPF(NPDE,M,T,TOUT,PDEDEF,BNDARY,UVINIT,Y,
$           NNPTS,X,NV,ODEDEF,NXI,XI,NEQN,RTOL,ATOL,
$           ITOL,NORM,LAOPT,ALGOPT,REMESH,NXFIX,XFIX,
$           NRMESH,DXMESH,TRMESH,IPMINF,XRATIO,CONST,
$           D03PCL,W,NW,IW,NIW,ITASK,ITRACE,IND,IFAIL)

    write (*,*) "Leaving d03ppf..."
    CALL MONITR (NEQ,T,Y,RR)

```

```

C      IF(INFORM(1) .NE. 2) THEN
C          WRITE(LCONC1,300) INFORM(1)
C          GO TO 70
C      ENDIF

C.....  Sepatrate the concentration and temperature solutions
DO 205 KL = 1, NPDE
        DO 105 KM = 1, NPTS
            SOL(KM,KL) = Y(NPDE*(KM-1)+KL)
105        CONTINUE
205    CONTINUE

        WRITE(LCONC1,250) T*TIMESC, Y(NEQ)*SOLLSC
        WRITE(LCONC1,200) (SOL(J,1)*OMG1SC, J=1, NPTS)
        WRITE(LCONC2,250) T*TIMESC, Y(NEQ)*SOLLSC
        WRITE(LCONC2,200) (SOL(J,2)*OMG2SC, J=1, NPTS)
        WRITE(LTEM,250) T*TIMESC, Y(NEQ)*SOLLSC
        WRITE(LTEM,200) (SOL(J,3)*TEMPSC-273.15, J=1, NPTS)
        WRITE(LCONT,400) T*TIMESC, SOL(NPTS,1)*OMG1SC,
$           SOL(NPTS,2)*OMG2SC
        WRITE(LCONB,400) T*TIMESC, SOL(1,1)*OMG1SC,
$           SOL(2,2)*OMG2SC

C.....  Calculate the chemical potentials for components 1 & 2
C      at every time step.
        WRITE(LCHMP1,250) T*TIMESC, Y(NEQ)*SOLLSC
        WRITE(LCHMP2,250) T*TIMESC, Y(NEQ)*SOLLSC
        DO 503 K = 1, NPTS
            DST(1) = SOL(K,1)
            DST(2) = SOL(K,2)
            CALL CHEMPT (0.0, 2, DST, 4, XNONSL, XSOLV)
            CHP1(K) = XNONSL
            CHP2(K) = XSOLV
C.....  Write out diffusion coefficients
            IF(K.EQ.NPTS) THEN
                IFLAG = 1
                CALL COEFFI(0.0, NPDE, DST, 0.0,
$                   FF1, FF2, GG1, GG2, HH1, HH2, IFLAG)
C      WRITE(LDIF,397) T*TIMESC,FF1*F1SC,FF2*F2SC,GG1*G1SC,GG2*G2SC
                IFLAG = 9999
                CALL COEFFI(0.0, NPDE, DST, 0.0,
$                   FF1, FF2, GG1, GG2, HH1, HH2, IFLAG)
C      WRITE(LDMU,397) T*TIMESC,FF1,FF2,GG1,GG2

                ENDIF
503    CONTINUE
        WRITE(LCHMP1,200) (CHP1(J), J=1, NPTS)
        WRITE(LCHMP2,200) (CHP2(J), J=1, NPTS)

C.....  Final integration time is reached, stop the program
        IF(TOUT .GT. TFIN) GO TO 53

        GO TO 54

53    CONTINUE

```

```

C      WRITE(LCONC1,350) INFORM(1)

70     CONTINUE
910    FORMAT('MAIN: Switching to sparse at T(s) ',1X,F12.5)

      CLOSE(LCONC1, STATUS='KEEP')
      CLOSE(LCONC2, STATUS='KEEP')
C      CLOSE(LRHO1, STATUS='KEEP')
C      CLOSE(LRHO2, STATUS='KEEP')
      CLOSE(LLT, STATUS='KEEP')
      CLOSE(LMASS, STATUS='KEEP')
      CLOSE(LTEM, STATUS='KEEP')
      CLOSE(LSURFT, STATUS='KEEP')
      CLOSE(LSUB, STATUS='KEEP')
C      CLOSE(LGEL, STATUS='KEEP')
      CLOSE(LWARN, STATUS='KEEP')
      CLOSE(LCONT, STATUS='KEEP')
      CLOSE(LCONB, STATUS='KEEP')
      CLOSE(LCONGR, STATUS='KEEP')
      CLOSE(LTEMGR, STATUS='KEEP')
      CLOSE(LCHMP1, STATUS='KEEP')
      CLOSE(LCHMP2, STATUS='KEEP')
      CLOSE(LDIF, STATUS='KEEP')
      CLOSE(LDMU, STATUS='KEEP')
      CLOSE(ladv, status='keep')
      CLOSE(lpen, status='keep')
      CLOSE(lpent, status='keep')
      CLOSE(ladvl, status='keep')

90     FORMAT(1X, 5(F12.8,2X))
200    FORMAT(6(F12.8,1X))
201    FORMAT(6(F10.4,2X))
250    FORMAT('TIME(s) ',2(F15.9, 2X))
270    FORMAT('Negative concentration')
300    FORMAT(2X,'UNSUCCESSFULL INFORM(1) = ',I3)
350    FORMAT(2X,'SUCCESSFULL INFORM(1) = ',I3)
397    FORMAT(1X, 5(F12.8,2X))
400    FORMAT(2X,F15.7,5X,2(F20.15,2X))
550    FORMAT(A16)
1060   FORMAT(2X,'TIME(S)',5X,'DM1DO1, DM1DO2, DM2DO1, DM2DO2')
1070   FORMAT(5X,'TIME(s)',5X,'L(t)(cm)',5X,'L(t)(dimenlss)')
1080   FORMAT(2X,'TIME(s)',5X,'NS + S TO POLY MASS RATIO',5X,'TOT MAS')
1090   FORMAT(2X,'TIME(s)',5X,'SURF SOL TEMP(C)')
1095   FORMAT(2X,'TIME(s)',5X,'SURF SUB TEMP(C)')
1100   FORMAT(1X,'T(s)',5X,'NS FLX',5X,'S FLX',5X,'NS EQ INTF CON',
$       5X,'S EQ CON')
1110   FORMAT(1X,'TIME(s)',5X,'NS MAS FRAC(TOP)',5X,'S MAS FRAC(TOP)')
1120   FORMAT(1X,'TIME(s)',5X,'NS MAS FRAC(BOT)',5X,'S MAS FRAC(BOT)')
1130   FORMAT(1X,'TIME(S)',5X,'NODIM SURF NS&S M FRAC GRAD',5X,'DIMNAL
$       SURF M DENS NS&S GRAD')
1140   FORMAT(1X,'TIME(S)',5X,'DIMLSS SURF TEM GRAD',5X,'DIMNAL SURF
$       TEM GRAD')

      STOP
      END

```

```

C.....          ***** USER SUBROUTINES *****

C*****
C*              SUBROUTINE UVINIT                      *
C*      This subroutine initializes the pdes and the odes.      *
C*****

      SUBROUTINE UVINIT( NPDE, NPTS,NXI, X, XI, U, NV,V)
      IMPLICIT DOUBLE PRECISION (A-H , O-Z)
      IMPLICIT INTEGER (I-N)
      DOUBLE PRECISION X(NPTS), U(NPDE,NPTS)

      DOUBLE PRECISION V(NV)

      COMMON /SCALES/ RHOSC, DIF1SC, DIF2SC, SOLLSC, SUBLSC, TIMESC,
$  VELSC, TEMPSC, F1SC, F2SC, G1SC, G2SC, HEATSC, FLX1SC, FLX2SC
$  ,OMG1SC, OMG2SC
      COMMON /INPUTS/ OMG1IN, OMG2IN, YK1, TEMPIN, TEMAMB
$  , FLMIN, GELTIM, PTOT

      DO 10 I = 1,NPTS
      U(1,I) = OMG1IN/OMG1SC
      U(2,I) = OMG2IN/OMG2SC
      U(3,I) = TEMPIN/TEMPSC
      U(4,I) = TEMPIN/TEMPSC
10    CONTINUE

      V(1)=FLMIN/SOLLSC ! This is from SVINIT from SPRINT.

      RETURN
      END

C*****
C*              SUBROUTINE ODEDEF                      *
C*      The ode coupled at the interface is defined in this      *
C*      subroutine.                                             *
C*****

      SUBROUTINE ODEDEF (NPDE,T,NV,V,VDOT,NXI,XI,UI,UXI,RI,
$  UTI,UTXI,VRES,IRES)

      IMPLICIT DOUBLE PRECISION (A-H , O-Z)
      IMPLICIT INTEGER (I-N)
      DOUBLE PRECISION XI(NXI), UI(NPDE,NXI), UXI(NPDE,NXI),
$  RI(NPDE,NXI), UTI(NPDE,NXI), UTXI(NPDE,NXI), VRES(NV),
$  V(NV), VDOT(NV)
      COMMON /SCALES/ RHOSC, DIF1SC, DIF2SC, SOLLSC, SUBLSC, TIMESC,
$  VELSC, TEMPSC, F1SC, F2SC, G1SC, G2SC, HEATSC, FLX1SC, FLX2SC
$  ,OMG1SC, OMG2SC
      COMMON /BLK2/ GF1, GF2

      IF(IRES.EQ.-1) THEN
      VRES(1) = VDOT(1)

```

```

ELSE
CALL DENSTY (T, NPDE, UI, IFLAG, RHO)
CALL FLXHET (T, UI, NPDE, NV, V, VDOT, RHOGA,
$          FLUXG1, FLUXG2, HTRSFC, HV1, HV2, IFG)
GF1 = FLUXG1
GF2 = FLUXG2
C          PRINT *, 'GF1=', GF1, GF2
C..... Set component densities (g/cm^3)
RH01 = 1.0
RH02 = 0.7857
RH03 = 1.31
RH13 = (1.0D0/RH01) - (1.0D0/RH03)
RH23 = (1.0D0/RH02) - (1.0D0/RH03)
DIMM1 = (F1SC*TIMESC)/(RHOSC*(SOLLSC**2.0D0))
DIMM2 = TIMESC/(RHOSC*SOLLSC)

C          PRINT*, ' RHO is ', RHO
C          PRINT*, ' RHOGA... ', RHOGA
C          CALL COEFFI(T, NPDE, UI, 0.0, FF1, FF2, GG1, GG2, HH1, HH2, IFLAG)
C          PRINT*, 'FF1 , UXIs are ', FF1, UXI(1,1), UXI(2,1)
          VRES(1) = VDOT(1) - DIMM1*RH13*RI(1,1)/V(1) - DIMM1*RH23*RI(2,1)/V(1) +
(FLUXG1 + (FLX2SC/FLX1SC)*FLUXG2)/(RHO)

ENDIF
IF(V(1) .LT. 0.0D0 .OR. IFG .EQ. 99) IRES = 2
RETURN
END

```

```

C*****
C*          SUBROUTINE PDEDEF          *
C*    The pdes are defined in this subroutine.          *
C*****

```

```

SUBROUTINE PDEDEF (NPDE,T,X,U,DUDX,NV,V,VDOT,C,Q,RR,IRES)

IMPLICIT DOUBLE PRECISION (A-H , O-Z)
IMPLICIT INTEGER (I-N)
DOUBLE PRECISION U(NPDE), DUDX(NPDE),
$          C(NPDE,NPDE), Q(NPDE), RR(NPDE), V(NV), VDOT(NV)
DOUBLE PRECISION LAMBDA

COMMON /CONST/ RH01, RH02, RH03, RH013, RH023, SV1, SV2
$ , SV3, WM1, WM2, WM3, WMAIR, V1, V2, V3, R, V12, V21
$ , V13, V23, ETA, LAMBDA, GAMMA, ALPHA, BETA, FUJD0
$ , FUJA, FUJB, G
COMMON /SCALES/ RHOSC, DIF1SC, DIF2SC, SOLLSC, SUBLSC, TIMESC,
$ VELSC, TEMPSC, F1SC, F2SC, G1SC, G2SC, HEATSC, FLX1SC, FLX2SC
$ ,OMG1SC, OMG2SC
COMMON /PLYPAR/ TCONPS, CPPS, EPSLON, SIGMA
COMMON /GLSPAR/ TCONGL, RHOGLS, CPGLS, SUBTHK, WPLATE, ALFSUB
COMMON /GRADS/ UX1LFT, UX1RHT, UX2LFT, UX2RHT, UTLFT, UTRHT
COMMON /GRDOMG/ GDU1(130,3), GDU2(130,3)

CALL DENSTY(T, NPDE, U, IFG, RHO)
IFLAG = 1
CALL COEFFI(T, NPDE, U, DUDX, FF1, FF2, GG1, GG2, HH1, HH2, IFLAG)

```

RH01 = 1.0
 RH02 = 0.7857
 RH03 = 1.31
 RH13 = (1.0D0/RH01) - (1.0D0/RH03)
 RH23 = (1.0D0/RH02) - (1.0D0/RH03)
 DIM1 = (RHOSC*SOLLSC**2)/(F1SC*TIMESC)

C..... Component (1) (nonsolvent) mass transport equation
 C(1,1) = DIM1*RHO*V(1)**2
 C(2,1) = 0.0D0
 C(3,1) = 0.0D0
 C(4,1) = 0.0D0
 Q(1) = - DIM1*RHO*V(1)*X*DUDX(1)*VDOT(1) +
 RHO*(RH13*(FF1*DUDX(1)+GG1*DUDX(2)) + RH23*(FF2*DUDX(1)+GG2*DUDX(2)))*DUDX(1)
 RR(1) = - (FF1*DUDX(1)+GG1*DUDX(2))

C DIM2 = (RHOSC*SOLLSC**2)/(G2SC*TIMESC)

C..... Component (2) (solvent) mass transport equation
 C(1,2) = 0.0D0
 C(2,2) = DIM1*RHO*V(1)**2
 C(3,2) = 0.0D0
 C(4,2) = 0.0D0
 Q(2) = - DIM1*RHO*V(1)*X*DUDX(2)*VDOT(1) +
 RHO*(RH13*(FF1*DUDX(1)+GG1*DUDX(2)) + RH23*(FF2*DUDX(1)+GG2*DUDX(2)))*DUDX(2)
 RR(2) = - (FF2*DUDX(1)+GG2*DUDX(2))

DIM3 = (SOLLSC**2)*RHOSC*CPPS/(TIMESC*TCONPS)
 DIM31 = F1SC/(RHOSC*SOLLSC)

C..... Energy transport equation (polymer solution)
 C(1,3) = 0.0D0
 C(2,3) = 0.0D0
 C(3,3) = DIM3*RHO*V(1)*V(1)
 C(4,3) = 0.0D0
 Q(3) = - DIM3*RHO*V(1)*X*VDOT(1)*DUDX(3) +
 (DIM31*DIM3*TIMESC/SOLLSC)*(RH13*(FF1*DUDX(1)+GG1*DUDX(2)) +
 RH23*(FF2*DUDX(1)+GG2*DUDX(2)))*(V(1)**2)*DUDX(3)
 RR(3) = DUDX(3)

C C(1,3) = 0.0D0
 C C(2,3) = 0.0D0
 C C(3,3) = DIM3*RHO*V(1)*V(1)
 C C(4,3) = 0.0D0
 C Q(3) = - DIM3*RHO*V(1)*X*VDOT(1)*DUDX(3)
 C RR(3) = DUDX(3)

DIM4 = SUBLSC*SUBLSC/(TIMESC*ALFSUB)

C..... Energy transport equation (glass plate)
 C(1,4) = 0.0D0
 C(2,4) = 0.0D0
 C(3,4) = 0.0D0
 C(4,4) = DIM4
 Q(4) = 0.0D0
 RR(4) = DUDX(4)

ICNT = 0

```

C...      Count empty space in GDUs
DO 2001 J=1, 130
      IF (GDU1(J,1) .EQ. 0.0D0) THEN
            ICNT = ICNT + 1
      ENDIF
2001 CONTINUE

C...      If there is any empty space in GDUs then fill it with mass frc. grad and location.
IF (ICNT .GT. 0) THEN
      DO 2058 J=1,130
            IF (GDU1(J,1) .EQ. X) THEN
                  ICNT=ICNT+1
            ENDIF
2058      CONTINUE
            GDU1(130-ICNT+1,1) = X
            GDU1(130-ICNT+1,2) = DUDX(1)
            GDU1(130-ICNT+1,3) = (F1SC/(SOLLSC*V(1)))*((1.0D0/RH01 - 1.0D0/RH03)*RR(1)
+ (1.0D0/RH02 - 1.0D0/RH03)*RR(2))
            GDU2(130-ICNT+1,1) = X
            GDU2(130-ICNT+1,2) = DUDX(2)
C          GDU2(130-ICNT+1,3) = (F1SC/(SOLLSC*V(1)))*RR(1)/(RHO*U(1))
            GDU2(130-ICNT+1,3) = TCONPS/(RHO*CPPS)
      ENDIF

C...      If there is no empty space in GDUs then find the location and fill it with frc. grad.
IF (ICNT .EQ. 0) THEN
      DO 2002 J=1,130
            IF (GDU1(J,1) .EQ. X) THEN
                  GDU1(J,2) = DUDX(1)
                  GDU2(J,2) = DUDX(2)
                  GDU1(J,3) = (F1SC/(SOLLSC*V(1)))*((1.0D0/RH01 -
1.0D0/RH03)*RR(1) + (1.0D0/RH02 - 1.0D0/RH03)*RR(2))
C          GDU2(J,3) = (F1SC/(SOLLSC*V(1)))*RR(1)
                  GDU2(J,3) = TCONPS/(RHO*CPPS)
            ENDIF
2002      CONTINUE
      ENDIF

C.....   Store the gradients at the right boundary (X=1)
IF(X .GE. 1.0) THEN
      UX1RHT = DUDX(1)
      UX2RHT = DUDX(2)
      UTRHT = DUDX(3)
      ENDIF
      RETURN
      END

```

```

C*****
C*          SUBROUTINE BNDARY          *
C*      The boundary conditions are defined in this subroutine.          *
C*****

```

```

$      SUBROUTINE BNDARY(NPDE,T,U,UX,NV,V,VDOT,
      IBND,BBETA,GAMA,IRES)

```

```

      IMPLICIT DOUBLE PRECISION (A-H , O-Z)

```

```

    IMPLICIT INTEGER (I-N)
    DOUBLE PRECISION BBETA(NPDE), GAMA(NPDE), U(NPDE), UX(NPDE)
$      ,V(1), VDOT(1)
    DOUBLE PRECISION LAMBDA

INTEGER IBND

    CHARACTER*1 TISO, BINRY
    COMMON /CONST/ RH01, RH02, RH03, RH013, RH023, SV1, SV2
$   , SV3, WM1, WM2, WM3, WMAIR, V1, V2, V3, R, V12, V21
$   , V13, V23, ETA, LAMBDA, GAMMA, ALPHA, BETA, FUJD0
$   , FUJA, FUJB, G
    COMMON /SCALES/ RHOSC, DIF1SC, DIF2SC, SOLLSC, SUBLSC, TIMESC,
$   VELSC, TEMPSC, F1SC, F2SC, G1SC, G2SC, HEATSC, FLX1SC, FLX2SC
$   ,OMG1SC, OMG2SC
    COMMON /PLYPAR/ TCONPS, CPPS, EPSLON, SIGMA
    COMMON /INPUTS/ OMG1IN, OMG2IN, YK1, TEMPIN, TEMAMB
$   , FLMIN, GELTIM, PTOT
    COMMON /CHARA/ TISO, BINRY
    COMMON /GLSPAR/ TCONGL, RHOGLS, CPGLS, SUBTHK, WPLATE, ALFSUB
    COMMON /BLK2/ GF1, GF2

    IF (IBND .EQ. 0) THEN
C..... Mass transport, component (1) (water)
        BBETA(1) = 0.0D0
        GAMA(1) = UX(1)

C..... Mass transport, component (2) (acetone)
        BBETA(2) = 0.0D0
        GAMA(2) = UX(2)

C..... Energy transport(polymer solution)
        BBETA(3) = 0.0D0
        GAMA(3) = U(3) - U(4)

C..... Energy transport(glass plate)
        BBETA(4) = 1.0D0
        GAMA(4) = - (SUBLSC*TCONPS/(SOLLSC*TCONGL))*(UX(3)/V(1))
    ELSE
C      CALL DENSTY (T, NPDE, U, IFG, RHO)
C      CALL FLXHET (T, U, NPDE, NV, V, VDOT, RHOGA,
C $      FLUXG1, FLUXG2, HTRSFC, HV1, HV2, IFG)
C      FLUXG1 = GF1
C      FLUXG2 = GF2

C      IF(IFG .EQ. 99) THEN
C          IRES = 2
C          RETURN
C      ENDIF

C..... Set component densities (g/cm^3)
C      RH01 = 1.0
C      RH02 = 0.7857
C      RH03 = 1.31

C      Neglect gas density

```



```

C          UI1 = 0.0D0
C          UI2 = 0.0D0

C          CALL COEFFI(T, NPDE, U, UX, FF1, FF2, GG1, GG2, HH1, HH2, IFLAG)

C          DDIM1 = RHO*U(1)
C          DDIM2 = RHO*U(2)
C          RH13 = (1.0D0/RH01) - (1.0D0/RH03)
C          RH23 = (1.0D0/RH02) - (1.0D0/RH03)
C          DDIM11 = (RHOSC*SOLLSC**2)/(F1SC*TIMESC)
CCCCCCCCCCCCCCCCCCCCCCCCCCCCCCCCCCCCCCCCCCCCCCCCCCCCCCCC
C.....    Mass transport after local equilibrium at the top
C.....    Mass transport, component (1) (nonsolvent)
C          BBETA(1) = - (1.0D0 - RHO*U(1)*RH13)/V(1)
C          GAMA(1) = DDIM11*DDIM1*VDOT(1) + RHO*U(1)*RH23*(FF2*UX(1) +
GG2*UX(2))/V(1) - FLUXG1*(SOLLSC/F1SC)

C.....    Mass transport, component (2) (solvent)
C          BBETA(2) = - (1.0D0 - RHO*U(2)*RH23)/V(1)
C          GAMA(2) = DDIM11*DDIM2*VDOT(1) + RHO*U(2)*RH13*(FF1*UX(1) +
GG1*UX(2))/V(1) + FLUXG2*(SOLLSC/F1SC)

CCCCCCCCCCCCCCCCCCCCCCCCCCCCCCCCCCCCCCCCCCCCCCCCCCCCCCCC
          CALL FLXHET (T, U, NPDE, NV, V, VDOT, RHOGA,
$          FLUXG1, FLUXG2, HTRSFC, HV1, HV2, IFG)
          IF(IFG .EQ. 99) THEN
              PRINT *, 'IFG=99', FLUXG1, FLUXG2
              IRES = 2
              RETURN
          ENDIF

          DDIM1 = (FLX1SC*SOLLSC)/F1SC
C.....    Mass transport, component (1) (nonsolvent)
          BBETA(1) = 1.0D0
          GAMA(1) = (V(1)*DDIM1)*(- FLUXG1*((1.0D0/OMG1SC) - U(1))
$          + (FLX2SC/FLX1SC)*FLUXG2*U(1) )

          DDIM2 = (FLX1SC*SOLLSC)/G2SC
C.....    Mass transport, component (2) (solvent)
          BBETA(2) = 1.0D0
          GAMA(2) = (V(1)*DDIM2)*( FLUXG1*U(2)
$          - (FLX2SC/FLX1SC)*FLUXG2*((1.0D0/OMG2SC) - U(2)))
C.....    Change the boundary condition of the thermal equation for polymer
C          solution at the solution/air interface for isothermal runs.
C          The heat flux condition changes to constant temp condition.

C.....    Energy transport (polymer solution)
          IF(TISO .EQ. 'Y') THEN
              BBETA(3) = 0.0D0
              GAMA(3) = U(3) - TEMPIN/TEMPSC
          ELSE
              GRUP1 = SOLLSC*HTRSFC/TCONPS
              GRUP2 = EPSLON*SIGMA*SOLLSC*TEMPSC**3/TCONPS
              GRUP3 = FLX1SC*SOLLSC*HEATSC/(TEMPSC*TCONPS)

```

```

RATIO = TEMAMB/TEMPSC

BBETA(3) = 1.0D0
GAMA(3) = V(1)*( GRUP1*(RATIO-U(3)) +
$ GRUP2*(RATIO**4 - U(3)**4) - GRUP3*(
$ FLUXG1*HV1 + (FLX2SC/FLX1SC)*FLUXG2*HV2))
ENDIF

C..... Energy transport (glass plate)
        BBETA(4) = 1.0D0
        GAMA(4) = 0.0D0
        ENDIF
        RETURN
        END

C*****
C*          SUBROUTINE MONITR          *
C*    This subroutine handles the output after every time step.  *
C*****

SUBROUTINE MONITR (NEQ, T, Y, RR)
IMPLICIT DOUBLE PRECISION (A-H , O-Z)
IMPLICIT INTEGER (I-N)
DOUBLE PRECISION Y(NEQ), RR(NEQ),
$ DX(9000), TIME(9000), GFLX1(9000), GFLX2(9000)
DOUBLE PRECISION LAMBDA, PLYDEN(1000), SOLDEN(1000), NSLDEN(1000)
DOUBLE PRECISION US(1000,10), UU(2), NSLOS, NSOLNT, NSOLVM,
$ STOR(10), UNORML(1000,10)

DOUBLE PRECISION DOMG1D(NPTSM-1, 2), DOMG2D(NPTSM-1,2)

CHARACTER*1 TISO, BINRY
COMMON /CONST/ RH01, RH02, RH03, RH013, RH023, SV1, SV2
$ , SV3, WM1, WM2, WM3, WMAIR, V1, V2, V3, R, V12, V21
$ , V13, V23, ETA, LAMBDA, GAMMA, ALPHA, BETA, FUJD0
$ , FUJA, FUJB, G
C
COMMON /GLSPAR/ TCONGL, RHOGLS, CPGLS, SUBTHK, WPLATE, ALFSUB
COMMON /PLYPAR/ TCONPS, CPPS, EPSLON, SIGMA
COMMON /GASPAR/ TCONGS, VISGAS
COMMON /SCALES/ RHOSC, DIF1SC, DIF2SC, SOLLSC, SUBLSC, TIMESCS,
$ VELSC, TEMPSC, F1SC, F2SC, G1SC, G2SC, HEATSC, FLX1SC, FLX2SC
$ ,OMG1SC, OMG2SC
COMMON /INPUTS/ OMG1IN, OMG2IN, YK1, TEMPIN, TEMAMB
$ , FLMIN, GELTIM, PTOT
COMMON /CHARA/ TISO, BINRY
COMMON /BLK1/ RHOINT, C1MASI, C2MASI, C3MASI, DX, JCT,
$ KCT, AREA, NPTSM, NPDEM
COMMON /BLK2/ GF1, GF2
COMMON /DEVICE/ LCONC1, LCONC2, LRHO1, LRHO2, LLT, LDMU,
$ LMASS, LTEM, LSURFT, LSUB, LGEL, LWARN, LFLX
$ , LCONT, LCONB, LCONGR, LTEMGR, LCHMP1, LCHMP2, LDIF, LADV, LPEN,
LPENT
COMMON /FRCMOL/ YI1, YI2, YIA
COMMON /GRADS/ UX1LFT, UX1RHT, UX2LFT, UX2RHT, UTLFT, UTRHT

```

```

COMMON /GRDOMG/ GDU1(130,3), GDU2(130,3)
COMMON /DEVICE2/ LADVL

JSPIN = 0

C..... Separate the concentration and temperature solutions
DO 5 KL = 1, NPDEM
      DO 15 KM = 1, NPTSM
            US(KM,KL) = Y(NPDEM*(KM-1)+KL)
15      CONTINUE
5      CONTINUE

C..... Exit to main program if solution contains neg conc
DO 20 KL = 1, 2
      DO 22 KM = 1, NPTSM
            IF(US(KM,KL) .LT. 0.0D0) THEN
                  WRITE(LWARN,25) T*TIMESC, US(KM,KL)
                  IMON = -2
                  RETURN
            ENDIF
22      CONTINUE
20      CONTINUE
25      FORMAT(1X,' MONITR: Neg Conc at T(s) ', 2X, 2(F12.6,1X))

C.... Check to see whether the spinodal has been reached
IF(BINRY .EQ. 'N') THEN

      DO 35 NJ = 1, NPTSM
            STOR(1) = US(NJ,1)
            STOR(2) = US(NJ,2)
            IFLAG = 1
            CALL COEFFI(T, NPDEM, STOR, 0.0,
$           FF1, FF2, GG1, GG2, HH1, HH2, IFLAG)
            SPINOD = FF1*F1SC*GG2*G2SC - FF2*F2SC*GG1*G1SC
            IF(SPINOD .LT. 0.0D0) THEN
                  WRITE(LWARN,27) T*TIMESC, DX(NJ)*SOLLSC*Y(NEQ)
                  JSPIN = 1
            ENDIF
35      CONTINUE
      ENDIF
27      FORMAT(1X,' MONITR: Spinodal Is Reached at T(s) & Z(cm) '
$           (2X,F12.6,1X))

C..... Write out the values of time and L(t) and time Tsurf
REALT = T*TIMESC
XLT = Y(NEQ)*SOLLSC
WRITE(LLT,46) REALT, Y(NEQ)*SOLLSC, Y(NEQ)
WRITE(LSURFT,44) REALT, US(NPTSM,3)*TEMPSC-273.15, US(NPTSM,3)
WRITE(LSUB,45) REALT, US(NPTSM,4)*TEMPSC-273.15
44      FORMAT(3(F15.9,2X))
45      FORMAT(2(F15.9,2X))
46      FORMAT(3(F15.9,2X))

C..... Calculate and write out the component mass conc. gradients
C..... Convert the dimensionless mass frac grad to dimensional grad
GRADNS = (2.*US(NPTSM,1)*RH013 + US(NPTSM,2)*RH023 + RH03)*

```

```

$          (UX1RHT/XLT) + (US(NPTSM,1)*RH023*(UX2RHT/XLT) )
GRADSL = (US(NPTSM,2)*RH013*(UX1RHT/XLT)) + (US(NPTSM,1)*
$          RH013 + 2.*US(NPTSM,2)*RH023 + RH03)*(UX2RHT/XLT)
WRITE(LCONGR,1100)REALT, UX1RHT, UX2RHT, GRADNS, GRADSL
1100  FORMAT(1X,F9.4,3X,4(F14.11,2X))

C.....  Calculate and write out the component mass fraction gradients
C.....  Convert the dimensionless mass frac grad to dimensional grad
DO 2004 J=1, NPTSM-1
      DOMG1D(J,1) = GDU1(J,1)*XLT
      DOMG1D(J,2) = GDU1(J,2)/XLT
      DOMG2D(J,1) = GDU2(J,1)*XLT
      DOMG2D(J,2) = GDU2(J,2)/XLT
2004  CONTINUE

C....    Write out dimensional mass-average velocity
WRITE(LADV,2010) REALT, XLT
WRITE(LADV,2009) (GDU1(J,3), J=1, NPTSM-1)

2009  FORMAT(6(F19.8,1X))
2010  FORMAT("TIME(s) ",2(F15.9, 2X))

C.....  Write out location for mass-average velocity
WRITE(LADV,2016) REALT, XLT
WRITE(LADV,2017) (GDU1(J,1), J=1, NPTSM-1)

2017  FORMAT(6(F19.8,1X))
2016  FORMAT("TIME(s) ",2(F15.9, 2X))

C....    Write out pecllet number for mass transfer at near the top
WRITE(lpen,2111) REALT, GDU1(NPTSM-1,3)*XLT/1.0D-5, XLT
2111  FORMAT(3(F19.8,1X))

C....    Write out pecllet number for heat transfer at near the top
WRITE(25,2115) REALT, GDU1(NPTSM-1,3)*XLT/GDU2(NPTSM-1,3), XLT
2115  FORMAT(3(F19.8,1X))

C.....  Calculate and write out the surface temp grad
TGRADNT = UTRHT*TEMPSC/XLT
c       WRITE(LTEMGR,1110) REALT, UTRHT, TGRADNT
1110   FORMAT(1X,F9.4,3X,2(F20.10,3X))

      TIME(1) = 0.0D0
      GFLX1(1) = 0.0D0
      GFLX2(1) = 0.0D0
      TIME(KCT+2) = REALT
      GFLX1(KCT+2) = GF1*FLX1SC
      GFLX2(KCT+2) = GF2*FLX2SC

C.....  Write out the values of fluxes (g/(cm^2-s))
WRITE(LFLX, 57) REALT, GFLX1(KCT+2), GFLX2(KCT+2), YI1, YI2
57     FORMAT(5(E12.5,2X))

C....    Store the normalized and non-normalized concentrations
DO 37 NK = 1, NPTSM

```

```

        UNORML(NK,1) = US(NK,1)
        UNORML(NK,2) = US(NK,2)
        US(NK,1) = US(NK,1)*OMG1SC
        US(NK,2) = US(NK,2)*OMG2SC
37  CONTINUE

      IF (JCT*1 .EQ. KCT) THEN
        write(6,222) realt, us(nptsm,1), us(nptsm,2),
          $      us(nptsm,3)*tempsc-273.15
          $      , us(nptsm,4)*tempsc-273.15
222  format(5(f15.10,1x))

c    WRITE(LCONC1,250) realt, Y(NEQ)*SOLLSC
c    WRITE(LCONC1,200) (US(J,1), J=1, NPTSM)
c    WRITE(LCONC2,250) realt, Y(NEQ)*SOLLSC
c    WRITE(LCONC2,200) (US(J,2), J=1, NPTSM)
c    WRITE(LTEM,250) realt, Y(NEQ)*SOLLSC
c    WRITE(LTEM,201) (US(J,3)*TEMPSC-273.15, J=1, NPTSM)

200  FORMAT(6(F12.8,1X))
201  FORMAT(6(F10.4,2X))
250  FORMAT('TIME(s) ',2(F15.9, 2X))
208  FORMAT(1X,F14.10,1X,8(F7.5,1X))

C..... Integrate flux vs time to obtain amounts of non-solvent (NSLOS)
C      and solvent (SOLOS) evaporated.
      SOLVNT = 0.0D0
      NSOLNT = 0.0D0
      DO 30 L = 1, KCT+1
        NSOLNT = NSOLNT + (GFLX1(L+1) + GFLX1(L))*(TIME(L+1)-TIME(L))
30     SOLVNT = SOLVNT + (GFLX2(L+1) + GFLX2(L))*(TIME(L+1)-TIME(L))
        NSLOS = NSOLNT*0.5D0*AREA
        SOLOS = SOLVNT*0.5D0*AREA

C      PRINT *, 'NSLOS, SOLOS=', NSLOS, SOLOS
C..... Write out the initial component masses
      IF(KCT .EQ. 0) THEN
        WRITE(LMASS,400) C1MASI, C2MASI, C3MASI
400    FORMAT(' Intl masses of NS, S, and P ', 3X, 3(F15.10,2X))
      ENDIF

C..... Calculate the components spatial mass density
      DO 999 LJ = 1, NPTSM
C..... Note that the normalized concentrations are needed for DENSTY
        UU(1) = UNORML(LJ,1)
        UU(2) = UNORML(LJ,2)
        CALL DENSTY(T, 2, UU, IFG, RHO)
        NSLDEN(LJ) = RHO*US(LJ,1)*RHOSC
        SOLDEN(LJ) = RHO*US(LJ,2)*RHOSC
        PLYDEN(LJ) = RHO*( 1.0D0 - US(LJ,1) - US(LJ,2) ) *RHOSC
999    CONTINUE

C..... Locate the space position at which gelation has occurred
      DO 1000 LJ = 1, NPTSM
        IF(SOLDEN(LJ) .LE. GELTIM) THEN
          gelthk=Y(NEQ)*SOLLCS-DX(LJ)*Y(NEQ)*SOLLSC

```

```

C          WRITE(LGEL,1005) REALT, DX(LJ), DX(LJ)*Y(NEQ)*SOLLSC
          write(LGEL,1005) T, GELTHK/SOLLSC, REALT, GELTHK
          GO TO 1001
        ENDIF
1000      CONTINUE
1001      CONTINUE
C1005    FORMAT(3(F20.13,2X))
1005     FORMAT(4(F20.13,2X))

C.....   Integrate the polymer & acetone mass density vs distance
          SUMNS = 0.D0
          SUMSL = 0.D0
          SUMPL = 0.D0
          DO 10 L = 1 , NPTSM - 1
          SUMNS = SUMNS +
$         (NSLDEN(L+1)+NSLDEN(L))*(DX(L+1)-DX(L))*FLMIN*Y(NEQ)

          SUMSL = SUMSL +
$         (SOLDEN(L+1)+SOLDEN(L))*(DX(L+1)-DX(L))*FLMIN*Y(NEQ)

          SUMPL = SUMPL +
$         (PLYDEN(L+1)+PLYDEN(L))*(DX(L+1)-DX(L))*FLMIN*Y(NEQ)
10      CONTINUE

C.....   Calculate the component and total mass
          NSOLVM = AREA*SUMNS/2.D0
          SOLVTM = AREA*SUMSL/2.D0
          POLYMM = AREA*SUMPL/2.D0
          TOTMAS = NSOLVM + SOLVTM + C3MASI

          WRITE(LMASS,300) REALT, (NSOLVM+SOLVTM)/C3MASI, TOTMAS
300     FORMAT(2X, 2(F15.10,3X), F15.7)
          JCT = JCT + 1
          ENDIF
          KCT = KCT + 1

C.....   Stop the numerical computation if spinodal is reached
          IF(JSPIN .EQ. 1) IMON = -2

          RETURN
          END

```

```

C*****
C*          SUBROUTINE FLXHET          *
C*   In this subroutine the component fluxes in the gas phase,   *
C*   heat transfer coefficeint, and heat of vaporations for     *
C*   non-solvent and solvent are calculated.                    *
C*****

```

```

$          SUBROUTINE FLXHET (T, UU, N, NV, VV, VVT, RHOGA,
          FLUXG1, FLUXG2, HTRSFC, HV1, HV2, IFLAG)

```

```

PARAMETER (PI = 3.14159265359)

```

```

IMPLICIT DOUBLE PRECISION (A-H , O-Z)
IMPLICIT INTEGER (I-N)

```

```

DOUBLE PRECISION UU(N), VV(NV), VVT(NV), TCLOW(2,2),
$      TCHIGH(2,2), DFLUX(2), TFLUX(2), CORR(2,2)
DOUBLE PRECISION LAMBDA

double precision sum,DX2DZatZ0

CHARACTER*1 TISO, BINRY
COMMON /CONST/ RH01, RH02, RH03, RH013, RH023, SV1, SV2
$ , SV3, WM1, WM2, WM3, WMAIR, V1, V2, V3, R, V12, V21
$ , V13, V23, ETA, LAMBDA, GAMMA, ALPHA, BETA, FUJDO
$ , FUJA, FUJB, G

COMMON /GLSPAR/ TCONGL, RHOGLS, CPGLS, SUBTHK, WPLATE, ALFSUB
COMMON /PLYPAR/ TCONPS, CPPS, EPSLON, SIGMA
COMMON /GASPAR/ TCONGS, VISGAS
COMMON /SCALES/ RHOSC, DIF1SC, DIF2SC, SOLLSC, SUBLSC, TIMESC,
$ VELSC, TEMPSC, F1SC, F2SC, G1SC, G2SC, HEATSC, FLX1SC, FLX2SC
$ ,OMG1SC, OMG2SC
COMMON /INPUTS/ OMG1IN, OMG2IN, YK1, TEMPIN, TEMAMB
$ , FLMIN, GELTIM, PTOT
COMMON /CHARA/ TISO, BINRY
COMMON /DEVICE/ LCONC1, LCONC2, LRHO1, LRHO2, LLT, LDMU,
$      LMASS, LTEM, LSURFT, LSUB, LGEL, LWARN, LFLX
$      , LCONT, LCONB, LCONGR, LTEMGR, LCHMP1, LCHMP2, LDIF, LADV, LPEN,
LPENT
COMMON /FRCMOL/ YI1, YI2, YIA

IF(T .LE. 0.0D0) THEN
    FLUXG1 = 0.0D0
    FLUXG2 = 0.0D0
    HTLOWF = 0.0D0
    HV1 = 0.0D0
    HV2 = 0.0D0
    HTRSFC = HTLOWF
    RETURN
ENDIF

C..... The first section of this subroutine calculates the gas
C phase fluxes of water (1) and acetone (2) by the method
C outlined in the paper by Krishna and Standart
C AIChE J., Vol 22, P 383, 1976. The mass transfer coefficients are
C corrected using the film theory model. Note that in this paper the
C coordinate system is placed such that z=0 is the bulk of the gas and
C z=delta is the liquid/gas interface. Therefore, one should keep
C the coordinate orientation in mind when interpreting the direction
C of the component fluxes. In my system the coordinate system is
C in the opposite direction to that of the paper cited above.
C Therefore, by simply changing the sign on the final mass fluxes or
C by switching the interfacial and bulk values one obtains the fluxes
C corresponding to my coordinate system.

C..... The second part evaluates the heat transfer coefficient using the
C same correlation as in the mass transfer part and heat of
C vaporization of non-solvent and solvent.

C..... Note that the mass fluxes and heat of vaporizations are in

```

C dimensionless form. However, the heat transfer coefficient has
 C the units of J/(cm²-s-K).

C..... ***** MASS TRANSFER *****

C..... The variable ICOUNT is used to bypass the convergence criterion
 C first time through.
 ICOUNT = 0

C..... Evaluate the vapor pressure using the Antoine equation. The
 C coefficients are obtained from The Properties of Gases and Liquids.
 C The pressure is in mmHg and the temperature is in degrees Kelvin. Note
 C that the temperature UU(3) is dimensionless. The total pressure is
 C mmHg.

```
IF(TISO .EQ. 'Y') THEN
    PSAT1 = DEXP(18.3036 - (3816.44/(TEMPSC - 46.13)))
    PSAT2 = DEXP(16.6513 - (2940.46/(TEMPSC - 35.93)))
    TAVE = TEMPSC
ELSE
    PSAT1 = DEXP(18.3036 - (3816.44/(UU(3)*TEMPSC - 46.13)))
    PSAT2 = DEXP(16.6513 - (2940.46/(UU(3)*TEMPSC - 35.93)))
```

C..... Average temperature (K)
 TAVE = (TEMAMB + (TEMPSC*UU(3))) / 2.0
 ENDIF

```
IF(UU(3) .LT. 0.0D0) THEN
    PSAT1 = 0.0D0
    PSAT2 = 0.0D0
ENDIF
```

C..... Set the flag for the subroutine CHEMPT
 IF(BINRY .EQ. 'Y') THEN
 IFG = 0
 ELSE
 IFG = 1
 ENDIF

C..... Calculate the chemical potential divided by RT
 CALL CHEMPT(T, N, UU, IFG, DELCP1, DELCP2)

C..... Calculate the ternary gas phase mole fractions in equilibrium
 C with the polymer solution at interface.
 YI1 = DEXP(DELCP1)*PSAT1 / PTOT
 YI2 = DEXP(DELCP2)*PSAT2 / PTOT
 YIA = 1.0 - YI1 - YI2

C..... Convert the mole fractions to mass fractions
 DENOM = YI1*WM1 + YI2*WM2 + YIA*WMAIR
 OMG1GS = YI1*WM1/DENOM
 OMG2GS = YI2*WM2/DENOM
 OMGAGS = YIA*WMAIR/DENOM

C..... Ternary mole fractions of Water, Acetone, and Air in the bulk.
 C Water mole fraction(YK1) is a common variable in the common
 C block INPUTS and is based on the relative humidity.
 YK2 = 0.0

$YKA = 1.0 - YK1 - YK2$

C..... Set the moles of water at interface and in the bulk to zero in the
 C solvent/polymer binary limit.
 IF (BINRY .EQ. 'Y') THEN
 $YI1 = 0.0$
 $YK1 = 0.0$
 $YIA = 1.0 - YI1 - YI2$
 $YKA = 1.0 - YK1 - YK2$
 ENDIF

C..... Ternary average mole fractions for water, acetone, and air.
 $YAV1 = (YI1 + YK1) / 2.0$
 $YAV2 = (YI2 + YK2) / 2.0$
 $YAVA = (YIA + YKA) / 2.0$

C..... Calculate the molecular weight of the gas phase from weighted sum
 C of the individual molecular weights ($M_{gas} = \sum (YAV_i * M_i)$).
 $WMGAS = YAV1 * WM1 + YAV2 * WM2 + YAVA * WM_{AIR}$

C..... Convert the pressure to units of atmosphere
 $PATM = PTOT / 760.0$

C..... Using ideal gas law evaluate total gas mass density (g/cm^3)
 $RHOGAS = (PATM * WMGAS) / (82.05 * TAVE)$
 $CONGAS = RHOGAS / WMGAS$

C..... _____ BINARY SYSTEM (Acetone-Air (2A)) _____

C..... The mass transfer correlation should be for a denser gas
 C evaporating into a less dense gas.

C..... Binary interfacial concentration
 $Y2AB2I = YI2 / (YIA + YI2)$
 $Y2ABAI = YIA / (YIA + YI2)$

C..... Binary bulk cocentration
 $Y2AB2K = YK2 / (YKA + YK2)$
 $Y2ABAK = YKA / (YKA + YK2)$

C..... Binary average properties are used in the subsequent calculations.
 $WMG2A = ((Y2AB2I + Y2AB2K) * WM2 + (Y2ABAI + Y2ABAK) * WM_{AIR}) / 2.0$
 $RHOG2A = (PATM * WMG2A) / (82.05 * TAVE)$

C..... Values of viscosities($g/(cm \cdot s)$) are taken from Krantz et al (1986)
 C J Mem Sci V29, p11
 $VIS2A = (1.69D-04 + 1.66D-04) / 2.0$

C..... Since the gas phase is ideal, the concentration in the gas phase
 C for ternary case is the same as the binary pairs.
 $CONC2A = RHOG2A / WMG2A$

C..... The diffusion coefficient(cm^2/s) is calculated using Chapman-Enskog
 C relation and it is averaged at 5 and 25 C temperatures.
 $D2A = (0.10279 + 0.08989) / 2.0$

```

C..... The coefficient of concentration volume expansion is defined
C (for ideal gases) as;
C  $EXPN_{ij} = - (1/RHO_{ij}) * (P/RT) * (W_{Mi} - W_{Mj})$ . The negative sign is
C absorbed in the change in the concentrations in the Gr number.
C  $EXPN2A = (1.0/RHOG2A) * (PATM/(82.05 * TAVE)) * (WM2 - WMAIR)$ 

C..... The coefficient of thermal expansion in the case of ideal gases
C is equal to  $1/T$ .
C  $EXPNT = 1.0 / TAVE$ 

*****

C Don't need this for MCA model
C..... Binary (2A) Mass Transfer Coefficient
C The correlation given in by Singh(1960) for the case of heat
C transfer from a cooled plate facing upward is used
C  $(Nu1A = 0.816 (Gr Sc)^{0.20})$ .
C  $GR2A = EXPN2A * (Y2AB2I - Y2AB2K)$ 
C  $GRTEMP = EXPNT * (TEMAMB - UU(3) * TEMPSC)$ 

GRTOT = (WPLATE/2.)**3.0*(RHOG2A**2.0)*G*(GR2A+GRTEMP)
$ / (VIS2A)**2.0
SC2A = VIS2A / (RHOG2A*D2A)
IF(GRTOT .LT. 0.0) THEN
    GRTOT = - GRTOT
ENDIF

C..... Mass transfer coefficient at low flux (mole/(cm^2 s))
C  $TC2A = ((CONC2A * D2A / (WPLATE/2.)) * 0.816 * (GRTOT * SC2A))^{0.20}$ 
*****

C MTC for MCA model
C sum=0
C DO 714 countern=1,50
C 714 sum=sum+DEXP(-D2A*T*TIMESC*(countern*PI/0.1)**2)
C DX2DZatZ0=-(YI2/0.1)*(1+2*sum) ! should YI2
C TC2A = -CONC2A*D2A*DX2DZatZ0/YI2 ! should be /YI2
C write (*,*) "dx2dzatz0",DX2DZatZ0
C write (*,*) "TC2A",TC2A

C..... Obtain an estimate of the film thickness at low fluxes(cm).
C  $FLMST2 = CONC2A * D2A / TC2A$ 
C  $FLMEST = FLMST2$ 

c IF(GR2A*SC2A .LT. 3.0D05 .OR. GR2A*SC2A .GT. 1.0D10) THEN
c WRITE(LWARN,10) T*TIMESC, GR2A*SC2A
c ENDF
10 FORMAT('FLXHET: @ T(s) MTC not valid', 1X, F10.2, 2X, E12.5)

C..... _____BINARY SYSTEM (Water-Air (1A))_____

IF(BINRY .EQ. 'Y') THEN
Y1AB1I = 0.0
Y1AB1K = 0.0
Y1AB1A = 1.0
Y1AB1A = 1.0
ELSE

```

```

C..... Binary interfacial concentration
        Y1AB1I = YI1 / (YI1 + YIA)
        Y1ABAI = YIA / (YI1 + YIA)

C..... Binary bulk cocentration
        Y1AB1K = YK1 / (YK1 + YKA)
        Y1ABAK = YKA / (YK1 + YKA)
        ENDIF

        WMG1A = ((Y1AB1I+Y1AB1K)*WM1 + (Y1ABAI+Y1ABAK)*WMAIR) / 2.0
        RHOG1A = (PATM*WMG1A)/(82.05*TAVE)
        D1A = (0.21410 + 0.18674) / 2.0
        CONC1A = RHOG1A / WMG1A
        TC1A = CONC1A*D1A/FLMST2

C..... _____BINARY SYSTEM (Water-Acetone (12))_____

C..... Binary interfacial concentration
        IF(BINRY .EQ. 'Y') THEN
        Y12B1I = 0.0
        Y12B1K = 0.0
        Y12B2I = 1.0
        Y12B2K = 1.0
        ELSE
        Y12B1I = YI1 / (YI1 + YI2)
        Y12B2I = YI2 / (YI1 + YI2)

C..... Binary bulk cocentration
        Y12B1K = YK1 / (YK1 + YK2)
        Y12B2K = YK2 / (YK1 + YK2)
        ENDIF

        WMG12 = ((Y12B1I+Y12B1K)*WM1 + (Y12B2I+Y12B2K)*WM2) / 2.0
        RHOG12 = (PATM*WMG12)/(82.05*TAVE)
        D12 = (0.08937 + 0.07772) / 2.0
        CONC12 = RHOG12 / WMG12
        TC12 = CONC12*D12/FLMEST

c      print*, 'tc2a, tc1a, tc12', tc2a, tc1a, tc12
      JCONVG = 1
2010  CONTINUE
C..... Calculate zero flux M. T. C. at bulk gas phase conditions using
C      zero flux binary M. T. C.
      S = YK1*TC2A + YK2*TC1A + YKA*TC12
      TCLOW(1,1) = TC1A*(YK1*TC2A + (1.0-YK1)*TC12)/S
      TCLOW(1,2) = YK1*TC2A*(TC1A-TC12)/S
      TCLOW(2,1) = YK2*TC1A*(TC2A-TC12)/S
      TCLOW(2,2) = TC2A*(YK2*TC1A + (1.0-YK2)*TC12)/S

C..... As an initial guess assume the MTCs at low fluxes are the same at
C      high fluxes (or the correction matrix is identity).
      TCHIGH(1,1) = TCLOW(1,1)
      TCHIGH(1,2) = TCLOW(1,2)
      TCHIGH(2,1) = TCLOW(2,1)
      TCHIGH(2,2) = TCLOW(2,2)

```

```

C..... Flux evaluation (DFLUX and TFLUX represent the diffusional
C      and total fluxes).
3020  DFLUX(1) = TCHIGH(1,1)*(YK1-YI1) + TCHIGH(1,2)*(YK2-YI2)
      DFLUX(2) = TCHIGH(2,1)*(YK1-YI1) + TCHIGH(2,2)*(YK2-YI2)

C..... In total flux calculation the bulk concentration is used by Krishan
C      and Standart. Why bulk properties? I think interfacial properties
C      should be used.
c      TFLUX(1) = (DFLUX(1) + DFLUX(2)*(YK1/(1.0-YK2)))*
c $      ((1.0-YK2)/(1.0-YK1-YK2))
c      TFLUX(2) = (DFLUX(2) + DFLUX(1)*(YK2/(1.0-YK1)))*
c $      ((1.0-YK1)/(1.0-YK1-YK2))

      TFLUX(1) = (DFLUX(1) + DFLUX(2)*(YI1/(1.0-YI2)))*
$      ((1.0-YI2)/(1.0-YI1-YI2))
      TFLUX(2) = (DFLUX(2) + DFLUX(1)*(YI2/(1.0-YI1)))*
$      ((1.0-YI1)/(1.0-YI1-YI2))

      IF (ICOUNT.EQ.0) THEN
      TOLD1 = TFLUX(1)
      TOLD2 = TFLUX(2)
      ICOUNT = 1
      GO TO 3010
      ELSE
      IF (BINRY .EQ. 'Y') THEN
          IF (ABS((TFLUX(2)-TOLD2)/TFLUX(2)).LT.1.D-03) THEN
              GO TO 3000
          ELSE
              TOLD2 = TFLUX(2)
              JCONVG = JCONVG + 1
              GO TO 3010
          ENDIF
      ELSE
          IF (ABS((TFLUX(1)-TOLD1)/TFLUX(1)).LT.1.D-03.AND.
$      ABS((TFLUX(2)-TOLD2)/TFLUX(2)).LT.1.D-03) THEN
              GO TO 3000
          ELSE
              TOLD1 = TFLUX(1)
              TOLD2 = TFLUX(2)
              JCONVG = JCONVG + 1
              GO TO 3010
          ENDIF
      ENDIF
      ENDIF
      ENDIF

C..... Calculate the correction matrix.
3010  PH1  = (TFLUX(1)/TC1A) + (TFLUX(2)/TC2A)
      PH2  = (TFLUX(1) + TFLUX(2))/TC12
      EH1  = PH1 / (DEXP(PH1) - 1.0)
      EH2  = PH2 / (DEXP(PH2) - 1.0)
      PH12 = - TFLUX(1) * ((1./TC12) - (1./TC1A))
      PH21 = - TFLUX(2) * ((1./TC12) - (1./TC2A))
      CORR(1,1) = (EH1*PH12 + EH2*PH21) / (PH1 - PH2)
      CORR(1,2) = (EH1 - EH2)*PH12 / (PH1 - PH2)
      CORR(2,1) = (EH1 - EH2)*PH21 / (PH1 - PH2)

```

```

CORR(2,2) = (EH1*PH21 + EH2*PH12) / (PH1 - PH2)
CCCCCCCCCCCCCCCCCCCCCCCCCCCCCCCC

C..... Obtain new estimate of MTC at high flux
TCHIGH(1,1) = TCLOW(1,1)*CORR(1,1) + TCLOW(1,2)*CORR(2,1)
TCHIGH(1,2) = TCLOW(1,1)*CORR(1,2) + TCLOW(1,2)*CORR(2,2)
TCHIGH(2,1) = TCLOW(2,1)*CORR(1,1) + TCLOW(2,2)*CORR(2,1)
TCHIGH(2,2) = TCLOW(2,1)*CORR(1,2) + TCLOW(2,2)*CORR(2,2)
c WRITE(6,313) tchigh(1,1),tchigh(1,2),tchigh(2,1),tchigh(2,2)

C..... Terminate the program if more than 5000 steps needed to
C converge on fluxes
IF(JCONVG .GT. 5000) THEN
WRITE(LWARN,413) T*TIMESC
RETURN
ENDIF
413 FORMAT('FLXHET: Too many steps at T(s) ', 1X, F12.6)

GO TO 3020
313 FORMAT(1X, 4(E12.5, 2X))

C..... Convert molar fluxes to mass fluxes (change the signs) and
C nondimensionlize.
3000 FLUXG1 = - (TFLUX(1) * WM1) / FLX1SC
FLUXG2 = - (TFLUX(2) * WM2) / FLX2SC
C 3000 FLUXG1 = - (TFLUX(1) * WM1)
C FLUXG2 = - (TFLUX(2) * WM2)
IF(FLUXG1.LT.0.0.OR.GFLUXG2.LT.0.0) THEN
WRITE(LWARN,414) T*TIMESC, FLUXG1, FLUXG2
PRINT*,' MOLE FRAC INT & BLK',Y11,Y12,Y1A,YK1,YK2,YKA
C..... Abort the execution
write (*,*) "about to set IFLAG = 99"
IFLAG = 99
RETURN
ENDIF
414 FORMAT('FLXHET: Neg Gas Flux @ T(s)',2X,F12.6,1X,2(F12.7,1X))

IF(TISO .EQ. 'Y') THEN
HV1 = 0.0D0
HV2 = 0.0D0
HTRSFC = 0.0D0
RETURN
ENDIF

C..... ***** HEAT TRANSFER ***** .....

C..... Calculate the latent heat of vaporization as a function of T.
C The Pitzer Acentric-Factor equation given on pages
C 199-200 of "The properties of gases and liquids" by Reid,
C Prauznitz, and Sherwood is used for the acetone. The correlation
C on page 210 is used for the water. The validity of these
C correlation should be verified using experimental data. The
C correlations compare very well to the experimental
C data(see notes 7/24/91).

C..... Set critical tem (K) and acentric factors for water and acetone.

```

```

CRITC1 = 647.3
CRITC2 = 508.1
ACENT1 = 0.344
ACENT2 = 0.309

C..... Calculate reduced temperature. Note that UU(3) is dimensionless.
TRDUC1 = UU(3)*TEMPSC/CRITC1
TRDUC2 = UU(3)*TEMPSC/CRITC2
IF(TRDUC1 .GT. 1.0D0) TRDUC1 = 1.0D0
IF(TRDUC2 .GT. 1.0D0) TRDUC2 = 1.0D0

IF(BINRY .EQ. 'Y') THEN
HV1 = 0.0D0
HV2 = (R*CRITC2/(WM2*HEATSC))*(7.08*(1.0-TRDUC2)**0.354 +
$ 10.95*ACENT2*(1.0-TRDUC2)**0.456)
ELSE
HV1 = (2501.7/HEATSC)*
$ ((1.-(273.16/CRITC1))/(1.-TRDUC1))**0.378
HV2 = (R*CRITC2/(WM2*HEATSC))*(7.08*(1.0-TRDUC2)**0.354 +
$ 10.95*ACENT2*(1.0-TRDUC2)**0.456)
ENDIF

C..... Use the same correlation to evaluate heat transfer coefficient
C at low mass fluxes as the one used for the mass
C transfer(Singh, 1960)

C..... Heat capacity of water, acetone, air, and the ideal gas mixture
C (j/(mole-c)) with temperature in degrees C.
TAVEC = TAVE - 273.15
CP1GAS = 33.46 + 0.688D-02*TAVEC + 0.7604D-05*(TAVEC*TAVEC)
$ - 3.593D-09*(TAVEC*TAVEC*TAVEC)
CP2GAS = 71.96 + 20.1D-02*TAVEC - 12.78D-05*(TAVEC*TAVEC)
$ + 34.76D-09*(TAVEC*TAVEC*TAVEC)
CPAGAS = 28.94 + 0.4147D-02*TAVEC + 0.3191D-05*(TAVEC*TAVEC)
$ - 1.965D-09*(TAVEC*TAVEC*TAVEC)

C..... Mixture heat capacity (ideal mixing, since ideal gas is assumed)
CPGAS = CP1GAS*YAV1 + CP2GAS*YAV2 + CPAGAS*YAVA

C..... Heat capacity of binary solvent/polymer
CPGASB = (CP2GAS*(Y2AB2I+Y2AB2K) + CPAGAS*(Y2ABAI+Y2ABAK))*0.5

C..... Calculate the binary(solvent-air) heat transfer coefficient
C at low fluxes
c IF(UU(3)*TEMPSC.EQ.TEMAMB)THEN
c GRTEMP = ((WPLATE/2.):**3.0)*(RHOGAS**2.0)*G*EXPNT*
c $ (1.0D-06) / (VISGAS**2.0)
c ELSE
c GRTEMP = ((WPLATE/2.):**3.0)*(RHOGAS**2.0)*G*EXPNT*
c $ (TEMAMB - (UU(3)*TEMPSC)) / (VISGAS**2.0)
c ENDIF
c IF(GRTEMP .LT. 0.0D0) GRTEMP = -GRTEMP
c PRTEMP = CPGASB*VISGAS/TCONGS
c PRTEMP = CPGAS*VISGAS/TCONGS

```

c FACTOR OF TWO ERROR IN HEAT TRANSFER COEFF. IS HERE!!!!!! MP 6/29/99

$$HTLOWF = (TCONGS/(WPLATE/2.))*0.816*(GRTOT*PRTEMP)**0.20$$

C HTLOWF = (TCONGS/(WPLATE))*0.816*(GRTOT*PRTEMP)**0.20

*** Bottom line (with CC) is correct, but don't want this for MCA.

*** For MCA want:

C HTLOWF=TC2A*TCONGS/(CONC2A*D2A)

C..... High flux correction to the heat transfer coefficient

C using the film theory. B. S. L. page 661 equation 21.5-29.

C..... Note the signs on the fluxes are changed.

$$\begin{aligned} \text{HTRSFC} &= (-\text{TFLUX}(1)*\text{CP1GAS} - \text{TFLUX}(2)*\text{CP2GAS}) / \\ \$ &(\text{DEXP}((-\text{TFLUX}(1)*\text{CP1GAS} - \text{TFLUX}(2)*\text{CP2GAS})/\text{HTLOWF}) - 1.\text{D0}) \end{aligned}$$

c print*, 'htrsfc, htlowf', htrsfc, htlowf

RETURN

END

C*****

C* SUBROUTINE CONSTS *

C* This subroutine is called to initialize the constants which *

C* are specific to the system. *

C*****

SUBROUTINE CONSTS

IMPLICIT DOUBLE PRECISION (A-H, O-Z)

IMPLICIT INTEGER (I-N)

DOUBLE PRECISION LAMBDA, DX(9000)

CHARACTER*1 TISO, BINRY

COMMON /CONST/ RH01, RH02, RH03, RH013, RH023, SV1, SV2

\$, SV3, WM1, WM2, WM3, WMAIR, V1, V2, V3, R, V12, V21

\$, V13, V23, ETA, LAMBDA, GAMMA, ALPHA, BETA, FUJD0

\$, FUJA, FUJB, G

COMMON /GLSPAR/ TCONGL, RHOGLS, CPGLS, SUBTHK, WPLATE, ALFSUB

COMMON /PLYPAR/ TCONPS, CPPS, EPSLON, SIGMA

COMMON /GASPAR/ TCONGS, VISGAS

COMMON /SCALES/ RHOSC, DIF1SC, DIF2SC, SOLLSC, SUBLSC, TIMESC,

\$ VELSC, TEMPSC, F1SC, F2SC, G1SC, G2SC, HEATSC, FLX1SC, FLX2SC

\$, OMG1SC, OMG2SC

COMMON /INPUTS/ OMG1IN, OMG2IN, YK1, TEMPIN, TEMAMB

\$, FLMIN, GELTIM, PTOT

COMMON /CHARA/ TISO, BINRY

COMMON /BLK1/ RHOINT, C1MASI, C2MASI, C3MASI, DX, JCT,

\$ KCT, AREA, NPTSM, NPDEM

COMMON /DEVICE/ LCONC1, LCONC2, LRHO1, LRHO2, LLT, LDMU,

\$ LMASS, LTEM, LSURFT, LSUB, LGEL, LWARN, LFLX

\$, LCONT, LCONB, LCONGR, LTEMGR, LCHMP1, LCHMP2, LDIF, LADV, LPEN,

LPENT

C..... Set component densities (g/cm^3)

RH01 = 1.0

RH02 = 0.7857

RH03 = 1.31

RH013 = RH01 - RH03

RH023 = RH02 - RH03

C..... Calculate the specific volumes (cm³/g)
SV1 = 1.0/RH01
SV2 = 1.0/RH02
SV3 = 1.0/RH03

C..... Molecular weights (g/mole)
WM1 = 18.0
WM2 = 58.08
WM3 = 40000.0
WMAIR = 29.0

V1 = SV1*WM1
V2 = SV2*WM2
V3 = SV3*WM3
R = 8.314
G = 980.0
SIGMA = 5.67D-12

C..... Calculate pure molar volume ratios
V12 = V1/V2
V21 = V2/V1
V13 = V1/V3
V23 = V2/V3

C..... Calculate ratios of pure molar volumes to molecular weights
ETA = V1/WM1
LAMBDA = V2/WM2
GAMMA = V3/WM3
ALPHA = ETA - GAMMA
BETA = LAMBDA - GAMMA

C..... Set parameters in Fujita's expression
FUJD0 = 7.70133D-17
FUJA = 3.35087D-02
FUJB = 3.37608D-03

C..... Set parameters specific to the support
TCONGL = 0.23D-02
RHOGLS = 1.41
CPGLS = 1.7

C..... Calculate the thermal diffusivity of the glass support
ALFSUB = TCONGL/(RHOGLS*CPGLS)
WPLATE = 2.0 * 2.54
AREA = WPLATE**2.0

C..... Set parameters specific to the polymer solution
C The following values were taken from Tantekin's thesis for
C binary solution (CA/ACET). Values for ternary must be obtained.
TCONPS = 0.2d-02
CPPS = 2.5
EPSLON = 0.81


```

C..... Set parameters specific to the gas phase
C      The following values are for pure air averaged over 280 and 300 K
      TCONGS = 2.5456d-04
      VISGAS = 1.7984D-04

C..... Set the scaling values
      RHOGIN = 1.0D0*WMAIR/(82.0*TEMPIN)
*      RHOSC = (RH01 + RH02 + RH03)/3.0D0
      RHOSC = 1.0D0
      DIF1SC = 1.0D-06
      DIF2SC = DIF1SC
      SOLLSC = FLMIN
      SUBLSC = SUBTHK
c      FLX1SC = 0.5*RHOGIN
      XK01A = 3.0D-05
      XH0 = 2.0D-03
      FLX1SC = WM1*XK01A
      FLX2SC = FLX1SC
      TIMESC = SOLLSC*RHOSC/FLX2SC
      TEMPSC = TEMPIN
      F1SC = RHOSC*DIF1SC
      G2SC = RHOSC*DIF2SC
      F2SC = F1SC
      G1SC = G2SC
c      OMG1SC = OMG1IN
c      OMG2SC = OMG2IN
      OMG1SC = 1.0
      OMG2SC = 1.0

C..... Scale factor for the heat of vaporization is the heat of
C      vaporization of acetone at 25 C (J/g).
      HEATSC = 550.0

C..... Calculate the constant dimensionless groups
      P3DMLS = WM2/WM1
      P4DMLS = OMG1IN
      P5DMLS = OMG2IN
      Q2DMLS = TEMAMB/TEMPIN
      Q8DMLS = SUBTHK/FLMIN
      Q9DMLS = TCONPS/TCONGL
      R1DMLS = (TEMAMB**3*SIGMA*EPSLON*SUBTHK)/TCONPS
      R2DMLS = TCONPS/(RHOSC*CPPS*DIF1SC)
      R3DMLS = (CPPS*TEMAMB)/HEATSC
      R4DMLS = ALFSUB/DIF1SC
      R5DMLS = (XK01A*WM1*SUBTHK*CPPS)/TCONPS
      R6DMLS = (SUBTHK*XH0)/TCONPS
      R7DMLS = WPLATE/(SUBTHK*2.0)
      WRITE(LLT,101)
      WRITE(LLT,*) P3DMLS, P4DMLS, P5DMLS, Q2DMLS, Q8DMLS,
$           Q9DMLS, R1DMLS, R2DMLS, R3DMLS, R4DMLS, R5DMLS,
$           R6DMLS, R7DMLS
101  FORMAT(1X,'P3, P4, P5, P5, Q2, Q8, Q9, R1, R2, R3,
$       R4, R5, R6, R7')
      RETURN
      END

C*****

```

```

C*          SUBROUTINE COEFFI          *
C*      This subroutine is used to calculate the coefficients of the *
C*      pde. These are f1, f2, g1, g2, h1, and h2.          *
C*****
      SUBROUTINE COEFFI(T, N, UV, UVX, F1, F2, G1, G2, H1, H2, IFLAG)
      IMPLICIT DOUBLE PRECISION (A-H, O-Z)
      IMPLICIT INTEGER (I-N)
      DOUBLE PRECISION UV(N), UVX(N), LAMBDA

      CHARACTER*1 TISO, BINRY
      COMMON /CONST/ RH01, RH02, RH03, RH013, RH023, SV1, SV2
$ , SV3, WM1, WM2, WM3, WMAIR, V1, V2, V3, R, V12, V21
$ , V13, V23, ETA, LAMBDA, GAMMA, ALPHA, BETA, FUJDO
$ , FUJA, FUJB, G
      COMMON /GLSPAR/ TCONGL, RHOGLS, CPGLS, SUBTHK, WPLATE, ALFSUB
      COMMON /PLYPAR/ TCONPS, CPPS, EPSLON, SIGMA
      COMMON /GASPAR/ TCONGS, VISGAS
      COMMON /SCALES/ RHOSC, DIF1SC, DIF2SC, SOLLSC, SUBLSC, TIMESCS,
$ VELSC, TEMPSC, F1SC, F2SC, G1SC, G2SC, HEATSC, FLX1SC, FLX2SC
$ ,OMG1SC, OMG2SC
      COMMON /INPUTS/ OMG1IN, OMG2IN, YK1, TEMPIN, TEMAMB
$ , FLMIN, GELTIM, PTOT
      COMMON /CHARA/ TISO, BINRY

      OMG1 = UV(1)*OMG1SC
      OMG2 = UV(2)*OMG2SC
      OMG3 = 1.D0 - OMG1 - OMG2

C..... Calculate the volume fractions from mass fractions
      DUMMY = ALPHA*OMG1 + BETA*OMG2 + GAMMA
      PHI1 = ETA*OMG1/DUMMY
      PHI2 = LAMBDA*OMG2/DUMMY
      PHI3 = GAMMA*(1.0-OMG1-OMG2)/DUMMY

C..... Calculate binary 12 volume fractions from ternary volume fractions
      U1 = PHI1/(PHI1+PHI2)
      U2 = PHI2/(PHI1+PHI2)

      ABODON = GAMMA + ALPHA*OMG1 + BETA*OMG2

C..... Calculate derivatives of ternary volume frac w.r.t. mass frac.
      DP1O1 = -(ALPHA*ETA*OMG1/(ABODON)**2)
$ + ETA/(ABODON)
      DP1O2 = -(BETA*ETA*OMG1/(ABODON)**2)
      DP2O1 = -(ALPHA*LAMBDA*OMG2/(ABODON)**2)
      DP2O2 = -(BETA*LAMBDA*OMG2/(ABODON)**2)
$ + LAMBDA/(ABODON)
      DP3O1 = -(ALPHA*GAMMA*(1. - OMG1 - OMG2)/(ABODON)**2)
$ - GAMMA/(ABODON)
      DP3O2 = -(BETA*GAMMA*(1. - OMG1 - OMG2)/(ABODON)**2)
$ - GAMMA/(ABODON)

C..... Sum of the derivatives w.r.t. mass fractions is zero
      SUMO1 = DP1O1 + DP2O1 + DP3O1
      SUMO2 = DP1O2 + DP2O2 + DP3O2

```

C..... Begin calculation of the friction coefficients.

C..... Calculate the binary(2,3) density (solvent/polymer) using
C the following equation of state;
C
$$RHOB23 = OM23B2 * RH02 + OM23B3 * RH03.$$
C Note that the binary mass fractions are expressed in terms of
C ternary mass fractions.
C
$$RHOB23 = ((OMG2 * RH023) / (1.0 - OMG1)) + RH03$$
C
$$RHOB23 = 1.0D0 / ((OMG2 / (1.0D0 - OMG1)) * (1.0D0 / RH02 - 1.0D0 / RH03)) + 1.0D0 / RH03)$$
C..... Calculate the self diffusion coefficients from Fujita's experssion.
C The binary volume fractions are evaluated in terms of ternary
C volume fractions.
C
$$D2STAR = FUJD0 * DEXP(PHI2 / (FUJA * PHI2 + FUJB * (1. - PHI1)))$$
C..... Calculate the friction coefficients XIij. Note that the
C friction coefficients are evaluate without the RT part.
C That is, the actual friction coefficient exi12 is equal
C to variable XI12 * RT. This is because the RTs cancel when the
C friction coefficients are multiplied by the gradients of chemical
C potentials divided by friction coefficients squared.
C
$$XI12 = V2 / 5.03D - 05$$
C
$$XI23 = (((2.0 * (OMG2 / (1. - OMG1)) * RH023) + RH03) * WM3)$$
C
$$/ (D2STAR * (RHOB23 ** 2.0))$$
C \$
c
$$XI13 = 0.25 * V12 * XI23$$
C
$$XI13 = 2.05D - 08 * V12 * XI23$$
C..... Calculate various parts of Fi, Gi, and Hi.
C
$$PRT1 = XI12 * XI13 * OMG1 / (WM1 * WM3)$$
C
$$PRT2 = XI12 * XI23 * OMG2 / (WM2 * WM3)$$
C
$$PRT3 = XI13 * XI23 * OMG3 / (WM3 * WM3)$$
C
$$THETA = PRT1 + PRT2 + PRT3$$
C
$$AA = (XI12 * OMG2 / WM2) + (XI13 * (1.0D0 - OMG2) / WM3)$$
C
$$BB = (XI12 * OMG2 / WM2) - (XI13 * OMG2 / WM3)$$
C
$$CC = (XI12 * OMG1 / WM1) + (XI23 * (1.0D0 - OMG1) / WM3)$$
C
$$DD = (XI12 * OMG1 / WM1) - (XI23 * OMG1 / WM3)$$
C..... Note that the functions H1 and H2 reduce to -OMG1 and
C -OMG2, respectively. However, these functions will be
C calculated using the long experssions in order to check the
C friction coefficient functions.
C
$$H1 = -(OMG1 / (WM3 * THETA)) * (CC * XI13 + BB * XI23)$$
C
$$H2 = -(OMG2 / (WM3 * THETA)) * (DD * XI13 + AA * XI23)$$
c
$$IFLAG = 1$$
C
$$CALL FHINTP(T, U1, U2, PHI1, PHI2, PHI3, G12, G23, G13,$$
C \$
$$DG12, DG23, DG13, DDG12, DDG23, DDG13, IFLAG)$$
C..... Calculate the components needed for gradient of chemical potential
C That is, Q1, Q2, Q3, S1, S2, and S3.
C
$$Q1 = (1.0 / PHI1) - 1.0 + ((PHI1 - (2.0 * U2)) * (U2 ** 2.0) * DG12)$$
C \$
$$+ (U1 * (U2 ** 3.0) * DDG12) - ((PHI3 ** 2.0) * DG13)$$
C
$$Q2 = -V12 + (G12 * ((2.0 * PHI2) + PHI3)) + (G13 - (V12 * G23)) * PHI3 +$$
C \$
$$(U1 * U2 * ((2.0 * U2) - PHI1 - 1.0) * DG12) - ((U1 ** 2.0) * (U2 ** 2.0)$$
C \$
$$* DDG12) - (V12 * (PHI3 ** 2.0) * DG23)$$
C
$$Q3 = -V13 + (G13 * (2.0 * PHI3 + PHI2)) + (PHI2 * (G12 - (V12 * G23))) -$$

```

$ (3.0*V12*PHI2*PHI3*DG23)+((1.0-3.0*PHI1)*PHI3*DG13)-
$ (V12*PHI2*(PHI3**2.0)*DDG23)-(PHI1*(PHI3**2.0)*DDG13)

S1 = -V21 +(PHI3*(G23-(V21*G13)))+(V21*G12*(2.0*PHI1+PHI3))
$ +(V21*U1*U2*(1.0+PHI2-(2.0*U1))*DG12)-((U1**2.0)*
$ (U2**2.0)*V21*DDG12)-(PHI3**2.0)*V21*DG13)
S2 = (1.0/PHI2) -1.0+((U1**3.0)*U2*V21*DDG12)+((U1**2.0)
$ *V21*(2.0*U1-PHI2)*DG12)-(PHI3**2.0)*DG23)
S3 = -V23+(V21*PHI1*(G12-G13))+(G23*(2.0*PHI3+PHI1))+
$ ((1.0-3.0*PHI2)*PHI3*DG23)-(PHI2*(PHI3**2.0)*DDG23)
$ -(PHI1*(PHI3**2)*V21*DDG13)-(3.0*V21*PHI1*PHI3*DG13)

```

```

C..... Assemble the gradient of chemical potentials w.r.t. mass frac
C Note! Here again the gradients will be evaluated without the
C RT part, just as in the friction coefficient evaluation.
DM1O1 = Q1*DP1O1 + Q2*DP2O1 + Q3*DP3O1
DM1O2 = Q1*DP1O2 + Q2*DP2O2 + Q3*DP3O2
DM2O1 = S1*DP1O1 + S2*DP2O1 + S3*DP3O1
DM2O2 = S1*DP1O2 + S2*DP2O2 + S3*DP3O2

```

```

C..... Write out the gradients of chem pot w.r.t. omegas
IF(IFLAG.EQ. 9999) THEN
F1 = DM1O1
F2 = DM1O2
G1 = DM2O1
G2 = DM2O2
RETURN
ENDIF

```

```

C..... Calculate the functions F1, G1, H1, F2, G2, and H2.
C The functions F1, F2, G1, and G2 are dimensionless.
F1 = -(OMG1/THETA)*(CC*DM1O1 + BB*DM2O1) / F1SC
F2 = -(OMG2/THETA)*(DD*DM1O1 + AA*DM2O1) / F2SC
G1 = -(OMG1/THETA)*(CC*DM1O2 + BB*DM2O2) / G1SC
G2 = -(OMG2/THETA)*(DD*DM1O2 + AA*DM2O2) / G2SC

```

```

C..... For the limiting case of binary
IF(BINRY.EQ. 'Y') THEN
F2 = 1.0D0
G1 = 0.0D0
H1 = 0.0D0
ENDIF

RETURN
END

```

```

C*****
C* SUBROUTINE FHINTP *
C* This subroutine is used to calculate the Flory-Huggins *
C* interactions parameters and their various derivatives. *
C*****

```

```

SUBROUTINE FHINTP(T, U1, U2, PHI1, PHI2, PHI3, G12, G23, G13,
$ DG12, DG23, DG13, DDG12, DDG23, DDG13, IFLAG)
IMPLICIT DOUBLE PRECISION (A-H, O-Z)
IMPLICIT INTEGER (I-N)

```

```

IF(IFLAG .EQ. 0) THEN

C..... Binary (polymer/solvent) system
C..... Calculate Flory-Huggins (F-H) interaction parameter
          G23 = 0.535 + 0.11*PHI3
          G12 = 0.0
          G13 = 0.0

C..... Calculate the first derivatives of G23 w.r.t. PHI2 (Appdx G2
C equation 10)
          DG23 = - 0.11
          DG12 = 0.0
          DG13 = 0.0

C..... Calculate the second derivatives of G23 w.r.t. PHI2
          DDG23 = 0.0
          DDG12 = 0.0
          DDG13 = 0.0

ELSE
C..... Ternary (polymer/solent/nonsolvent) system
          G12 = 0.661 + (0.417/(1.0-(U2*0.755)))
          G23 = 0.535 + 0.11*PHI3
          G13 = 1.4

          DG12 = 0.417*0.755/((1.0 - U2*0.755)**2.0)
          DG23 = 0.11
          DG13 = 0.0

          DDG12 = (2.0*0.755/(1.0 - U2*0.755))*DG12
          DDG23 = 0.0
          DDG13 = 0.0

ENDIF
RETURN
END

C*****
C*                SUBROUTINE CHEMPT                *
C* This subroutine is used to calculate the change in chemical *
C potential divided by RT.                            *
C*****

SUBROUTINE CHEMPT(T, N, UV, IFG, DELCP1, DELCP2)
IMPLICIT DOUBLE PRECISION (A-H , O-Z)
IMPLICIT INTEGER (I-N)
DOUBLE PRECISION UV(N)
DOUBLE PRECISION LAMBDA

COMMON /CONST/ RH01, RH02, RH03, RH013, RH023, SV1, SV2
$ , SV3, WM1, WM2, WM3, WMAIR, V1, V2, V3, R, V12, V21
$ , V13, V23, ETA, LAMBDA, GAMMA, ALPHA, BETA, FUJDO
$ , FUJA, FUJB, G
COMMON /SCALES/ RHOSC, DIF1SC, DIF2SC, SOLLSC, SUBLSC, TIMESCS,
$ VELSC, TEMPSC, F1SC, F2SC, G1SC, G2SC, HEATSC, FLX1SC, FLX2SC
$ ,OMG1SC, OMG2SC

```

C..... It is necessary to evaluate the activity coefficient times mole
C fraction of acetone and water for use in subroutine FLXHET. The
C activity coefficient multiplied by mole fraction for each component
C is given by: (Act Coef i)*Xi = DEXP(del chem pot/RT).
C The change in chemical potential divided by RT is evaluated in this
C subroutine.

OMG1 = UV(1)*OMG1SC
OMG2 = UV(2)*OMG2SC
OMG3 = 1.D0 - OMG1 - OMG2

C..... Calculate the volume fractions using mass fractions
DUMMY = ALPHA*OMG1 + BETA*OMG2 + GAMMA
PHI1 = ETA*OMG1/DUMMY
PHI2 = LAMBDA*OMG2/DUMMY
PHI3 = GAMMA*(1.0-OMG1-OMG2)/DUMMY

C..... Calculate binary 12 volume fractions from ternary volume fractions
U1 = PHI1/(PHI1+PHI2)
U2 = PHI2/(PHI1+PHI2)

CALL FHINTP(T, U1, U2, PHI1, PHI2, PHI3, G12, G23, G13,
\$ DG12, DG23, DG13, DDG12, DDG23, DDG13, IFG)

C..... Binary solvent/polymer system

DELCP1 = 0.0D0
\$ DELCP2 = DLOG(PHI2) + PHI3*(1.D0 - V23 +
\$ PHI3*(G23 + PHI2*DG23))

C..... Ternary system

DELCP1 = DLOG(PHI1) + 1.0 - PHI1 - V12*PHI2 - V13*PHI3 +
\$ (G12*PHI2 + G13*PHI3)*(PHI2 + PHI3) - G23*V12*PHI2*PHI3 -
\$ U1*U2*PHI2*DG12 - PHI1*DG13*PHI3**2.0 -
\$ V12*PHI2*DG23*PHI3**2.0

DELCP2 = DLOG(PHI2) + 1.0 - PHI2 - V21*PHI1 - V23*PHI3 +
\$ U1*U2*PHI1*V21*DG12 - PHI1*V21*DG13*PHI3**2.0 -
\$ G13*PHI1*PHI3*V21 + (G12*V21*PHI1 + G23*PHI3)*(PHI1 + PHI3)
\$ - PHI2*DG23*PHI3**2.0

IF(IFG .EQ. 3) PRINT*, OMG1, OMG2, DELCP1, DELCP2
ENDIF
RETURN
END

C*****
C* SUBROUTINE DENSTY *
C* This subroutine calculates the density of the solutions *
C* using the following equation of state; *
C* RHO = OMG1*RH01 + OMG2*RH02 + OMG3*RH03 *
C*****

SUBROUTINE DENSTY (T, N, UV, IFG, RHO)
IMPLICIT DOUBLE PRECISION (A-H , O-Z)
IMPLICIT INTEGER (I-N)
DOUBLE PRECISION UV(N)
DOUBLE PRECISION LAMBDA

```

COMMON /CONST/ RH01, RH02, RH03, RH013, RH023, SV1, SV2
$ , SV3, WM1, WM2, WM3, WMAIR, V1, V2, V3, R, V12, V21
$ , V13, V23, ETA, LAMBDA, GAMMA, ALPHA, BETA, FUJDO
$ , FUJA, FUJB, G
COMMON /SCALES/ RHOSC, DIF1SC, DIF2SC, SOLLSC, SUBLSC, TIMESCS,
$ VELSC, TEMPSC, F1SC, F2SC, G1SC, G2SC, HEATSC, FLX1SC, FLX2SC
$ ,OMG1SC, OMG2SC

```

```

OMG1 = UV(1)*OMG1SC
OMG2 = UV(2)*OMG2SC
OMG3 = 1.0D0 - OMG1 - OMG2

```

```

C..... RHO is dimensionless.
RHO = 1/(OMG1/RH01 + OMG2/RH02 + OMG3/RH03)

```

```

RETURN
END

```

APPENDIX C

TERNARY DAIGRAM

The most common way to display the concentration change of a ternary system due to mass transfer is to put instantaneous local compositions on a ternary phase diagram, as shown in Figure C.1. Each apex represents a pure component. For example, the point X in Figure C.1 represents the composition of an A/B/C mixture. The labels on each base indicate the distance from the base to its opposite apex and therefore the fraction of each species in the mixture. The base opposite the apex representing pure A is the line connecting the apex of pure B and the apex of pure C. The fraction of A in the mixture can be obtained by drawing a line from the point X parallel to this base and then reading or the distance (0.3). The fractions of B and C in the mixture X are 0.5 and 0.2, respectively. Obviously, summation of all fractions is 1 for any point in the ternary diagram.

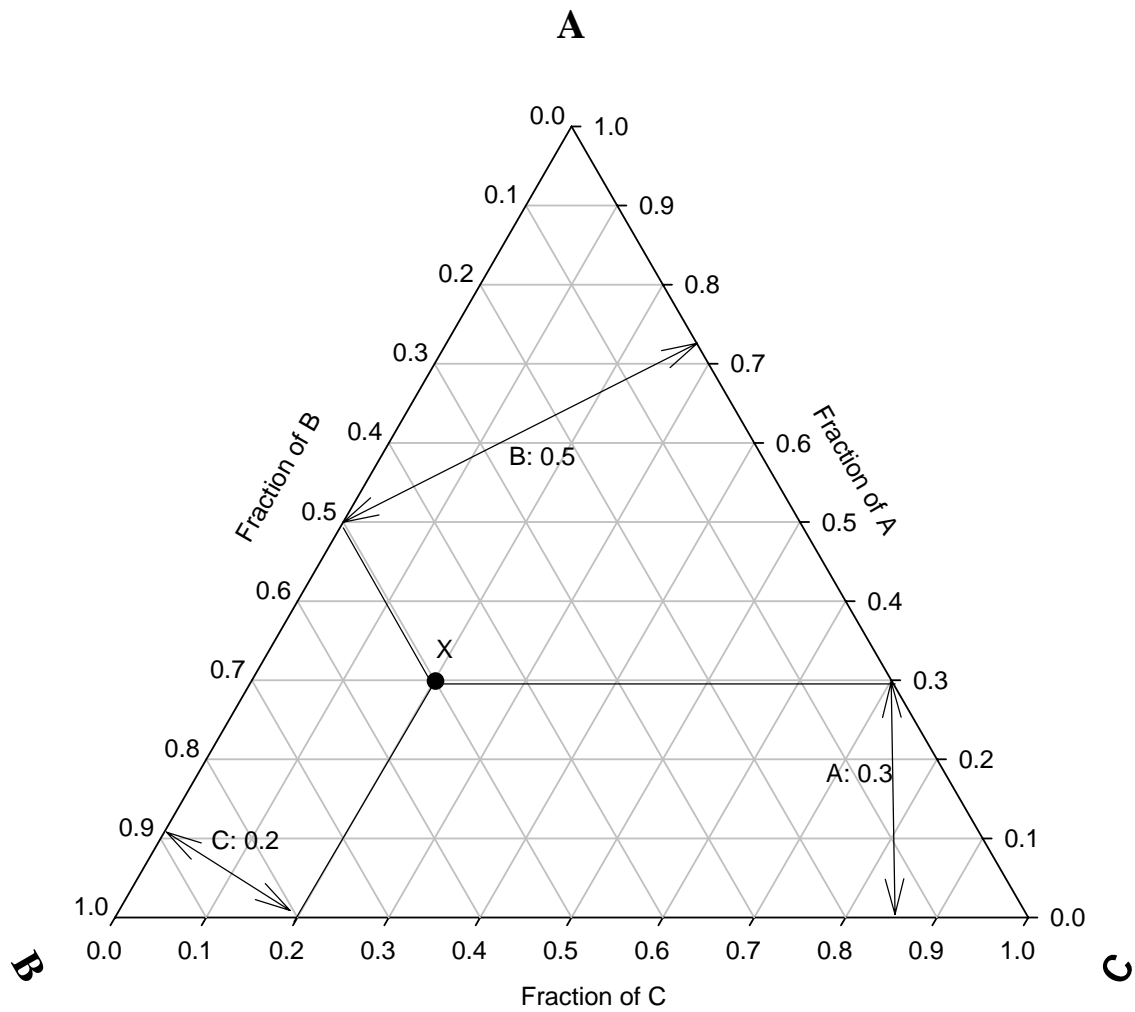


Figure C.1: Ternary phase diagram for an A / B / C system and an example composition X of the mixture.

A typical ternary phase diagram has two distinct regions, as shown in Figure C.2. A one-phase region represents all possible compositions of mixtures which produce a single-phase, homogeneous and stable solution. The binodal is the boundary between a one-phase region and a two-phase region. A mixture of this composition placed in a two-phase region will phase-separate into two liquid phases. These solutions are referred to as either metastable- or unstable solutions depending on their location within the two-phase region. The tie line connects the points between two compositions in equilibrium. For example, points M and N represent the compositions of two neighboring phases in equilibrium. Since M has more polymer fraction than N, M is called the polymer-rich phase and N is the polymer-lean phase. At the plait point, the two phases in equilibrium have the same composition.

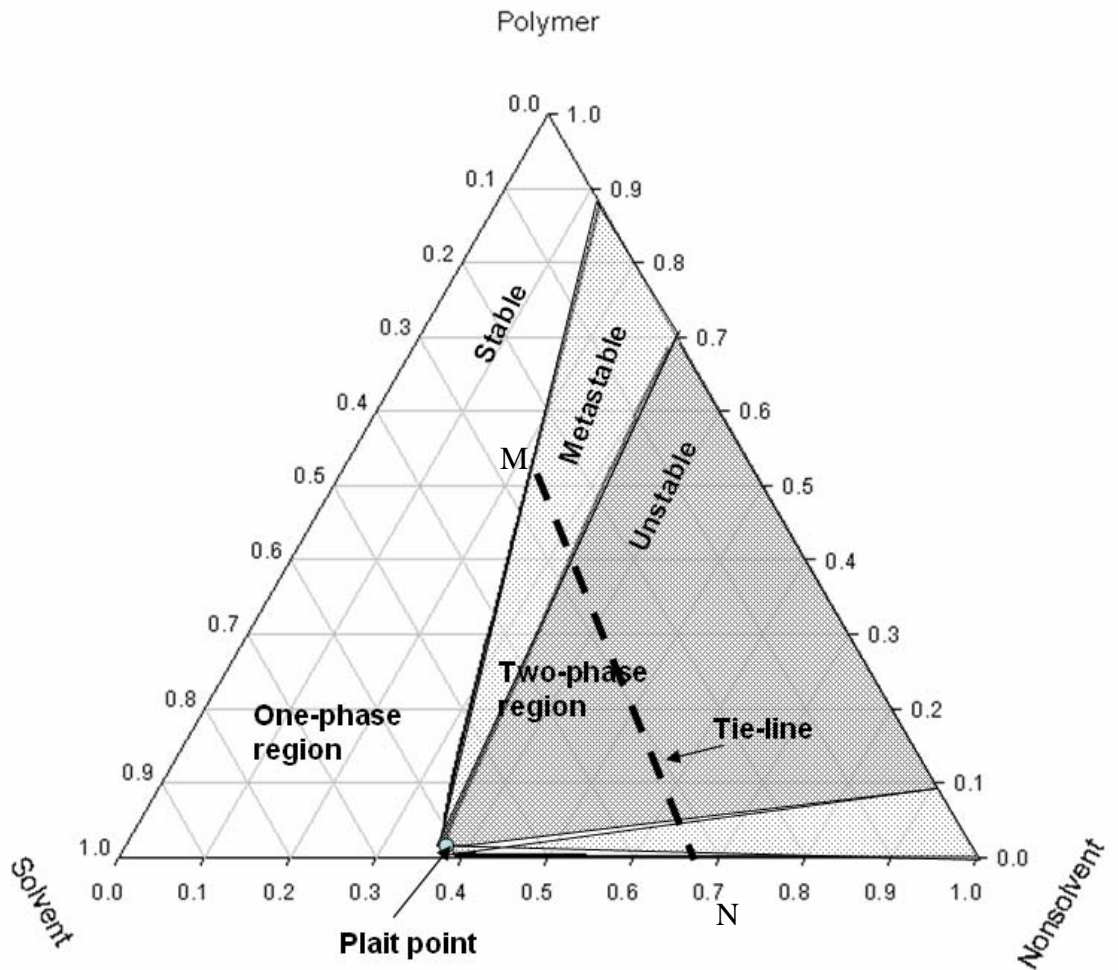


Figure C.2: Hypothetical ternary phase diagram for a polymer / solvent / nonsolvent system which can be one-phase or two-phase.

APPENDIX D

VOLUME-AVERAGE VELOCITY

The volume-average velocity is defined as:

$$W^V = \frac{\sum_i \bar{V}_i v_i}{\sum_k \bar{V}_k} \quad (\text{D.1})$$

where \bar{V}_i and v_i are the partial volume and velocity of species i , respectively. The zero volume-of-mixing implies

$$V = \sum_i \bar{V}_i \quad (\text{D.2})$$

From Equations (D.1) and (D.2), the volume-average velocity is

$$W^V = \sum_i \phi_i v_i \quad (\text{D.3})$$

where ϕ_i is the volume fraction of component i and is related to mass fractions by the following equation:

$$\phi_i = \frac{\frac{\omega_i}{\rho_i^\circ}}{\sum_k \frac{\omega_k}{\rho_k^\circ}} \quad (\text{D.4})$$

Combining Equations (D.3) and (D.4) yields the following volume-average velocity equation as a function of mass fractions:

$$W^V = \sum_i \left(\frac{\frac{\omega_i v_i}{\rho_i^\circ}}{\sum_k \left(\frac{\omega_k}{\rho_k^\circ} \right)} \right) \quad (\text{D.5})$$

Multiplying both the numerator and the denominator of Equation (D.5) by the density ρ yields

$$W^V = \sum_i \left(\frac{\rho_i v_i}{\rho_i^\circ \sum_k \left(\frac{\rho_k}{\rho_k^\circ} \right)} \right) \quad (\text{D.6})$$

Note that the numerator of Equation (D.6) is mass flux of component i . Therefore, the volume-average velocity and mass flux are related by the following equation:

$$W^V = \sum_i \left(\frac{n_i}{\rho_i^\circ \sum_k \left(\frac{\rho_k}{\rho_k^\circ} \right)} \right) \quad (\text{D.7})$$

Tsay and McHugh [51] found the following relationship of fluxes from the zero volume-of-mixing.

$$\sum_i \left(\frac{n_i}{\rho_i^\circ} \right) = 0 \quad (\text{D.8})$$

Clearly, the left-hand side (LHS) of Equation (D.8) is not necessarily volume-average velocity as they claimed, since $\rho_k = \omega_k \rho$ and $\rho_k \neq \omega_k \rho_k^\circ$. Their claim is true only when all species have the same pure density. Therefore, the diffusion equation in terms of the unit of volume does not always incorporate convection due to the non-zero mass-average velocity.

APPENDIX E

WET-CASTING MASS-TRANSPORT PROGRAM

The FORTRAN code developed to solve the wet-casting mass-transfer equations incorporating convection is presented below. This code uses the commercial PDE solver, NAG®.

```
PROGRAM MCAWETCAST
IMPLICIT DOUBLE PRECISION (A-H , O-Z)
IMPLICIT INTEGER (I-N)

PARAMETER (NPTS=131, M=0,NXI=1,NV=1,NCODE=NV)
PARAMETER (NXFIX=0, NPDE=2)
C PARAMETER (NWKRES=NPDE*(3*NPDE*NPTS+21)+7*(NPTS+NXFIX+3))
PARAMETER (NWKRES=NPDE*(3*NPDE+6*NXI+NPTS+15)+NXI+NCODE+
$ 7*NPTS+NXFIX+2+9000)
PARAMETER (NEQN=NPDE*NPTS+NCODE)
PARAMETER (NIW=25*NEQN+25+NXFIX+90000)
PARAMETER (LENODE=(6+5)*NEQN+50)
C PARAMETER (NW=NEQN*NEQN+NEQN+NWKRES+LENODE)
PARAMETER (NW=4*NEQN+11*NEQN/2+1+NWKRES+LENODE+90000)

DOUBLE PRECISION Y (NEQN), X (NEQN), RTOL (NEQN), ATOL (NEQN),
$ XI (1), XBK (11), DX (9000), XFIX (1), IW (NIW), W (NW),
$ SOL (1000,10), CHP1 (NEQN), CHP2 (NEQN), DST (2)

C Variables for NRTL equation
DOUBLE PRECISION LAMBDA
DOUBLE PRECISION TNRTLA12, TNRTLA21, TNRTLALPHA12
DOUBLE PRECISION DELCP11, DELCP22

INTEGER ITERATION
INTEGER INFORM (14+NEQN)
INTEGER ITASK

INTEGER IGRAVITY

LOGICAL THETA
DOUBLE PRECISION ALGOPT (30)
CHARACTER*1 LAOPT
INTEGER NRMESH, IPMINF
REAL DXMESH, TRMESH, XRATIO, CONST
```

```

CHARACTER*16 ZID

CHARACTER*1 NORM

EXTERNAL UVINIT,ODEDEF,PDEDEF,BNDARY,SPDEF1,D03PPF,MONITR,
$   D03PCL

COMMON /SDEV2/ ITRACE, IDEV
COMMON /DEVICE/ LCONC1, LCONC2, LRHO1, LRHO2, LLT, LDMU,
$   LMASS, LVEL, LSURFT, LSUB, LGEL, LWARN, LFLX, LDOMG1, LDOMG2
$   , LCONT, LCONB, LCONGR, LTEMGR, LCHMP1, LCHMP2, LDIF, LADV, LPEN
COMMON /CONST/ RH01, RH02, RH03, RH013, RH023, SV1, SV2
$   , SV3, WM1, WM2, WM3, WMAIR, V1, V2, V3, R, V12, V21
$   , V13, V23, ETA, LAMBDA, GAMMA, ALPHA, BETA, FUJD0
$   , FUJA, FUJB, G
C
COMMON /GLSPAR/ TCONGL, RHOGLS, CPGLS, SUBTHK, WPLATE, ALFSUB
COMMON /PLYPAR/ TCONPS, CPPS, EPSLON, SIGMA
COMMON /GASPAR/ TCONGS, VISGAS
COMMON /SCALES/ RHOSC, DIF1SC, DIF2SC, SOLLSC, SUBLSC, TIMESC,
$   VELSC, TEMPSC, F1SC, F2SC, G1SC, G2SC, FLX1SC, FLX2SC
$   ,OMG1SC, OMG2SC
COMMON /INPUTS/ OMG1IN, OMG2IN, YK1, TEMPIN, TEMAMB, FLMIN, GELTIM, PTOT
COMMON /BLK1/ RHOINT, C1MASI, C2MASI, C3MASI, DX, JCT,
$   KCT, AREA, NPTSM, NPDEM
COMMON /FRMOL/ YI1, YI2, YIA, UI1, RHOGA
COMMON /CHEMP/ DELCP11, DELCP22
COMMON /NRTL/ TNRTLA12, TNRTLA21, TNRTLALPHA12
COMMON /BLK2/ GF1, GF2
COMMON /GRVT/ IGRAVITY
C
COMMON /ADVCTN/ AMAV(130)
COMMON /GRDOMG/ GDU1(130,3), GDU2(130,3)
COMMON /CONT/ UTOP(2)

```

```

theta = .false.
neq = neqn
nnpts = nppts
norm = 'A'

```

```

kct = 0
jct = 0

```

```

lconc1 = 1
lconc2 = 2
lrho1 = 3
lrho2 = 4

```

```

lmass = 7
lvel = 8
lsurft = 9
lsub = 10
lgel = 11
lwarn = 12
lflx = 13
llt = 14
lcont = 15
lconb = 16
lcongr = 17
ltemgr = 18
lchmp1 = 19

```

```

lchmp2 = 20
ldif = 21
ldmu = 22
lchp = 23
ldomg1 = 24
ldomg2 = 25
ladv = 26
lpen = 27

itrace = 1
idev = 6

open (lconc1, file='conc1.8dat', status='new')
open (lconc2, file='conc2.8dat', status='new')
C open (lrho1, file='rho1.dat', status='new')
C open (lrho2, file='rho2.dat', status='new')
open (llt, file='lstar.8dat', status='new')
C open (lmass, file='mass.8dat', status='new')
open (lvel, file='velocity.8dat', status='new')
open (lsurft, file='surft.8dat', status='new')
open (lsub, file='subt.8dat', status='new')
open (lgel, file='gel.8dat', status='new')
open (lwarn, file='err.8dat', status='new')
open (lflx, file='flx.8dat', status='new')
open (lcont, file='topc.8dat', status='new')
open (lconb, file='botc.8dat', status='new')
open (lcongr, file='gradc.8dat', status='new')
open (ltemgr, file='gradt.8dat', status='new')
open (lchmp1, file='chemp1.8dat', status='new')
open (lchmp2, file='chemp2.8dat', status='new')
open (ldif, file='diff.8dat', status='new')
open (ldmu, file='dmudo.8dat', status='new')
open (lchp, file='chp.8dat', status='new')
open (ldomg1, file='domg1.8dat', status='new')
open (ldomg2, file='domg2.8dat', status='new')
open (ladv, file='adv.8dat', status='new')
open (lpen, file='pe.8dat', status='new')
C..... The time increment at which the control is returned to the main
C program. The smaller this time step the smaller the error.
TINC = 1.00D0
TFINAL = 300.0D0

C..... Initial conditions for the problem

C..... Experiment identification number
ZID = "T091092.600.15.3"

OMG1IN = 0.000000001D0
OMG2IN = 0.850D0
UTOP(1) = 0.1600D0
UTOP(2) = 0.1229D0
YK1 = 0.9999999999D0
FLMIN = 0.0200D0
TEMPIN = 298.15D0
IGRAVITY = 0

C..... Parameters for NRTL equation of Acetone/water mixture
TNRTLA12 = 631.0463
TNRTLA21 = 1197.4101
TNRTLALPHA12 = 0.5343

```



```

          PTOT = 632.0
C..... Ambient temperature, usually the same as initial temp
          TEMAMB = 297.15
          SUBTHK = 1.0
          GELTIM = 0.55D0

C..... Initialize the constants specific to the system of interest
CALL CONSTS

          write(LDMU,1060)
          write(LLT,1070)
          write(LMASS,1080)
          write(LSURFT,1090)
          write(LSUB,1095)
          write(LFLX,1100)
          write(LCONT,1110)
          write(LCONB,1120)
C          write(LVEL,1121)
          write(LCONGR,1130)
          write(LTEMGR,1140)
          write(LCONC1,550) ZID
          write(LCONC1,13) OMG1IN, OMG2IN, FLMIN, TEMPIN, YK1,
$              TISO, BINRY
13  FORMAT('THE INPUT VALUES ', 5(F10.6,1X),2(2X,A1))

          WRITE(LCONC1,*) RHOSC, DIF1SC, DIF2SC, SOLLSC, SUBLSC,
$              TIMES, TEMPSC, F1SC, F2SC, G1SC, G2SC, VELSC,
$              FLX1SC, FLX2SC, OMG1SC, OMG2SC

          WRITE(LDIF,103)
103  FORMAT('TIME(S)', 5X, ' DIMENSIONAL F1, F2, G1, G2')

C..... Calculate the initial mass of nonsolvent(NS)(1), solvent(S)(2),
C      and polymer(P)(3).
C      RHOINT = RH01*OMG1IN + RH02*OMG2IN + RH03*(1.D0-OMG1IN-OMG2IN)
          RHOINT = 1.0D0/((RH01/OMG1IN) + (RH02/OMG2IN) + (RH03/(1.D0-OMG1IN-OMG2IN)))
          C1MASI = RHOINT*OMG1IN*AREA*FLMIN
          C2MASI = RHOINT*OMG2IN*AREA*FLMIN
          C3MASI = RHOINT*(1.0D0 - OMG1IN - OMG2IN)*AREA*FLMIN

C..... Start SPRINT initialization
C      NPDE = 4 ! turned into a parameter
          NPDEM = NPDE

C..... M = geometry (0 = planar, 1 = cylindrical, 2 = spherical)
C      M = 0 turned into a parameter

          ITASK = 2

          DO 16 I=1,30
          ALGOPT(I)=0.0D0
16  CONTINUE
          ALGOPT(4)=2.0D0 !don't do the Petzold test.
          ALGOPT(29)=0.5
          ALGOPT(30)=1D-300

          LAOPT='S' !use the sparse matrix routines

C..... Define the mesh positions in the array X(I)

```

```

X(1) = 0.0D0
XBK(1) = 0.0D0
DX25 = 1.0D0 / DBLE(25.0D0)
DX50 = 1.0D0 / DBLE(50.0D0)
DX100 = 1.0D0 / DBLE(100.0D0)
DX200 = 1.0D0 / DBLE(200.0D0)
DX400 = 1.0D0 / DBLE(400.0D0)
DX800 = 1.0D0 / DBLE(800.0D0)
DX1600 = 1.0D0 / DBLE(1600.0D0)
DX1047 = 1.0D0 / DBLE(130.0D0)
DX1057 = 1.0D0 / DBLE(260.0D0)
DX1067 = 1.0D0 / DBLE(12500.0D0)
DX1087 = 124.0D0 / (30.0D0 * 125.0D0)
DX1077 = 1.0D0 / DBLE(DX1087)

X(NPTS) = 1.0D0
ncase = 1047

IF(NCASE .EQ. 2) THEN
c npts=131
    DO 5 J=2,21
5      X(J) = X(J-1) + DX50

    DO 6 J = 22, 51
6      X(J) = X(J-1) + DX100

    DO 7 J = 52, 91
7      X(J) = X(J-1) + DX200

    DO 8 J = 92, 130
8      X(J) = X(J-1) + DX400
    PRINT*, 'NPTS = ', NPTS
    ENDIF

        IF(NCASE .EQ. 6) THEN
C          npts = 80
c          npts = 5
          PRINT*, 'NPTS = ', NPTS
          DXXP = 1.0D0 / DBLE(NPTS-1)
          DO 650 J = 2, NPTS
650      X(J) = X(J-1) + DXXP
        ENDIF
    IF(NCASE .EQ. 4) THEN
C npts=191
    PRINT *, 'NPTS = ', NPTS
    DO 55 j=2,21
55      X(J) = X(J-1) + DX50

    DO 66 J = 22, 51
66      X(J) = X(J-1) + DX100

    DO 77 J = 52, 91
77      X(J) = X(J-1) + DX200

    DO 88 J = 92, 111
88      X(J) = X(J-1) + DX400

    DO 89 J = 112, 190
89      X(J) = X(J-1) + DX1600
    ENDIF

        IF(NCASE .EQ. 3) THEN

```

```

C      NPTS = 261
      PRINT*, ' NPTS = ', NPTS
      DO 1 J = 2, 41
1       X(J) = X(J-1) + DX100

      DO 2 J = 42, 101
2       X(J) = X(J-1) + DX200

      DO 3 J = 102, 181
3       X(J) = X(J-1) + DX400

      DO 4 J = 182, 260
4       X(J) = X(J-1) + DX800
      ENDIF

      IF(NCASE .EQ. 5) THEN
C      NPTS = 521
      PRINT*, ' NPTS = ', NPTS
      DO 555 J = 2, 81
555    X(J) = X(J-1) + DX200

      DO 666 J = 82, 201
666    X(J) = X(J-1) + DX400

      DO 777 J = 202, 361
777    X(J) = X(J-1) + DX800

      DO 888 J = 362, 520
888    X(J) = X(J-1) + DX1600
      ENDIF

      IF (NCASE .EQ. 1047) THEN
C      NPTS = 131 and equally distributed mesh
      PRINT*, ' NPTS = ', NPTS
      DO 1047 J=2, 130
1047   X(J) = X(J-1) + DX1047
      ENDIF

      IF (NCASE .EQ. 1057) THEN
C      NPTS = 131
      PRINT*, ' NPTS := ', NPTS, DX1067, DX1077, DX1087

      DO 31057 J = 2, 31
31057   X(J) = X(J-1) + DX1087

      DO 41057 J = 32, 130
41057   X(J) = X(J-1) + DX1067
      ENDIF

      X(NPTS) = 1.0D0
      NPTSM = NPTS

C....   GDU(J,1) contains a normalized location.
      DO 2005 J=1, NPTS-1 !Dimension of GDU1 and GDU2 should be changed accordingly.
      GDU1(J,1) = 0.0D0
      GDU2(J,1) = 0.0D0
2005    CONTINUE

C.....  Transfer x values into the DX for use in subroutine MONITR
      DO 41 KP = 1 , NPTS
      WRITE(LCONC1,57) X(KP)
      WRITE(LCONC2,57) X(KP)

```

```

WRITE(LCHMP1,57) X(KP)
WRITE(LCHMP2,57) X(KP)
C WRITE(LTEM,57) X(KP)
41 DX(KP) = X(KP)
57 FORMAT(F20.15)

C..... Coupled O.D.E. at the solution/air interface (moving boundary)
C NV = 1 turned into a parameter
C NXI = 1 turned into a parameter
C Coupled point(XI) is the top of the casting solution(x)
  XI(1) = 1.0D0
C NCODE=NV Turned into a parameter

  REMESH = .FALSE.
  MAXNPT = NNPTS
  T = 0.0D0
C IBAND =
  ITIME = 1

  NRMESH = 0
  DXMESH = 0.0
  TRMESH = 1.0
  IPMINF = 0
  XRATIO = 1.5
  CONST = 2.0/(NNPTS-1)

  NMOSS = 2
  SENS = 0.0D0
  IRET = 0

C..... Set convergence criterion
DO 52 I = 1,NEQ
  RTOL(I) = 1.0D-4
52 ATOL(I) = 1.0D-4
  ITOL = 4

DO 99 I = 1 , 14
99 INFORM(I) = 0
  INFORM(2) = 1
  INFORM(3) = 1
  INFORM(4) = 9000
C SNORM = 'L2NORM'
  NEQMAX = NEQ + 1

WRITE(LCONC1,*) TFINAL, NPTS, ATOL(1), MAXORD

C..... Write the initial conc and mass fractions of components 1 & 2
WRITE(LCONC1,250) T*TIMESC, Y(NEQ)*SOLLSC
WRITE(LCONC1,200) (Y(J)*OMG1SC, J=1, NEQ-1, NPDE)
C WRITE(LRHO1,250) T*TIMESC, Y(NEQ)*SOLLSC
C WRITE(LRHO1,200) (RHOACT(J), J=1, NEQ-1, NPDE)

WRITE(LCONC2,250) T*TIMESC, Y(NEQ)*SOLLSC
WRITE(LCONC2,200) (Y(J)*OMG2SC, J=2, NEQ-1, NPDE)
C WRITE(LRHO2,250) T*TIMESC, Y(NEQ)*SOLLSC
C WRITE(LRHO2,200) (RHOACT(J), J=2, NEQ-1, NPDE)

C..... Write out the initial chemical potentials for components 1 & 2
WRITE(LCHMP1,250) T*TIMESC, Y(NEQ)*SOLLSC
WRITE(LCHMP2,250) T*TIMESC, Y(NEQ)*SOLLSC

```

```

DO 603 K = 1 , NPTS
DST(1) = OMG1IN/OMG1SC
DST(2) = OMG2IN/OMG2SC
CALL CHEMPT (0.0, 2, DST, 4, XNONSL, XSOLV)
CHP1(K) = XNONSL
CHP2(K) = XSOLV
603 CONTINUE
WRITE(LCHMP1,200) (CHP1(J), J=1, NPTS)
WRITE(LCHMP2,200) (CHP2(J), J=1, NPTS)
C..... Write the initial mass avg. vel. at interface in the polymer solution
C WRITE(LVEL,250) T*TIMESC, Y(NEQ)*SOLLSC
C WRITE(LVEL,201) (Y(J)*VELSC, J = 3, NEQ-1, NPDE)
C WRITE(LVEL,250) T*TIMESC, Y(NEQ)*SOLLSC
JSPARS = 0

C Nondimensionize the final time
TFIN = TFINAL / TIMESC
TOUT = 0.0
LNO = 0
LINO = 1
C 54 TOUT = T + TINC/TIMESC
54 TOUT = TOUT + TINC/TIMESC

```

IFAIL = -1

```

write (*,*) NPDE,M,T,TOUT,NNPTS,NEQN
ITERATION=ITERATION+1
write (*,*) ITERATION
write (*,*) "Entering d03ppf..."
CALL D03PPF(NPDE,M,T,TOUT,PDEDEF,BNDARY,UVINIT,Y,
$ NNPTS,X,NV,ODEDEF,NXI,XI,NEQN,RTOL,ATOL,
$ ITOL,NORM,LAOPT,ALGOPT,REMESH,NXFIX,XFIX,
$ NRMESH,DXMESH,TRMESH,IPMINF,XRATIO,CONST,
$ D03PCL,W,NW,IW,NIW,ITASK,ITRACE,IND,IFAIL)

```

write (*,*) "Leaving d03ppf..."

```

CALL MONTR (NEQ,T,Y,RR)

C IF(INFORM(1) .NE. 2) THEN
C WRITE(LCONC1,300) INFORM(1)
C GO TO 70
C ENDIF

C..... Sepatrte the concentration solutions
DO 205 KL = 1, NPDE
DO 105 KM = 1, NPTS
SOL(KM,KL) = Y(NPDE*(KM-1)+KL)
105 CONTINUE
205 CONTINUE

WRITE(LCONC1,250) T*TIMESC, Y(NEQ)*SOLLSC
WRITE(LCONC1,200) (SOL(J,1)*OMG1SC, J=1, NPTS)
WRITE(LCONC2,250) T*TIMESC, Y(NEQ)*SOLLSC
WRITE(LCONC2,200) (SOL(J,2)*OMG2SC, J=1, NPTS)
C WRITE(LVEL,250) T*TIMESC, Y(NEQ)*SOLLSC
C WRITE(LVEL,200) (SOL(J,3)*VELSC, J=1, NPTS)
C WRITE(LVEL,401) T*TIMESC, SOL(NPTS,3)*VELSC
WRITE(LCONT,400) T*TIMESC, SOL(NPTS,1)*OMG1SC,
$ SOL(NPTS,2)*OMG2SC

```

```

WRITE(LCONB,400) T*TIMESC, SOL(1,1)*OMG1SC,
$           SOL(1,2)*OMG2SC
C..... Calculate the chemical potentials for components 1 & 2
C       at every time step.
WRITE(LCHMP1,250) T*TIMESC, Y(NEQ)*SOLLSC
WRITE(LCHMP2,250) T*TIMESC, Y(NEQ)*SOLLSC

DO 503 K = 1, NPTS
DST(1) = SOL(K,1)
DST(2) = SOL(K,2)
CALL CHEMPT (0.0, 2, DST, 4, XNONSL, XSOLV)
CHP1(K) = XNONSL
CHP2(K) = XSOLV
C..... Write out diffusion coefficients
IF(K.EQ.NPTS) THEN
IFLAG = 1
CALL COEFFI(0.0, NPDE, DST, 0.0,
$           FF1, FF2, GG1, GG2, HH1, HH2, IFLAG)
C       WRITE(LDIF,397) T*TIMESC,FF1*F1SC,FF2*F2SC,GG1*G1SC,GG2*G2SC
IFLAG = 9999
CALL COEFFI(0.0, NPDE, DST, 0.0,
$           FF1, FF2, GG1, GG2, HH1, HH2, IFLAG)
C       WRITE(LDMU,397) T*TIMESC,FF1,FF2,GG1,GG2

ENDIF
503 CONTINUE
WRITE(LCHMP1,200) (CHP1(J), J=1, NPTS)
WRITE(LCHMP2,200) (CHP2(J), J=1, NPTS)
WRITE(lchp,1141) T*TIMESC, CHP1(NPTS), CHP2(NPTS), SOL(NPTS,1)*OMG1SC,
SOL(NPTS,2)*OMG2SC

C..... Final integration time is reached, stop the program
IF(TOUT .GT. TFIN) GO TO 53

GO TO 54

53 CONTINUE

C       WRITE(LCONC1,350) INFORM(1)

910 FORMAT('MAIN: Switching to sparse at T(s) ',1X,F12.5)

CLOSE(LCONC1, STATUS='KEEP')
CLOSE(LCONC2, STATUS='KEEP')
C       CLOSE(LRHO1, STATUS='KEEP')
C       CLOSE(LRHO2, STATUS='KEEP')
CLOSE(LLT, STATUS='KEEP')
CLOSE(LMASS, STATUS='KEEP')
C       CLOSE(LVEL, STATUS='KEEP')
CLOSE(LSURFT, STATUS='KEEP')
CLOSE(LSUB, STATUS='KEEP')
C       CLOSE(LGEL, STATUS='KEEP')
CLOSE(LWARN, STATUS='KEEP')
CLOSE(LCONT, STATUS='KEEP')
CLOSE(LCONB, STATUS='KEEP')
CLOSE(LCONGR, STATUS='KEEP')
CLOSE(LTEMGR, STATUS='KEEP')
CLOSE(LCHMP1, STATUS='KEEP')
CLOSE(LCHMP2, STATUS='KEEP')
CLOSE(LDIF, STATUS='KEEP')

```

```

CLOSE(LDMU, STATUS='KEEP')
CLOSE(lchp, status='keep')
CLOSE(ldomg1, status='keep')
CLOSE(ldomg2, status='keep')
CLOSE(ladv, status='keep')
CLOSE(lpen, status='keep')

90   FORMAT(1X, 5(F12.8,2X))
200  FORMAT(6(F12.8,1X))
201  FORMAT(6(F10.4,2X))
250  FORMAT('TIME(s) ',2(F15.9, 2X))
270  FORMAT('Negative concentration')
300  FORMAT(2X,'UNSUCCESSFULL INFORM(1) = ',I3)
350  FORMAT(2X,'SUCCESSFULL INFORM(1) = ',I3)
397  FORMAT(1X, 5(F12.8,2X))
400  FORMAT(2X,F15.7,5X,2(F20.15,2X))
401  FORMAT(2X,F15.7,5X,F20.15,2X)
550  FORMAT(A16)
1060 FORMAT(2X,'TIME(S)',5X,'DM1DO1, DM1DO2, DM2DO1, DM2DO2')
1070 FORMAT(5X,'TIME(s)',5X,'L(t)(cm)',5X,'L(t)(dimenlss)')
1080 FORMAT(2X,'TIME(s)',5X,'NS + S TO POLY MASS RATIO',5X,'TOT MAS')
1090 FORMAT(2X,'TIME(s)',5X,'SURF SOL TEMP(C)')
1095 FORMAT(2X,'TIME(s)',5X,'SURF SUB TEMP(C)')
1100 FORMAT(1X,'T(s)',5X,'NS FLX',5X,'S FLX',5X,'NS EQ INTF CON',
$      5X,'S EQ CON')
1110 FORMAT(1X,'TIME(s)',5X,'NS MAS FRAC(TOP)',5X,'S MAS FRAC(TOP)')
1120 FORMAT(1X,'TIME(s)',5X,'NS MAS FRAC(BOT)',5X,'S MAS FRAC(BOT)')
1121 FORMAT(1X,'TIME(s)',5X,'MAS AVG VEL(TOP)')
1130 FORMAT(1X,'TIME(S)',5X,'NODIM SURF NS&S M FRAC GRAD',5X,'DIMNAL
$      SURF M DENS NS&S GRAD')
1140 FORMAT(1X,'TIME(S)',5X,'DIMLSS SURF TEM GRAD',5X,'DIMNAL SURF
$      TEM GRAD')
1141 FORMAT(5(E12.5,1X))
      STOP
      END

```

C..... ***** USER SUBROUTINES *****

```

C*****
C*          SUBROUTINE UVINIT          *
C*    This subroutine initializes the pdes and the odes.    *
C*****

```

```

      SUBROUTINE UVINIT(NPDE, NPTS,NXI, X, XI, U, NV,V)
      IMPLICIT DOUBLE PRECISION (A-H , O-Z)
      IMPLICIT INTEGER (I-N)
      DOUBLE PRECISION X(NPTS), U(NPDE,NPTS), UU(NPDE)

```

```

c
      DOUBLE PRECISION V(NV)

```

```

c
      COMMON /SCALES/ RHOSC, DIF1SC, DIF2SC, SOLLSC, SUBLSC, TIMESC,
$  VELSC, TEMPSC, F1SC, F2SC, G1SC, G2SC, FLX1SC, FLX2SC
$  ,OMG1SC, OMG2SC
      COMMON /INPUTS/ OMG1IN, OMG2IN, YK1, TEMPIN, TEMAMB, FLMIN, GELTIM, PTOT
      COMMON /PLYPAR/ TCONPS, CPPS, EPSLON, SIGMA
      COMMON /GLSPAR/ TCONGL, RHOGLS, CPGLS, SUBTHK, WPLATE, ALFSUB
      COMMON /GRADS/ UX1LFT, UX1RHT, UX2LFT, UX2RHT
      COMMON /CONT/ UTOP(2)

```

```

DO 10 I = 1,NPTS
U(1,I) = OMG1IN/OMG1SC
U(2,I) = OMG2IN/OMG2SC

10    CONTINUE
      V(1)=FLMIN/SOLLSC  ! This is from SVINIT from SPRINT.

      U(1,NPTS) = UTOP(1)
      U(2,NPTS) = UTOP(2)
      RETURN
      END

C*****
C*          SUBROUTINE PDEDEF                      *
C*    The pdes are defined in this subroutine.      *
C*****

      SUBROUTINE PDEDEF (NPDE,T,X,U,DUDX,NV,V,VDOT,C,Q,RR,IRES)

      IMPLICIT DOUBLE PRECISION (A-H , O-Z)
      IMPLICIT INTEGER (I-N)
      DOUBLE PRECISION U(NPDE), DUDX(NPDE),
$       C(NPDE,NPDE), Q(NPDE), RR(NPDE), V(NV), VDOT(NV)
      DOUBLE PRECISION LAMBDA

      COMMON /CONST/ RH01, RH02, RH03, RH013, RH023, SV1, SV2
$   , SV3, WM1, WM2, WM3, WMAIR, V1, V2, V3, R, V12, V21
$   , V13, V23, ETA, LAMBDA, GAMMA, ALPHA, BETA, FUJD0
$   , FUJA, FUJB, G

C
      COMMON /SCALES/ RHOSC, DIF1SC, DIF2SC, SOLLSC, SUBLSC, TIMESC,
$   VELSC, TEMPSC, F1SC, F2SC, G1SC, G2SC, FLX1SC, FLX2SC
$   ,OMG1SC, OMG2SC
      COMMON /PLYPAR/ TCONPS, CPPS, EPSLON, SIGMA
      COMMON /GLSPAR/ TCONGL, RHOGLS, CPGLS, SUBTHK, WPLATE, ALFSUB
      COMMON /GRADS/ UX1LFT, UX1RHT, UX2LFT, UX2RHT
C
      COMMON /ADVCTN/ AMAV(130)
      COMMON /GRDOMG/ GDU1(130,3), GDU2(130,3)

      CALL DENSTY(T, NPDE, U, IFG, RHO)
      IFLAG = 1
      CALL COEFFI(T, NPDE, U, DUDX, FF1, FF2, GG1, GG2, HH1, HH2, IFLAG)

C
      PRINT*, 'RHO in PDEDEF = ', RHO
      DIM1 = (FLX1SC*SOLLSC)/F1SC

C.....  Component (1) (nonsolvent) mass transport equation
      C(1,1) = RHO*(V(1)**2.0D0)
      C(2,1) = 0.0D0

      Q(1) = RHO*(1.0D0/RH01 - 1.0D0/RH03)*(FF1*DUDX(1) + GG1*DUDX(2))*DUDX(1) +
RHO*(1.0D0/RH02 - 1.0D0/RH03)*(FF2*DUDX(1) + GG2*DUDX(2))*DUDX(1) -
RHO*V(1)*X*VDOT(1)*DUDX(1)
      RR(1) = - (FF1*DUDX(1) + GG1*DUDX(2))

C.....  Component (2) (solvent) mass transport equation
      C(1,2) = 0.0D0
      C(2,2) = RHO*(V(1)**2.0D0)

```



```

      Q(2) = RHO*(1.0D0/RH01 - 1.0D0/RH03)*(FF1*DUDX(1) + GG1*DUDX(2))*DUDX(2) +
      RHO*(1.0D0/RH02 - 1.0D0/RH03)*(FF2*DUDX(1) + GG2*DUDX(2))*DUDX(2) -
      RHO*V(1)*X*VDOT(1)*DUDX(2)
      RR(2) = - (FF2*DUDX(1) + GG2*DUDX(2))

```

```

C..... Store the gradients at the right boundary (X=1)

```

```

      IF(X .GE. 1.0) THEN
          UX1RHT = DUDX(1)
          UX2RHT = DUDX(2)
          UX3RHT = DUDX(3)

```

```

C

```

```

      ENDIF

```

```

      ICNT = 0

```

```

C.... Count empty space in GDUs

```

```

      DO 2001 J=1, 130
          IF (GDU1(J,1) .EQ. 0.0D0) THEN
              ICNT = ICNT + 1
          ENDIF

```

```

2001

```

```

      CONTINUE

```

```

C... If there is any empty space in GDUs then fill it with mass frc. grad and location.

```

```

      IF (ICNT .GT. 0) THEN
          DO 2058 J=1,130
              IF (GDU1(J,1) .EQ. X) THEN
                  ICNT=ICNT+1
              ENDIF

```

```

2058

```

```

      CONTINUE
      GDU1(130-ICNT+1,1) = X
      GDU1(130-ICNT+1,2) = DUDX(1)
      GDU1(130-ICNT+1,3) = (F1SC/(SOLLSC*V(1)))*((1.0D0/RH01 - 1.0D0/RH03)*RR(1) +
(1.0D0/RH02 - 1.0D0/RH03)*RR(2))
      GDU2(130-ICNT+1,1) = X
      GDU2(130-ICNT+1,2) = DUDX(2)
      GDU2(130-ICNT+1,3) = (F1SC/(SOLLSC*V(1)))*RR(1)/(RHO*U(1))
      ENDIF

```

```

C... If there is no empty space in GDUs then find the location and fill it with frc. grad.

```

```

      IF (ICNT .EQ. 0) THEN
          DO 2002 J=1,130
              IF (GDU1(J,1) .EQ. X) THEN
                  GDU1(J,2) = DUDX(1)
                  GDU2(J,2) = DUDX(2)
                  GDU1(J,3) = (F1SC/(SOLLSC*V(1)))*((1.0D0/RH01 - 1.0D0/RH03)*RR(1) +
(1.0D0/RH02 - 1.0D0/RH03)*RR(2))
                  GDU2(J,3) = (F1SC/(SOLLSC*V(1)))*RR(1)/(RHO*U(1))
              ENDIF

```

```

2002

```

```

      CONTINUE
      ENDIF

```

```

      RETURN
      END

```

```

C*****
C* SUBROUTINE BNDARY *
C* The boundary conditions are defined in this subroutine. *
C*****

```

```

      SUBROUTINE BNDARY(NPDE,T,U,UX,NV,V,VDOT,

```

```

$      IBND,BBETA,GAMA,IRES)

      IMPLICIT DOUBLE PRECISION (A-H , O-Z)
      IMPLICIT INTEGER (I-N)
      DOUBLE PRECISION BBETA(NPDE), GAMA(NPDE), U(NPDE), UX(NPDE)
$      ,V(1), VDOT(1)

      INTEGER IBND

      COMMON /SCALES/ RHOSC, DIF1SC, DIF2SC, SOLLSC, SUBLSC, TIMESC,
$  VELSC, TEMPSC, F1SC, F2SC, G1SC, G2SC, FLX1SC, FLX2SC
$      ,OMG1SC, OMG2SC
      COMMON /PLYPAR/ TCONPS, CPPS, EPSLON, SIGMA
      COMMON /INPUTS/ OMG1IN, OMG2IN, YK1, TEMPIN, TEMAMB
$  , FLMIN, GELTIM, PTOT

      COMMON /GLSPAR/ TCONGL, RHOGLS, CPGLS, SUBTHK, WPLATE, ALFSUB
      COMMON /BLK2/ GF1, GF2
      COMMON /FRMOL/ YI1, YI2, YIA, UI1, RHOGA
      COMMON /CONT/ UTOP(2)
C      COMMON /ADVCTN/ AMAV(130)

      IF (IBND .EQ. 0) THEN
C.....  Mass transport, component (1) (water)
          BBETA(1) = 0.0D0
          GAMA(1) = UX(1)

C.....  Mass transport, component (2) (acetone)
          BBETA(2) = 0.0D0
          GAMA(2) = UX(2)

      ELSE
C      PRINT*, ' BNDARY '
          CALL DENSTY (T, NPDE, U, IFG, RHO)
          PRINT*, ' RHO = ', RHO
          CALL FLXHET (T, U, NPDE, NV, V, VDOT, RHOGA
$          GF1, GF2, HTRSFC, HV1, HV2, IFG)

          FLUXG1 = GF1
          FLUXG2 = GF2

          PRINT*, ' FLUXG1 and FLUXG2 is ', FLUXG1, FLUXG2

C      PRINT*, ' RHOGA, UI1 are ', RHOGA, UI1
C      IF (RHOGA .EQ. 0.0D0) THEN

C      RHOGA = 0.7857
C      PRINT*, 'RHOGA was zero'
C      ENDIF

          PRINT*, ' RHOGA, UI1 = ', RHOGA, UI1

          IF(IFG .EQ. 99) THEN
              IRES = 2
              RETURN
          ENDIF

C.....  Set component densities (g/cm^3)
          RH01 = 1.0
          RH02 = 0.7857
          RH03 = 1.31

```

```

UI2 = 1.0D0 - UI1

CALL COEFFI(T, NPDE, U, UX, FF1, FF2, GG1, GG2, HH1, HH2, IFLAG)

DDIMB = RHO - RHOGA
DDIM1 = (RHO*U(1) - RHOGA*UI1)
DDIM2 = (RHO*U(2) - RHOGA*UI2)
RH13 = (1.0D0/RH01) - (1.0D0/RH03)
RH23 = (1.0D0/RH02) - (1.0D0/RH03)

CCCCCCCCCCCCCCCCCCCCCCCCCCCCCCCCCCCCCCCCCCCCCCCCCCCCCCCC
C.....  Mass transport after local equilibrium at the top
C.....  Mass transport, component (1) (nonsolvent)
C          BBETA(1) = - (1.0D0 - RHO*U(1)*RH13)/V(1)
C          GAMA(1) = DDIM1*VDOT(1) +
C $          RHO*U(1)*DDIM2*(FF2*UX(1) + GG2*UX(2))/V(1) + FLUXG1

C.....  Mass transport, component (2) (solvent)
C          BBETA(2) = - (1.0D0 - RHO*U(2)*RH23)/V(1)
C          GAMA(2) = DDIM2*VDOT(1) +
C $          RHO*U(2)*DDIM1*(FF1*UX(1) + GG1*UX(2))/V(1) + FLUXG2

CCCCCCCCCCCCCCCCCCCCCCCCCCCCCCCCCCCCCCCCCCCCCCCCCCCCCCCC
C.....  Mass transport after vitrification at the top
          BBETA(1) = 0.0D0
C          GAMA(1) = U(1) - 0.156198D0
          GAMA(1) = U(1) - UTOP(1)

          BBETA(2) = 0.0D0
C          GAMA(2) = U(2) - 0.128232D0
          GAMA(2) = U(2) - UTOP(2)

      ENDIF
      RETURN
      END

C*****
C*          SUBROUTINE ODEDEF          *
C*  The ode coupled at the interface is defined in this *
C*  subroutine.          *
C*****

      SUBROUTINE ODEDEF (NPDE,T,NV,V,VDOT,NXI,XI,UI,UXI,RI,
$          UTI,UTXI,VRES,IRES)

      IMPLICIT DOUBLE PRECISION (A-H , O-Z)
      IMPLICIT INTEGER (I-N)
      DOUBLE PRECISION XI(NXI), UI(NPDE,NXI), UXI(NPDE,NXI),
$          RI(NPDE,NXI), UTI(NPDE,NXI), UTXI(NPDE,NXI), VRES(NV),
$          V(NV), VDOT(NV)
      COMMON /SCALES/ RHOSC, DIF1SC, DIF2SC, SOLLSC, SUBLSC, TIMESC,
$  VELSC, TEMPSC, F1SC, F2SC, G1SC, G2SC, FLX1SC, FLX2SC
$  ,OMG1SC, OMG2SC
      COMMON /BLK2/ GF1, GF2
      COMMON /FRCMOL/ YI1, YI2, YIA, UI1, RHOGA
C      COMMON /ADVCTN/ AMAV(130)

      IF(IRES.EQ.-1) THEN
          CALL DENSTY (T, NPDE, UI, IFLAG, RHO)

```

```

VRES(1) = VDOT(1)*(RHO - RHOGA)

PRINT*, 'IRES for ODEDEF is -1 and VRES=', VRES(1), VDOT(1)
ELSE
C PRINT*, ' ODEDEF '

CALL DENSTY (T, NPDE, UI, IFLAG, RHO)
CALL FLXHET (T, UI, NPDE, NV, V, VDOT, RHOGA
$ GF1, GF2, HTRSFC, HV1, HV2, IFG)

C..... Set component densities (g/cm^3)
RH01 = 1.0
RH02 = 0.7857
RH03 = 1.31
RH13 = (1.0D0/RH01) - (1.0D0/RH03)
RH23 = (1.0D0/RH02) - (1.0D0/RH03)

PRINT*, ' RHO is ', RHO
PRINT*, ' RHOGA... ', RHOGA
CALL COEFFI(T, NPDE, UI, 0.0, FF1, FF2, GG1, GG2, HH1, HH2, IFLAG)
PRINT*, 'FF1 , UXIs are ', FF1, UXI(1,1), UXI(2,1)

FLUXG1 = GF1
FLUXG2 = GF2

C Incompressible fluid assumption
VRES(1) = VDOT(1)*(RHO - RHOGA) - RHO*RH13*RI(1,1)/V(1) - RHO*RH23*RI(2,1)/V(1)
+ (FLUXG1 + FLUXG2)

ENDIF

RETURN
END

```

```

C*****
C* SUBROUTINE MONITR *
C* This subroutine handles the output after every time step. *
C*****

```

```

SUBROUTINE MONITR (NEQ, T, Y, RR)
IMPLICIT DOUBLE PRECISION (A-H , O-Z)
IMPLICIT INTEGER (I-N)
DOUBLE PRECISION Y(NEQ), RR(NEQ),
$ DX(9000), TIME(9000), GFLX1(9000), GFLX2(9000)
DOUBLE PRECISION LAMBDA, PLYDEN(1000), SOLDEN(1000), NSLDEN(1000)
DOUBLE PRECISION US(1000,10), UU(2), NSLOS, NSOLNT, NSOLVM,
$ STOR(10), UNORML(1000,10)
DOUBLE PRECISION DOMG1D(NPTSM-1, 2), DOMG2D(NPTSM-1,2)

```

```

COMMON /CONST/ RH01, RH02, RH03, RH013, RH023, SV1, SV2
$ , SV3, WM1, WM2, WM3, WMAIR, V1, V2, V3, R, V12, V21
$ , V13, V23, ETA, LAMBDA, GAMMA, ALPHA, BETA, FUJDO
$ , FUJA, FUJB, G

```

```

C COMMON /GLSPAR/ TCONGL, RHOGLS, CPGLS, SUBTHK, WPLATE, ALFSUB
COMMON /PLYPAR/ TCONPS, CPPS, EPSLON, SIGMA
COMMON /GASPAR/ TCONGS, VISGAS
COMMON /SCALES/ RHOSC, DIF1SC, DIF2SC, SOLLSC, SUBLSC, TIMESCS,

```

```

$ VELSC, TEMPSC, F1SC, F2SC, G1SC, G2SC, FLX1SC, FLX2SC
$   ,OMG1SC, OMG2SC
COMMON /INPUTS/ OMG1IN, OMG2IN, YK1, TEMPIN, TEMAMB
$   , FLMIN, GELTIM, PTOT

COMMON /BLK1/ RHOINT, C1MASI, C2MASI, C3MASI, DX, JCT,
$   KCT, AREA, NPTSM, NPDEM
COMMON /BLK2/ GF1, GF2
COMMON /DEVICE/ LCONC1, LCONC2, LRHO1, LRHO2, LLT, LDMU,
$   LMASS, LTEM, LSURFT, LSUB, LGEL, LWARN, LFLX, LDOMG1, LDOMG2
$   , LCONT, LCONB, LCONGR, LTEMGR, LCHMP1, LCHMP2, LDIF, LADV, LPEN
COMMON /FRMOL/ Y11, Y12, Y1A, UI1, RHOGA
COMMON /GRADS/ UX1LFT, UX1RHT, UX2LFT, UX2RHT
COMMON /GRDOMG/ GDU1(130,3), GDU2(130,3)

JSPIN = 0

C..... Separate the concentration and temperature solutions
DO 5 KL = 1, NPDEM
      DO 15 KM = 1, NPTSM
            US(KM,KL) = Y(NPDEM*(KM-1)+KL)
15      CONTINUE
5      CONTINUE

C..... Exit to main program if solution contains neg conc
DO 20 KL = 1, 2
      DO 22 KM = 1, NPTSM
            IF(US(KM,KL) .LT. 0.0D0) THEN
                  WRITE(LWARN,25) T*TIMESC, US(KM,KL)
                  IMON = -2
                  RETURN
            ENDIF
22      CONTINUE
20      CONTINUE
25      FORMAT(1X, ' MONITR: Neg Conc at T(s) ', 2X, 2(F12.6,1X))

C.... Check to see whether the spinodal has been reached

      DO 35 NJ = 1, NPTSM
            STOR(1) = US(NJ,1)
            STOR(2) = US(NJ,2)
            IFLAG = 1
            CALL COEFFI(T, NPDEM, STOR, 0.0,
$           FF1, FF2, GG1, GG2, HH1, HH2, IFLAG)
            SPINOD = FF1*F1SC*GG2*G2SC - FF2*F2SC*GG1*G1SC
            IF(SPINOD .LT. 0.0D0) THEN
                  WRITE(LWARN,27) T*TIMESC, DX(NJ)*SOLLSC*Y(NEQ)
                  JSPIN = 1
            ENDIF
35      CONTINUE

27      FORMAT(1X, ' MONITR: Spinodal Is Reached at T(s) & Z(cm) '
$           (2X,F12.6,1X))

C..... Write out the values of time and L(t) and time Tsurf
REALT = T*TIMESC
XLT = Y(NEQ)*SOLLSC
WRITE(LLT,46) REALT, Y(NEQ)*SOLLSC, Y(NEQ)
WRITE(LSURFT,44) REALT, US(NPTSM,3)*TEMPSC-273.15, US(NPTSM,3)
WRITE(LSUB,45) REALT, US(NPTSM,4)*TEMPSC-273.15
44      FORMAT(3(F15.9,2X))

```

```

45     FORMAT(2(F15.9,2X))
46     FORMAT(3(F15.9,2X))

C..... Calculate and write out the component mass conc. gradients
C..... Convert the dimensionless mass frac grad to dimensional grad
      GRADNS = (2.*US(NPTSM,1)*RH013 + US(NPTSM,2)*RH023 + RH03)*
      $      (UX1RHT/XLT) + (US(NPTSM,1)*RH023*(UX2RHT/XLT))
      GRADSL = (US(NPTSM,2)*RH013*(UX1RHT/XLT)) + (US(NPTSM,1)*
      $      RH013 + 2.*US(NPTSM,2)*RH023 + RH03)*(UX2RHT/XLT)
      WRITE(LCONGR,1100)REALT, UX1RHT, UX2RHT, GRADNS, GRADSL
1100   FORMAT(1X,F9.4,3X,4(F14.11,2X))

C..... Calculate and write out the component mass fraction gradients
C..... Convert the dimensionless mass frac grad to dimensional grad
      DO 2004 J=1, NPTSM-1
          DOMG1D(J,1) = GDU1(J,1)*XLT
          DOMG1D(J,2) = GDU1(J,2)/XLT
          DOMG2D(J,1) = GDU2(J,1)*XLT
          DOMG2D(J,2) = GDU2(J,2)/XLT
2004   CONTINUE

      WRITE(LDOMG1,2008) REALT, XLT
      WRITE(LDOMG1,2007) (DOMG1D(J,2), J=1, NPTSM-1)
      WRITE(LDOMG2,2008) REALT, XLT
      WRITE(LDOMG2,2007) (DOMG2D(J,2), J=1, NPTSM-1)

2007   FORMAT(6(F19.8,1X))
2008   FORMAT("TIME(s) ",2(F15.9, 2X))

C....      Write out dimensional mass-average velocity
      WRITE(LADV,2010) REALT, XLT
      WRITE(LADV,2009) (GDU1(J,3), J=1, NPTSM-1)

2009   FORMAT(6(F19.8,1X))
2010   FORMAT("TIME(s) ",2(F15.9, 2X))

C....      Write our pecllet number at top
      WRITE(lpen,2111) REALT, XLT, GDU1(NPTSM-1,3)*XLT/1.0D-6
C      WRITE(lpen,2111) REALT, XLT, GDU1(NPTSM-1,3)/GDU2(NPTSM-1,3)
2111   FORMAT(3(F19.8,1X))

C..... Calculate and write out the surface temp grad
      TGRADNT = UX3RHT*TEMPSC/XLT
c      WRITE(LTEMGR,1110) REALT, UX3RHT, TGRADNT
1110   FORMAT(1X,F9.4,3X,2(F20.10,3X))

      TIME(1) = 0.0D0
      GFLX1(1) = 0.0D0
      GFLX2(1) = 0.0D0
      TIME(KCT+2) = REALT
      GFLX1(KCT+2) = GF1*FLX1SC
      GFLX2(KCT+2) = GF2*FLX2SC

C..... Write out the values of fluxes (g/(cm^2-s))
      WRITE(LFLX, 57) REALT, GFLX1(KCT+2), GFLX2(KCT+2), YI1, YI2, US(NPTSM,1), US(NPTSM,2)
57     FORMAT(7(E12.5,2X))

C....      Store the normalized and non-normalized concentrations
      DO 37 NK = 1, NPTSM

```

```

                UNORML(NK,1) = US(NK,1)
                UNORML(NK,2) = US(NK,2)
                US(NK,1) = US(NK,1)*OMG1SC
                US(NK,2) = US(NK,2)*OMG2SC
37      CONTINUE

      IF (JCT*1 .EQ. KCT) THEN
        write(6,222) reat, us(nptsm,1), us(nptsm,2),
$          us(nptsm,3)*tempsc-273.15
$          , us(nptsm,4)*tempsc-273.15
222      format(5(f15.10,1x))

200      FORMAT(6(F12.8,1X))
201      FORMAT(6(F10.4,2X))
250      FORMAT('TIME(s) ',2(F15.9, 2X))
208      FORMAT(1X,F14.10,1X,8(F7.5,1X))

C.....  Integrate flux vs time to obtain amounts of non-slovent (NSLOS)
C        and solvent (SOLOS) evaporated.
        SOLVNT = 0.0D0
        NSOLNT = 0.0D0
        DO 30 L = 1, KCT+1
          NSOLNT = NSOLNT + (GFLX1(L+1) + GFLX1(L))*(TIME(L+1)-TIME(L))
30        SOLVNT = SOLVNT + (GFLX2(L+1) + GFLX2(L))*(TIME(L+1)-TIME(L))
          NSLOS = NSOLNT*0.5D0*AREA
          SOLOS = SOLVNT*0.5D0*AREA

C.....  Write out the initial component masses
        IF(KCT .EQ. 0) THEN
          WRITE(LMASS,400) C1MASI, C2MASI, C3MASI
400        FORMAT(' Intil masses of NS, S, and P ', 3X, 3(F15.10,2X))
          ENDIF

C.....  Calculate the components spatial mass density
        DO 999 LJ = 1, NPTSM
C.....  Note that the normalized concentrations are needed for DENSTY
          UU(1) = UNORML(LJ,1)
          UU(2) = UNORML(LJ,2)
          CALL DENSTY(T, 3, UU, IFG, RHO)
          NSLDEN(LJ) = RHO*US(LJ,1)*RHOSC
          SOLDEN(LJ) = RHO*US(LJ,2)*RHOSC
          PLYDEN(LJ) = RHO*( 1.0D0 - US(LJ,1) - US(LJ,2) ) *RHOSC
999        CONTINUE

C.....  Locate the space position at which gelation has occurred
        DO 1000 LJ = 1, NPTSM
          IF(SOLDEN(LJ) .LE. GELTIM) THEN
            gelthk=Y(NEQ)*SOLLCS-DX(LJ)*Y(NEQ)*SOLLSC
C          WRITE(LGEL,1005) REALT, DX(LJ), DX(LJ)*Y(NEQ)*SOLLSC
            write(LGEL,1005) T, GELTHK/SOLLSC, REALT, GELTHK
            GO TO 1001
          ENDIF
1000       CONTINUE
1001       CONTINUE
C1005      FORMAT(3(F20.13,2X))
1005      FORMAT(4(F20.13,2X))

C.....  Integrate the polymer & acetone mass density vs distance
        SUMNS = 0.D0
        SUMSL = 0.D0

```

```

SUMPL = 0.D0
DO 10 L = 1 , NPTSM - 1
SUMNS = SUMNS +
$ (NSLDEN(L+1)+NSLDEN(L))*(DX(L+1)-DX(L))*FLMIN*Y(NEQ)

SUMSL = SUMSL +
$ (SOLDEN(L+1)+SOLDEN(L))*(DX(L+1)-DX(L))*FLMIN*Y(NEQ)

SUMPL = SUMPL +
$ (PLYDEN(L+1)+PLYDEN(L))*(DX(L+1)-DX(L))*FLMIN*Y(NEQ)
10 CONTINUE

C..... Calculate the component and total mass
NSOLVM = AREA*SUMNS/2.D0
SOLVTM = AREA*SUMSL/2.D0
POLYMM = AREA*SUMPL/2.D0
TOTMAS = NSOLVM + SOLVTM + C3MASI

300 WRITE(LMASS,300) REALT, (NSOLVM+SOLVTM)/C3MASI, TOTMAS
FORMAT(2X, 2(F15.10,3X), F15.7)
JCT = JCT + 1
ENDIF
KCT = KCT + 1

C..... Stop the numerical computation if spinodal is reached
IF(JSPIN .EQ. 1) IMON = -2

RETURN
END

C*****
C* SUBROUTINE FLXHET *
C* In this subroutine the component fluxes in the gas phase, *
C* heat transfer coefficient, and heat of vaporations for *
C* non-solvent and solvent are calculated. *
C*****

SUBROUTINE FLXHET (T, UU, N, NV, VV, VVT, RHOGA
$ FLUXG1, FLUXG2, HTRSFC, HV1, HV2, IFLAG)

PARAMETER (PI = 3.14159265359)

IMPLICIT DOUBLE PRECISION (A-H , O-Z)
IMPLICIT INTEGER (I-N)
DOUBLE PRECISION UU(N), VV(NV), VVT(NV), TLOW(2,2), THIGH(2,2)
DOUBLE PRECISION LAMBDA

DOUBLE PRECISION UI1

COMMON /CONST/ RH01, RH02, RH03, RH013, RH023, SV1, SV2
$ , SV3, WM1, WM2, WM3, WMAIR, V1, V2, V3, R, V12, V21
$ , V13, V23, ETA, LAMBDA, GAMMA, ALPHA, BETA, FUJD0
$ , FUJA, FUJB, G

COMMON /GLSPAR/ TCONGL, RHOGLS, CPGLS, SUBTHK, WPLATE, ALFSUB
COMMON /PLYPAR/ TCONPS, CPPS, EPSLON, SIGMA
COMMON /GASPAR/ TCONGS, VISGAS
COMMON /SCALES/ RHOSC, DIF1SC, DIF2SC, SOLLSC, SUBLSC, TIMESCS,
$ VELSC, TEMPSC, F1SC, F2SC, G1SC, G2SC, FLX1SC, FLX2SC
$ ,OMG1SC, OMG2SC
COMMON /INPUTS/ OMG1IN, OMG2IN, YK1, TEMPIN, TEMAMB
$ , FLMIN, GELTIM, PTOT

```



```

COMMON /DEVICE/ LCONC1, LCONC2, LRHO1, LRHO2, LLT, LDMU,
$          LMASS, LTEM, LSURFT, LSUB, LGEL, LWARN, LFLX, LDOMG1, LDOMG2
$          , LCONT, LCONB, LCONGR, LTEMGR, LCHMP1, LCHMP2, LDIF,LADV, LPEN
COMMON /FRMOL/ Y11, Y12, Y1A, UI1, RHOA
COMMON /NRTL/ TNRTLA12, TNRTLA21, TNRTLALPHA12
COMMON /CHEMP/ DELCP11, DELCP22
COMMON /BLK2/ GF1, GF2
COMMON /GRVT/ IGRAVITY
COMMON /CONT/ UTOP(2)

C....  Variables for wet-casting and NRTL equation
INTEGER          NOUT
PARAMETER        (NOUT=6)
DOUBLE PRECISION          TNRTLFX, TNRTLTX, TNRTLY
INTEGER          TNRTLIFAIL, TNRTLIND, TNRTLIR
REAL            TNRTLC(17)
DOUBLE PRECISION          TNRTLF
EXTERNAL        TNRTLF

C.....  Variables for Mass transfer coefficients for wet-casting
EXTERNAL        C05AZF
DOUBLE PRECISION          D12
DOUBLE PRECISION          D12A, D12B, D12C, D12D, D12E
DOUBLE PRECISION          RAYLEIGH1, RAYLEIGH2, GRASHOF1, GRASHOF2,
$                          SCHMIDT1, SCHMIDT2,
$                          PARAM11, PARAM12, PARAM21, PARAM22

C.....  NRTL constants for Water(1)-Acetone(2) system
TNRTLA12 = 631.0463
TNRTLA21 = 1197.4101
TNRTLALPHA12 = 0.5343

C...  Initialize fluxes
IF(T .LE. 0.0D0) THEN
C          FLUXG1 = 0.0D0
          FLUXG2 = 0.0D0
          RETURN
ENDIF

C.....  ***** MASS TRANSFER ***** .....

C.....  The variable ICOUNT is used to bypass the convergence criterion
C          first time through.
          ICOUNT = 0

C.....  Set the flag for the subroutine CHEMPT

          IFG = 1

C.....  Calculate the chemical potential divided by RT
          CALL CHEMPT(T, N, UU, IFG, DELCP1, DELCP2)

C.....  Calculate the equilibrium molar concentration of the coagulation bath
C.....  at the interface using NRTL equation.
C.....  the NRTL equation is defined in the Function NRTL()

          TNRTLTX = 1.0D-6
          TNRTLY = 1.0D0
          TNRTLX = 0.0D0

```

```

TNRTLIR = 0
TNRTLIFAIL = -1
TNRTLIND = 1

DELCP11 = DELCP1
DELCP22 = DELCP2

PRINT*, 'DELCP11 is ', DELCP11

C      333      CALL C05AZF(TNRTLX, TNRTLY, TNRTLFX, TNRTLTO LX, TNRTLIR, TNRTLC,
TNRTLIND, TNRTLIFAIL)

C      IF (TNRTLIND .NE. 0) THEN
C          DELCP11 = DELCP1
C          TNRTLFX = TNRTLF(TNRTLX)
C          GO TO 333

C      ELSE
C          YI2 = TNRTLY
C          YI1 = 1.0D0 - YI2
C          YIA = 0.0D0
C          PRINT*, 'MOLE FRAC INT & BLK= ', YI1, YI2, YIA
C      ENDIF

C          OMG2GS = UU(2) + (0.06D0/0.35D0)*(0.35D0-UU(2)) + 0.09D0
C          OMG2GS = UTOP(2)
C          OMG1GS = 1.0D0 - OMG2GS

C          DENOM = OMG1GS/WM1 + OMG2GS/WM2
C          YI1 = (OMG1GS/WM1)/DENOM
C          YI2 = 1.0D0 - YI1
C          YI2 = UU(2)
C          YI1 = 1.0D0 - YI2

C..... Ternary mole fractions of Water, Acetone, and Air in the bulk.
C      Water mole fraction(YK1) is a common variable in the common
C      block INPUTS.
C          YK2 = 1.0D0 - YK1
C          YKA = 0.0D0

C..... Ternary average mole fractions for water, acetone, and air.
C          YAV1 = (YI1 + YK1) / 2.0D0
C          YAV2 = (YI2 + YK2) / 2.0D0
C          YAVA = 0.0D0

C..... Calculate the molecular weight of the coagulation phase from weighted sum
C      of the individual molecular weights (Mgas = Sum (YAVi*Mi)).
C          WMGAS = YAV1*WM1 + YAV2*WM2 + YAVA*WMAIR

C..... Binary interfacial concentration
C          Y12B1I = YI1
C          Y12B2I = YI2

C..... Binary bulk cocentration
C          Y12B1K = YK1 / (YK1 + YK2)
C          Y12B2K = YK2 / (YK1 + YK2)

C          PRINT*, 'TIME=', T*TIMESC

```

```

C          PRINT*, ' MOLE FRACTIONS ARE ', Y12B1I, Y12B2I, Y12B1K, Y12B2K

C....    Calculate the density of coagulation bath at the interface
          WMG12 = (Y12B1I*WM1) + (Y12B2I*WM2)
          UI1 = (Y12B1I*WM1)/WMG12
          UI2 = (Y12B2I*WM2)/WMG12
          RHOG12 = 1.0D0/((OMG1GS/RH01) + (OMG2GS/RH02))
          RHOGA = RHOG12/RHOSC

C.....   Binary interfacial mass fraction of component(1)-water
          UI1 = (Y12B1I*WM1)/WMG12

          PRINT*, 'T, RHOga and UI1', T*TIMESC, RHOGA, UI1
C....    Diffusion coefficient depending on concentration at the interface
          D12A = 15.211
          D12B = -24.151
          D12C = 18.961
          D12D = -6.1798
          D12E = 1.2801
          D12 = ((D12A*(Y12B2I**4.0)) + (D12B*(Y12B2I**3.0)) + (D12C*(Y12B2I**2.0)) +
(D12D*Y12B2I) + D12E)*1.0D-05

          CONC12 = ((Y12B1I*RH01)/WM1) + ((Y12B2I*RH02)/WM2)
          PRINT*, ' YI2, D12= ', Y12B2I, D12

          IF (IGRAVITY .EQ. 0) THEN

CCCCCCCCCCCCCCCCCCCCCCCCCCCCCCCCCCCCCCCCCCCCCCCCCCCCCCCC
C
C          No convection (0-G)
C
CCCCCCCCCCCCCCCCCCCCCCCCCCCCCCCCCCCCCCCCCCCCCCCCCCCCCCCC
          FLMST = 1.0D0*((0.000050D0*T*TIMESC)**0.5D0)
C          FLMST = 1.90D0
          sum=0
          DO 9714 countern=1,50
9714          sum=sum+DEXP(-D12*T*TIMESC*(countern*PI/FLMST)**2.0D0)

C.....   Equi-mass mass transport
          DX2DZatZ0=-(RHOGA*OMG2GS/FLMST)*(1.0D0+2.0D0*sum)
          TC2A = RHOG12*D12*DX2DZatZ0/OMG2GS

          PRINT*, 'FL1s= ', DX1DZatZ0, DX2DZatZ0
12346   CONTINUE
          PRINT*, 'vvt=', VVT(1)
          FLUXG1 = (1.0D0 + OMG1GS*(1.0D0/RH01-1.0D0/RH02))*D12*DX2DZatZ0/FLX1SC
          FLUXG2 = -(1.0D0 - OMG2GS*(1.0D0/RH01-1.0D0/RH02))*D12*DX2DZatZ0/FLX2SC
          PRINT*, 'FLns=', RHOGA*(FLUXG1+FLUXG2)*OMG2GS/RHOGA -
RHOGA*D12*DX2DZatZ0, FLUXG2, FLUXG2*FLX2SC
          GF1 = FLUXG1
          GF2 = FLUXG2
C          FLUXG1 = (TCHIGH(1,2) * (Y12B1K - Y12B1I))*WM1 / FLX1SC
          PRINT*, 'FLUXG1, FLUXG2, GF1, GF2 = ', FLUXG1, FLUXG2, GF1, GF2
C          PRINT*, ' FLUXGs, Vdot, conc_CS= ', FLUXG1, FLUXG2, VVT(1), UU(1), UU(2), UU(3)

          ELSE

CCCCCCCCCCCCCCCCCCCCCCCCCCCCCCCCCCCCCCCCCCCCCCCCCCCCCCCC

```

```

C
C      Free Convection (1-G, 2-G)
C
CCCCCCCCCCCCCCCCCCCCCCCCCCCCCCCCCCCCCCCCCCCCCCCCCCCCCCCC
      FLMST = 1.0D0*((0.000050D0*T*TIMESC)**0.5D0)
C      FLMEST= 1.90D0
      sum=0
      DO 19714 countern=1,50
19714      sum=sum+DEXP(-D12*T*TIMESC*(countern*PI/FLMST)**2)
              DX2DZatZ0=-((OMG2GS/1.9)*(1-2*sum)
      TC2A = RHOG12*D12*DX2DZatZ0/OMG2GS  ! should be /YI2
C      write (*,*) "dx2dzatz0",DX2DZatZ0
C      write (*,*) "TC2A",TC2A
      PRINT*, 'FLMST= ', FLMST
C.....  Obtain an estimate of the film thickness at low fluxes(cm).
C      FLMST2 = RHOG12*D12/TC2A
C      FLMEST = 1.90D0
C      PRINT*, 'FLMEST = ', FLMEST

C      Evluate (Rayligh number)^0.25 = (Grashof number)^0.25 * (Schmidt number)^0.25
C
      PARAM11 = 0.27D0
      PARAM12 = 0.25D0

      PARAM21 = 0.54D0
      PARAM22 = 0.25D0

      IF (IGRAVITY .EQ. 1) THEN
C      1-G
      GRASHOF1 = (((FLMST)**3.0D0) * (RHOG12**2.0D0) * 9.8D0 * 1.0D0 *(Y12B1K -
Y12B1I)) / ((1.0D-02)**2.0D0)**PARAM12
      GRASHOF2 = (((FLMST)**3.0D0) * (RHOG12**2.0D0) * 9.8D0 * 1.0D0 *(Y12B2I -
Y12B2K)) / ((1.0D-02)**2.0D0)**PARAM22
      PRINT*, 'Grashof1, Grashof2= ', GRASHOF1, GRASHOF2
      PRINT*, 'RHOG12, Y12B1K, Y12B1I= ', RHOG12, Y12B1K, Y12B1I

      ELSE
C      2-G
      GRASHOF1 = (((FLMST)**3.0D0) * (RHOG12**2.0D0) * 9.8D0 * 2.0D0 * (Y12B1K -
Y12B1I)) / ((1.0D-02)**2.0D0)**PARAM12
      GRASHOF2 = (((FLMST)**3.0D0) * (RHOG12**2.0D0) * 9.8D0 * 2.0D0 *(Y12B2I -
Y12B2K)) / ((1.0D-02)**2.0D0)**PARAM22
      PRINT*, 'Grashof1, Grashof2= ', GRASHOF1, GRASHOF2
      ENDIF

      SCHMIDT1 = ((1.0D-02) / (RHOG12 * D12))**PARAM12
      SCHMIDT2 = ((1.0D-02) / (RHOG12 * D12))**PARAM22
      PRINT*, 'Schmidt1, Schmidt2= ', SCHMIDT1, SCHMIDT2
      RAYLEIGH1 = GRASHOF1 * SCHMIDT1
      RAYLEIGH2 = GRASHOF2 * SCHMIDT2

      PRINT*, 'Rayligh1, Rayligh2= ', RAYLEIGH1, RAYLEIGH2

C      TCLOW(1,2) = (CONC12 * D12 / FLMST) * (PARAM11 * (RAYLEIGH1))
C      TCLOW(2,1) = (CONC12 * D12 / FLMST) * (PARAM21 * (RAYLEIGH2))
      TCLOW(1,2) = (CONC12 * D12 / FLMST) * (10.0D0**0.1D0)
      TCLOW(2,1) = (CONC12 * D12 / FLMST) * (10.0D0**0.1D0)
      PRINT*, ' TCLOWs= ', TCLOW(1,2), TCLOW(2,1)

      FLUXG2 = - (TCLOW(2,1) * (Y12B2K - Y12B2I)) * WM2 / FLX2SC
      FLUXG1 = - (TCLOW(1,2) * (Y12B1K - Y12B1I)) * WM1 / FLX1SC

```

```
RVALUE = (Y12B1I - Y12B1K)/((FLUXG1/(FLUXG1+FLUXG2)) - Y12B1I)
THVALUE = (DLOG(RVALUE + 1.0D0))/RVALUE
```

```
TCHIGH(2,1) = THVALUE*TCLOW(2,1)
TCHIGH(1,2) = THVALUE*TCLOW(1,2)
PRINT*, ' TCHIGHss= ', TCHIGH(1,2), TCHIGH(2,1)
PRINT*, 'R and Th= ', RVALUE, THVALUE
```

```
FLUXG2 = - (TCHIGH(2,1) * (Y12B2K - Y12B2I)) * WM2 / FLX2SC
FLUXG1 = - (TCHIGH(1,2) * (Y12B1K - Y12B1I)) * WM1 / FLX1SC
C FLUXG1 = FLUXG2
PRINT*, ' FLUXG1, FLUXG2 = ', FLUXG1, FLUXG2
C PRINT*, ' FLUXGs, Vdot, conc_CS= ', FLUXG1, FLUXG2, VVT(1), UU(1), UU(2), UU(3)
GF1 = FLUXG1
GF2 = FLUXG2
```

```
ENDIF
```

```
RETURN
END
```

```
C*****
C* SUBROUTINE CONSTS *
C* This subroutine is called to initialize the constants which *
C* are specific to the system. *
C*****
```

```
SUBROUTINE CONSTS
IMPLICIT DOUBLE PRECISION (A-H , O-Z)
IMPLICIT INTEGER (I-N)
DOUBLE PRECISION LAMBDA, DX(9000)
```

```
COMMON /CONST/ RH01, RH02, RH03, RH013, RH023, SV1, SV2
$ , SV3, WM1, WM2, WM3, WMAIR, V1, V2, V3, R, V12, V21
$ , V13, V23, ETA, LAMBDA, GAMMA, ALPHA, BETA, FUJD0
$ , FUJA, FUJB, G
COMMON /GLSPAR/ TCONGL, RHOGLS, CPGLS, SUBTHK, WPLATE, ALFSUB
COMMON /PLYPAR/ TCONPS, CPPS, EPSLON, SIGMA
COMMON /GASPAR/ TCONGS, VISGAS
COMMON /SCALES/ RHOSC, DIF1SC, DIF2SC, SOLLSC, SUBLSC, TIMESC,
$ VELSC, TEMPSC, F1SC, F2SC, G1SC, G2SC, FLX1SC, FLX2SC
$ ,OMG1SC, OMG2SC
COMMON /INPUTS/ OMG1IN, OMG2IN, YK1, TEMPIN, TEMAMB
$ , FLMIN, GELTIM, PTOT

COMMON /BLK1/ RHOINT, C1MASI, C2MASI, C3MASI, DX, JCT,
$ KCT, AREA, NPTSM, NPDEM
COMMON /DEVICE/ LCONC1, LCONC2, LRHO1, LRHO2, LLT, LDMU,
$ LMASS, LTEM, LSURFT, LSUB, LGEL, LWARN, LFLX, LDOMG1, LDOMG2
$ , LCONT, LCONB, LCONGR, LTEMGR, LCHMP1, LCHMP2, LDIF, LADV, LPEN
```

```
C..... Set component densities (g/cm^3)
RH01 = 1.0
RH02 = 0.7857
RH03 = 1.31
```

```
RH013 = RH01 - RH03
RH023 = RH02 - RH03
```

C..... Calculate the specific volumes (cm³/g)
SV1 = 1.0/RH01
SV2 = 1.0/RH02
SV3 = 1.0/RH03

C..... Molecular weights (g/mole)
WM1 = 18.0
WM2 = 58.08
WM3 = 40000.0
WMAIR = 29.0

V1 = SV1*WM1
V2 = SV2*WM2
V3 = SV3*WM3
R = 8.314
G = 980.0
SIGMA = 5.67D-12

C..... Calculate pure molar volume ratios
V12 = V1/V2
V21 = V2/V1
V13 = V1/V3
V23 = V2/V3

C..... Calculate ratios of pure molar volumes to molecular weights
ETA = V1/WM1
LAMBDA = V2/WM2
GAMMA = V3/WM3
ALPHA = ETA - GAMMA
BETA = LAMBDA - GAMMA

C..... Set parameters in Fujita's expression
FUJD0 = 7.70133D-17
FUJA = 3.35087D-02
FUJB = 3.37608D-03

C..... Set parameters specific to the support
TCONGL = 0.23D-02
RHOGLS = 1.41
CPGLS = 1.7

C..... Calculate the area of MCA casting solution cavity.
AREA = 3.141592D0*(0.5**2.0D0)

C..... Set parameters specific to the polymer solution
C The following values were taken from Tantekin's thesis for
C binary solution (CA/ACET). Values for ternary must be obtained.
TCONPS = 0.2d-02
CPPS = 2.5
EPSLON = 0.81

C..... Set parameters specific to the gas phase
C The following values are for pure air averaged over 280 and 300 K
TCONGS = 2.5456d-04
VISGAS = 1.7984D-04

C..... Set the scaling values
C RHOGIN = 1.0D0*WMAIR/(82.0*TEMPIN)
RHOSC = 1.0D0
C RHOSC = (RH01 + RH02 + RH03)/3.0D0
C DIF1SC = 1.0D-06
C DIF1SC = 5.0D-05

```

C      DIF2SC = 1.28D-05
      DIF2SC = 5.0D-05
      SOLLSC = FLMIN
      SUBLSC = SUBTHK
c      FLX1SC = 0.5*RHOGIN
      VELSC = DIF1SC/SOLLSC

C      XK01A = 1.7772546781866D-05
C      XK02A = 3.5545093563732D-05
      XK01A = 1.50D-05
      XK02A = 1.50D-05
      XH0 = 2.0D-03
C      FLX1SC = WM1*XK01A
C      FLX2SC = WM2*XK02A
      FLX1SC = RHOSC*DIF1SC/SOLLSC
      FLX2SC = RHOSC*DIF1SC/SOLLSC
C      FLX2SC = FLX1SC
C      TIMESC = SOLLSC*RHOSC/FLX1SC
      TIMESC = (SOLLSC**2.0D0)/DIF1SC
      TEMPSC = TEMPIN
      F1SC = RHOSC*DIF1SC
      G2SC = RHOSC*DIF2SC
      F2SC = F1SC
      G1SC = G2SC
c      OMG1SC = OMG1IN
c      OMG2SC = OMG2IN
      OMG1SC = 1.0D0
      OMG2SC = 1.0D0

C..... Calculate the constant dimensionless groups
      P3DMLS = WM2/WM1
      P4DMLS = OMG1IN
      P5DMLS = OMG2IN

      WRITE(LLT,101)
      WRITE(LLT,*) P3DMLS, P4DMLS, P5DMLS
101    FORMAT(1X,'P3, P4, P5')

      RETURN
      END

C*****
C*          SUBROUTINE COEFFI          *
C*      This subroutine is used to calculate the coefficients of the *
C*      pde. These are f1, f2, g1, g2, h1, and h2.          *
C*****

      SUBROUTINE COEFFI(T, N, UV, UVX, F1, F2, G1, G2, H1, H2, IFLAG)
      IMPLICIT DOUBLE PRECISION (A-H, O-Z)
      IMPLICIT INTEGER (I-N)
      DOUBLE PRECISION UV(N), UVX(N), LAMBDA

      COMMON /CONST/ RH01, RH02, RH03, RH013, RH023, SV1, SV2
$ , SV3, WM1, WM2, WM3, WMAIR, V1, V2, V3, R, V12, V21
$ , V13, V23, ETA, LAMBDA, GAMMA, ALPHA, BETA, FUJD0
$ , FUJA, FUJB, G
      COMMON /GLSPAR/ TCONGL, RHOGLS, CPGLS, SUBTHK, WPLATE, ALFSUB
      COMMON /PLYPAR/ TCONPS, CPPS, EPSLON, SIGMA
      COMMON /GASPAR/ TCONGS, VISGAS
      COMMON /SCALES/ RHOSC, DIF1SC, DIF2SC, SOLLSC, SUBLSC, TIMESC,
$ VELSC, TEMPSC, F1SC, F2SC, G1SC, G2SC, FLX1SC, FLX2SC

```

```

$      ,OMG1SC, OMG2SC
COMMON /INPUTS/ OMG1IN, OMG2IN, YK1, TEMPIN, TEMAMB
$      ,FLMIN, GELTIM, PTOT

OMG1 = UV(1)*OMG1SC
OMG2 = UV(2)*OMG2SC
OMG3 = 1.D0 - OMG1 - OMG2

C..... Calculate the volume fractions from mass fractions
DUMMY = ALPHA*OMG1 + BETA*OMG2 + GAMMA
PHI1 = ETA*OMG1/DUMMY
PHI2 = LAMBDA*OMG2/DUMMY
PHI3 = GAMMA*(1.0-OMG1-OMG2)/DUMMY

IF (PHI1 .LT. 0.0D0 .OR. PHI2 .LT. 0.0D0 .OR. PHI3 .LT. 0.0D0) THEN
F1 = 0.0D0
F2 = 0.0D0
G1 = 0.0D0
G2 = 0.0D0
RETURN
ENDIF

C..... Calculate binary 12 volume fractions from ternary volume fractions
U1 = PHI1/(PHI1+PHI2)
U2 = PHI2/(PHI1+PHI2)

ABODON = GAMMA + ALPHA*OMG1 + BETA*OMG2

C..... Calculate derivatives of ternary volume frac w.r.t. mass frac.
DP1O1 = -(ALPHA*ETA*OMG1/(ABODON)**2)
$      + ETA/(ABODON)
DP1O2 = -(BETA*ETA*OMG1/(ABODON)**2)
DP2O1 = -(ALPHA*LAMBDA*OMG2/(ABODON)**2)
DP2O2 = -(BETA*LAMBDA*OMG2/(ABODON)**2)
$      + LAMBDA/(ABODON)
DP3O1 = -(ALPHA*GAMMA*(1. - OMG1 - OMG2)/(ABODON)**2)
$      - GAMMA/(ABODON)
DP3O2 = -(BETA*GAMMA*(1. - OMG1 - OMG2)/(ABODON)**2)
$      - GAMMA/(ABODON)

C..... Sum of the derivatives w.r.t. mass fractions is zero
SUMO1 = DP1O1 + DP2O1 + DP3O1
SUMO2 = DP1O2 + DP2O2 + DP3O2

C..... Begin calculation of the friction coefficients.

C..... Calculate the binary(2,3) density (solvent/polymer) using
C the following equation of state;
RHOB23 = 1.0D0/((OMG2/(1.0D0-OMG1))*(1.0D0/RH02 + 1.0D0/RH03) + 1.0D0/RH03)

C..... Calculate the self diffusion coefficients from Fujita's experssion.
C The binary volume fractions are evaluated in terms of ternary
C volume fractions.
D2STAR = FUJD0*DEXP(PHI2/(FUJA*PHI2+FUJB*(1.-PHI1)))

C..... Calculate the friction coefficients XIij. Note that the
C friction coefficients are evaluate without the RT part.
C That is, the actual friction coefficient exi12 is equal
C to variable XI12 * RT. This is because the RTs cancel when the
C friction coefficients are multiplied by the gradients of chemical
C potentials divided by friction coefficients squared.
XI12 = V2/5.03D-05

```



```

C      XI23 = (((2.0*(OMG2/(1.-OMG1))*RH023)+RH03)*WM3)
C $      / (D2STAR*(RHOB23**2.0))
      XI23 = (RH03*WM3)/D2STAR
c      XI13 = 0.25*V12*XI23

C..... Shojai's C value is 2.05D-08
      XI13 = 2.05D-08*V12*XI23

C..... Ruever's C value is 0.5
C      XI12 = 0.5D0*V12*XI23

C..... Calculate various parts of Fi, Gi, and Hi.
      PRT1 = XI12*XI13*OMG1/(WM1*WM3)
      PRT2 = XI12*XI23*OMG2/(WM2*WM3)
      PRT3 = XI13*XI23*OMG3/(WM3*WM3)
      THETA = PRT1 + PRT2 + PRT3
      AA = (XI12*OMG2/WM2) + (XI13*(1.0D0-OMG2)/WM3)
      BB = (XI12*OMG2/WM2) - (XI13*OMG2/WM3)
      CC = (XI12*OMG1/WM1) + (XI23*(1.0D0-OMG1)/WM3)
      DD = (XI12*OMG1/WM1) - (XI23*OMG1/WM3)

C..... Note that the functions H1 and H2 reduce to -OMG1 and
C      -OMG2, respectively. However, these functions will be
C      calculated using the long expressions in order to check the
C      friction coefficient functions.
      H1 = -(OMG1/(WM3*THETA))*(CC*XI13 + BB*XI23)
      H2 = -(OMG2/(WM3*THETA))*(DD*XI13 + AA*XI23)

c      IFLAG = 1
      CALL FHINTP(T, U1, U2, PHI1, PHI2, PHI3, G12, G23, G13,
      $          DG12, DG23, DG13, DDG12, DDG23, DDG13, IFLAG)

C..... Calculate the components needed for gradient of chemical potential
C      That is, Q1, Q2, Q3, S1, S2, and S3.
      Q1 = (1.0/PHI1) - 1.0 + ((PHI1 - (2.0*U2))*(U2**2.0)*DG12)
      $ + (U1*(U2**3.0)*DDG12) - ((PHI3**2.0)*DG13)
      Q2 = -V12 + (G12*((2.0*PHI2)+PHI3)) + (G13-(V12*G23))*PHI3 +
      $ (U1*U2*((2.0*U2)-PHI1-1.0)*DG12) - ((U1**2.0)*(U2**2.0)
      $ *DDG12) - (V12*(PHI3**2.0)*DG23)
      Q3 = -V13 + (G13*(2.0*PHI3+PHI2)) + (PHI2*(G12-(V12*G23))) -
      $ (3.0*V12*PHI2*PHI3*DG23) + ((1.0-3.0*PHI1)*PHI3*DG13) -
      $ (V12*PHI2*(PHI3**2.0)*DDG23) - (PHI1*(PHI3**2.0)*DDG13)

      S1 = -V21 + (PHI3*(G23-(V21*G13))) + (V21*G12*(2.0*PHI1+PHI3))
      $ + (V21*U1*U2*(1.0+PHI2-(2.0*U1))*DG12) - ((U1**2.0)*
      $ (U2**2.0)*V21*DDG12) - ((PHI3**2.0)*V21*DG13)
      S2 = (1.0/PHI2) - 1.0 + ((U1**3.0)*U2*V21*DDG12) + ((U1**2.0)
      $ *V21*(2.0*U1-PHI2)*DG12) - ((PHI3**2.0)*DG23)
      S3 = -V23 + (V21*PHI1*(G12-G13)) + (G23*(2.0*PHI3+PHI1)) +
      $ ((1.0-3.0*PHI2)*PHI3*DG23) - (PHI2*(PHI3**2.0)*DDG23)
      $ - (PHI1*(PHI3**2.0)*V21*DDG13) - (3.0*V21*PHI1*PHI3*DG13)

C..... Assemble the gradient of chemical potentials w.r.t. mass frac
C      Note! Here again the gradients will be evaluated without the
C      RT part, just as in the friction coefficient evaluation.
      DM1O1 = Q1*DP1O1 + Q2*DP2O1 + Q3*DP3O1
      DM1O2 = Q1*DP1O2 + Q2*DP2O2 + Q3*DP3O2
      DM2O1 = S1*DP1O1 + S2*DP2O1 + S3*DP3O1
      DM2O2 = S1*DP1O2 + S2*DP2O2 + S3*DP3O2

C..... Write out the gradients of chem pot w.r.t. omegas
      IF(IFLAG.EQ.9999) THEN

```

```

F1 = DM1O1
F2 = DM1O2
G1 = DM2O1
G2 = DM2O2
PRINT*, IFLAG= , IFLAG
RETURN
ENDIF

C..... Calculate the functions F1, G1, H1, F2, G2, and H2.
C The functions F1, F2, G1, and G2 are dimensionless.
F1 = - (OMG1/THETA)*(CC*DM1O1 + BB*DM2O1) / F1SC
F2 = - (OMG2/THETA)*(DD*DM1O1 + AA*DM2O1) / F2SC
G1 = - (OMG1/THETA)*(CC*DM1O2 + BB*DM2O2) / G1SC
G2 = - (OMG2/THETA)*(DD*DM1O2 + AA*DM2O2) / G2SC

RETURN
END

C*****
C* SUBROUTINE FHINTP *
C* This subroutine is used to calculate the Flory-Huggins *
C* interactions parameters and their various derivatives. *
C*****

SUBROUTINE FHINTP(T, U1, U2, PHI1, PHI2, PHI3, G12, G23, G13,
$ DG12, DG23, DG13, DDG12, DDG23, DDG13, IFLAG)
IMPLICIT DOUBLE PRECISION (A-H , O-Z)
IMPLICIT INTEGER (I-N)

C..... Ternary (polymer/solent/nonsolvent) system
G12 = 0.661 + (0.417/(1.0-(U2*0.755)))
G23 = 0.535 + 0.11*PHI3
G13 = 1.4

DG12 = 0.417*0.755/((1.0 - U2*0.755)**2.0)
DG23 = 0.11
DG13 = 0.0

DDG12 = (2.0*0.755/(1.0 - U2*0.755))*DG12
DDG23 = 0.0
DDG13 = 0.0

RETURN
END

C*****
C* SUBROUTINE CHEMPT *
C* This subroutine is used to calculate the change in chemical *
C* potential divided by RT. *
C*****

SUBROUTINE CHEMPT(T, N, UV, IFG, DELCP1, DELCP2)
IMPLICIT DOUBLE PRECISION (A-H , O-Z)
IMPLICIT INTEGER (I-N)
DOUBLE PRECISION UV(N)
DOUBLE PRECISION LAMBDA

COMMON /CONST/ RH01, RH02, RH03, RH013, RH023, SV1, SV2

```

```

$ , SV3, WM1, WM2, WM3, WMAIR, V1, V2, V3, R, V12, V21
$ , V13, V23, ETA, LAMBDA, GAMMA, ALPHA, BETA, FUJDO
$ , FUJA, FUJB, G
COMMON /SCALES/ RHOSC, DIF1SC, DIF2SC, SOLLSC, SUBLSC, TIMESC,
$ VELSC, TEMPSC, F1SC, F2SC, G1SC, G2SC, FLX1SC, FLX2SC
$ ,OMG1SC, OMG2SC

C..... It is necessary to evaluate the activity coefficient times mole
C fraction of acetone and water for use in subroutine FLXHET. The
C activity coefficient multiplied by mole fraction for each component
C is given by: (Act Coef i)*Xi = DEXP(del chem pot/RT).
C The change in chemical potential divided by RT is evaluated in this
C subroutine.

OMG1 = UV(1)*OMG1SC
OMG2 = UV(2)*OMG2SC
OMG3 = 1.D0 - OMG1 - OMG2

C..... Calculate the volume fractions using mass fractions
DUMMY = ALPHA*OMG1 + BETA*OMG2 + GAMMA
PHI1 = ETA*OMG1/DUMMY
PHI2 = LAMBDA*OMG2/DUMMY
PHI3 = GAMMA*(1.0-OMG1-OMG2)/DUMMY

C PRINT*, 'PHI1,2,3 = ', PHI1, PHI2, PHI3

C..... Calculate binary 12 volume fractions from ternary volume fractions
U1 = PHI1/(PHI1+PHI2)
U2 = PHI2/(PHI1+PHI2)

CALL FHINTP(T, U1, U2, PHI1, PHI2, PHI3, G12, G23, G13,
$ DG12, DG23, DG13, DDG12, DDG23, DDG13, IFG)

C..... Ternary system
DELCP1 = DLOG(PHI1) + 1.0 - PHI1 - V12*PHI2 - V13*PHI3 +
$ (G12*PHI2 + G13*PHI3)*(PHI2 + PHI3) - G23*V12*PHI2*PHI3 -
$ U1*U2*PHI2*DG12 - PHI1*DG13*PHI3**2.0 -
$ V12*PHI2*DG23*PHI3**2.0

DELCP2 = DLOG(PHI2) + 1.0 - PHI2 - V21*PHI1 - V23*PHI3 +
$ U1*U2*PHI1*V21*DG12 - PHI1*V21*DG13*PHI3**2.0 -
$ G13*PHI1*PHI3*V21 + (G12*V21*PHI1 + G23*PHI3)*(PHI1 + PHI3)
$ - PHI2*DG23*PHI3**2.0

IF (PHI1 .LT. 0.0D0 .OR. PHI2 .LT. 0.0D0 .OR. PHI3 .LT. 0.0D0) THEN
DELCP1 = 0.0D0
DELCP2 = 0.0D0
PRINT*, 'BINODAL??'
ENDIF
C IF(IFG .EQ. 3) PRINT*, OMG1, OMG2, DELCP1, DELCP2
C ENDIF

C IF (DELCP1 .EQ. NaN .OR. DELCP2 .EQ. NaN) THEN
C PRINT*, 'DELCP is NaN'
C ENDIF
RETURN
END

C*****
C* SUBROUTINE DENSTY *
C* This subroutine calculates the density of the solutions *
```

```

C*      using the following equation of state;
C*      RHO = OMG1*RH01 + OMG2*RH02 + OMG3*RH03
C*****

      SUBROUTINE DENSTY (T, N, UV, IFG, RHO)
      IMPLICIT DOUBLE PRECISION (A-H , O-Z)
      IMPLICIT INTEGER (I-N)
      DOUBLE PRECISION UV(N)
      DOUBLE PRECISION LAMBDA

      COMMON /CONST/ RH01, RH02, RH03, RH013, RH023, SV1, SV2
$ , SV3, WM1, WM2, WM3, WMAIR, V1, V2, V3, R, V12, V21
$ , V13, V23, ETA, LAMBDA, GAMMA, ALPHA, BETA, FUJDO
$ , FUJA, FUJB, G
      COMMON /SCALES/ RHOSC, DIF1SC, DIF2SC, SOLLSC, SUBLSC, TIMESCS,
$ VELSC, TEMPSC, F1SC, F2SC, G1SC, G2SC, FLX1SC, FLX2SC
$ ,OMG1SC, OMG2SC

      OMG1 = UV(1)*OMG1SC
      OMG2 = UV(2)*OMG2SC
      OMG3 = 1.0D0 - OMG1 - OMG2

C      PRINT*, '1,2,3 = ', OMG1, OMG2, OMG3
C..... RHO is dimensionless.
      RHO = 1.0D0/(OMG1/RH01 + OMG2/RH02 + OMG3/RH03)
      RETURN
      END

C*****
C*      FUNCTION TNRTLF
C*      This subroutine defines activity coefficients of
C*      the surface of casting solution using NRTL equation
C*
C*****

      FUNCTION TNRTLF(AX)

      IMPLICIT DOUBLE PRECISION (A-H , O-Z)
      IMPLICIT INTEGER (I-N)

      DOUBLE PRECISION AX
      DOUBLE PRECISION TNRTLTAU12
      DOUBLE PRECISION TNRTLTAU21
      DOUBLE PRECISION TNRTLGA12
      DOUBLE PRECISION TNRTLGA21

      DOUBLE PRECISION TNRTLA12, TNRTLA21, TNRTLALPHA12
C      DOUBLE PRECISION DELCP01
      DOUBLE PRECISION DELCP11, DELCP22

      COMMON /INPUTS/ OMG1IN, OMG2IN, YK1, TEMPIN, TEMAMB, FLMIN, GELTIM, PTOT
      COMMON /NRTL/ TNRTLA12, TNRTLA21, TNRTLALPHA12
      COMMON /CHEMP/ DELCP11, DELCP22

      TNRTLA12 = 631.0463
      TNRTLA21 = 1197.4101
      TNRTLALPHA12 = 0.5343

      PRINT*, ' DELCP22= ', DELCP22
      TNRTLTAU12 = TNRTLA12/(1.98721D0*TEMPIN)
      TNRTLTAU21 = TNRTLA21/(1.98721D0*TEMPIN)

```

```

TNRTL12 = DEXP(-TNRTLALPHA12*TNRTLTAU12)
TNRTL21 = DEXP(-TNRTLALPHA12*TNRTLTAU21)

TNRTLF = (DEXP(DELC22)/(DEXP(0.0D0 - ((1-AX)**2.0D0)*
$      ((TNRTLTAU12*((TNRTL12/(AX+(1-AX)*TNRTL12))**2.0D0)) +
$      ((TNRTLTAU21*TNRTL21)/(((1-AX)+AX*TNRTL21)**2.0D0)))))) - AX

RETURN
END

```